ASTROGEOLOGIC STUDIES

ANNUAL PROGRESS REPORT

July 1, 1965 to July 1, 1966

PART B
CRATER INVESTIGATIONS

DEPARTMENT OF THE INTERIOR

UNITED STATES GEOLOGICAL SURVEY

ASTROGEOLOGIC STUDIES

ANNUAL PROGRESS REPORT

July 1, 1965 to

July 1, 1966

PART B: CRATER INVESTIGATIONS

November 1966

This preliminary report is distributed without editorial and technical review for conformity with official standards and nomenclature. It should not be quoted without permission.

This report concerns work done on behalf of the National Aeronautics and Space Administration.

DEPARTMENT OF THE INTERIOR
UNITED STATES GEOLOGICAL SURVEY

CONTENTS

PART B--CRATER INVESTIGATIONS

INTRODUCTION

This Annual Report is the sixth of a series describing the results of research conducted by the U.S. Geological Survey on behalf of the National Aeronautics and Space Administration. This report, which covers the period July 1, 1964 to July 1, 1965, is in four volumes corresponding to three main areas of research: Part A, Lunar and Planetary Investigations; Part B, Crater Investigations; Part C, Cosmic Chemistry and Petrology; and Part D, Space Flight Investigations; and a map supplement. An additional volume presents in abstract form summaries of the papers in Parts A-D.

The major long-range objectives of the astrogeologic studies program are to determine and map the stratigraphy and structure of the Moon's crust, to work out from these the sequence of events that led to the present condition of the Moon's surface, and to determine the processes by which these events took place. Work being carried out that leads toward these objectives includes a program of lunar geologic mapping; studies on the discrimination of geologic materials on the lunar surface by their photometric, polarimetric, and infrared properties; field studies of structures of impact, explosive, and volcanic origin; laboratory studies on the behavior of rocks and minerals subjected to shock; and study of the chemical, petrographic and physical properties of materials of possible lunar origin and the development of special techniques for their analysis.

Part B, Crater Investigations, contains the results of field and laboratory studies of craters and related phenomena. Field investigations have been made of naturally formed craters and roots of craters: (1) the Flynn Creek structure in east Tennessee, (2) the Sierra Madera structure in west Texas, (3) the Manicouagan Lake structure in Quebec, Canada, and (4) the Moses Rock diatreme in Utah. The first three are thought to be eroded impact structures; the fourth is the root of a maar-type crater.

Results of two experimental studies of impact craters are reported in (1) "Craters Produced by Missile Impacts," and (2) "Hypervelocity Impact Craters in Pumice"; a third paper provides a compilation of data on craters formed by explosives. Another paper describes a new technique for field explosive shock experiments.

Summaries of field and laboratory studies of shock-induced changes in rocks are given in three papers: (1) "Impact Metamorphism," (2) "Nickel-Iron Spherules from the Aouelloul Glass of Mauritania, Africa," and (3) "Influence of Stress History on Low-Temperature Thermoluminescence of Halite."

HISTORY AND ORIGIN OF THE FLYNN CREEK CRATER, TENNESSEE: FINAL REPORT

By David J. Roddy

INTRODUCTION

The Flynn Creek structure in north-central Tennessee (fig. 1) consists of a partly exhumed crater about 330 feet deep and 11,500 feet in diameter that is filled with breccia and Upper Devonian shale and Lower Mississippian chert that were deposited after the crater formed. The crater is surrounded by a folded and faulted rim composed of Middle and Upper Ordovician limestones, and its center is occupied by a hill of uplifted Lower Ordovician strata (figs. 2, 3).

The origin of this unusual structure has been the subject of controversy for nearly a century Of the various origins proposed, impact and volcanic gas-phreatic explosions have been suggested as the most likely causes. But only one short, inconclusive study has been actually directed toward this problem (Wilson and Born, 1936). Most of the specific information presented here was gathered during the recent study by the author, and it is now apparent that the structural deformation is very anomalous and is restricted to the area occupied by the crater and the surrounding strata in the rim. The deformation and chaotic mixing of fragments in the breccia, and the presence of a large ejected mass of breccia on the rim imply the occurrence of at least one dynamic event, presumably violent in nature. The observed deformational features could have originated at or very near the ground surface during middle Paleozoic time, and only a moderate amount of erosion might have occurred before the crater was buried. Reconnaissance studies of several hundred square miles surrounding the Flynn Creek area show

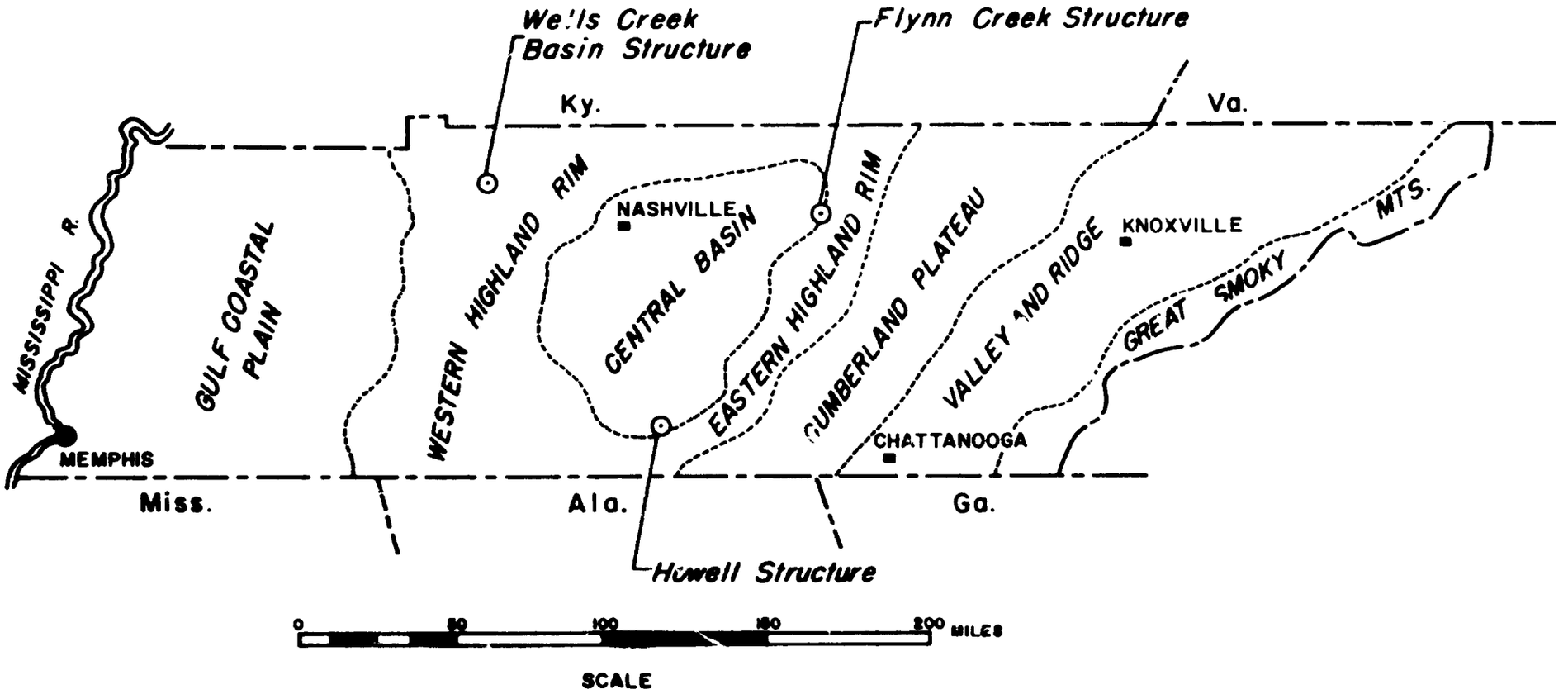

Figure 1.--Index map of the Flynn Creek structure, Tennessee. Dotted lines show the boundaries of the physiographic provinces.

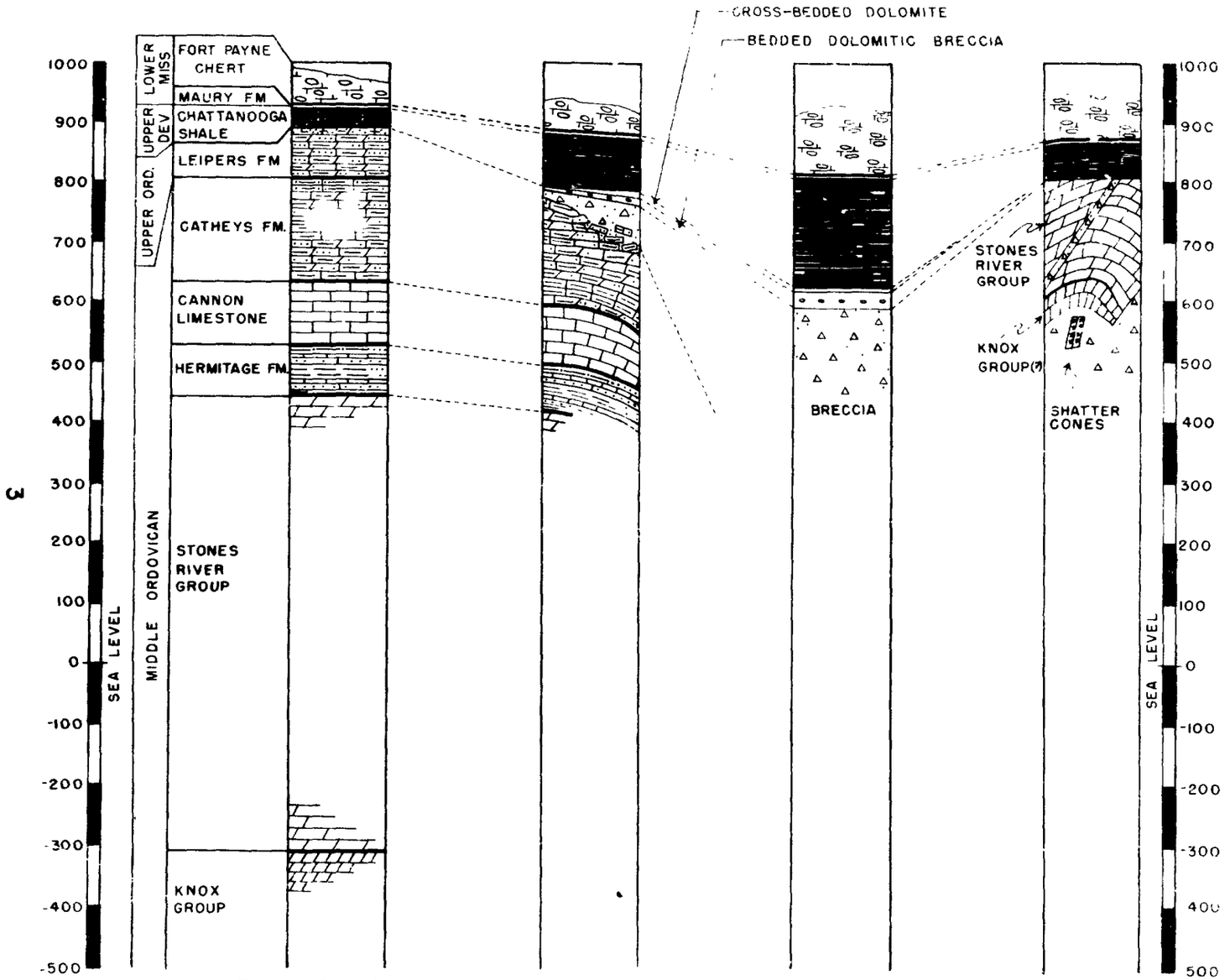

Figure 2.--Generalized columnar sections along the western half of the cross section of the Flynn Creek structure.

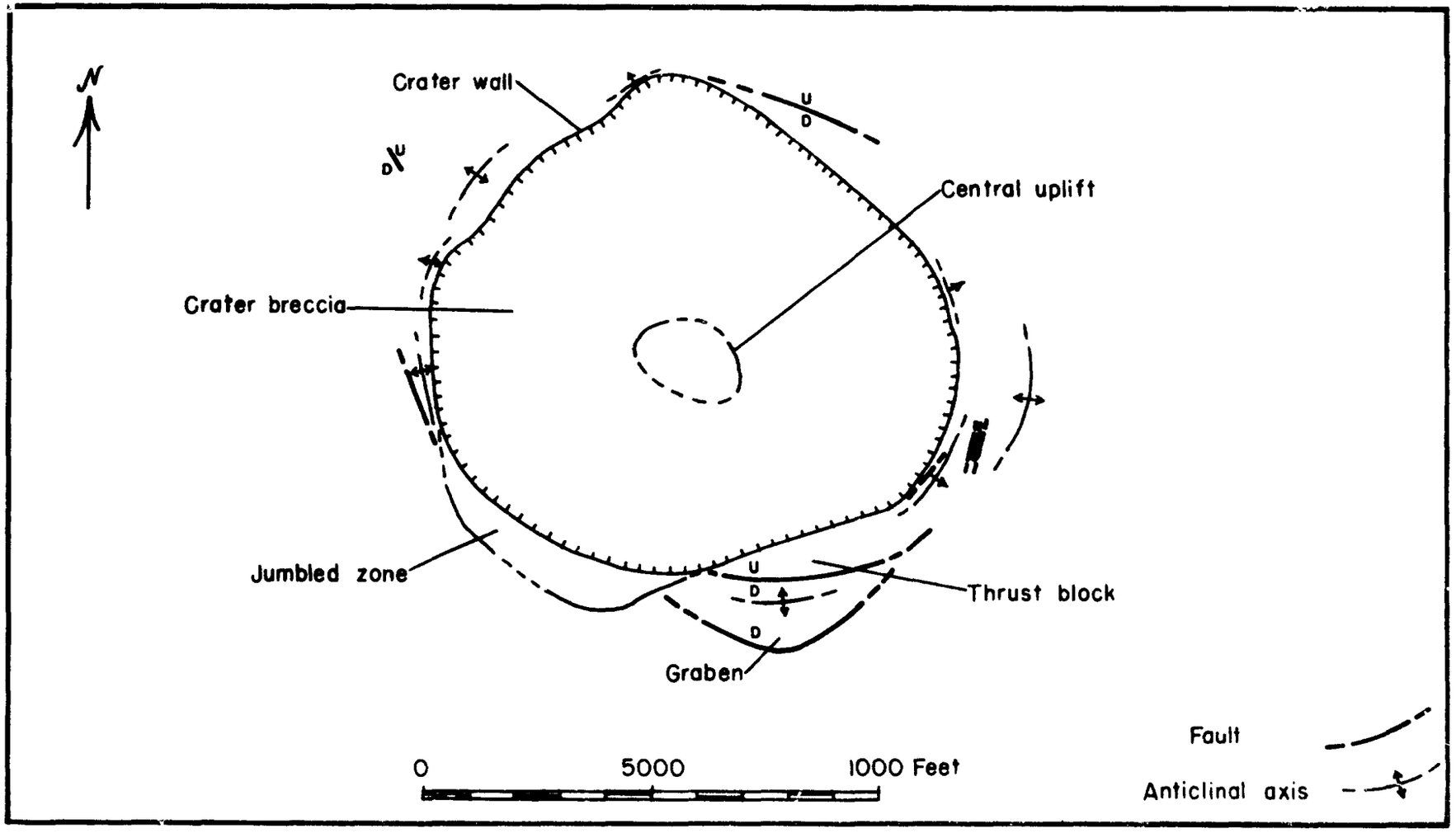

Figure 3.--Schematic map of major structural elements at the Flynn Creek crater, Tennessee.

that the normal regional attitude of the strata is undeformed and nearly flat lying. Until now no synthesis of this recent information with other available data has been made, and arguments for different origins have been left to speculation.

The purpose of this paper is to discuss the most likely mode of origin of the crater at Flynn Creek. The arguments are based on the author's recent geological and laboratory studies (Roddy, 1963, 1964a, 1964b, 1965, 1966) and on the published and unpublished studies of a number of other workers. A second aim is to present as complete a post-crater history as possible.

GEOLOGIC HISTORY OF THE FLYNN CREEK CRATER

The geologic history of the crater at Flynn Creek is important for two reasons: it aids in 1) determining the origin of the crater and in 2) establishing the time of formation. A thorough understanding of geologic history has been necessary to show that the crater has been only moderately eroded. This information has helped establish that the observed structural deformation at Flynn Creek is at or near the original level of the crater. Without this knowledge, structural comparisons could not be made between the Flynn Creek crater and other craters known to have formed at the ground surface, such as meteorite impact and maar craters. The time of formation of the crater is necessary for an understanding of the rates of erosion and of depositional filling. The age of the crater is also relevant to studies of the rate of terrestrial impact cratering.

The geologic environment of the Interior Lowlands during early Paleozoic time has been discussed at length by King (1959), Freeman (1953, 1959), Wilson (1949) and many others. It has been generally accepted that regionally extensive shallow seas periodically covered most of the Interior Lowlands during Cambrian and Ordovician time. Wilson (1962) has described conditions in central Tennessee as characterized by shallow seas with periodic uplifts

exposing the Nashville Dome to areal erosion. Wilson (1962, p. 504) stated that during Late Ordovician time the Nashville and Ozark swells were uplifted, and Leipers strata (Maysville time) were eroded from the higher parts of the Nashville dome. Immediately north of the Flynn Creek area only the upper 25 to 50 feet of Leipers strata was eroded from that area. This was probably also true in the Flynn Creek area, except that the level of erosion was slightly lower.

Near the end of Ordovician time the Richmond sea covered central Tennessee including the Nashville dome and the Flynn Creek area. The Sequatchie sediments were deposited as a calcareous ooze in silt-free water over a large part of the State (Wilson, 1949, p. 343). Several changes in depositional conditions occurred during late Richmond time, and limestones, shales, and silts were deposited as interbedded units north and west of the Flynn Creek area. At the end of the Ordovician and possibly at the beginning of Silurian time, central Tennessee was exposed to erosion, and unknown amounts of older strata were eroded from different areas. Erosion in the Flynn Creek area did not go below the Sequatchie strata.

During the Silurian Period, shallow seas advanced and withdrew several times, and a series of limestones, shales, and siltstones was deposited. Marine carbonates and shales of Silurian age are present in the extreme northern and northwestern part of the Nashville basin in central Tennessee (Wilson, 1949, p. 239-279). The Silurian strata are restricted to the western side of the present Nashville dome, a distance of nearly 30 miles from the Flynn Creek area. The nearest probable Silurian strata to the east are nearly 50 miles from the Flynn Creek area, as suggested by data from test wells (Born and Lockwood, 1945).

During Early and Middle Devonian time several incursions of shallow seas again occurred and were accompanied by periods of extensive erosion. Middle Devonian strata are absent on the

eastern side of the Nashville dome except for a small isolated deposit of Pegram Formation in west-central Jackson County about 12 miles northwest of the Flynn Creek area. Only a rubble of weathered Pegram sandstone blocks covering a few thousand square feet is present in this area; it represents the only remains of what was once probably a continuous shoreline deposit. The sandstone blocks lie directly upon Leipers strata in a way that suggests that they were let down from an earlier erosional surface. The nearest Pegram strata, lying in their normal stratigraphic position, occur along the western flanks of the Nashville dome, 30 miles from the Flynn Creek area. Lower and Middle Devonian strata have not been described in the subsurface from east of the Flynn Creek area to the Valley and Ridge province of east Tennessee.

It is not yet possible to say if Middle Devonian seas covered the Flynn Creek area. The distribution of the Pegram strata, according to Wilson (1949, p. 346), suggests that a Middle Devonian sea rose very high on the eastern flank of the Nashville dome. If this is true, then the Flynn Creek area was almost certainly covered.

A major interval of erosion followed the withdrawal of the Pegram sea, and the newly deposited sandstone and limestone were widely removed from much of central Tennessee. During Middle Devonian time the area immediately north of Flynn Creek was reduced to a rolling lowland with less than 100 feet of relief and with gentle slopes (Barnes, personal commun., 1964; Maher, personal commun., 1964). In some localities the Sequatchie rocks have been removed, and part of the top of the Leipers strata is also eroded away.

In the Flynn Creek area the Leipers strata were eroded 50 to 100 feet below the level of the highest Leipers horizons exposed 15 miles to the north. Most of the Sequatchie strata and the upper Leipers units of Platystrophia ponderosa limestone were probably eroded from the area. The down-faulted blocks on the southeastern

rim of the crater, however, preserve 75 to 150 feet of upper Leipers unit of Platystrophia ponderosa limestone and brecciated fragments of Sequatchie dolomite.

The crater probably formed within this interval in Middle Devonian time, possibly during a period of extensive regional erosion. The presence of Sequatchie fragments in the breccia clearly indicates a post-Richmond age for the crater. The apparent absence of any type of Silurian and Lower or Middle Devonian rocks in the bottom of the crater suggests that the crater is considerably younger than post-Richmond and more probably is Middle to post-Middle Devonian in age. If the crater had been present during this period of time, and if no Silurian or Devonian seas had covered the area, then almost certainly lake deposits would be present above the crater breccia. Instead, the first bedded deposits that are observed are marine breccias that were derived locally within the crater and are of early Late Devonian age.

Fragments from the upper Leipers unit of Platystrophia ponderosa limestone age are rare in the crater breccia, and Sequatchie fragments have not been found in the crater, yet both these rocks are present in the down-faulted block in the southern rim. The area was probably a rolling lowland with the low hills capped with Sequatchie rocks which were underlain by 75 to 150 feet of upper Leipers unit of Platystrophia ponderosa limestone. If a complete cover of these rocks had been present when the crater was formed, then more fragments should be present in the breccia of the crater, both from the initial deformation and from later erosion of the crater wall. The region could have been in a coastal-plain environment if the Middle Devonian sea was still in the immediate area.

The crater probably could not have existed for long before being destroyed by erosion and deposition. Instead, crater walls are still present as steep cliffs in parts of the crater, and the central uplift still remains with little obvious erosional destruction.

An age of late Middle Devonian to early Late Devonian seems most consistent with the available evidence.

The crater apparently formed during the impact of a comet or a meteorite, and a large amount of rock was ejected and fell as an ejecta blanket around the crater. A crude inversion of the strata occurred during the ejection and was later preserved on the southern rim. Presumably the central uplift and the intense folding and faulting in the rim occurred during the brief period of cratering. The large thrusts on the southeastern rim were probably formed during the impact, but other fault blocks, such as the down-faulted block on the southeastern rim, may have subsided for some time after the event. The southernmost fault zone was probably an open fracture at one period of time. Sequatchie breccia fills most of the fault zone and is present at the base of the overlying ejected breccia. The Sequatchie rocks, which were ejected and scattered at the base of the ejecta blanket, probably dropped into the opening fault zone as the block slowly subsided. The block probably continued to slump toward the crater until it formed a depression in the rim which preserved part of the ejecta blanket. (See Roddy, 1964b, p. 167.)

Erosion began to act immediately upon the ejecta and crater, and the entire ejecta blanket was eventually removed, except for that part preserved in the down-faulted block. Ejecta breccia over the block settled enough to allow a small talus deposit of upper Leipers Platystrophia ponderosa rocks to develop. Some of the ejecta and rim strata must have been eroded and deposited at the base of the crater walls and spread out over the crater floor. A very crude lineation in the long direction of some breccia fragments can be seen in a few of the breccia outcrops near the crater walls, suggesting that these breccias were washed or deposited over the crater slopes with a very crude bedding.

Slumping is evident along some of the crater walls where large megabreccia blocks are nearly at their original stratigraphic levels but are now tilted and separated a few hundred feet from the

rim strata. Subsidence probably occurred over all the crater floor as solution removed finer breccia fragments from lower levels.

Lake beds and alluvium may have formed on the crater floor, but they would now be covered by breccia washed in from the rim strata and ejecta blanket. Erosion proceeded to form small valleys and gulleys in the crater walls, but the rim was apparently never breached and opened to outside drainage. Erosional cliffs are present in parts of the crater walls. An internal drainage system developed in the crater, and much of the ejecta blanket that washed over the rim was carried to the low areas surrounding the flanks of the central uplift.

Apparently the Chattanooga sea had begun to cover the area by this time, or possibly it was present slightly earlier. If a high ejecta blanket surrounded the crater, it could have prevented a shallow sea from initially flooding the crater. However, owing to the unconsolidated nature of the ejecta, a surrounding body of water probably would have quickly removed it. On the other hand, much, if not all, of the breccia may have been removed by pre-Chattanooga erosion.

The first clearly bedded deposits in the crater appear to be poorly bedded breccias composed of reworked crater breccia. These poorly bedded breccias cover the crater floor and wedge out low on the crater walls. Apparently they were reworked and distributed over the crater floor and were then overlain by well-bedded breccia derived mainly from the highest horizons in the crater walls. A single massive bed of dolomite was then deposited on the well-bedded breccia throughout the crater.

The bedded breccias and dolomite were apparently deposited in a marine environment, because conodonts of early Late Devonian age are present in these rocks; they form the local, basal units of the Chattanooga Shale within the crater. No trace of ejecta or bedded breccia is present outside the crater.

During early Late Devonian time, sediments of the Chattanooga Shale filled the crater and prevented further erosion of the structure.

Nearly 300 feet of the lower unit of the black shale filled the crater to a level about equal with the surrounding rim surface. Younger units of the shale then covered the nearly level area over the crater.

Deposition appears to have been continuous into Early Mississippian time with the Maury and Fort Payne Formations. The shale in the crater continued to compact until it had decreased in thickness to about 200 feet, and a broad sag formed in all the filling sediments. Pennsylvanian sediments later covered the area but were removed during more recent erosion. Drainage patterns were established during Quaternary and Tertiary time, probably contemporaneously with a gentle uplift of the Nashville dome and surrounding region. The Cumberland River and its many tributaries, including Flynn Creek, continued their downward cutting to form a complicated drainage pattern of incised stream valleys. The heads of the many stream valleys are slowly eroding into the flat uplands of the Highland Rim to the east and northeast of the Flynn Creek area. To the west the streams empty into the Cumberland River where it flows across the rolling lowlands of the northern end of the Nashville basin. The once deeply buried crater at Flynn Creek is now exposed in the walls and floors of the many valleys that have more recently been incised into the older rocks.

ORIGIN OF THE FLYNN CREEK CRATER

The formation of the Flynn Creek crater and similar structures has been ascribed to cavern collapse (Lusk, 1927), salt-dome or anhydrite expansion (Wilson and Born, 1936), natural-gas blowout (Wilson and Born, 1936), tectonic folding (Kellberg, 1965), hydraulic fracture (Goguel, 1963), volcanic-gas explosion (Bucher, 1936, 1963; Amstutz, 1965; Currie, 1965; Snyder and Gerdemann, 1965), and meteorite impact (Wilson and Born, 1936; Boon and Albritton, 1937; Wilson, 1953; Dietz, 1960; and others). The last two mechanisms are the most widely accepted and are discussed in detail below. Reasons for rejection of the others are reported elsewhere (Roddy, 1966).

Bucher (1963, p. 642) included the Flynn Creek crater as a "cryptoexplosion" feature and suggested that the structure was not of impact origin. According to Shoemaker and Eggleton (1961), it is a "buried crater with the form and structure of a meteorite crater." The central point of the argument has resolved basically to comparison of the deformation at Flynn Creek with the structures observed in volcanic, impact, and other shock-produced craters. If good structural comparisons can be established with craters produced by one mechanism, and if comparisons with other types of craters are poor, at least a specific model will be available to test with further studies. Data relevant to the discussion of origin of the Flynn Creek crater have been discussed at length in earlier studies (Roddy, 1963, 1964a, 1964b, 1965, 1966) and are outlined below.

A. Geologic data (see figs. 2-5):

1. Regional:

   a. Strata of Middle and Late Ordovician age surrounding the crater are flat lying and undeformed except for very gentle anticlinal and synclinal folding which is typical of the region. Dips on the flanks of these folds rarely exceed 2°. Faulting has not been observed in the several hundred square miles surrounding the Flynn Creek area.

   b. Mineralized breccia zones along what appear to be poorly exposed faults are present in central Tennessee, but none are closer than 12 miles to the Flynn Creek structure. Mineralization includes calcite, barite, fluorite, galena, and sphalerite.

   c. The nearest deformed areas in Tennessee which are similar to the Flynn Creek structure are the Howell structure in the south-central part of the State, the Wells Creek structure in the northwestern part of the State, and the Dycus structure about 12 miles northwest of the Flynn Creek area.

2. Crater:

   a. A nearly circular crater with a diameter of about 11,500 feet was formed in the flat-lying limestones.

   b. The original topographic form was a crater with moderately to steeply dipping walls.

c. The average depth of crater measured from the top of the walls to the lowest point on the floor is about 330 feet. This is the depth after an unknown amount of breccia washed back over the earliest crater floor.

d. A chaotic, nonbedded breccia forms the floor of the crater and is composed of angular fragments ranging from a fraction of an inch to megabreccia blocks 300 feet in length. The megabreccia occurs along the outside of the crater. The breccia is composed of the same Middle and Upper Ordovician limestones that were present in the area where the crater was formed. The breccia is cemented by a fine-grained calcite to dolomitic calcite matrix.

3. Central uplift:

a. A sequence of steeply dipping folded faulted and brecciated limestone and dolomite of Middle-Early Ordovician age has been uplifted in the center of the crater. Before the crater was filled the central uplift represented a hill which rose about 300 feet above the crater floor and was nearly 2,500 feet in diameter at its base.

b. The oldest strata in the central uplift have been raised about 1,000 feet and contain the only shatter cones found.

c. Strata of the Knox Group of Early Ordovician age and of the Stones River Group of Middle Ordovician age are now recognized as forming the central uplift.

4. Crater rim:

a. The strata in the rim are commonly uplifted and tilted away from the crater. The width of the deformation band in the rim strata varies from a few hundred feet to nearly 3,000 feet.

b. Anticlines and synclines are common in the rim strata and become more pronounced near the crater. The trends of most of the axes of these folds are concentric with the crater wall, but some fold axes are radial to the crater. Tight folding in parts of the rim produces radial shortening as great as 35 percent. Tight folds in the northern and eastern rims grade upward in less than 100 feet into progressively more open folding.

c. A sharp anticlinal to monoclinal downfold is common in the rim strata adjacent to the crater wall. The width of this fold is commonly less than 100 feet.

d. A large fault zone is present in the southern and southeastern rim with dips up to 50° toward the crater. The upper part of the Hermitage Formation of Middle Ordovician age, unexposed elsewhere in the area, is present in the lower part of the thrust plate. Displacement along the fault zone is at least 500 feet.

e. The aforementioned fault zone forms the northern boundary of a tilted graben in the southern rim. The southern part of the graben is bounded by a brecciated zone dipping 30° to 50° toward the crater. Displacement along this fault zone is about 300 feet. Units of upper Leipers Platystrophia ponderosa strata that have been removed from the surrounding area are preserved in the graben.

f. The aforementioned fault zones die out as sharp anticlinal folds in the eastern rim strata and grade westward into jumbled strata of the southern rim.

g. Breccia of Sequatchie strata of Richmond age (Late Ordovician) is present in the fault zone south of the graben.

h. Breccia with a very crude inversion in the stratigraphy overlies the graben mentioned above (e) and its lithology is identical with that of the crater breccia, except for the presence of fragments of the upper Leipers Platystrophia ponderosa unit and possible Sequatchie strata.

i. Minor low-angle thrust faults are present in the eastern rim, and minor high-angle normal faults are present in the northern and southwestern rim. All faulting is roughly concentric with the crater and restricted to the more tightly folded parts of the rim.

j. The contact between the rim strata in the crater wall and the breccia in the crater is sharp and well defined in some areas and gradational elsewhere.

5. Crater-filling deposits:

a. A bedded breccia, locally poorly bedded, wedges out high on the crater walls and thickens to at least 50 feet near the center of the crater around the the flanks of the central uplift. Fragments in the breccia consist of the same rock types found

in the underlying crater breccia and in the crater walls. Fragments from the upper Leipers unit are abundant.

b. The aforementioned bedded breccia is overlain by a single bed of dolomite, locally crossbedded, that averages 3 feet in thickness and thins out high on the crater walls. The dolomite locally thickens to 25 feet in some parts of the crater floor.

c. The Chattanooga Shale lies unconformably on a relatively flat surface with low relief surrounding the crater. The lower unit of the shale thickens from about 10 feet to about 170 feet in the crater. The rest of the overlying units of the black shale are nearly constant in thickness in the crater.

d. Conodont studies indicate an early Late Devonian age for the bedded breccia, the bedded dolomite, and the basal Chattanooga Shale.

e. Strata of Mississippian age cover the area and sag gently over the crater.

6. Exposures:

The area is now highly dissected by Flynn Creek and its tributaries. Good exposures of the rim structure, crater walls, and central uplift are now present on the valley walls. The original crater floor is exposed on the floors and lower walls of some of the present deeper valleys.

B. Geophysical data:

1. Gravity:

A detailed gravity study indicates that no gravity anomaly on the level of 1 milligal is associated with the Flynn Creek crater (Roddy, 1966).

2. Magnetics:

A detailed magnetic study indicates that no large magnetic anomalies are associated with the structure. Several small magnetic lows within the crater appear to be associated with manmade disturbances and probably are not related to the structure (Roddy, 1966).

C. Laboratory data:

1. Petrography:

a. No meteoritic or volcanic materials were found in the breccia fragments or in the breccia matrix. No chemical or mineral alterations involving high

temperatures or metasomatic-hydrothermal processes were recognized.

b. Fracturing and microfracturing are common in an irregular zone several tens to hundreds of feet wide in the rim strata adjacent to the crater wall.

c. Twinning and abundant to intense microtwinning are present in calcite in the aforementioned zone. The most intense twinning and microtwinning is irregularly distributed, even on the scale of inches, but is generally confined to the rocks immediately adjacent to the crater wall. Some of the fragments in the crater breccia also contain highly twinned and microtwinned calcite.

d. Studies of well cuttings from three wells immediately south and southwest of the crater show no mineralization or deformation in the rocks down to a depth of 1,150 feet, the deepest level of the wells.

2. Geochemical search for volcanic or meteoritic meterial:

a. Trace-element abundances appear to be relatively constant within individual horizons outside the crater.

b. Trace-element abundances of rocks in the breccia are nearly identical with the values found for the parent rocks in the rim.

c. The trace-element abundances in the breccia matrix are very nearly identical with the levels in the rim strata, and no anomalous values were found in rocks inside or outside the crater.

3. Search for high-pressure polymorphs:

An X-ray search for aragonite, coesite, and stishovite in the more intensely deformed breccia fragments was not successful.

4. Thermoluminescence:

Thermoluminescence studies indicate the possibility of a modification of the 270°C emission peak in the deformed rim strata, but the current results are inconclusive (Roddy, 1966).

Although a large amount of other field and laboratory data have been previously described (Roddy, 1963, 1964a, b, 1965), the preceding summary lists the information most pertinent to discussion of the origin of the Flynn Creek crater.

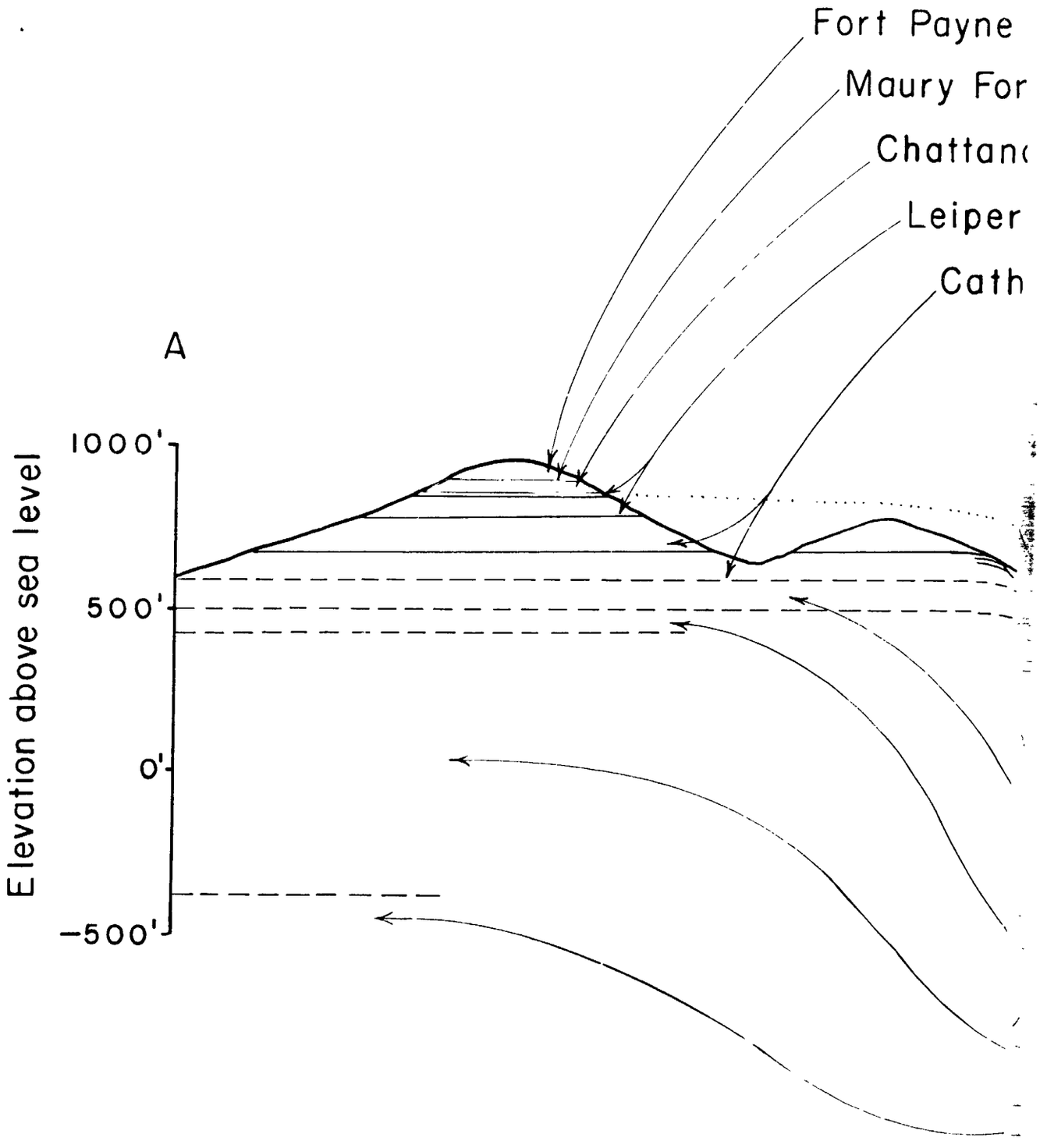
Fort Payne
Maury For
Chattan
Leiper
Cath
A
1000'
500'
0'
-500'
Elevation above sea level

Chert

mation

ɔoga Shale

s Formation

eys Formation

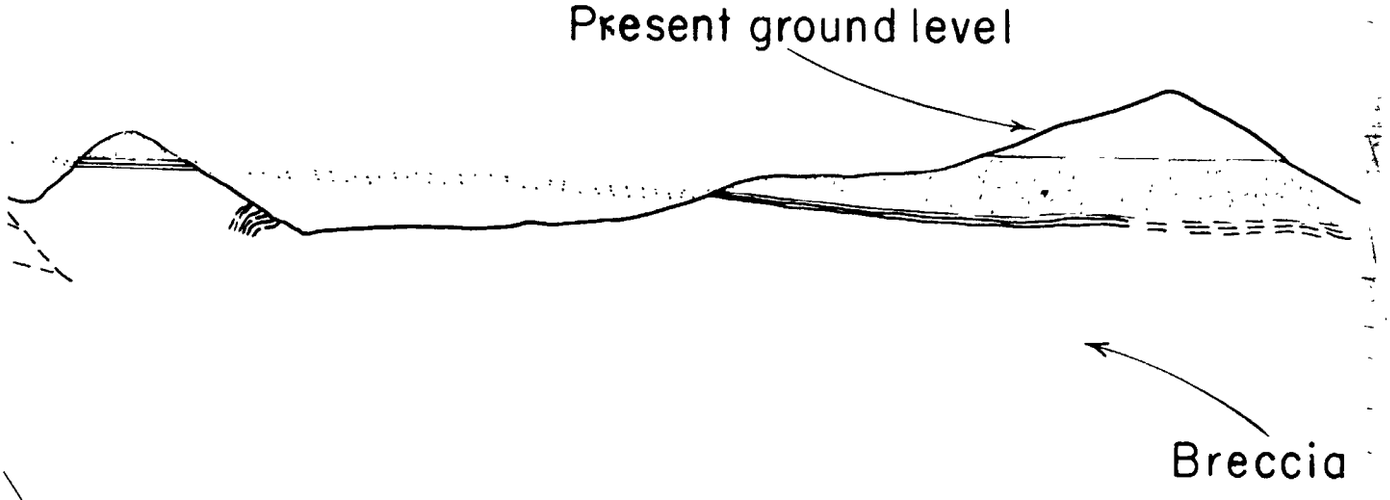

Cannon Limestone

Hermitage Formation

Stones River Group

Knox Group

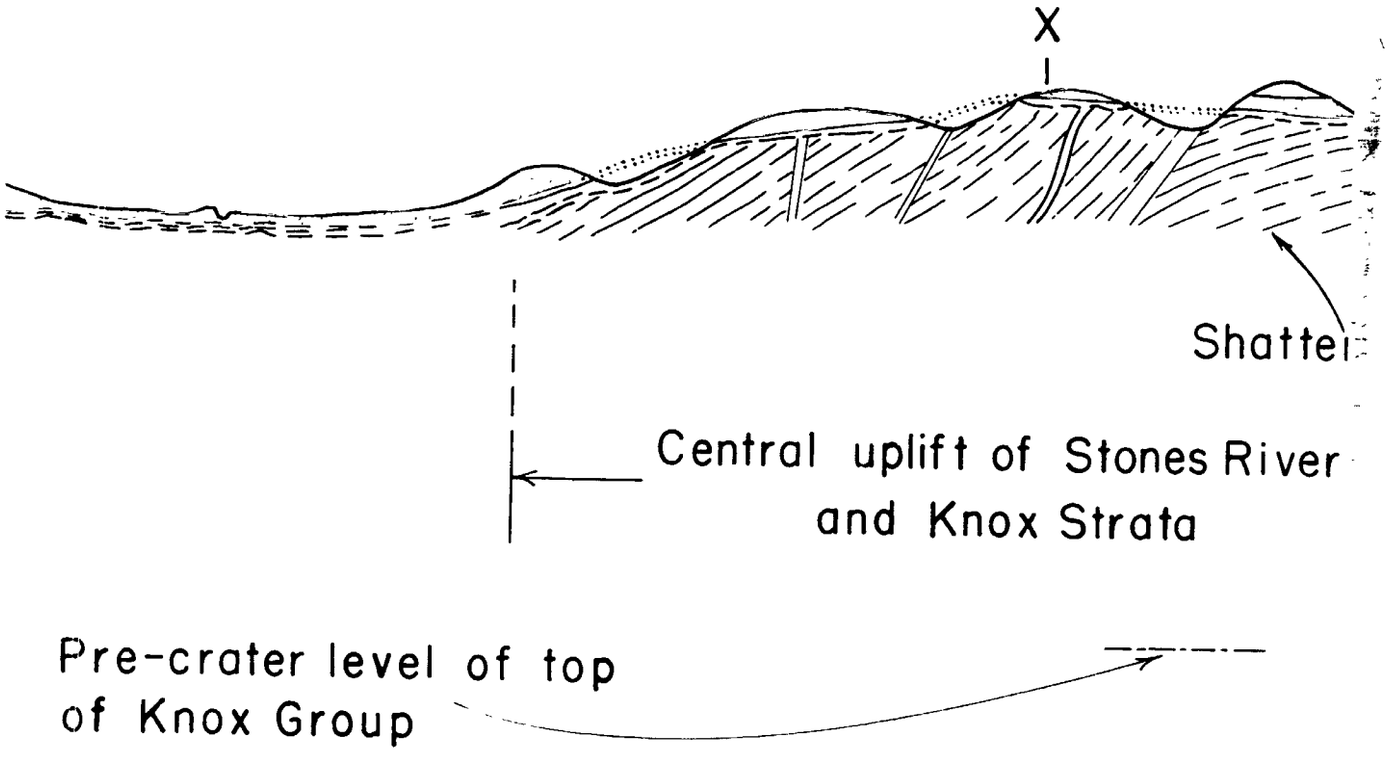

Figure 4.--Cross section A-A' of

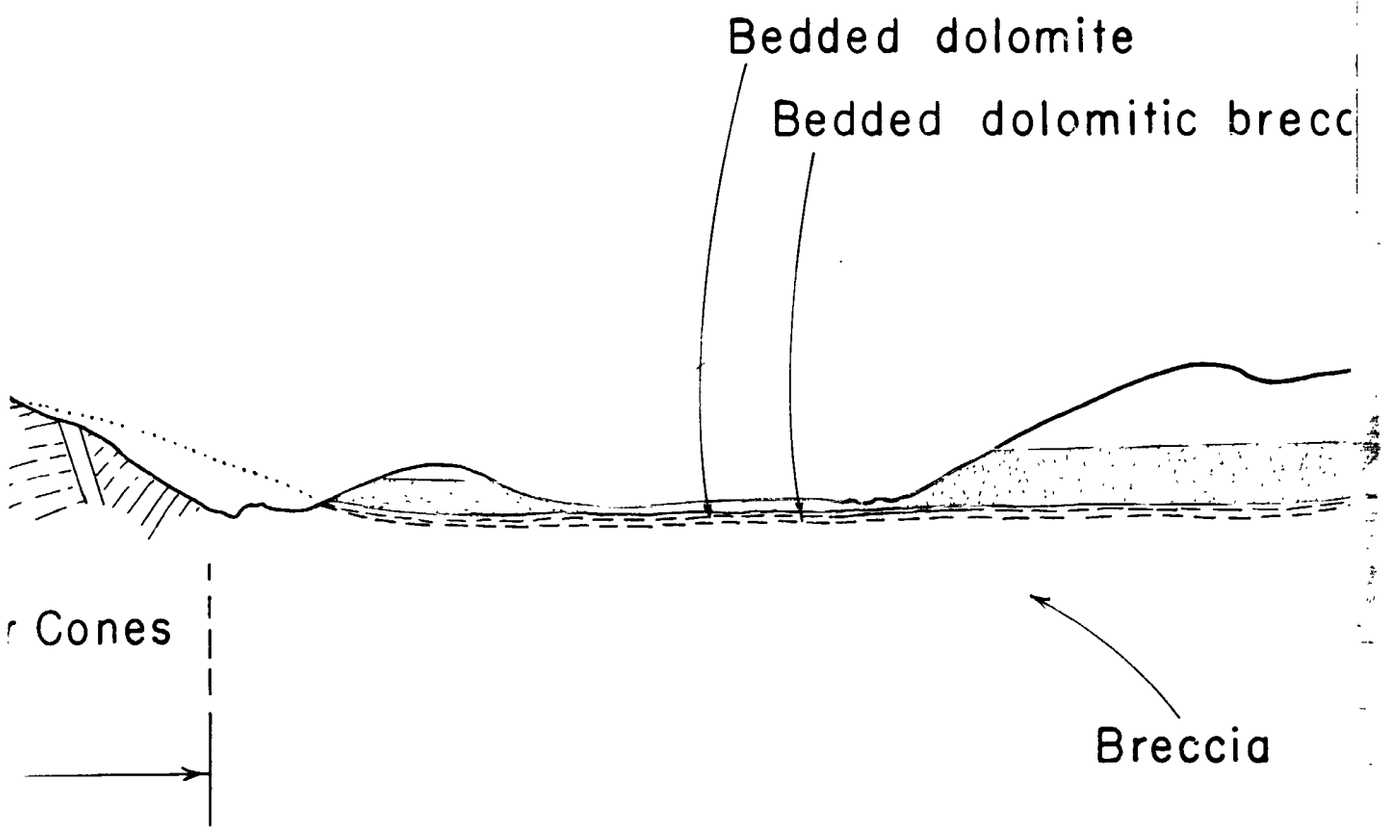

cale 1:6000

cale 1:6000

the Flynn Creek crater, Tennessee

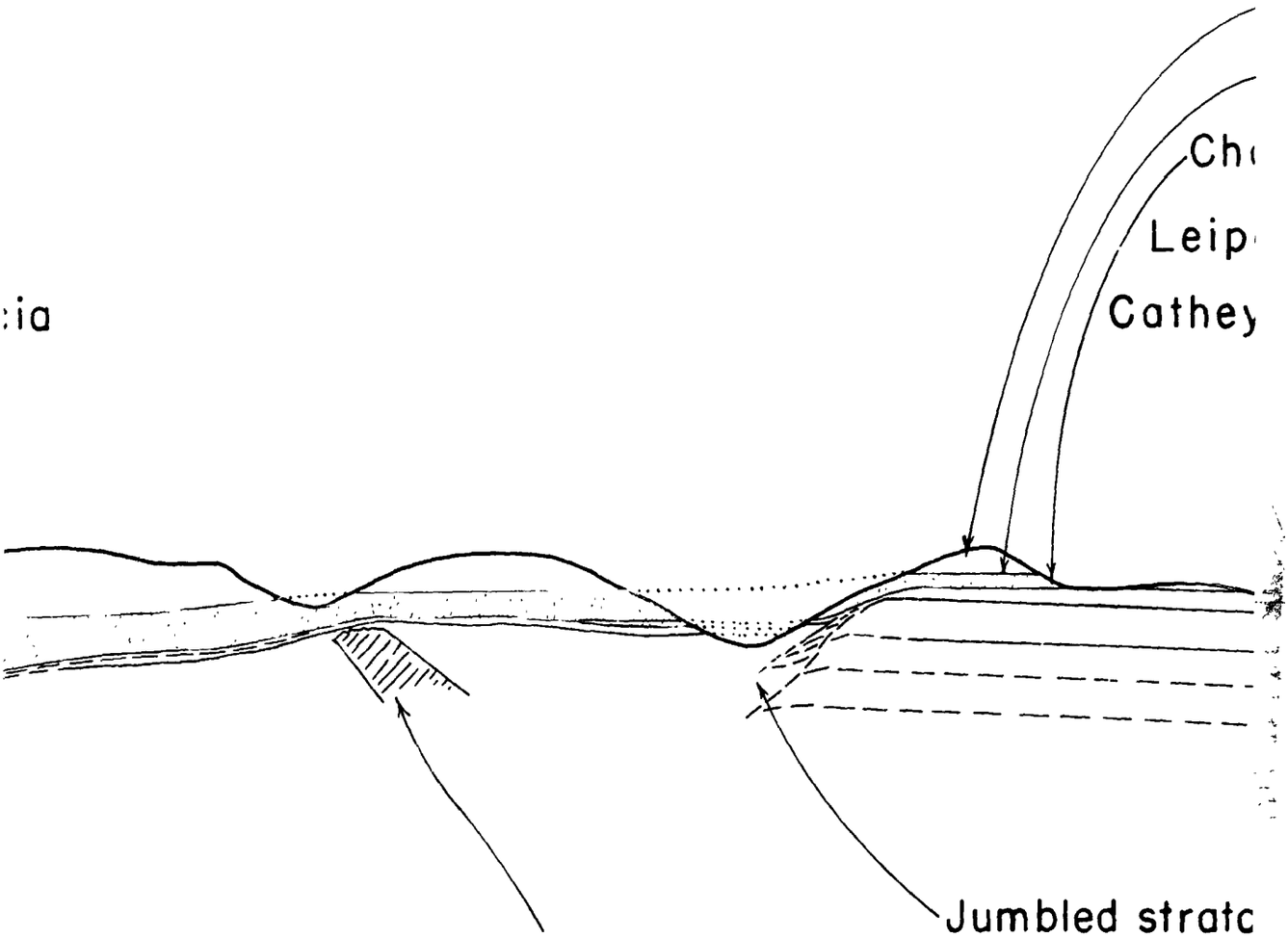

Exposed contact

Approximate position of contact

Inferred position of contact

—Fort Payne Chert

·Maury Formation

ɹttanooga Shale

ers Formation

ɹs Formation

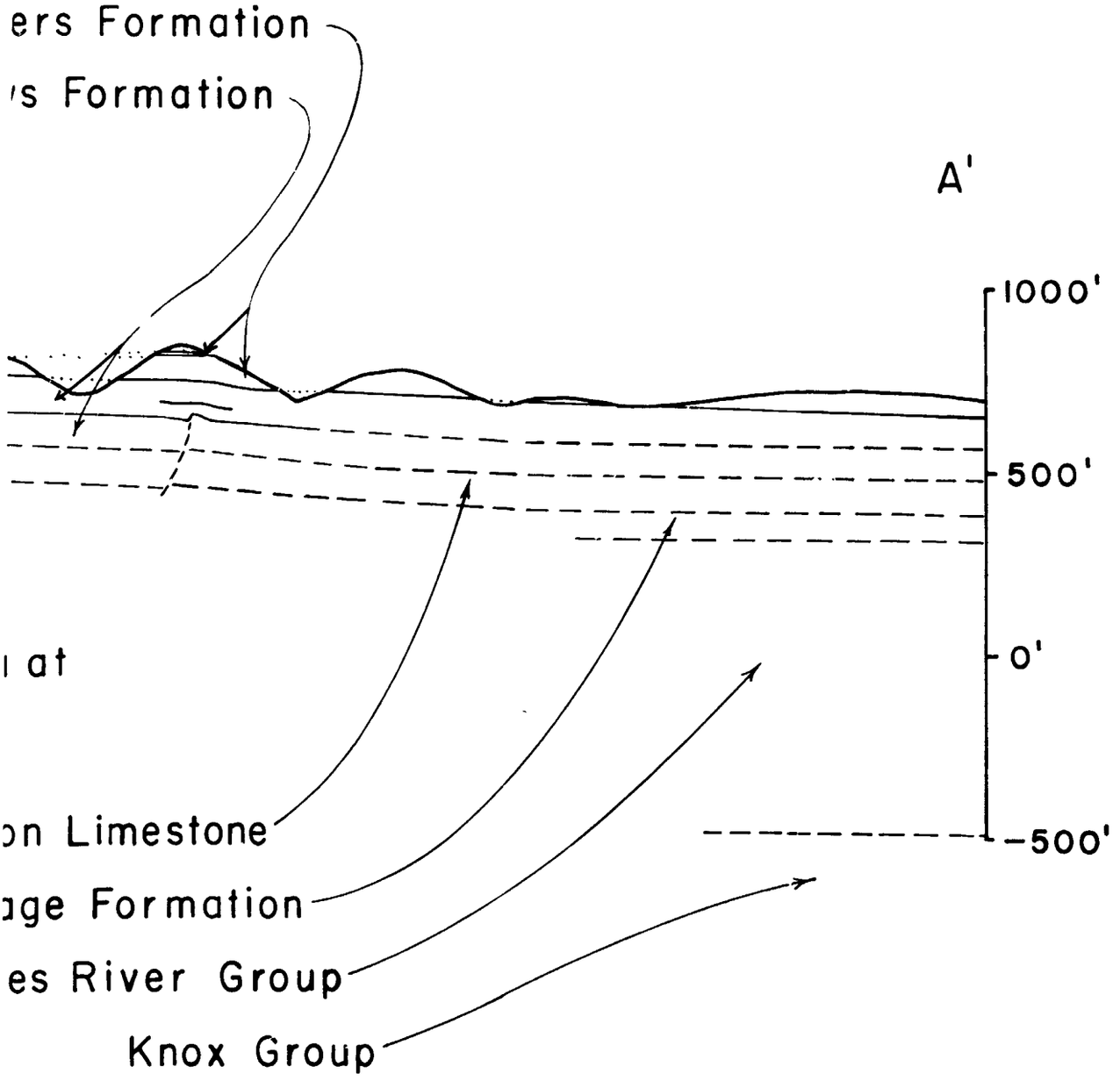

ı at

ɔn Limestone

ɹge Formation

es River Group

Knox Group

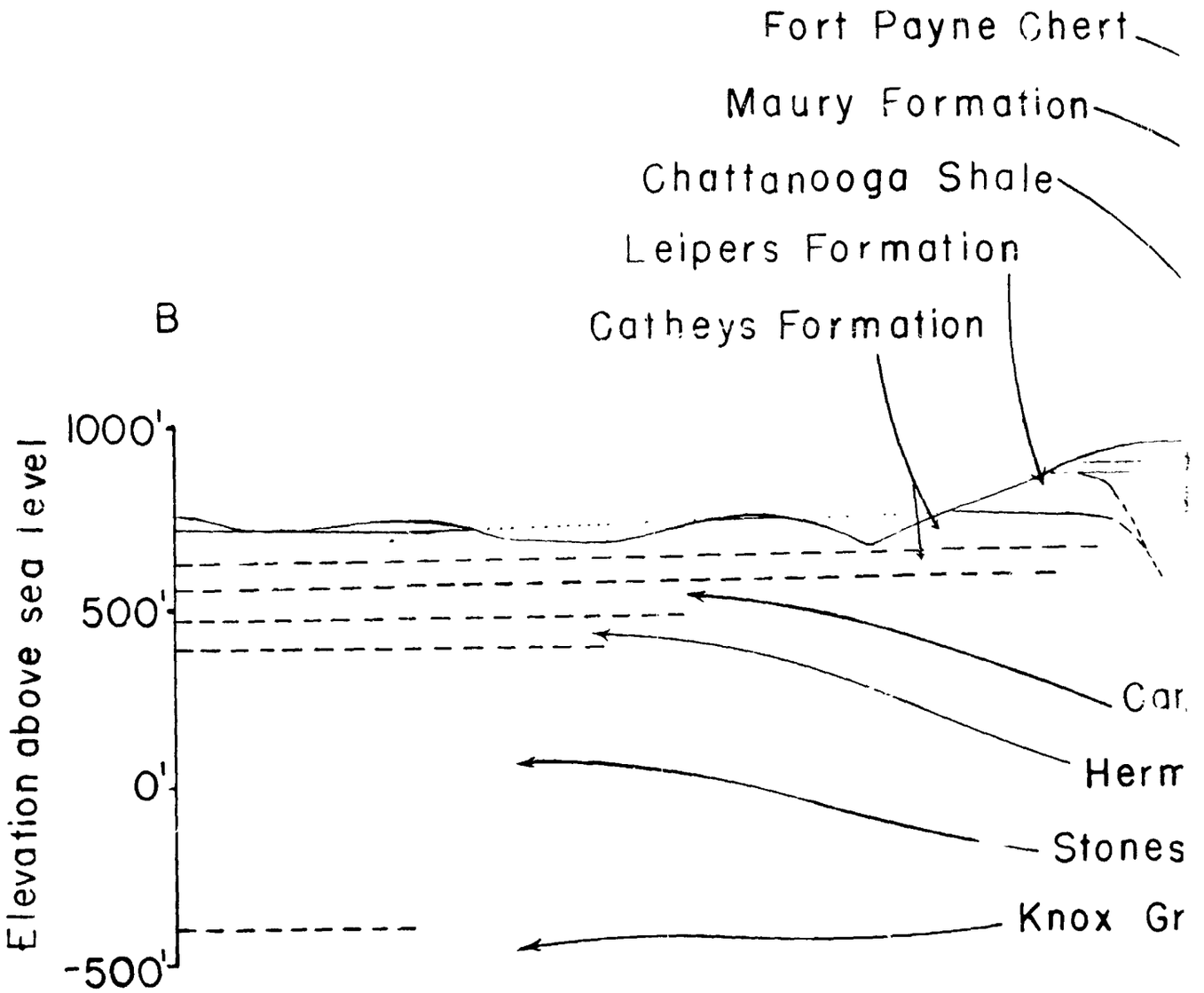
Fort Payne Chert
Maury Formation
Chattanooga Shale
Leipers Formation
Catheys Formation
B
1000'
500'
0'
-500'
Elevation above sea level
Car
Herm
Stones
Knox Gr

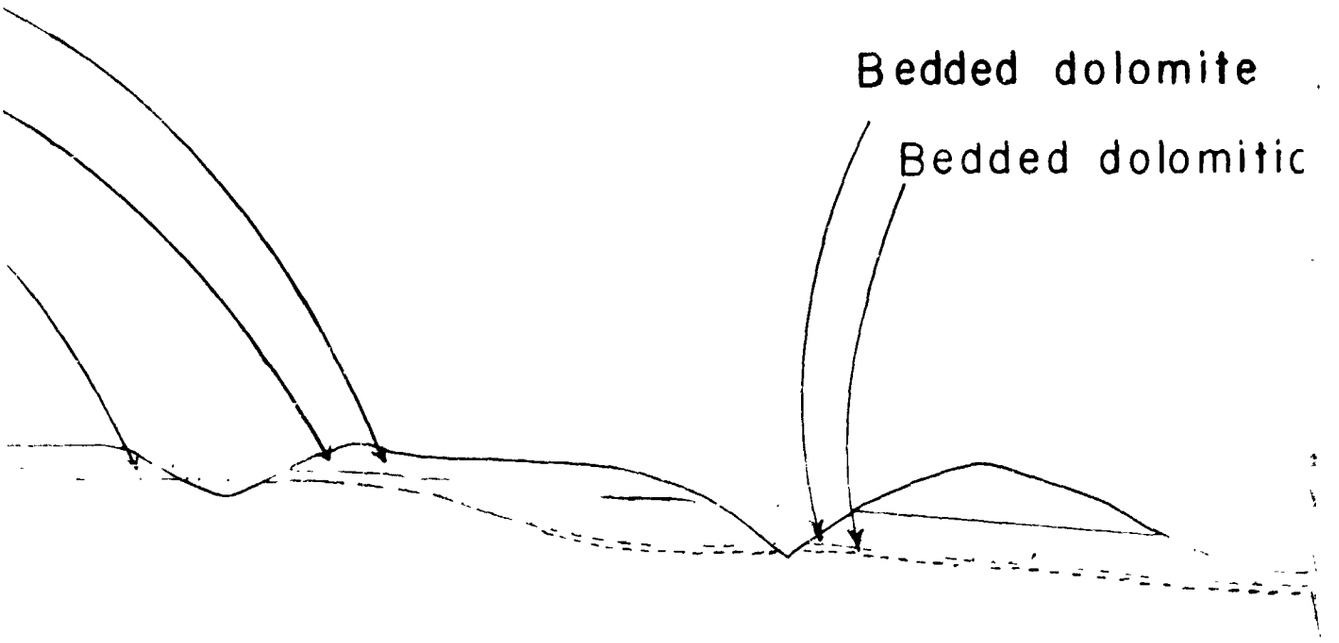

ınon Limestone

ıitage Formation

River Group

oup

breccia

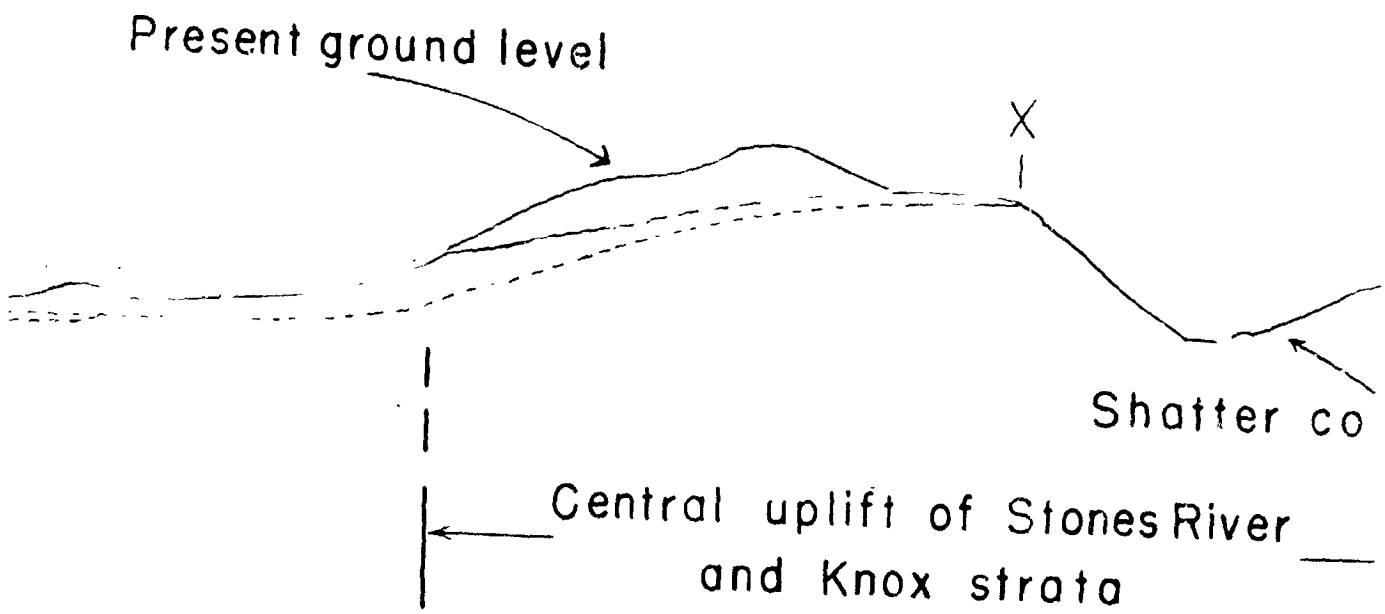

Figure 5.--Cross section B-B' of the Flyi

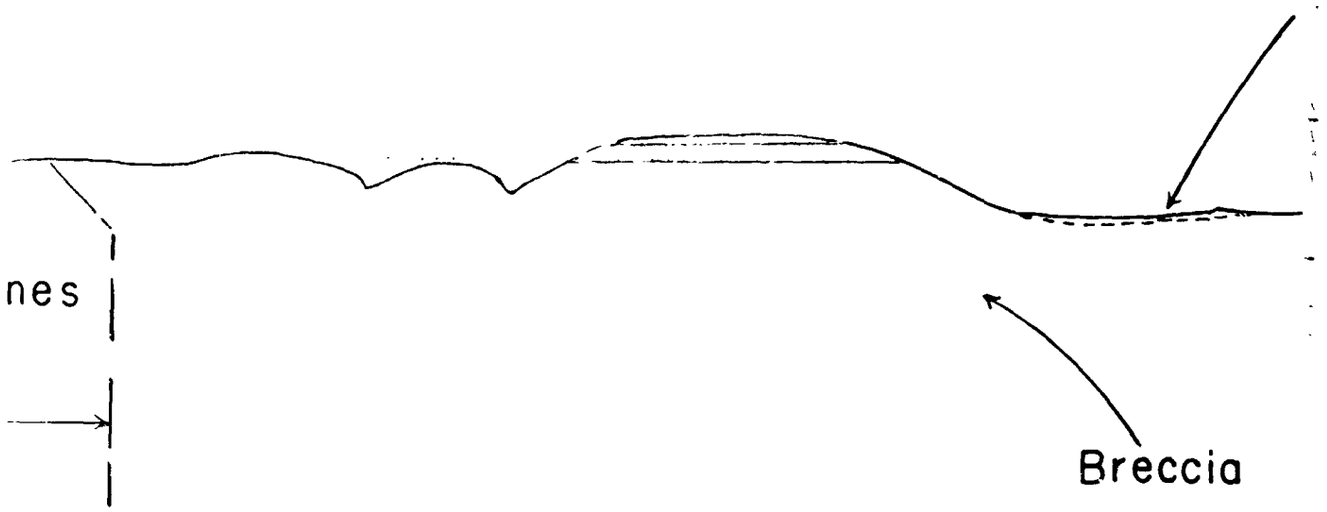

1500 2000 2500 feet

ale 1:6000

ale 1:6000

— E

--- A

---- Ir

n Creek crater, Tennesse.

For

Maur

Chattano

Leipers F

Catheys Fo

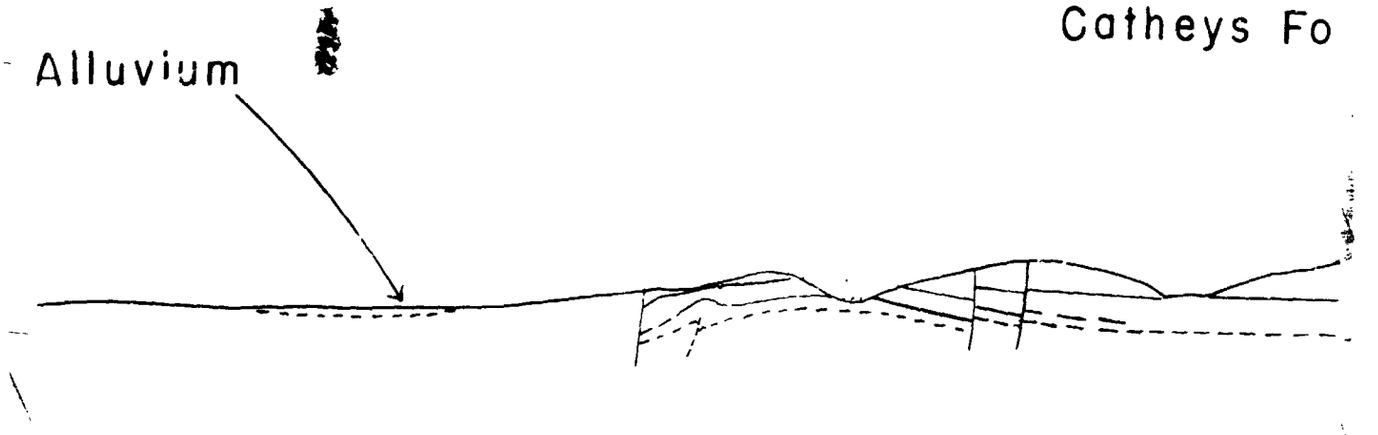

Cannon L

Hermitage

Stones I

xposed contact

pproximate position of contact

nferred position of contact

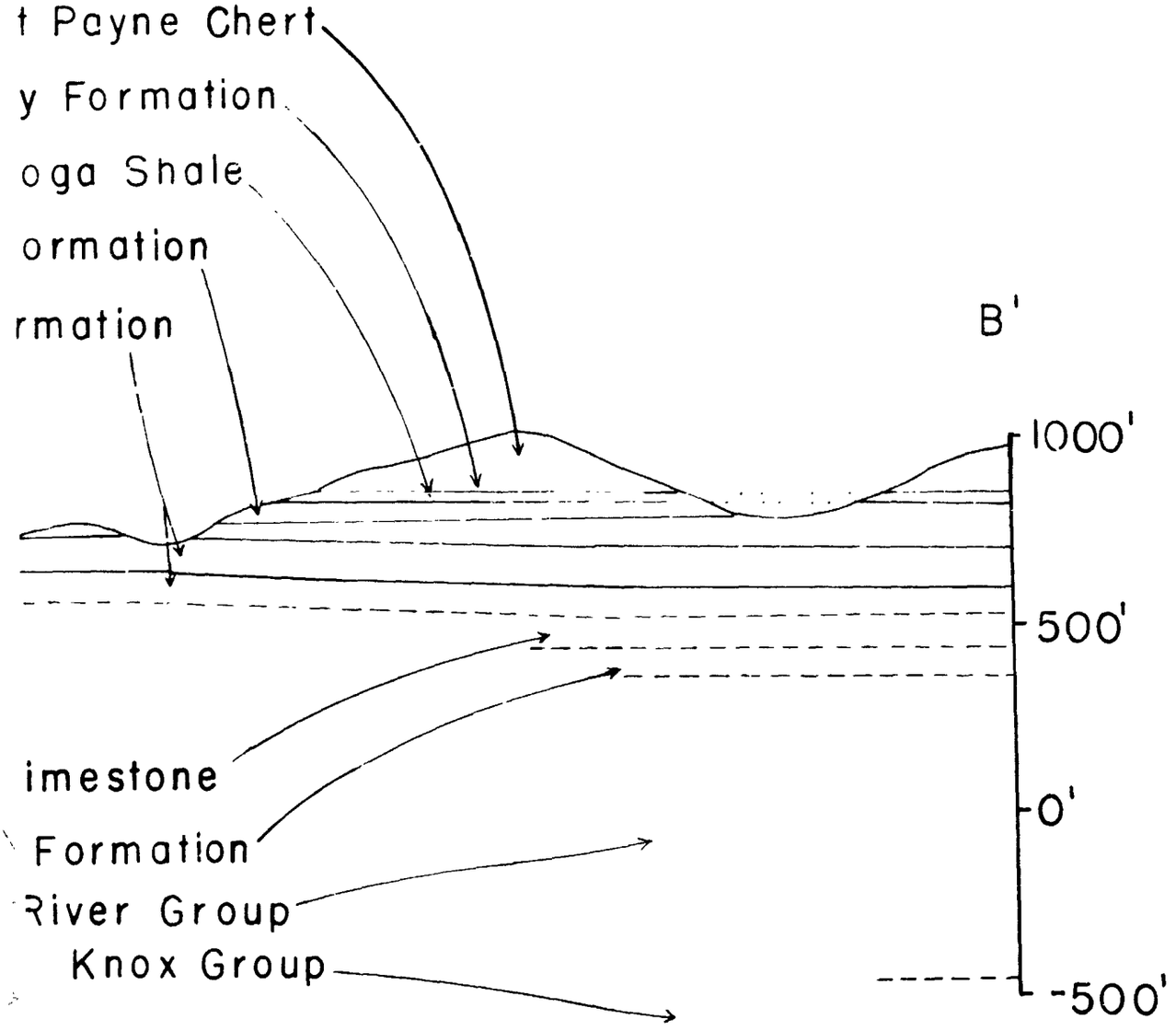
t Payne Chert
y Formation
oga Shale
ormation
rmation
B'
1000'
500'
0'
-500'
imestone
Formation
River Group
Knox Group

"Cryptovolcanic" Explosion Hypothesis

The "cryptovolcanic" or volcanic gas explosion hypothesis has been most strongly advocated by Bucher (1936, 1963). In his discussion of the problem, he noted that "cryptovolcanic" structures have several distinctive features: a circular outline, a central uplift surrounded by a ring-shaped depression, concentric marginal folds, rock deformation which indicates an "explosive force", and no signs of volcanic material or "thermal action" (Bucher, 1936, p. 1074). However, his concept of the deforming process was less definitive, and he referred to it simply as a "subterranean blast." In a later report (1963, p. 642), he speculated that enormous pressures from a rapidly crystallizing water-rich magma penetrated the overlying strata, "crushing and partly pulverizing the rock in gouging out irregularly shaped pathways to the surface * * *." He stated that the "explosive action" might exhaust itself at depth, or end in a unsuccessful attempt to eject the rock and thereby produce a "cryptoexplosion" structure. This general description of the proposed "crypto"-mechanism has been widely accepted as an explanation for "cryptoexplosion" structures in other parts of the world. Amstutz (1965), Currie (1965), and Snyder and Gerdemann (1965) have restated Bucher's general hypothesis without significant addition.

More recently, Bucher (1963, p. 600) agreed that certain features of the "cryptoexplosion" structures could also be accounted for by meteorite impact and listed the following: "The highly disordered structure of the central uplift consisting of rocks carried above their original positions (and the limitation of the shatter cones to these central uplifts). The corresponding downward displacement of a ring-shaped belt of rock concentric with the central uplift. In some cases, the development of a seemingly wave-like up-and-down movement in one or two rings surrounding the first rim syncline. The relatively shallow depth to which these cryptoexplosion structures seem to

extend, judging from the few drill holes the results of which have become available." Bucher then stated that if meteorite impact had produced the cryptoexplosion structures they must be-- "(1) Randomly distributed, e.g., not demonstrably related to structures of purely terrestrial origin; (2) Independent of magmatic activity in the region; (3) Structurally of a nature that is comprehensible in terms of instantaneous impact and its immediate consequences."

Mainly on the basis of points 1 and 2, Bucher (1963) presented reasonable arguments for the nonmeteoritic "cryptovolcanic" origin of the Ries structure in Germany, the Vredefort dome in South Africa, and the Wells Creek structure in Tennessee. The main argument offered for each structure was that it lay on or within some general volcanic or tectonic lineament or zone; however, the structures were not proved to be genetically related to the regional volcanic or tectonic activity.

A good argument for the association of a structure with widespread volcanism and tectonic activity was presented by Hager (1949, 1953) for Meteor Crater in Arizona. Meteor Crater directly overlies a large monoclinal fold, and the extensive field of explosive volcanic vents of the Hopi Buttes is less than 50 miles to the north (Shoemaker, 1960). Yet there is no doubt that Meteor Crater is actually an impact crater (Shoemaker, 1960).

One of the serious problems in applying Bucher's points 1 and 2 as the test for an origin is that it is difficult to locate any place in the Interior Lowlands that does not have some regional tectonic or volcanic feature nearby. On the other hand, impact craters would be expected to be random in their location and could just as easily be located on or near a regional tectonic or volcanic feature. The writer fully agrees with Bucher that the first step in examining the "cryptoexplosion" structure is to establish its position in the regional tectonic and volcanic framework. The writer disagrees that this approach alone will establish an individual origin.

Bucher (1963, p. 600) listed a third point which he did not pursue at length, but it in effect stated that the structure of each feature must be consistent with the proposed origin. This important step has not been followed until now, mainly because there was very little structural data available for the "cryptoexplosion" features. Structural comparisons and relationships are outlined in the following sections in order to examine the possible origin of the Flynn Creek crater.

Relationship of the Flynn Creek crater to regional structure and volcanism

The Flynn Creek area is on the eastern flank of the Nashville dome. The crest of the dome in this area trends northeast and is about 30 miles west of the crater at Flynn Creek. The regional attitude of the strata surrounding the crater is nearly flat lying, with a gentle dip towards the east. Many small folds are present throughout the region. Local dips on the flanks of these rarely exceed 5°. Broad flat-plunging anticlines and synclines that cover many square miles are also present. The Flynn Creek area appears to be situated on one of the broad eastward-plunging anticlines. The dips on the limbs of these folds and their plunges are only about 1° to 2°.

Faults are uncommon in central Tennessee and in the Flynn Creek area. The breccia in the existing fault zones is locally mineralized with various combinations of calcite, barite, fluorite, galena, and sphalerite. The nearest mineralized zone is a small limestone breccia with fluorite, about 15 miles south of the Flynn Creek crater.

No volcanic rocks are exposed in central Tennessee. The nearest extrusive igneous rock is a small dike of mica peridotite in the Valley and Ridge province in east Tennessee.

Present knowledge of the regional geologic setting indicates that no volcanic zones or tectonic lineaments appear to be genetically related to the Flynn Creek crater.

Comparison of the Flynn Creek crater with maars and diatremes

The most likely volcanic structures to compare with the Flynn Creek crater are those produced by violent gas eruptions, such as maars and diatremes. The term "maar" is the German word applied to the volcanic craters occupied by lakes in the Eifel region of Germany. The term has been used more generally for any volcanic crater of moderate size (less than about 5 km) that was produced by a violent gas eruption. The term "diatreme" refers to the pipe or vent exposed below a maar after the crater has been eroded away. Although the exact mechanisms which produce these structures are subject to debate, there is general agreement that they are the result of volcanic gas pressures, with or without associated violent surface eruptions. This type of mechanism is apparently what Bucher (1963, p. 642) had in mind, except that in "crypto-explosion" structures the eruption fails to continue after the initial gas breakthrough to the surface. Heated ground water accompanied by a phreatic "explosion" is also considered a possible part of some maar-forming processes (McBirney, 1959).

A discussion of maar and diatreme structures is given elsewhere (Roddy, 1966). In this earlier discussion volcanic structures comparable in size to the Flynn Creek crater have been stressed, and the descriptions are limited to volcanic structures which have penetrated sedimentary strata. The comparison of the structural deformation at these volcanic craters with the Flynn Creek crater is outlined below, and the detailed discussion is given in the earlier paper (Roddy, 1966).

1. The Flynn Creek crater is roughly circular with a partly polygonal outline. Maars and diatremes of similar size may be circular or elliptical, but few exhibit a well-defined polygonal outline.
2. Both maars and the Flynn Creek structure are craters formed in a preexisting terrain, with moderate to steep crater walls.

3. Maars and diatremes usually exist in groups. The Flynn Creek structure is an isolated crater.
4. Maar craters have an ash and agglomerate ejecta blanket on the rim. The Flynn Creek structure presumably had an ejecta blanket of sedimentary rock thrown out of the crater. A crude inversion of the ejecta stratigraphy is preserved in the fault block. Volcanic material is common in the breccia and rim ejecta of maars. No volcanic material is observed at the Flynn Creek crater.
5. The Flynn Creek crater has a large central hill or central uplift of older strata, with some units raised nearly 1,000 feet and containing shatter cones. Small volcanic cones occupy the craters of a few maars, but large blocks such as the central uplift at the Flynn Creek structure are unknown. Shatter cones have not been found in maar or diatreme breccias.
6. The breccias in the crater of the Flynn Creek structure were formed from the same rocks that are exposed in the surrounding sedimentary section. Some breccia blocks are severely deformed. Fractures, folds, and twinning are evidence of intense deformation. The agglomerates in maars and diatremes, particularly in those the size of the Flynn Creek structure, consist of a variable assemblage of volcanic tuff and breccia and occasional irregular intrusive and extrusive igneous dikes. The breccias of maars and diatremes generally contain igneous and occasionally metamorphic rocks from deeper horizons. If these structures penetrate sedimentary columns, abundant breccia from the sedimentary rocks is also common in the agglomerate. Deformation in these sedimentary blocks consists of moderate brecciation, fracturing, and occasional folding and induration.
7. Slumping within the crater and concentric normal faulting are features of both maars and the Flynn Creek structure. Thrust faulting, a feature of the Flynn Creek structure, is not found in maars.

8. Where structural deformation is present in the rims of maars and diatremes, it is commonly restricted to a narrow band a few feet wide. Some diatremes have a steep inward dip adjacent to the vent wall, but the fold is rarely wider than 30 feet and averages 5 feet. Most maars and diatremes have sharp boundaries with the surrounding strata and lack folds. A narrow fracture or breccia zone is also present in some of the vent walls. The size of the structure does not appear to affect the width of the inward-dipping fold or fracture zone. The same zone that is fractured is commonly somewhat indurated and may be mineralized.

In contrast with the maar and diatreme rims, the rim of the Flynn Creek structure is uplifted and generally tilted away from the crater, with many doubly plunging asymmetric anticlines and synclines. Most axes of folds in the rim are concentric with the crater wall, but the axes of some are radial to the crater wall. Tight folding in parts of the rim produces radial shortening as great as 35 percent. Tight folds in the northern and eastern rim are overlain by progressively more open folding. A sharp anticlinal to monoclinal downbend is common in the rim adjacent to the rim-breccia contact. A large thrust fault and a rotated fault block which forms a tilted graben are present in the southern rim. Much of the crater wall consists of deformed rocks--fractured and folded limestones containing an irregular zone of intensely twinned calcites. Microfractures are common in much of the folded rim strata near the crater wall. Elsewhere along the rim, the contact is jumbled and gradational. Mineralization related to hydrothermal or volcanic processes has not been recognized in the Flynn Creek area.

From the preceding outline it is clear that few structural comparisons can be drawn between the Flynn Creek structure and the structure of maars and diatremes. Also, it seems unlikely that a crater as large as the Flynn Creek structure with its extensive brecciation would not contain even a trace of volcanic material or

mineralization if it were of volcanic origin and related to maar-diatreme type activity. This is particularly true since fault breccias within 12 miles of the Flynn Creek area are highly mineralized with materials which probably had their source in hydrothermal solutions.

The point must be made that the lack of comparison between structural deformation at Flynn Creek and at maars and diatremes does not uniquely rule out some unusual type of volcanic gas origin (with or without ground--water steam) whose mechanism of eruption is foreign to current understanding.

In the earlier papers of Branca and Frass (1905), Bucher (1936), Wilson and Born (1936) and others, the meaning or physical concept of a "buried volcanic explosion" and how it could occur were never made clear. According to Bucher (1963, p. 042) it resulted from very high gas pressures derived from rapidly crystallizing water-rich magmas. He also equated "fluidization" and comminution of the rock with an "explosion." More recently, Snyder and Gerdemann (1965) also described high volcanic gas pressures and resultant fracturing and structural disordering as the conditions under which "cryptoexplosion" structures form. They suggested that where the sedimentary cover is thin, as at the Crooked Creek structure in Missouri, gas pressure domes the rocks until an "explosion" occurs and the strata collapse as a breccia into the crater.

It would seem unlikely that the process suggested by Snyder and Gerdemann would produce the particular types of folding observed in the rim strata and parts of the breccia at the Flynn Creek crater. This can be examined in at least a semiquanitative way by considering the minimum mechanical energy necessary to form the crater and relating this energy to gas pressures that might accompany the process. The gas pressures and their relationship to the folding in the rim strata can then be discussed.

If a cylindrical shape is assumed for the Flynn Creek structure at depth with a diameter equal to 11,500 feet and a depth of 1,500 feet (depth to lowest brecciated horizon known), a volume can be

calculated of 4.55 $\times$ 10^{15} cc. Assuming a density of 2.7 g per cc, the mass will equal 1.23 $\times$ 10^{16} g. A conservative estimate of the mass raised in the central uplift, plus the estimated mass of all blocks in the breccia raised above their normal stratigraphic position, plus the mass of the thrust fault in the southern rim is about 0.6 $\times$ 10^{16} g with an average increase in elevation of 100 m. The work necessary to raise this mass is approximately 6 $\times$ 10^{22} ergs This is a minimum estimate of work done in lifting material, because the rim ejecta is neglected.

The energy needed to fracture the total mass of rock can be estimated using comminution surface energy from the extensive work of Bergstom. The fracture energy is about 1.6 $\times$ $10^{23\pm1}$ ergs. The uncertainty is primarily because a mean fragment size must be assumed for the breccia to use Bergstrom's values. A volume of 15 cc was assumed for the mean size of the breccia fragments on the basis of estimates made from surface observations of the breccia.

The energy needed to eject the mass which occupied the crater must also be estimated. With a diameter of 11,500 feet and a depth of 330 feet, the volume equals 9.6 $\times$ 10^{14} cc, and the mass (assuming density equals 2.7 g per cc) equals 2.6 $\times$ 10^{15} g. The work necessary to lift this mass to the level of the original rim is about 2.6 $\times$ 10^{22} ergs. If one assumes a value of 30 m per sec for the acceleration of the ejected material, the total work involved will be about 7.8 $\times$ $10^{23 \pm 1}$ ergs. This value does not include the energy necessary to overcome the friction between breccia fragments during movement.

To estimate the minimum volume of gas (volcanic gas or steam from ground water) that would provide energies on the order of 10^{23} ergs if allowed to expand adiabatically, assume a 10 percent porosity in the limestone. If the limestone has a total volume of 4.55 $\times$ 10^{15} cc, the volume of pore space is about 0.5 $\times$ 10^{15} cc. If the gas is steam at 250°C and Goguel's (1953, p. 30) value of about

2.5×10^9 erg per cc is used as the rate of adiabatic expansion, the gas will have about 1.25×10^{24} ergs for expansion work. A pressure computed for gas under these P-T-V conditions is on the order of 1,000 to 2,000 bars, which is at least 100 times the pressure necessary to produce tension fracturing in limestone. Considering the uncertainties in such calculations, it still seems clear that even modest amounts of volcanic gas or steam (from ground water heated by a volcanic source) have sufficient energy to move the masses under consideration at Flynn Creek when one compares the 10^{24} ergs available for work versus the 10^{22-23} ergs of work necessary to be done. It is also important to note that this s at a pressure high enough to easily produce tensile . acturing.

The relationship of these gas pressures to the folding in the rim strata of the Flynn Creek crate . be discussed only qualitatively. Mechanical properties of rocks are affected by confining pressure, temperature, interstitial solutions, time, and previous physical history. Fortunately, several of these factors can be reasonably approximated for the Flynn Creek rocks before the deformation.

Field studies have shown that the original ground surface is present in the tilted graben on the southeastern rim. Thickness measurements made from this surface down to older horizons indicate that less than 150 feet of strata, and more probably less than 50 feet, was removed after the crater formed. Using this field information, lithostatic or confining pressures have been calculated for different levels known to be brecciated (table 1). Later in this section these confining pressures are related to laboratory investigations on rock deformation and comparisons made between brittle and plastic failure of limestone.

No thermal metamorphic effects have been noted either in the field or in petrographic studies. There are no signs of even the lowest temperature carbonate metamorphic reactions, so temperatures were probably below 200°C. The low porosity of the rocks in the

Flynn Creek area suggests that interstitial solutions probably were well below 10 percent by volume.

Table 1.--Predeformation lithostatic pressures calculated for selected stratigraphic horizons

[The original ground surface described in this paper as Sequatchie Formation (Upper Ordovician) is used as the 0 pressure surface. The lowest level of known brecciation is in the top of the Knox Group, at a depth of about 457 m]

Formation	Maximum original depth from ground surface to base of formation		Pressure (bars) at densities (g per cc) of--		
	Feet	Meters	2.50	2.70	3.00
Leipers	300	91	22.9	24.7	27.5
Catheys	475	145	36.3	39.2	43.5
Cannon	574	175	43.8	47.3	52.5
Hermitage	675	206	51.5	55.6	61.8
Stones River Group	1,476	450	112.5	121.5	135.0
Lowest known depth of brecciation	1,500	475	114.2	123.4	137.1
Knox Group-basement	6,000	1,829	457.3	493.8	548.7

The time factor and previous physical history would probably be of minor importance if deformation had been rapid. This is true for all the origins that have been offered for the crater. It is recognized that the varying roles these factors play in rock deformation allow, at the present time, only a qualitative application to natural systems, but some comments can be made concerning the nature of the deforming process and the low near-surface confining pressures that existed before the formation of the Flynn Creek structure.

Lithostatic pressures existing just before the deformation in the Flynn Creek area probably did not exceed about 150 bars at the lowest known depth of brecciation (top of the Knox Group) (table 1). At the present level of the exposed folded, tilted, and faulted rim strata, the predeformation lithostatic pressure probably did not

exceed about 50 bars (table 1). Laboratory investigations (Robertson, 1955; Handin and Hager, 1957) on the deformation of limestones and dolomites have shown that both rock types exhibit varying degrees of ductile behavior under the confining pressures calculated for the Flynn Creek structure. For a number of limestones tested, the range in ductility varied from about 2 percent to nearly 10 percent strain before rupture at confining pressures of 150 bars (Handin and Hager, 1957). Rupture occurred at about 1,000 to 1,500 bars compression under these conditions. Studies on the effects of temperature and confining pressure have shown that certain limestones will not deform more than 5 percent before rupture under 2,800 bars compression at 75°C and 500 bars confining pressure.

In general, previous work has shown that the brittle-ductile transition in limestones at room temperatures occurs at an effective confining pressure of about 1,000 bars (Robertson, 1955; Handin and Hager, 1957). Under the low confining pressures calculated for the Flynn Creek area, it is reasonable to expect the limestones to behave as nearly brittle material, or more appropriately as semi-ductile material (Robertson, 1955) under differential compression or extension pressures of a few thousand bars. When tensile stresses are considered, failure commonly occurs at values 50 to 100 times lower than for compressional stresses. Also if compressional stresses of 1,000 to 5,000 bars are applied rapidly, limestone invariably fails by brittle fracture.

Without other complicating factors it seems logical not to expect large-scale folding to occur from compression effects alone, whereas fracturing and small amounts of plastic flow should be common. Nevertheless, large-scale folds, in which the major stress component was apparently horizontal, are present in much of the rim strata of the Flynn Creek crater. Intense fracturing and minor plastic deformation are also present.

If a gas is introduced under high pressure near the surface, one might expect that under low confining pressures (as in the Flynn

Creek area) the rocks would exhibit a small amount of flow followed by extensive fracturing. This of course does not explain the major folding that occured in various parts of the rim. If the laboratory investigations of rock deformation can be extrapolated to the Flynn Creek structure in the manner described, one would expect fracturing to occur before large plastic folding is completed under the condition of low confining pressure. Arcuate faulting and subsidence at depth conceivably could explain some of the folding, but they cannot account for other rim folds that definitely appear to have had the major stress component in the horizontal direction. Consequently, the simple build up of gas pressure near the surface, as proposed by Snyder and Gerdemann (1965) and Bucher (1963), would not appear to explain this part of the structure at Flynn Creek.

Meteorite Impact Hypothesis

The crater at Flynn Creek was first proposed as a possible meteorite impact structure by Wilson and Born (1936), but they rejected the idea because of the raised strata in the central uplift. Boon and Albritton (1937) suggested that the argument of Wilson and Born overlooked the fact "that elasticity of rocks would cause a strong rebound following intense compression produced by impact and explosion." During a study of the deformation at the Wells Creek structure, Wilson (1953) revised his opinion on the origin of the Flynn Creek crater and referred to it as a possible impact crater. Dietz (1960) reported shatter cones from the central uplift at Flynn Creek and thereby argued for an impact origin.

No attempt was made in the earlier work to compare the crater at Flynn Creek with either impact or volcanic craters, partly because detailed structural studies had not yet been undertaken. Shoemaker (1960, 1962) described in detail the structural similarities between different impact craters and nuclear explosion craters, and developed a model for the penetration mechanics of a meteorite based on observation of nuclear cratering and the resulting structural

deformation. One of the important contributions of Shoemaker's study was that it demonstrated that plastic folding is a normal consequence of impact. His study also showed that the type of deformation in the rim strata is dependent on the depth of penetration of the meteorite. One of the long-standing objections of many workers to an impact origin had been the failure to recognize the wide variety of different types of structural deformation which result from impact. For example, Kellberg (1965) proposed a tectonic hypothesis for "cryptoexplosion" structures mainly because he was unaware of plastic folding at impact craters.

Shoemaker (1960) drew his structural comparisons between Meteor Crater, Ariz., and nuclear craters because of the obvious similarities in deformation. The comparison was strengthened because it was known that shock effects played a dominant role in the formation of both impact and nuclear craters. The study at the Flynn Creek crater has now provided sufficient information to see close structural similarities with several of the different "shock-produced" craters, such as meteorite craters, nuclear craters, and chemical-explosion craters. Deformation in the rim strata, ejecta, and crater breccia is similar in these craters to that seen at the Flynn Creek crater. One of the chemical explosion craters has a pronounced central uplift, and the rim strata have been deformed in much the same was as at the Flynn Creek crater.

Although direct evidence of shock cannot yet be demonstrated in the Flynn Creek rocks, excellent structural comparisons can be made between the types of deformation at Flynn Creek and those seen in impact, nuclear, and chemical-explosion craters. Structures of comparable size are chosen, where possible, for comparison to lessen complications that may occur in scaling.

Comparison of the Flynn Creek crater with meteorite impact craters

A number of features of the Flynn Creek crater are also present at Meteor Crater. Both structures formed in flat-lying sedimentary

rocks, and both are craters. Meteor Crater is bowl shaped, but the Flynn Creek crater has a flat floor because of depositional fill. An ejecta blanket is present on the rim of Meteor Crater and at one time was present at Flynn Creek. In both ejecta blankets the stratigraphy is crudely inverted.

The strata in the rims of both craters are raised and dip away from the crater walls. Strata exposed in the crater walls at Meteor Crater dip steeply away and in one place are overturned. At Flynn Creek the strata in parts of the crater walls dip steeply away from the crater; in other parts it is more common to have an anticline concentric to the crater wall with the limb on the crater side dipping steeply towards the crater.

Small thrust faults are present at both craters and appear to be approximately parallel with the regional joint systems. Normal faults are present at both craters and are approximately concentric with the crater walls, with authigenic breccia zones present along some of the faults at both craters. The upper plates of thrust faults at Meteor Crater moved toward the crater, whereas at Flynn Creek they moved away from the crater The upper plate of one smaller thrust, comparable in size to those at Meteor Crater, moved toward the crater.

Rocks in the crater walls at both craters are intensely fractured to brecciated. At Flynn Creek a jumbled zone is developed in some parts of the crater walls. In both craters, strata in the rim a few tens of feet from the crater wall commonly exhibit little deformation. Irregular zones of authigenic breccia are locally present in the rims of both craters.

The floors of Meteor Crater and Flynn Creek crater are underlain by a chaotic breccia of fragments derived from the local strata. The largest blocks are near the crater walls.

The structures at Flynn Creek and at Odessa, Tex., are both craters formed in flat-lying limestones. Rim strata have been uplifted and locally folded in rim anticlines adjacent to the crater walls of

both structures. The limbs of the rim anticlines dip toward the craters. The upper plates of most thrust faults moved away from the crater. The upper plates of one small thrust fault at Flynn Creek and one at Odessa moved toward the crater. Jumbled strata are present in the crater wall in one of the smaller craters at Odessa; they are common at Flynn Creek.

The Henbury Craters are in dipping siltstones and shales, whereas the Flynn Creek crater is in flat-lying limestones. Varying amounts of material have washed into both craters. Deformation in parts of the walls of both craters is characterized by jumbled strata with no sharp break between the crater breccia and rim strata.

Strata in the rims of both craters have been folded into synclines, anticlines, and monoclines, locally cut by low- to high-angle thrust faults. The upper plate is commonly thrust away at both Flynn Creek and Henbury. Deformation decreases rapidly away from the crater walls.

Comparisons of Flynn Creek crater with nuclear explosion craters

The crater at Flynn Creek and each of the nuclear explosion craters are in flat-lying strata. Strata in the rims of all nuclear craters are uplifted and dip away from the crater. The rim strata at Flynn Creek are also raised and commonly dip away from the crater.

Thrust faults are present in several of the nuclear craters, and the upper plate has commonly moved away from the crater as at Flynn Creek. According to Shoemaker (personal commun., 1966), other details of rim deformation and brecciation at the nuclear craters compare with deformation at the Flynn Creek crater.

Locally an anticline is concentric and adjacent to the crater wall at Flynn Creek, and the limb on the crater side dips steeply toward the crater. A similar fold is present in the rim of the Jangle U nuclear crater and is identical with the fold in the rim of the largest Odessa crater. A shallow depth of burial of the nuclear device at Jangle U crater produced a crater most like that

at Flynn Creek. A deeper burial of the nuclear device at Jackpot Ess Crater produced a crater most like Meteor Crater.

Comparison of Flynn Creek crater with chemical explosion crater

The Flynn Creek crater and the 500 ton TNT crater are both flat bottomed, formed in flat-lying strata, and have a pronounced central uplift. In the rims of both, uplifted strata and [illegible] anticlines are present, the latter adjacement to crater walls. The anticlines are identical with those at the larger Odessa crater and the Jangle U nuclear crater. A thrust fault cuts the top of the fold as at the Odessa crater. An ejecta blanket is present.

Tension fractures formed in the rim strata at the 500 ton crater, and the blocks subsided very slightly. A similar structural feature is present at Flynn Creek in the southern rim, except that the block dropped considerably.

Deformation in other parts of the rim strata of the 500 ton crater is intense but limited to a zone very close to the crater walls. Jumbling is also common in a few places in the rim. Both of these features are present at the Flynn Creek crater.

The central uplifts at both craters are structurally very similar. Faulting and brecciation are more common in the central uplift at Flynn Creek, whereas folding is more common in the central uplift of the 500 ton crater.

CONCLUSIONS

The crater at Flynn Creek exhibits nearly all the types of structural deformation found at Meteor Crater, the Odessa craters, and the Henbury craters. Comparisons with four nuclear explosion craters indicate that structurally the Flynn Creek crater is nearly identical with the Jangle U nuclear crater and has pronounced similarities with parts of the other nuclear craters. Structural deformation in the 500 ton TNT explosion crater is nearly identical with that in the Flynn Creek crater. These structural comparisons

are the basis of the conclusion that the crater at Flynn Creek was also produced by a shock mechanism, in this case an impact.

Other approaches to the problem of the origin of the Flynn Creek crater have been less definitive, but none contradict the concept of an impact.

The petrographic studies of the zone of intense twinning also indicate a very high pressure environment during the formation of the crater. Insofar as is known, this type of deformation has not been shown for maars or diatremes.

High-pressure phases, such as coesite and stishovite, are absent at Flynn Creek, as one would expect in such a low silica environment. The maximum amount of detrital quartz in the limestones does not exceed 1 percent. Thus far the high-pressure phases have been found only in rocks which are entirely silicates. Detrital quartz grains would probably be little affected in a matrix which deforms as easily as calcite. However, the exposed horizons at the Flynn Creek structure are not the ideal place to find the most intensely deformed material produced by an impact. Most of the breccias exposed on the crater floor are reworked and washed into the crater and would cover any fallout layer if one were present. The fallout layer, according to Shoemaker (1960), contains the most highly shocked material in an impact crater.

The data from trace-element studies did not indicate the presence of volcanic or meteoritic materials. It is not likely that volcanic materials are absent because of erosion; they have remained in other sites for similar lengths of time. If a nickel-iron meteorite or even a stoney meteorite had caused the crater, it is possible that the impact so highly fragmented the body that it was easily weathered and removed by solution. Certainly the amount of meteoritic material in the largest Odessa crater is small and not easily found. This is even true for the surface at Meteor Crater, Ariz. Until drilling has been done at the Flynn Creek structure, this question will not be answered.

The shallow depth of the Flynn Creek crater, the presence of a central uplift, and the anticlinal folding in the rim suggest that if an impact occurred, it probably was a "shallow impact" (i.e., the center of energy was near the surface). This is consistent with the 500 ton TNT surface explosion and the Jangle U nuclear crater. Such conditions could possibly be met by a comet impact in which the comet would not act as a dense body and would not penetrate as deeply as an iron meteorite. This would explain the absence of meteoritic iron or stony iron materials, if comets are "frozen gases" as postulated. Shoemaker has suggested that comets may actually be carbonaceous chondrites, which, of course, would not leave any trace after even a short period of erosion following impact.

Shatter cones have not been found in any proven impact craters, although they have been produced under laboratory hypervelocity-impact conditions (Shoemaker and others, 1963). Johnson and Talbot published (1964) a short theoretical treatment which suggests that a very high stress environment is necessary, but they did not specify a possible natural origin.

Both gravity and magnetic surveys did not find a buried igneous source for the speculated volcanic gases. Either an igneous plug is not present, or the density and magnetic susceptibility of the intrusive body are very close to those of the surrounding sedimentary rocks.

Field studies have shown that the level of the original land surface supports the idea that confining pressures were very low. Comparison of the low pressures necessary to fracture limestones under these confining pressures indicates that a high pressure cannot account for the plastic folding. Large meteorite impacts, on the other hand, can generate pressures that are adequate to cause the rim folding as well as brecciation.

Simple scaling laws from nuclear explosion craters and the 500 ton TNT explosion crater suggest that between 10^{24} and 10^{25} ergs

was necessary to form the Flynn Creek crater. Comminution energy calculations also give 10^{24} ergs as the work done in fracturing the volume of rock in the crater. For illustrative purposes, if a comet of density 3.33 g per cc produced the Flynn Creek structure, the size of the body can be calculated using an average impact velocity of 18 miles per second. The diameter of the mass would be approximately 280 feet.

The writer's suggestion that the evidence indicates an impact origin can be uniquely tested by a drilling program. From nuclear scaling, the depth of the lowest brecciated horizon should be less than 3,000 feet. This is at least 2,000 feet above basement rock. Finding a lower limit of brecciation at the approximate predicted level would not only help solve the Flynn Creek problem but would also aid in determining the origin of many other similar cryptoexplosion structures. In the absence of refutative subsurface data, the impact origin of the Flynn Creek crater is considered the most likely hypothesis.

REFERENCES CITED

Amstutz, G. C., 1965, A morphological comparison of diagenetic cone-in-cone structures and shatter cones in Geological problems in lunar research: New York Acad. Sci. Annals, v. 123, p. 1050-1056.

Boon, J. D., and Albritton, C. C., Jr., 1937, Meteorite scars in ancient rocks: Field and Lab., v. 5, no. 2, p. 53-64.

Born, K. E., and Lockwood, W. N., 1945, Oil and gas in the northern Cumberland Plateau, Tennessee: Tennessee Div. Geology, Oil and Gas Inv. 2.

Branca, W., and Fraas, E., 1905, Das Kryptovulkanische Becken von Steinheim: Kgl. Preriss. Akad. Wiss. Abh., 64 p.

Bucher, W. H., 1936, Cryptovolcanic structures in the United States: Internat. Geol. Cong., 16th, Washington, D.C., Rept., v. 2, p. 1055-1084.

Bucher, W. H., 1963, Cryptoexplosion structures caused from without or from within the earth? ("astroblemes" or "geoblemes"?): Am. Jour. Sci., v. 261, p. 597-649.

Currie, K. L., 1965, Analogues of lunar craters on the Canadian Shield in Geological problems in lunar research: New York Acad. Sci. Annals, v. 123, p. 915-940.

Dietz, R. S., 1960, Meteorite impact suggested by shatterconе n rocks: Science, v. 131, p. 1781-1784.

Freeman, L. B., 1953, Regional subsurface stratigraphy of the Cambrian and Ordovician in Kentucky and vicinity: Kentucky Geol. Survey Bull., ser. 9, no. 12, 352 p.

_____1959, Regional aspects of Silurian and Devonian stratigraphy in Kentucky: Kentucky Geol. Survey Bull., ser. 9, no. 6, 575 p.

Goguel, J., 1953, Le régime thermique de l´eau souterraine: Annales des Mines, Ministere de l´Industrie et de l´Energie, v. 10, p. 3-32.

_____1963, A hypothesis on the origin of the "cryptovolcanic structures" of the central platform of North America: Am. Jour. Sci., v. 261, p. 664-667.

Hager, D., 1949, Crater Mound (Meteor Crater), Arizona: Is its origin geologic or meteoritic? [abs.]: Pop. Astronomy, v. 57, p. 457.

_____1953, Crater Mound (Meteor Crater), Arizona, a geologic feature: Am. Assoc. Petrol. Geologists Bull., v. 37, p. 821.

Handin, J. W., and Hager, R. V., 1957, Experimental deformation of sedimentary rocks under confining pressure-tests at room temperature on dry samples: Am. Assoc. Petrol. Geologists Bull., v. 41, no. 1, p. 1-50.

Hubbert, M. K., and Rubey, W. W., 1959, Mechanics of fluid-filled porous solids and its application to overthrust faulting, pt. 1 of Role of fluid pressure in mechanics of overthrust faulting: Geol. Soc. America Bull., v. 70, p. 115-166.

Johnson, G. P., and Talbot, R. J., 1964, A theoretical study of the shock wave origin of shatter cones: Air Force Inst. of Technology, School of Eng., Wright-Patterson A.F.B., Ohio, 92 p.

Kellberg, J. M., 1965, Tectonic origin of cryptoexplosion structures [abs.]: Geol. Soc. America, Southeast Sec., p. 15.

King, P. B., 1959, The evolution of North America: Princeton Univ. Press, 190 p.

Lusk, R. G., 1927, A pre-Chattanooga sink hole: Science, v. 65, p. 579-580.

_____1935, Geology and oil and gas resources of the Gainesboro Quadrangle, Tennessee: Tennessee Div. of Geology, Bull. 45, unpub.

McBirney, A. R., 1959, Factors governing emplacement of volcanic necks: Am. Jour. Sci., v. 257, p. 431-448.

_____1963, Breccia pipe near Cameron, Arizona: discussion: Geol. Soc. America Bull., v. 74, p. 227-232.

McKnight, E. T., 1940, Geology of area between Green and Colorado Rivers, Grand and San Juan Counties, Utah: U.S. Geol Survey Bull. 908, 147 p.

Miltor L. J., 1965, Structural geology of the larger Henbury craters, in Crater investigations, pt. B of Astrogeologic Studies Ann. Prog. Rept., July 1964-July 1965: U.S. Geol. Survey open-file report, p. 26-49.

Nettleton, L. L., 1934, Fluid mechanics of salt domes: Am. Assoc. Petroleum Geologists Bull., v. 18, p. 1175-1204.

Robertson, E. C., 1955, Experimental study of the strength of rocks: Geol. Soc. America Bull., v. 66, p. 1275-1314.

Roddy, D. J., 1963, Flynn Creek structure, Tennessee, in Crater investigations, pt. B of Astrogeologic Studies Ann. Prog. Rept., Aug. 1961-Aug. 1962: U.S. Geol. Survey open-file report, p. 118-126.

_____1964a, Geologic section across the Flynn Creek structure, in Crater investigations, pt. B of Astrogeologic Studies Ann. Prog. Rept., Aug 1962-July 1963: U.S. Geol. Survey open-file report, p. 53-76.

Roddy, D. J., 1964b, Recent investigations of the Flynn Creek structure, in Crater investigations, pt. B of Astrogeologic Studies Ann. Prog. Rept., July 1963-July 1964: U.S. Geol. Survey open-file report, p. 163-180.

_____1965, Recent geologic and laboratory investigations of the Flynn Creek structure, Tennessee, in Crater investigations, pt. B of Astrogeologic Studies Ann. Prog. Rept., July 1964-July 1965: U.S. Geol. Survey open-file report, p. 50-59.

_____1966, The Paleozoic crater at Flynn Creek, Tennessee: Unpub. Ph.D. thesis, California Inst. Tech., 232 p.

Shoemaker, E. M., 1960, Penetration mechanics of high velocity meteorites illustrated by Meteor Crater, Arizona: Internat. Geol. Cong., pt. 17, p. 418-433

_____1962, Interpretation of lunar craters, in Kopal, Z., ed., Physics and astronomy of the moon; New York, Academic Press, p. 283-360.

Shoemaker, E. M., and Eggleton, R. E., 1961, Terrestrial features of impact origin, in Proc. of the Geophys. Lab., Lawrence Radiation Lab. cratering symposium: U.S. Atomic Energy Comm., U.C.R.L.-6438, pt. ., paper A, 27 p.

Shoemaker, E. M., Gault, D., Moore, H. J., and Lugn, R., 1963, Hypervelocity impact of steel in Coconino sandstone: Am. Jour. Sci., v. 261, p. 668-682.

Shoemaker, E. M., Hackman, R. J., and Eggleton, R. E., 1962, Interplanetary correlation of geologic time: Advances in Astronautical Sci., v. 8, New York, Plenum Press, p. 70-89.

Short, N. M., 1965, A comparison of features characteristic of nuclear explosion craters and astroblemes: New York Acad. Sci. Annals, v. 123, p. 573-616.

Snyder, F. G., and Gerdemann, P. E., 1965, Explosive igneous activity along an Illinois-Missouri-Kansas axis: Am. Jour. Sci., v. 263, p. 465-493.

Stearns, R. G., and others. 1966, The Wells Creek structure, Tennessee: Conf. on shock metamorphism of natural materials, Goddard Space Flight Center, April 1966. p. 48-49.

Wilson, C. W., Jr., 1948, The geology of Nashville, Tennessee: Tennessee Div. Geology Bull. 53, 172 p.

_____1949, Pre-Chattanooga stratigraphy in Central Tennessee: Tennessee Div. Geology Bull 56, 407 p.

_____1953, Wilcox deposits in explosion craters, Stewart County, Tennessee, and their relations to origin and age of Wells Creek Basin structure: Geol. Soc. America Bull., v. 64, p. 753-768.

_____1962, Stratigraphy and geologic histroy of Middle Ordovician rocks of central Tennessee: Geol. Soc. America Bull., v. 73, p. 481-504.

Wilson, C. W., Jr., and Born, K. E., 1936, The Flynn Creek disturbance, Jackson County, Tennessee: Jour. Geology, v. 44, p. 815-835.

GEOLOGY OF THE SIERRA MADERA STRUCTURE, TEXAS: PROGRESS REPORT

By H. G. Wilshire

INTRODUCTION

This paper describes the progress made in fiscal year 1966 on the geologic study of the Sierra Madera cryptoexplosion structure in west Texas. The area of detailed mapping (Wilshire, 1965) was extended, and new data were obtained on lithology and stratigraphic relations of the Permian rocks exposed at Sierra Madera and in the nearby Glass Mountains. Structural data obtained from records of deep drill holes on and near Sierra Madera indicate that all parts of the structure are raised above the regional trend of the formations identified.

STRATIGRAPHY

Permian rocks representing formations from the Tessey Limestone at the top to the Word Formation at the base are exposed in the central part of the Sierra Madera structure. The Permian section is unconformably overlain by a thin conglomerate of possible Triassic age (Bissett Formation; Shoemaker and Eggleton, 1964), and this in turn[1] is unconformably(?) overlain by the Cretaceous Basement Sandstone and Edwards Limestone. The general stratigraphic relations are shown in figure 1.

A comparison of lithologies of Permian to Cretaceous rocks exposed at Sierra Madera and in the northeastern Glass Mountains was made by Wilshire (1965). The distinctive features that allow subdivision of the section in the Glass Mountains are also present

[1] The Hunt Elsinore 51 well (fig. 3) penetrated 140 feet of limestone between the Basement Sandstone and Tessey dolomites which is possibly the Cretaceous Glen Rose Formation.

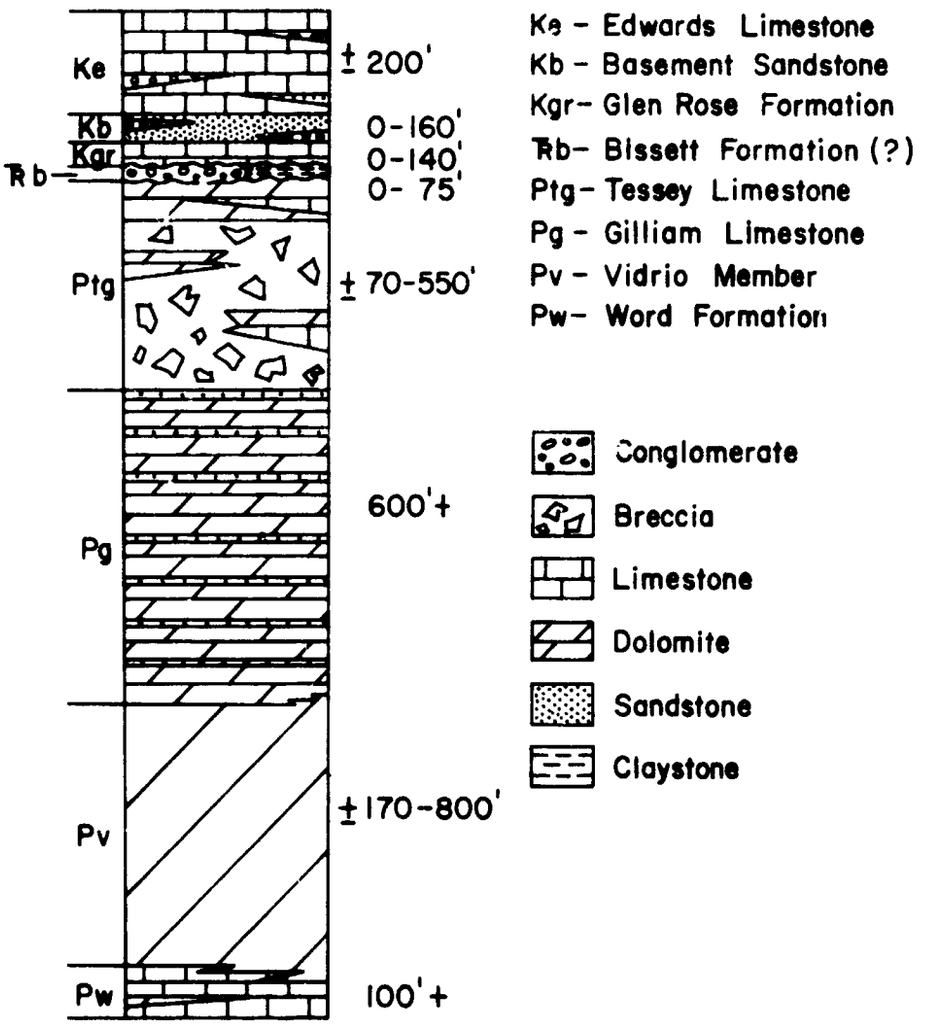

Figure 1.--Generalized columnar section showing relationships of the formations at Sierra Madera.

at Sierra Madera. The only major difference is that breccias are much more widespread at Sierra Madera. The diagnostic lithologies of the Permian formations are listed in table 1.

Table 1.--Dominant lithologies of Permian formations at Sierra Madera

Tessey Limestone	Interbedded dolomite, limestone. Dolomite most abundant, limestone unfossiliferous. Dolomite and limestone breccia abundant.
Gilliam Limestone	Interbedded dolomite, fine-grained sandstone. Dolomite most abundant, has close-spaced bedding-plane parting. Dolomite breccia common.
Vidrio Member of Word Formation	Dominantly massive, locally bedded dolomite. Thin stringers of coarse-grained sandstone, pebbly sandstone in places; limestone rare, generally near base where Vidrio and Word are intertongued. Dolomite breccia abundant.
Word Formation	Dominantly thick-bedded limestone interbedded with thin richly fossiliferous limestone. Upper part contains thin discontinuous gravel beds and interbedded massive dolomite. Lower part may contain more dolomite that resembles Vidrio.

The author (1965, p. 8) stated that the Vidrio Member of the Word Formation had not yet been recognized at Sierra Madera and that limestones of possible Word age were interbedded with dolomite breccias. Actually, a small part of the Gilliam-Vidrio contact had been mapped by Shoemaker and Eggleton (1964), but was not recorded in their report. A considerable section of Vidrio has now been mapped, and the dolomite breccias previously labeled Pw? (Wilshire, 1965, fig. 4) are now considered to be a part of the Vidrio Member. The thickness of the Vidrio Member so far mapped is extremely variable. Interfingering of Vidrio dolomite with Word limestone was definitely established, and slight interfingering at the upper contact with the Gilliam occurs locally. Rapid lateral changes in thickness of the Vidrio suggest that it is in part a reef deposit, and a small (125 by 250 feet) protrusion from the

upper contact into Gilliam dolomites resembles algal colonies described by Wolf (1965); the size of this protrusion is well within the range of known algal colonies (K. H. Wolf, oral commun., 1966). Although algae and other reef-forming fossils are well-preserved in Word limestones, no fossils of any kind have yet been found in the Vidrio dolomites at Sierra Madera.

A new formation of postdeformation age was found at Sierra Madera. In contrast with the common, monomict breccias of the Tessey, Gilliam, and Word formations, this unit is a mixed breccia that contains fragments of at least two formations (Gilliam and Word). Generally this breccia mantles the Gilliam, Vidrio, and Word and does not conform to the underlying structure; in three places, however, it appears to be interbedded with the Gilliam or Vidrio and is conformable with the local structure in those formations. Characteristically the breccia is an unsorted aggregate of large (to at least 4 feet) angular blocks of dolomite and smaller angular pebbles and boulders of dolomite, limestone, fine-grained sandstone, chert, and a kaolinite-rich rock of unknown origin, in a sandy carbonate matrix. Fragments of thin-bedded Gilliam dolomite commonly contain segments of shatter cones that are broken off irregularly at the edge of the fragment. Fine-grained sandstone fragments derived from the Gilliam, and rare medium-grained sandstone fragments and chert pebbles derived from the Word Formation are present. Fusulinid-bearing Word limestone fragments are moderately abundant even where the breccia overlies the Gilliam Limestone.

Mapping of this formation has not been completed, and its origin connot yet be stated with certainty. Alternative interpretations that are being considered are that it is a caliche-cemented slope-wash deposit possibly correlative with the Pliocene Ogallala Formation (Bretz and Horberg, 1949) or that it is allogenic (Shoemaker, 1960, p. 424) or allochthonous (Dence, 1965, p. 952) breccia formed by an impact event. The first interpretation is

supported by the apparent absence of shocked phases in the breccia and by the occurrence of small lenses of the breccia on the upslope side of massive Vidrio dolomites; in such places it appears that more rapid erosion or solution of the upslope Word limestones caused local ponding of slope wash behind the Vidrio dolomite. In this view, the apparently interbedded lenses of mixed breccia would represent infillings of solution-widened bedding-plane partings analogous to that illustrated by Bretz and Horberg (1949, pl. 1B). There is no direct evidence favoring the alternative interpretation, but the distribution of the deposit resembles that of the allochthonous breccia at West Clearwater Lake (Dence, 1965); in this view, the apparently interbedded mixed breccias may represent injection breccias.

For additional control on stratigraphy and subsurface structure, lithologic and electric logs and paleontologic records of deep drill holes on and near the structure were obtained (fig. 2). Six wells on the structure reached depths from 7,343 to 16,946 feet; six other wells within 7 miles of the structure reached depths of 4,481 to 23,400 feet. A number of driller's logs of shallower wells on and near the structure were obtained, but the lithologies will not be recorded until rock identifications can be confirmed. Commercial logs of the section penetrated to the Leonard or Wolfcamp formation are shown in figure 3 in generalized form. The choice of contacts is based primarily on lithology and fossils.

Two wells (Hunt 51, 57) on the structure penetrated Cretaceous rocks of the Comanchean Series. There is no lithologic break to allow subdivision of the Edwards Limestone and younger limestones, but the 840 feet of limestone is well in excess of the thickest (225 feet) section of Edwards Limestone reported by King (1930). The Hunt 57 well penetrated at most 10 feet of the Basement Sandstone, whereas the Hunt 51 well penetrated 160 feet (the maximum so far recorded) of this formation. In the Hunt 51 well, 140 feet of limestones beneath the Basement Sandstone may represent the Glen Rose Formation (basal Comanchean), and some limestones in

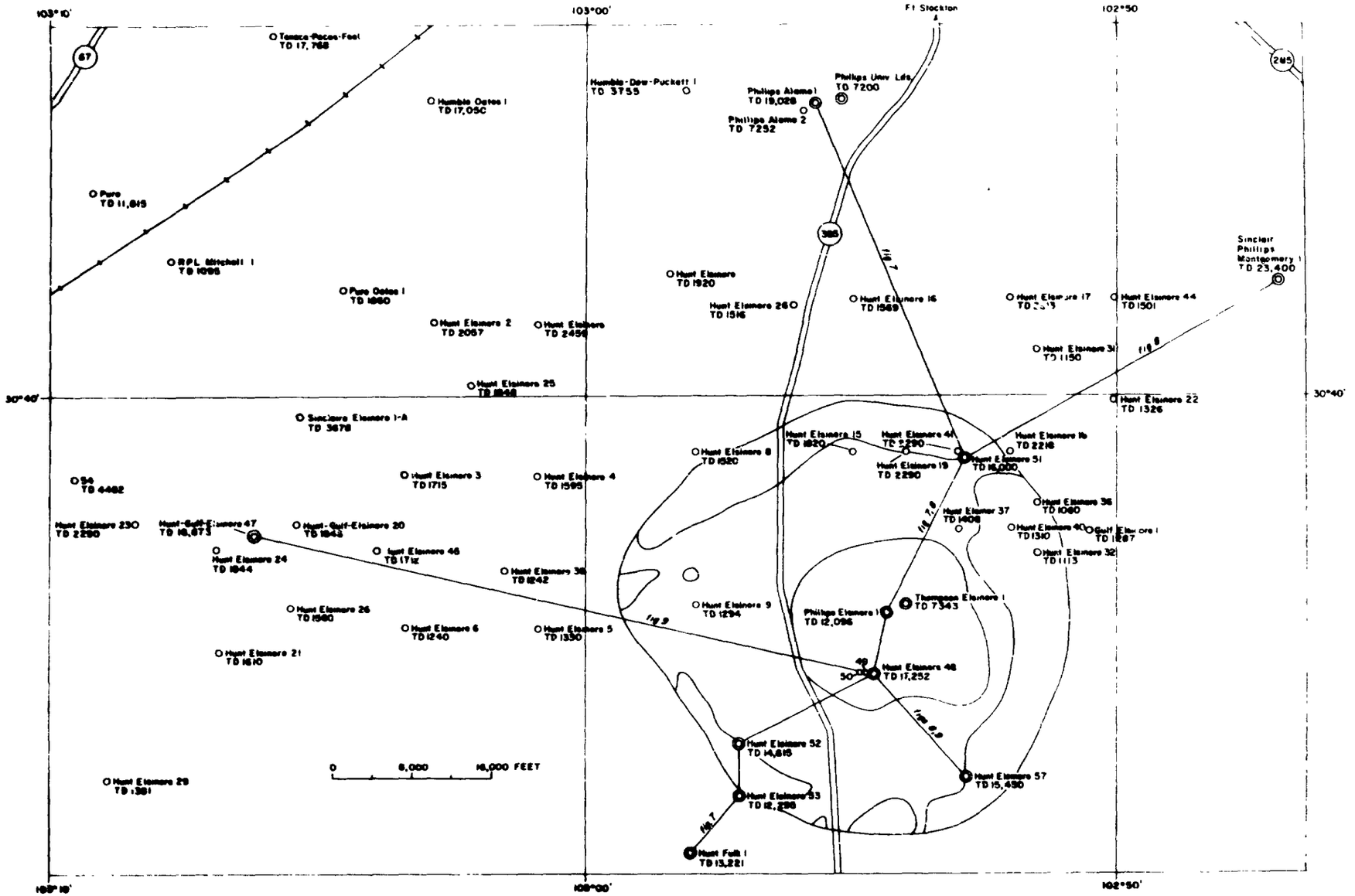

Figure 2.--The Sierra Madera structure showing wells. The inner zone is intensely deformed Permian and Cretaceous rocks; the outer zone is midly deformed dominantly Cretaceous rocks.

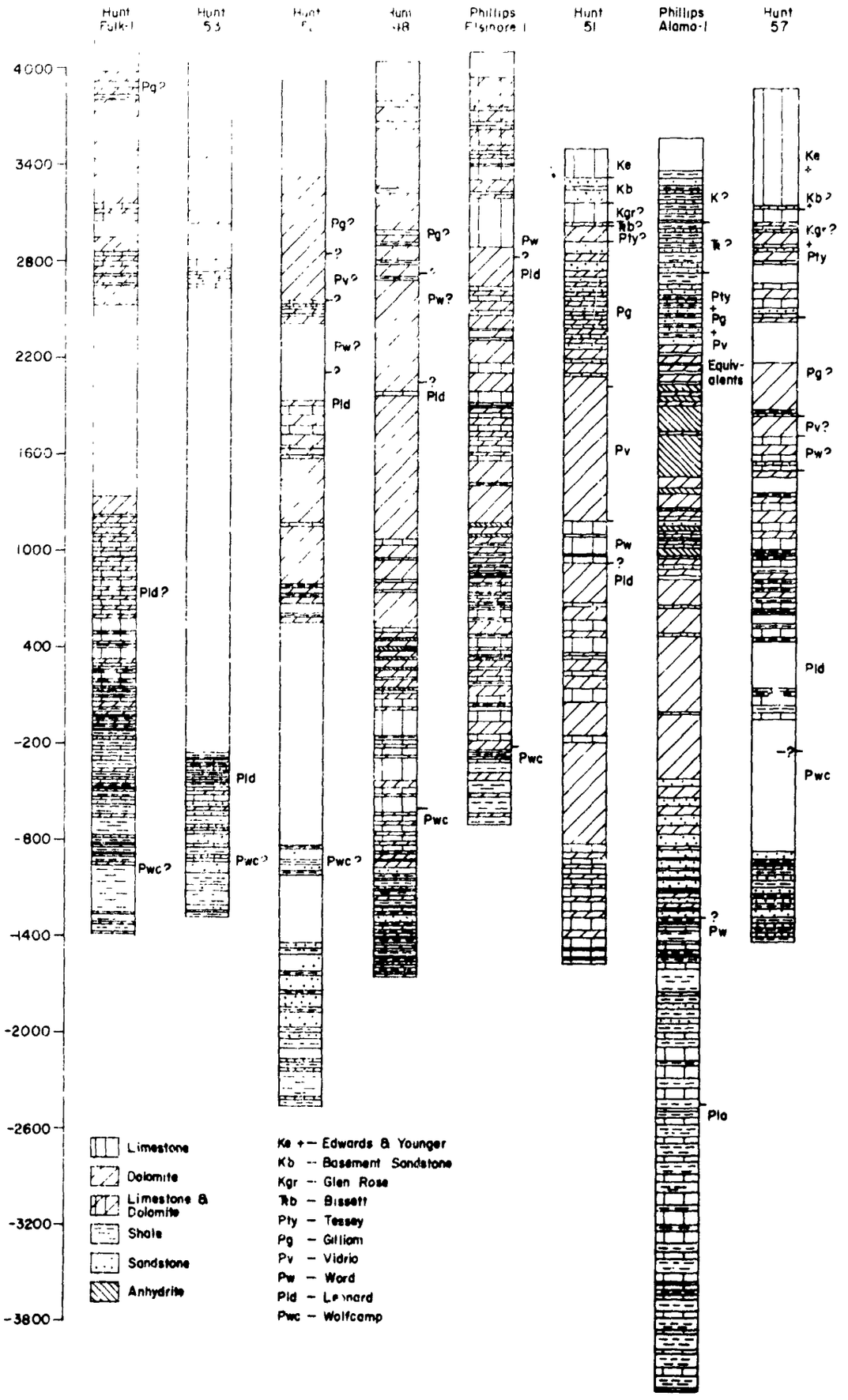

Figure 3.--Generalized lithologic logs of some deep drill holes on and near the Sierra Madera structure.

the same position in the Hunt 57 well are possibly Glen Rose strata but cannot be separated from Tessey limestone. Thicknesses[2] of Tessey Limestone range from 70 feet in the Hunt 51 well to about 550 feet in the Hunt 57 well; the formation is composed dominantly of dolomite with some limestone, sandstone, and shale, and grades northward (Vacuum Elsinore 1 and Phillips Alamo 1) into a dominantly saline section. The thickness of Gilliam Limestone penetrated by the various wells ranges from 620 feet (Hunt 57) to about 980 feet (Hunt 51). The formation consists of dolomite and sandstone in variable proportions with some shale; these grade northward into a section dominated by sandstone with some saline and carbonate rocks (Vacuum Elsinore 1) and to a section dominated by dolomite in the Phillips Alamo 1 well. There is no lithologic basis for separation of Gilliam and Vidrio in the Hunt 48 well. The Vidrio Member of the Word Formation ranges in thickness from 140 feet (Hunt 57) to more than 775 feet (Vacuum Elsinore 1) and consists dominantly of dolomite with minor sandstone and shale; this member changes to a section dominated by sandstone with some dolomite and shale in the Phillips Alamo 1 well. There is no lithologic basis for separating the Vidrio from the Word in the Hunt 48 well. The apparent thickness of Word Formation varies from about 800 feet (Hunt 57) to about 1,270 feet (Phillips Elsinore 1); there is no lithologic break between the Word and Leonard Formations, and determination of thicknesses depends on fossil identification. Fossil data that define the Word closely are available only in the structurally complex area drilled by the Phillips Elsinore 1, and true thickness may be grossly exaggerated. Generally the Word is composed of limestone and dolomite with limestone slightly more abundant, but the section in the Hunt 48 well is almost entirely dolomite. These rocks grade northward (Phillips Alamo 1) into a section composed dominantly

[2]All recorded thicknesses are apparent thicknesses penetrated by the wells. Possible structural causes of variation are not taken into account.

of shale with some sandstone, dolomite, and limestone. Inasmuch as the Word Formation (exclusive of the Vidrio Member) is only about 200-300 feet thick in the nearest Glass Mountains, it is important to note the lack of a distinctive lithologic break between the Word and Leonard in wells on the structure. The Leonard Formation may accordingly be exposed in the center of Sierra Madera, but this can be demonstrated only by study of the fossils.

PETROGRAPHY AND CHEMICAL COMPOSITION

Examination of thin sections of the various formations allows more precise classification of the rocks, as shown in table 2. Folk's scheme of classification of the carbonate rocks (1959, 1962) is used, and clastic rocks are classified according to Gilbert's scheme (Williams, Turner, and Gilbert, 1958). Dolomitic rocks are described by Folk's (1962, p. 70) terms under the heading "replacement dolomites," although no evidence was found in thin section to support or reject a replacement origin. The dolomite breccias from Sierra Madera are considered to be deformational rather than sedimentary and do not fit the classifications of either Folk or Gilbert; in table 2, the rock fragments of the breccias are described in terms of Folk's classification, but the interstitial recrystallized mylonite(?) is referred to as the "groundmass" to avoid use of "cement" or other terms that might imply a sedimentary origin. Chemical analyses of carbonate rocks (table 3) were made by J. A. Thomas to aid precise classification and as part of the study of the breccias and their goundmass components.

Table 2.--Petrography of the Permian formations

	Glass Mountains
Tessey Limestone	Finely to very finely crystalline dolomite, pellet dolomite; bedding laminae generally faint, caused by size-color variation. Sparry calcite veinlets common. Breccias consist of very finely crystalline dolomite

Table 2.--Petrography of the Permian formations--Continued

	and pellet dolomite fragments in aphanocrystalline, locally sandy matrix. Interbedded unfossiliferous micrite and medium crystalline limestone; some well-sorted fine-grained quartz arenites with medium crystalline calcite and microcrystalline silica cement; quartz angular-subangular, generally free of inclusions; undulose extinction common.
Gilliam Limestone	Finely to very finely crystalline dolomite and pellet dolomite. Minor subangular detrital quar'
Vidrio Member of Word Formation	Finely to very finely crystalline dolomite. Patchy distribution of sparry calcite. Rare, poorly preserved fossils. Concentrically zoned discoid cavity fill; most commonly outer zone of finely crystalline, clear calcite, intermediate zone medium crystalline calcite (often with minute inclusions), inner zone of botryoidal fibrous carbonate. Thin veinlets of sparry calcite and hematite common.
Word Formation	Micrite, biomicrite; locally very sandy and pebbly. Uncommon round interclasts(?) composed of irregular patches of microcrystalline silica surrounded by single sparry calcite grain; local replacement of fossils by microcrystalline or fibrous silica. Sand composed of angular-subangular quartz; pebbles of chert, quartzite. Quartz generally free of inclusions, commonly has undulose extinction.
Gravel member of Leonard Formation	Conglomerate composed of well-rounded to angular cobbles, pebbles, and granules of banded chert, quartz arenite, quartzite, and quartz cemented by locally sub-botryoidal finely crystalline dolomite or calcite. Minor fossil fragments, detrital zircon, tourmaline, and monazite(?); rare zircon inclusions in quartz. Quartz commonly has undulose extinction or deformation lamellae in quartzite fragments.
Hess Member of Leonard Formation	Finely to very finely crystalline dolomite and pellet dolomite. Minor detrital quartz, muscovite. Undulose extinction common in quartz. Local sandy, pebbly beds with granules of quartz, quartzite,

Table 2.--Petrography of the Permian formations--Continued

	quartz arenite in finely crystalline dolomite cement.
	Sierra Madera
Tessey Limestone	Finely to very finely crystalline dolomite and pellet dolomite; variable quantities of sparry calcite, minor detrital quartz and muscovite. Some interbedded pelmicrite. Rare fossil fragments. Dolomites commonly brecciated; fragments in aphanocrystalline, banded groundmass.
Gilliam Limestone	Finely to very finely crystalline dolomite and pellet dolomite and interbedded fine to very fine grained calcareous quartz arenite with minor detrital muscovite and heavy minerals. Dolomites commonly brecciated with fragments in aphanocrystalline, banded groundmass. Poorly preserved fusulinids rare.
Vidrio Member of Word Formation	Finely to medium crystalline dolomite. Dolomite breccia common with fragments in aphanocrystalline, banded groundmass; local lineation of elongate fragments in groundmass.
Word Formation	Biomicrite, locally sandy. Patchy distribution sparry calcite, locally with single set of multiple twins. Locally cut by thin, branching veinlets filled with aphanocrystalline carbonate. Sand dominantly subrounded quartz, some chert. Quartz commonly has undulose extinction.

Table 3.--Partial chemical analyses of carbonate rocks

[Analyst: J. A. Thomas]

Sample	Formation and location	Percentage of-- Ca	Mg	Molal ratio	Percentage of-- Total Carbonate	Fe_2O_3
SM-1	Vidrio, G.M.[1]	22.6	12.4	1.11	99.5	0.205
SM-19	Tessey, G.M.	25.7	10.2	1.53	99.7	.205
SM-48	Tessey, G.M.	39.3	.02	100.0	98.3	.070
SM-50	Tessey, G.M.	39.3	.08	100.0	98.3	.090
SM-53	Gilliam, S.M.[1]	22.0	12.6	1.06	98.8	.304
SM-24A[2]	Gilliam, S.M.	21.6	12.9	1.02	98.8	.130
SM-24M		22.1	12.8	1.05	99.7	.182
SM-26A	Gilliam, S.M.	20.7	12.3	1.02	94.5	.175
SM-26M		21.8	12.7	1.04	98.6	.210
SM-31A	Tessey, S.M.	22.5	12.4	1.10	99.3	.330
SM-31M		22.7	11.8	1.17	97.7	.445
SM-32	Tessey, S.M.	22.0	12.1	1.10	97.0	.120
SM-33A	Tessey, S.M.	21.7	12.7	1.04	98.4	.195
SM-33M		21.6	12.2	1.07	96.3	.197
SM-49	Tessey, G.M.	22.8	12.3	1.12	98.5	.130
SM-49A		22.8	12.2	1.13	99.3	.100
SM-49M		22.2	12.3	1.10	98.2	.152
SM-59A	Gilliam, S.M.	22.4	12.2	1.11	98.3	.225
SM-59M		21.8	11.8	1.12	95.4	.225
SM-60A	Vidrio, S.M.	21.8	12.2	1.08	96.8	.100
SM-60M		22.7	12.2	1.13	99.1	.100

[1] G.M. = Glass Mountains; S.M. = Sierra Madera.
[2] A = rock fragments; M = matrix.

Note.--Ca and Mg are accurate within ± 1 percent. Analysis by colormetric titration. Iron analysis by atomic absorption.

As shown in table 2, there is no difference in the dominant rock types of the various Permian formations between the Glass Mountains and Sierra Madera. Dolomites in all the formations are finely to very finely crystalline dolomites or pellet dolomites, generally slightly sandy, and rarely fossiliferous. The total carbonate content (table 3) ranges from 94.5 to 99.7 percent, and, with one exception (SM-19), rocks classified as dolomite in the field are composed of nearly pure dolomite (molal ratios 1.02-1.17). The Word Formation both in the Glass Mountains and at Sierra Madera consists of biomicrite, micrite, pelletiferous micrite, and dolomites not as yet studied in thin section. Sandstones, primarily from the Gilliam Limestone, are fine-grained calcareous quartz arenites composed largely of subangular quartz. Detrital quartz in the carbonate rocks as well as in the sandstones is generally free of inclusions and commonly exhibits undulose extinction or poorly developed strain lamellae.

Sampling of formations at Sierra Madera was heavily weighted towards the breccias that are abundant in all the Permian rocks; breccias are absent in equivalent rocks in the Glass Mountains except in the Tessey Limestone. It was previously suggested (Wilshire, 1965) that all the breccias at Sierra Madera are of sedimentary origin and indicate a shallower depositional environment than in the nearest Glass Mountains. This conclusion was based on the transition of laminated Tessey dolomites through mildly disturbed laminated units into completely mixed breccias, and on interbedding of massive and brecciated dolomites in the Gilliam Limestone. The macroscopic appearance of breccias from the Tessey in the Glass Mountains (fig. 4A, B) is the same as that of many Tessey breccias at Sierra Madera (fig. 4C, D), and structures such as nearly isoclinal folds (fig. 5A) occur in both places. Microscopic examination, however, revealed major differences between breccias of the Tessey Limestone from the Glass Mountains and those from Sierra Madera. In thin section the breccias from the

Figure 4A.--Brecciated laminated dolomite. Tessey Limestone, Glass Mountains. Note bending of thin, mildly brecciated beds over large piece of laminated dolomite below hammer. Breccia above hammer is thoroughly mixed.

Figure 4B.--Brecciated laminated dolomite. Tessey Limestone, Glass Mountains. Breccia is in core of a small fold.

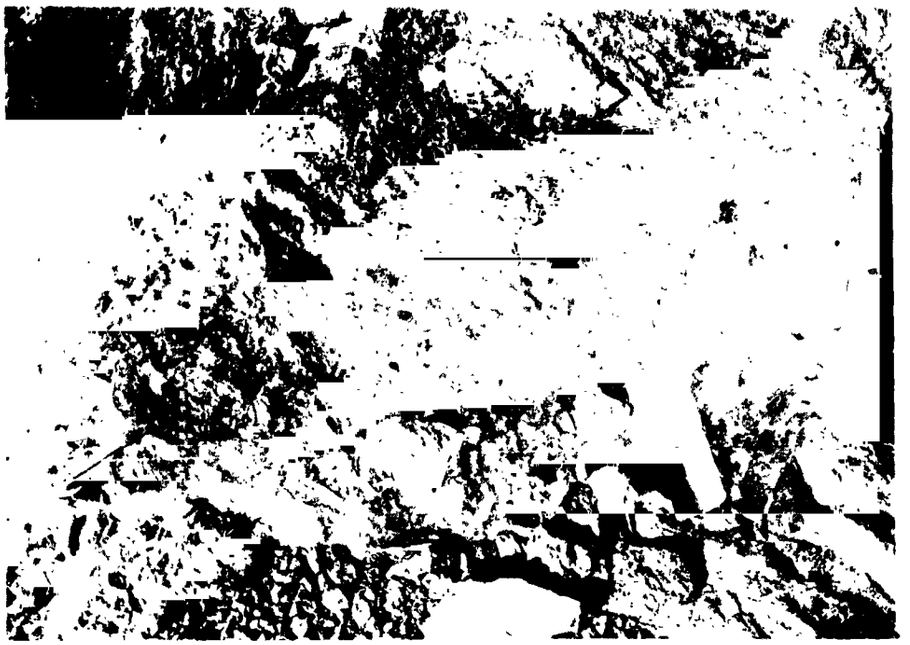

Figure 4C.--Brecciated dolomite. Tessey Limestone, Sierra Madera. Mildly brecciated beds near hammerhead grade down into thoroughly mixed breccia.

Figure 4D.--Brecciated dolomite. Tessey Limestone, Sierra Madera.

Figure 5A.--Tight, steep-sided fracture folds in laminated dolomite. Tessey Limestone, Glass Mountains.

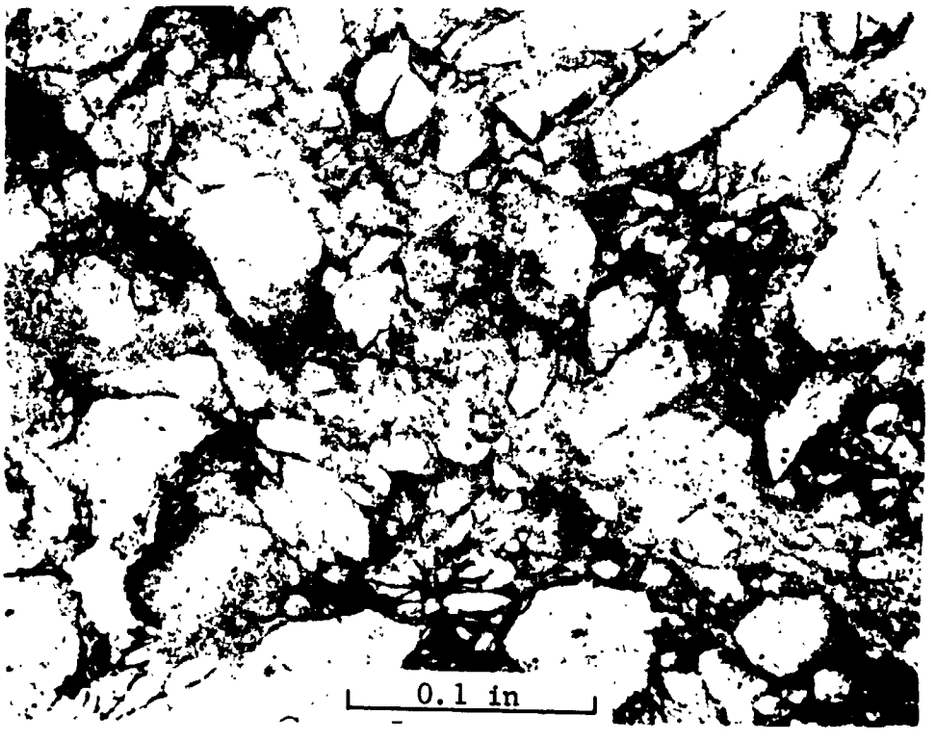

Figure 5B.--Photomicrograph of dolomite breccia. Gilliam Limestone, Sierra Madera. Note frayed color (and grain size) banding in groundmass.

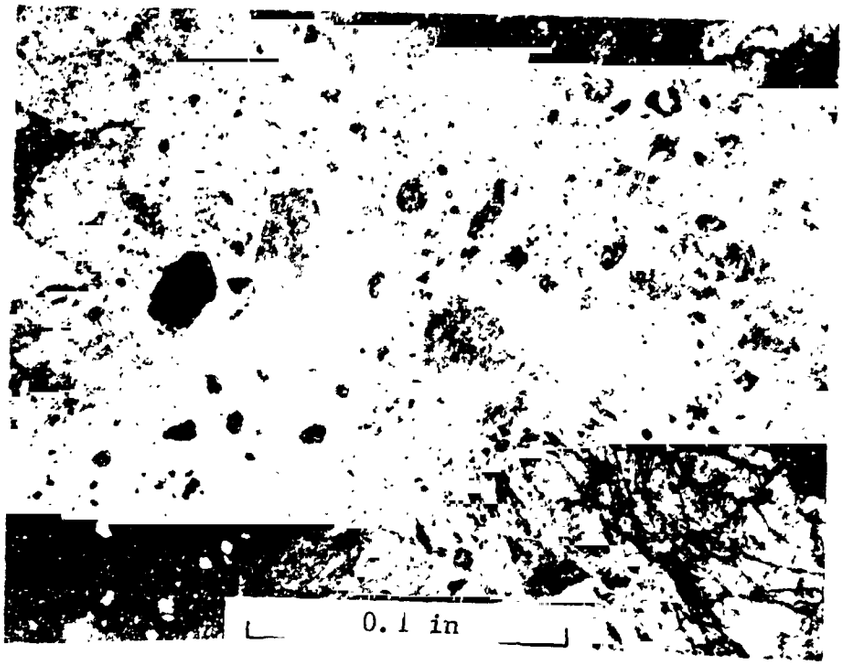

Figure 5C.--Photomicrograph of dolomite breccia. Tessey Limestone, Sierra Madera. Note finger of dark groundmass material extending diagonally across photograph from lower left corner. Extensive internal fracturing with slight rotation of parts in rock fragment, lower right corner of photograph; fractures filled with aphanocrystalline carbonate.

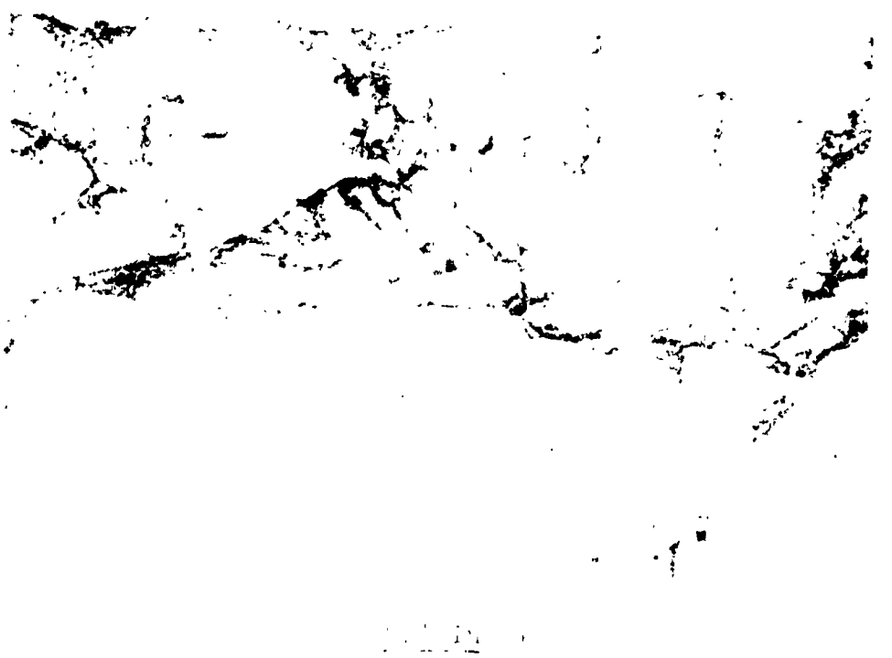

Figure 5D.--Photomicrograph of dolomite breccia. Vidrio Member, Sierra Madera. Extensive internal fracturing of rock fragments.

Glass Mountains are characterized by a nearly homogeneous matrix and the absence of internal fracturing of rock fragments; also, where the breccias are sandy (especially prominent where interbedded with sandstones), there is a concentration of detrital quartz in the matrix indicating reworking of dolomite by currents that could supply extraneous material. In contrast, the breccias in all Permian formations at Sierra Madera are characterized by an inhomogeneous, banded groundmass (fig. 5B,C), by internal fracturing of rock fragments with slight rotation of the parts (fig. 5C, D), and by a fairly homogeneous distribution of detrital quartz in rock fragments and groundmass. Locally there is a pronounced lineation of elongate fragments parallel to the trend of groundmass veinlets. The fractures in these breccias closely resemble those in mylonitized rock. They may, therefore, be of deformational origin despite the lack of any unusual fracturing or twinning of carbonate grains either in the rock fragments or in the groundmass. Detrital quartz likewise shows no exceptional internal structures or size diminution in the groundmass compared with quartz in the rock fragments, but it is a minor constituent. If the extremely fine grained carbonate of the groundmass does represent granulated rock, it has probably been recrystallized because the individual grains of the groundmass are interlocked in the same manner as those in the rock fragments.

Chemical analyses (table 3) were made of several breccias to determine compositional variations between rock fragments and groundmass, and to compare these variations in breccias from the Glass Mountains and from Sierra Madera. The latter comparison is preliminary as only one sample from the Glass Mountains has been analyzed. Samples of rock fragments and groundmass were obtained with a 1/8-inch diamond core drill; all groundmass samples contain an undetermined amount of small rock chips. With one exception (SM-49)--the one analyzed sample from the Glass Mountains--there is a slightly higher Ca/Mg ratio in the groundmass than in the rock fragments. Table 3 also shows a slight increase in iron from rock fragment to groundmass; from petrographic evidence, this is most likely due

to the presence of hematite stain in the groundmass rather than variation in siderite content of the carbonate fraction.

Both the style of fracturing as seen in thin section and the nature of the material filling the fractures of the breccias closely resemble those of shatter-cone segments from a Gilliam sandstone (fig. 6A). Quartz in and adjacent to the shatter-cone surfaces of the Gilliam sandstone shows no shock-induced structures such as those described by Short (1965). The fractures are filled with a mosaic of undeformed calcite grains much finer than the calcite cement of the host rock.

The mixed breccia that mantles the Gilliam and Word differs from the breccias of the Permian formations in that it is composed of an assortment of rock types derived from at least two formations, and internal fracturing of the rock fragments (excepting shatter-cone segments) is rare. Irregular fragments of a kaolinite-rich rock of unknown origin are fairly common in the breccia. These fragments are locally foliated (fig. 6B) and are composed primarily of kaolinite, authigenic quartz, calcite, and, locally, small muscovite flakes that are oriented in the plane of foliation. The shapes of some of these fragments (fig. 6B) suggest plastic deformation, and some sandstone fragments have irregularly sutured boundaries (fig. 6C). The matrix of the breccia is composed of sandy finely crystalline to aphanocrystalline carbonate. Quartz and carbonate grains in the matrix and rock fragments have no unusual internal structures.

Two thin sections of a small Recent caliche-cemented breccia of Word limestone were made for petrographic comparison with other breccias. This breccia resembles the mixed breccia described above in being composed of a heterogeneous assortment of rock fragments and in having an unbanded aphanocrystalline carbonate cement; the most conspicuous differences between the Recent and older breccias are the large number of cavities and the deep-brown color (possibly due to organic material) of the Recent caliche.

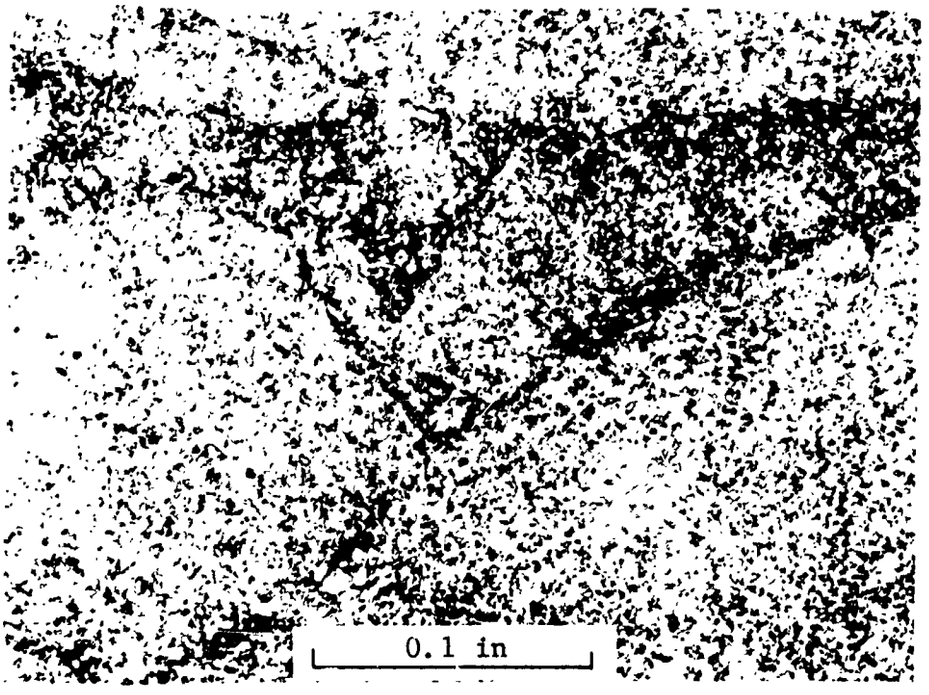

Figure 6A.--Photomicrograph of shatter-coned sandstone. Gilliam Limestone, Sierra Madera. Dark fractures are traces of shatter-cone surfaces and are filled with aphanocrystalline carbonate. Sandstone is composed largely of quartz (white) cemented by medium crystalline calcite (light gray).

Figure 6B.--Photomicrograph of mixed breccia. Sierra Madera. Foliation in light-colored fragment is defined by layering of carbonate (dark) and kaolinite plus authigenic quartz and some muscovite.

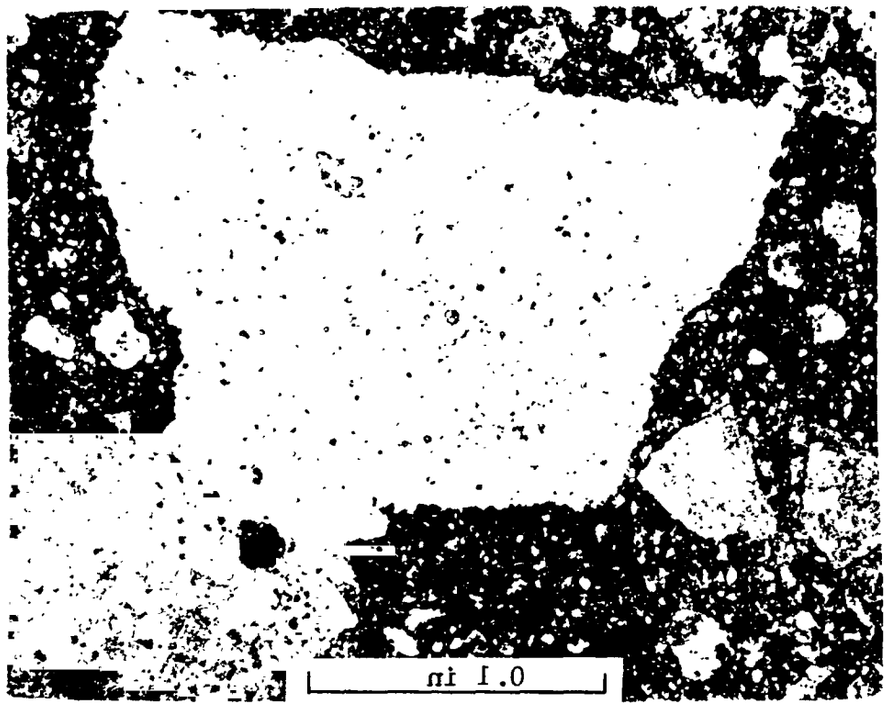

Figure 6C.--Photomicrograph of mixed breccia. Sierra Madera. Note locally sutured boundaries of light-colored calcareous quartz arenite.

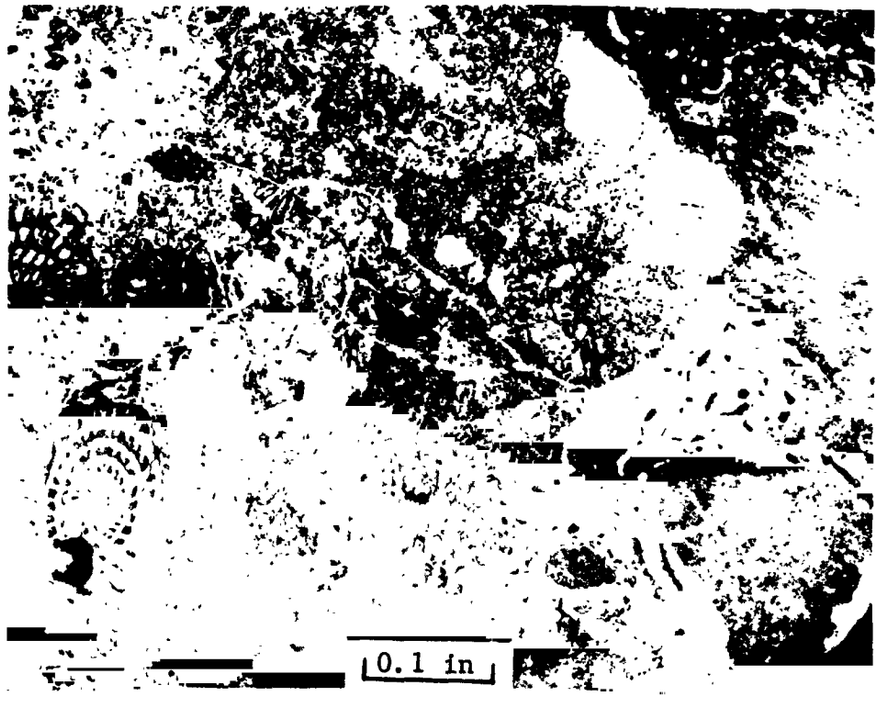

Figure 6D.--Photomicrograph of Recent caliche-cemented breccia. Caliche on right side of photograph (dark, with abundant irregular cavities). Large rock fragment (fusulinid Word limestone) is brecciated along line where fusulinids are truncated; upper part of the fragment is composed of brecciated Word biomicrite.

Rock fragments in the Recent caliche breccia include some that were obviously derived from previously brecciated Word biomicrite (fig. 6D).

STRUCTURE

Correlations of formations in the deep drill holes (figs. 7-9 reveal important elements of the regional structure as well as data relevant to the interpretation of Sierra Madera. The overall dip of all horizons is northward into the Delaware Basin. The section shown in figure 9 is most nearly parallel to the southern margin of the Delaware Basin, but the Hunt 47 well is farther from the upper Permian shelf area than the Hunt 57 well, and the same north-dipping trend is found as in figures 7 and 8. As shown in figure 7, the regional trend of pre-Permian formations is interrupted beneath the Hunt 52 and 53 wells by an anticlinal fold with approximately 800 feet of relief. Though the data are poor, this structure may be present in the middle Permian rocks also. Whether it is related to Sierra Madera is not know.

The Sierra Madera structure is revealed clearly in figures 7 and 8 in formations as low as the top of the Wolfcamp. Trends in formations from the base of the Wolfcamp down are drawn as though the structure were not present at those depths; there is, of course, no proof of this because the Phillips Elsinore 1 well did not reach the base of the Wolfcamp. The lower limit of the structure may possibly be defined (if it lies above the 12,000-foot depth of the Phillips Elsinore 1 well) by future studies of Wolfcamp fossils and the electric logs. There are indications that the structural relief diminishes downward from the apparent displacement of the Word-Leonard contact by about 1,000 feet and the Leonard-Wolfcamp contact by about 200 feet in the Phillips Elsinore 1 well; however, better data are needed on these contacts. The presence of anhydrite in the middle Leonard provides an important marker, the top of which is shown in Figures 7 and 8. Details of the anhydrite distribution are shown

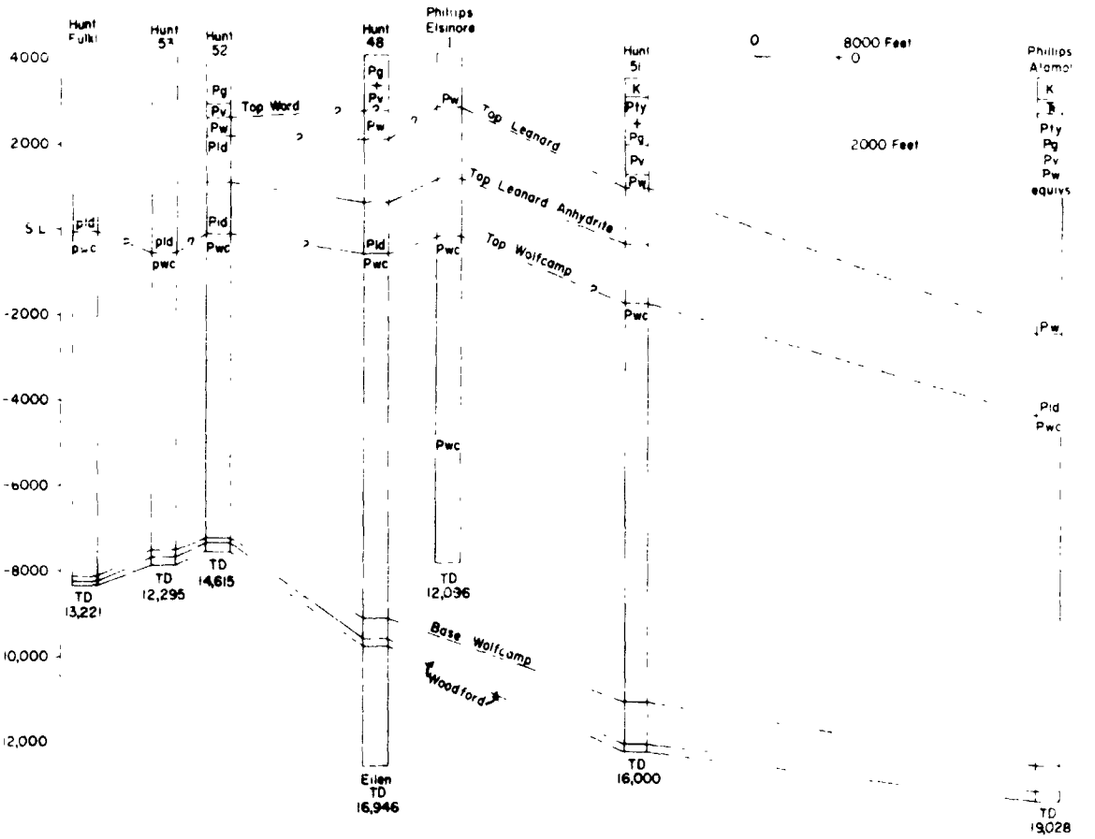
Hunt Fulk
Hunt 53
Hunt 52
Hunt 48
Phillips Elsinore 1
Hunt 51
Phillips Atoma
0
8000 Feet
0
2000 Feet
4000
2000
S L
-2000
-4000
-6000
-8000
10,000
12,000
Top Ward
Top Leonard
Top Leonard Anhydrite
Top Wolfcamp
Base Wolfcamp
Woodford
Pg
Pv
Pw
Pld
Pwc
K
Pty
equivs
TD 13,221
TD 12,295
TD 14,615
TD 12,036
Ellen TD 16,946
TD 16,000
TD 19,028

Figure 7.

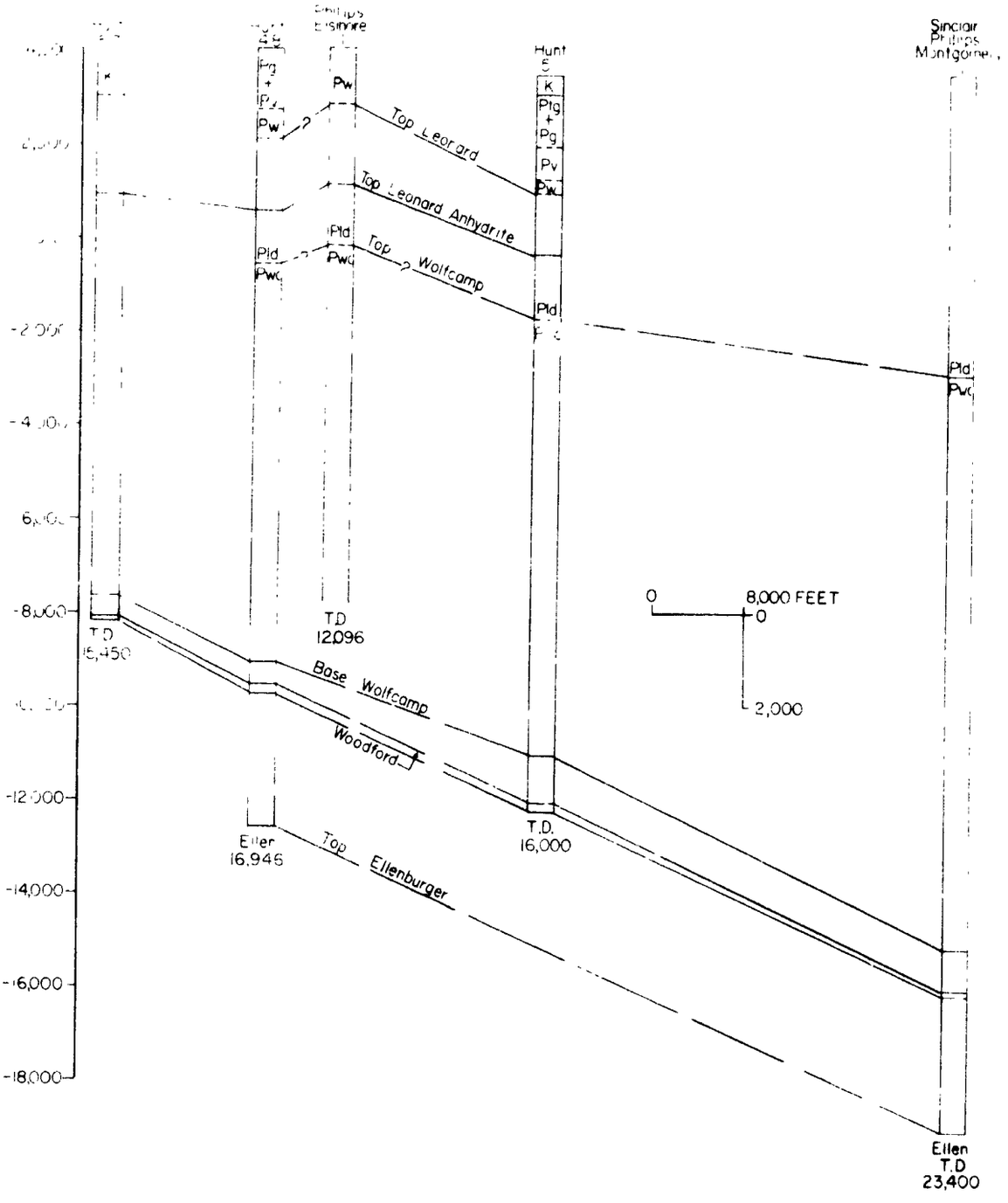
Phillips
Eisenhire
Hunt
Sinclair
Phillips
Montgomery
Pg
+
Pv
Pw
Top Leonard
Top Leonard Anhydrite
Top ? Wolfcamp
Pld
Pwc
-2,000
-4,000
-8,000
-12,000
-14,000
-16,000
-18,000
T.D
15,450
T.D
12,096
Base Wolfcamp
Woodford
Ellen
16,946
Top Ellenburger
T.D.
16,000
0
8,000 FEET
0
2,000
Ellen
T.D
23,400

Figure 8.

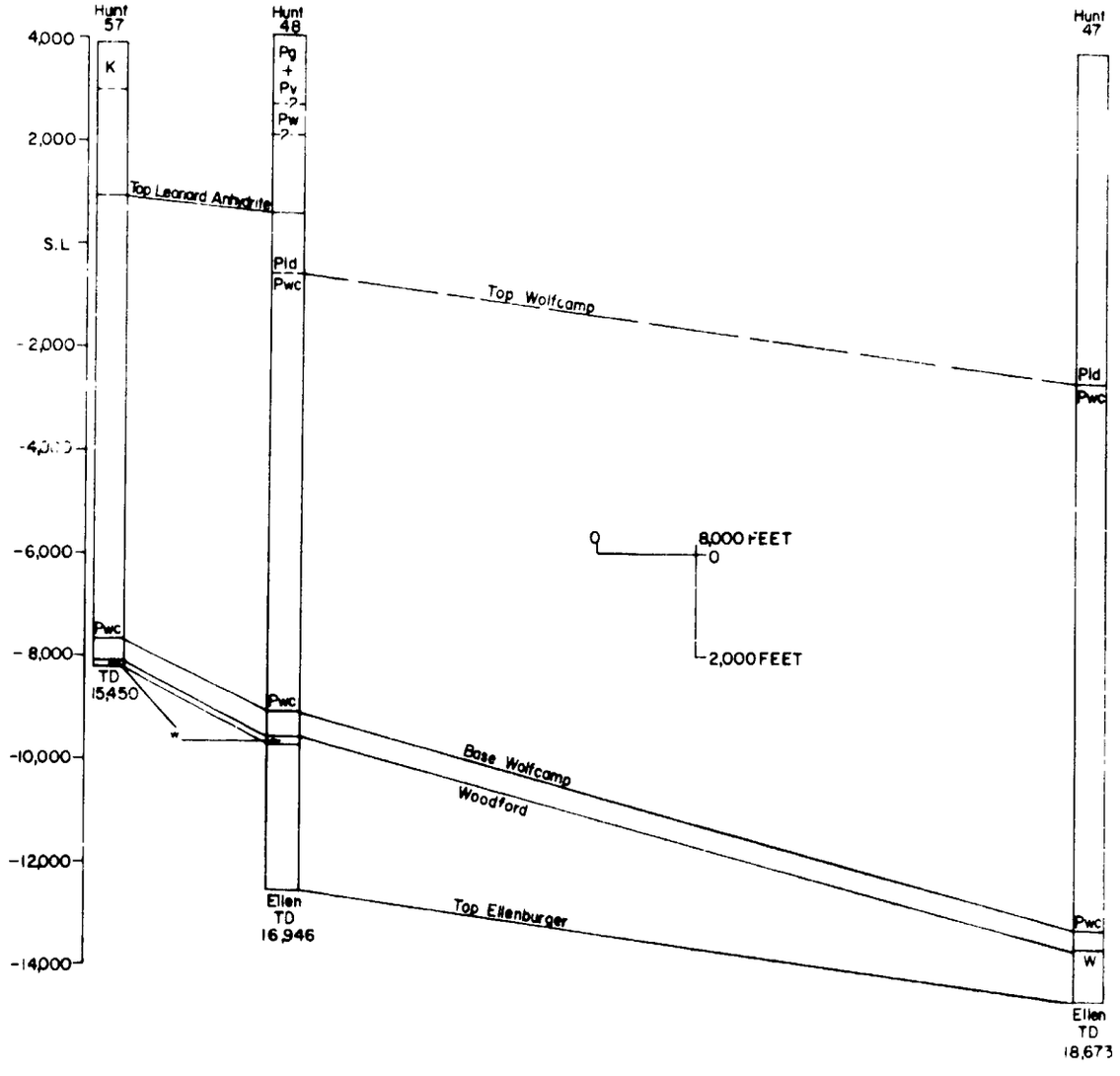
Hunt 57
Hunt 48
Hunt 47
4,000
2,000
S.L
-2,000
-6,000
-8,000
-10,000
-12,000
-14,000
K
Pg + Py
Pw
Top Leonard Anhydrite
Pld
Pwc
Top Wolfcamp
0
8,000 FEET
0
2,000 FEET
TD 15,450
Base Wolfcamp
Woodford
Ellen TD 16,946
Top Ellenburger
W
Ellen TD 18,673

Figure 9.

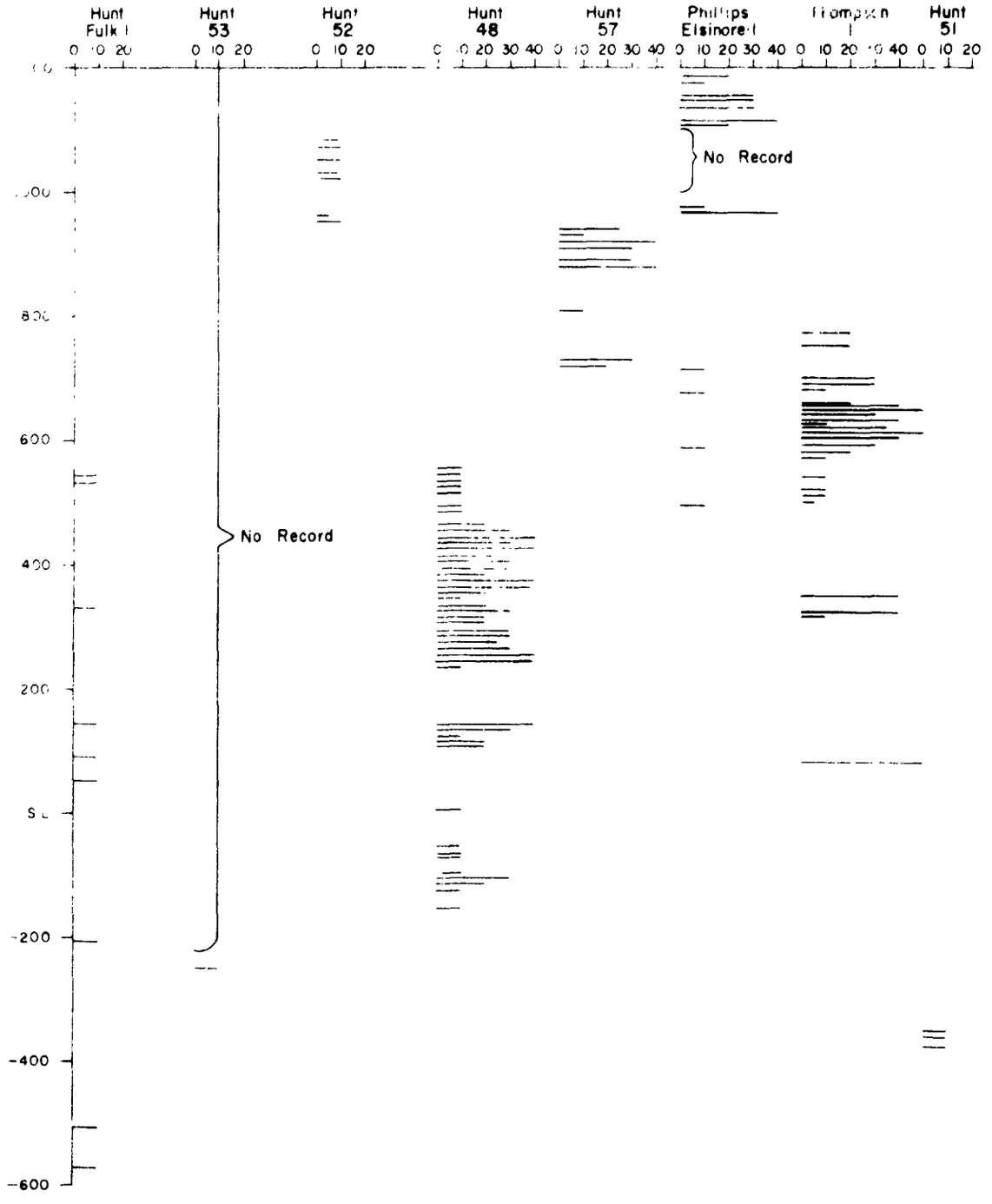
Hunt Fulk 1
Hunt 53
Hunt 52
Hunt 48
Hunt 57
Phillips Elsinore 1
Thompson 1
Hunt 51
No Record
No Record
600
400
200
-200
-400
-600

Figure 10.

in figure 10, which indicates that some caution must be used in correlating specific parts of the anhydritic interval. Although the Wolfcamp and younger formations dip inward from the outer rim of the structure (Hunt 52 and 57, figs. 2 and 7) toward the flank of the inner hill (Hunt 48, figs. 2 and 7), the lowest point of the Leonard-Wolfcamp contact is still about 200 feet above the regional trend. Inspection of the data presented in figures 7-9 shows that no part of the Sierra Madera structure has been displaced downward along the cross-section lines.

Available information on the Cretaceous rocks indicates the presence of local relief at Sierra Madera before deposition of the Cretaceous rocks. The Glen Rose Formation has not been identified in outcrop on the structure, and its closest known occurrence is in the Hunt 51 well. In addition, the Basement Sandstone locally pinches out on the east flank of the inner hill of the structure and in many other places on the east flank is considerably thinner than average. Although these relations indicate pre-Cretaceous deformation at Sierra Madera, this may have been part of the general pre-Cretaceous uplift of the ancestral Glass Mountains (King, 1930).

The area of detailed mapping (Wilshire, 1965) has been extended westward into the Word Formation. The salient facts revealed by this mapping are that the internal structure of the Gilliam Limestone is characterized by small, randomly oriented fold segments isolated by a mosaic of steep faults, and that the gross style of deformation shown by formational contacts is the same in the oldest (Word) as in the youngest (Edwards Limestone) formations in the central part of Sierra Madera.

In accordance with previous work (Eggleton and Shoemaker, 1961), the central hill was shown in figure 3 of last year's Annual Report as a megabreccia core surrounded by a belt of intensely deformed Permian to Cretaceous rocks. The megabreccia core was described by Eggleton and Shoemaker (1961) as consisting of blocks of carbonate rock up to several hundred feet across enclosed in a matrix of

angular fragments that grade progressively downward in size to microbreccia. They stated that in outcrop about half of the breccia is sufficiently fine grained to be recognizable as breccia in hand specimen. In addition, breccia was identified in well cuttings (Phillips Elsinore 1) from the surface to a depth of about 1,600 feet and again in the interval 2,600-2,800 feet beneath the surface.

Several observations made to date make the concept of a megabreccia core in the structure suspect. The boundary of the core as drawn by Eggleton and Shoemaker (1961) corresponds closely to the upper contact of the Vidrio Member of the Word Formation. There is generally an abrupt change at this contact from well-bedded Gilliam dolomites to poorly bedded or unbedded, often brecciated, dolomites of the Vidrio. The Vidrio is succeeded toward the center of the structure by Word limestones in which bedding is not prominent. This change from conspicuously bedded rock to poorly bedded rock gives an impression of a structural change but is in fact a stratigraphic change. Detailed mapping of upper and lower contacts of the Vidrio Member near the Thompson well (fig. 2) shows that the Vidrio conforms to gross structures recognized in the overlying Gilliam. Below the Vidrio, internal structures of the Word limestones are revealed only locally by interbedded dolomites. Although this gives an impression of large, isolated blocks of rock, detailed mapping shows that these are lenticular dolomites interbedded with limestone and not structurally isolated blocks encased in breccia; in fact, the limestones show no conspicuous brecciation at all. Detailed mapping has further shown rapid lateral changes in degree of brecciation of Vidrio dolomite as well as local apparent interbedding of brecciated and nonbrecciated Vidrio dolomites. Both the macroscopic and microscopic characteristics of breccias in the Vidrio are the same as those in the Gilliam dolomites, although the latter were consistently placed outside the megabreccia core by Eggleton and Shoemaker (1961). Accordingly, the information gathered to date indicates no change in style of deformation

throughout the central hill of the structure and lends no support to the concept of a megabreccia core or the inferences based on this concept.

REFERENCES CITED

Bretz, J H., and Horberg, L., 1949, The Ogallala Formation west of the Llano Extacado: Jour. Geology, v. 57, no. 5, p. 471-490.

Dence, M. R., 1965, The extraterrestrial origin of Canadian craters: New York Acad. Sci. Annals, v. 123, art. 2, p. 941-969.

Eggleton, R. E., and Shoemaker, E. M., 1961, Breccia at Sierra Madera, Texas: U.S. Geol. Survey Prof. Paper 424-D, p. 151-153.

Folk, R. L., 1959, Practical petrographic classification of limestones: Amer. Assoc. Petroleum Geologists Bull., v. 43, pt. 1, p. 1-38.

_____ 1962, Spectral subdivision of limestone types, in Classification of carbonate rocks, a symposium: Amer. Assoc. Petroleum Geologists Mem. 1, p. 62-84.

King, P. B., 1930, Descriptive geology, pt. 1 of The geology of the Glass Mountains, Texas: Univ. Texas Bull. 3038, 167 p.

Shoemaker, E. M., 1960, Penetration mechanics of high velocity meteorites, illustrated by Meteor Crater, Arizona: Internat. Geol. Cong., 21st, Copenhagen, 1960, Rept., pt. 18, p. 418-434.

Shoemaker, E. M., and Eggleton, R. E., 1964, Re-examination of the stratigraphy and structure of Sierra Madera, Texas, in Crater investigations, pt. B of Astrogeologic Studies Ann. Prog. Rept., Aug. 1962-July 1963: U.S. Geol. Survey open- file report, p. 98-106.

Short, N. M., 1965, A comparison of features characteristic of nuclear explosion craters and astroblemes: New York Acad. Sci. Annals., v. 123, art. 2, p. 573-616.

Williams, H., Turner, F. J., and Gilbert, C. M., 1958, Petrography: San Francisco, W. H. Freeman & Co., 406 p.

Wilshire, H. G., 1965, Geology of the Sierra Madera structure, Texas: Progress report, in Crater investigations, in Astrogeologic Studies Ann. Prog. Rept., July 1964-July 1965: U.S. Geol. Survey open-file report, p. 1-25.

Wolf, K. H., 1965, Gradational sedimentary products of calcareous algae: Sedimentology, v. 5, p. 1-37.

SOME ASPECTS OF THE MANICOUAGAN LAKE STRUCTURE IN QUEBEC, CANADA

By Stephen H. Wolfe

In northern Quebec, lat 51°28' N., long 68°37' W., two arcuate semicircular lakes, Manicouagan and Mushalagan, outline a nearly perfect circle some 35 miles in diameter. About a mile inside the inside shores of the lakes there is a ring of cliffs averaging 500-1,000 feet in height. Near the center of the ring formed by the lakes, there is an oblong mass of high ground, some points of which are 1,500 feet above the surrounding terrain. This mass is approximately 7 miles in length and 6 miles in width. At the present time, the outlet of the two lakes is being dammed, and the level of the water will be raised about 650 feet. The rising water will make the circularity of the cliff ring more apparent but will inundate some areas quite important to the interpretation of the history of the area. The topography inside the lakes is characterized by a series of "knobs" that trend generally north and rise 500-800 feet above the surrounding terrain. Outside the lakes, the relief of the land surface is somewhat greater (500-1,000 feet), but the hills are generally not as steep and do not show as pronounced a northward trend as the hills between the lakes.

The structure is in the Grenville province of Canada. The underlying basement rocks are Precambrian anorthosites and gneisses. Remnants of Ordovician limestone beds crop out in some places along the inner shores of the lakes; outside the lakes, marbles and iron-rich quartzites (probably Proterozoic) occur sporadically among the gneisses.

The data obtained during about 6 weeks field study, and subsequent petrographic analysis of samples obtained from the area, suggest that the structure is the result of the impact of a large meteoritic mass.

The sketch map (fig. 1) shows the general distribution of the various rock types (Berard, 1962).

The central mountain consists of a coarse-grained plagioclase-pyroxene-garnet rock that has been highly deformed Only about 10 percent of the rock consists of mafic minerals; the remainder is plagioclase, about An_{40}. The mafic minerals are alined in bands which give the rock a gneissic texture. Scapolite, sphene, and zircon are accessory minerals. Rocks of this type, termed anorthosites, are characteristic of the Grenville province. The presence of garnets in the rock may indicate regional metamorphism.

The textures of the deformed anorthosite exposed in the central mountain are unusual. The feldspars are commonly vitrified, the extinction undulatory, and the grains extensively fractured (on the order of 10-100 times as many cleavages per grain as in the undeformed material). The albite twinning of the grains is commonly still visible, although in many grains the twin lamellae show offsets of about one band thickness along fractures. Cores and edges of many grains are vitrified; two types of glass are common: a clear glass, $n = 1.540 \pm 0.002$, and a smokey-brown to a gray glass, $n = 1.531 \pm 0.002$. One specimen is especially noteworthy, sample 7-8-10. The hand specimen appears to be composed mainly of quartz with bands of garnet that give the rock a gneissic texture. The "quartz" is clear and conchoidally fractured, and its hardness is seven. X-ray diffraction patterns of the rock show only peaks identifiable as garnet. In thin section the rock appears to be composed of nearly 90 percent clear glass, $n = 1.540$. The glass displays a system of cracks which appear to represent the original grain boundaries. Small euhedral garnets are extensively fractured, and brown stains coat fractures and grain boundaries. A few grains with high birefringence (0.020) and moderate relief (1.55) give uniaxial negative figures. These appear to be scapolites. A spectrographic analysis of the sample shows an appreciable CaO content, and a set of modes calculated on

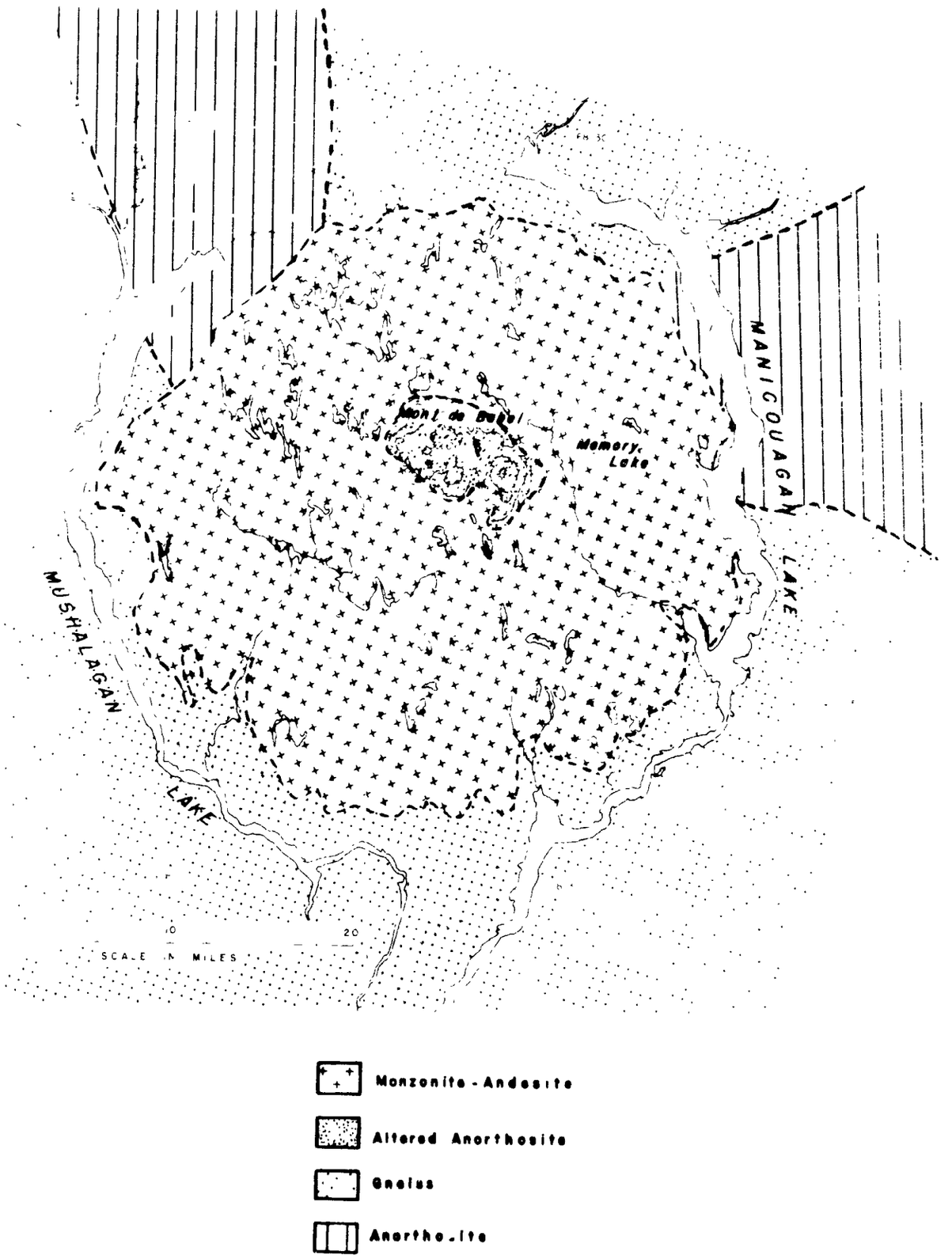

Figure 1.--Geologic sketch map of Manicouagan-Mushalagan Lakes area.

the basis of this analysis is consistent with an anorthosite composition. The rock is concluded to be primarily maskelynite or plagioclase glass. Other samples taken from the central mountain are fractured, contain brown glass, and are partly altered to the clear glass. In addition some of the mafic minerals have been transformed to opaque grains. Patches of brick-red and brown glass appear in veins and veinlets throughout the central mass. Many of these veins seem to be isolated blebs. Fracturing and partial vitrification are widespread features of the rock and apparently occur throughout the part of the central mountain sampled. The area sampled in the central mass includes points less than a quarter of a mile from the center of the mass.

The mode of formation of these rocks is debatable. Milton and DeCarli (1963) have produced similar clear plagioclase glasses by shock-loading samples of Stillwater gabbro to shock pressures of 250-300 kilobars. Currie reported (1965) that glasses resembling the brown to black glasses found at Manicouagan have been produced by rapidly heating amphibole-bearing rocks to 1,100°C. He believed that the clear glass mentioned above could be formed by rapidly heating pyroxene-bearing rocks. Extreme shock as a mode of formation of these textures, since it involves the passage of a rarefaction wave through the medium, would explain the extensive microfracturing observed in the samples.

Exposed around the central mountain is a ring of monzonites and andesites.[1] The monzonite is medium to fine grained, predominantly composed of 0.5-mm laths of plagioclase (An_{40}) rimmed by alkali feldspar. Optical and X-ray measurements suggest that the alkali feldspar is sanidine ($Ab_{10}Or_{90}$). The plagioclase shows

[1]The term "andesite" is applied to the rock on the basis of point counts of the crystalline fraction. A large amount of glass is present, however, and the rock may actually be a latite.

well-developed twinning. The laths are randomly oriented, and some intergranular quartz along with 2- to 3-mm grains of clinopyroxene occur. The rock contains abundant hematite (X-ray determination) and small amounts of hypersthene.

In the field, the monzonite forms the faces of cliffs on many of the knobs described above. In many places the unit forms outcrops several hundred feet thick, and it is generally overlain and underlain by andesites which contain abundant inclusions of deformed basement gneisses and anorthosites. One rather striking feature of the monzonites is their homogeneity throughout the area sampled. In the northwestern half of the ring, samples were obtained from 12 widely separated localities. These specimens are extremely difficult to distinguish from one another, either in hand specimen or in thin section. Slight differences in grain size and percentage of hypersthene are, however, detectable.

The paragenesis of these apparently igneous rocks is a matter of great controversy and is crucial to the correct interpretation of the formation of the structure.

Diamond drilling at the Brent crater in Ontario (Dence, 1965) pierced a layer some 60 meters thick of what appears to be andesite or latite. Rocks which mineralogically resemble the rocks from Brent crop out in West Clearwater Lake, and an analogous layer of rock has been identified by diamond drilling in East Clearwater Lake. Dence (1965) believed that the units from these three craters formed by a process of shock melting and he suggested that the breccia-lava series present at Manicouagan had a similar origin.

Currie (1965) believed that the rocks exposed at Manicouagan are the product of purely terrestrial igneous phenomena. He stated that since the major and minor element concentrations in the rocks are considerably different from those in the underlying basement, the rocks cannot have formed by shock melting. He did not, however, give any data.

Another alternative that has been suggested (Short, 1965) is that the sudden removal of a large volume of material from a crater might result in a pressure release sufficient to melt material somewhere below the crater. This material would subsequently be ejected along some of the many zones of weakness developed during the impact. If it is assumed that Manicouagan-Mushalagan originally had the shape of an explosion crater (and obeyed Baldwin's rules), then for a 35-mile-wide structure (an estimate based on the present diameter), Baldwin's rules would predict a depth of 10^4 feet or about 2 miles. Removing this volume of material would result in a pressure release of about 0.80 kilobars. It is questionable whether such a release would seriously affect equilibrium in the zone where molten material would be formed; however, the possibility is still open, especially if the material in the source region is for some reason very near its melting temperature.

A generalized section follows. It indicates the arrangement of the monzonite-andesite series exposed at Manicouagan. This section represents a slice through a knob whose relief is 1,500-2,000 feet. If the andesites and monzonites at Manicouagan were produced by shock melting, then the impacting body must have melted some 700-800 km^3 of material. Short (1965) calculated, by scaling up the amount of material melted in nuclear explosions, that for a structure the size of Manicouagan, some 200 km^3 of molten material would be produced. Such calculations show at least that the process of shock melting gives the right order of magnitude for material to be produced.

Generalized section of monzonite-andesite units exposed at Manicouagan

Thickness (feet)	Unit
300	Fine-grained andesite containing many inclusions of the basement.
800	Medium- to fine-grained monzonite, few or no inclusions.
400	Fine-grained andesite, containing many inclusions, occasional lenses of glass.
---	Basement gneiss and anorthosite, generally showing little macroscopic deformation.

Note.-The thicknesses shown vary widely from place to place and have not been accurately tabulated. The contacts between the various units are often obscured, but when observable can generally be located to within a few tens of feet, and sometimes to within a few inches.

As has already been mentioned, the fine-grained andesites at the bottom and top of the section contain many inclusions of deformed basement gneisses and anorthosites. These inclusions often weather out of the host rock, and many samples of these inclusions were collected. Large xenoliths, as much as 10-20 meters long, occur in the andesite, and their edges are easily confused with the andesite-basement contact. The inclusions vary in size from meters down to the centimeter and milimeter sizes found in thin sections. Most of the fragments show a rim of partially recrystallized material, which indicates that the andesite was hot at the time of emplacement. Inclusions of gneisses exhibit features observed in shocked granites: undulatory extinction, extensive fracturing, partial vitrification of the grains, and closely spaced parallel fracturing of the quartz grains. Such features have been observed by Short (1965) in granites shocked by nuclear explosions, and by Dence (1965) in rocks from West Clearwater Lake.

Several of the inclusions of shocked gneiss which in thin section seemed to show the most intense deformation were examined for high-pressure polymorphs of quartz. To this date, no coesite or stishovite have been found.

Three major rock units, distinct from the basement units, have been described: 1) the deformed anorthosite from the central mountain, 2) the series of andesites and monzonites found in a ring around the central mountain and inside the two lakes, and 3) the inclusions of deformed basement rocks generally found in the andesites. Of these three, the monzonites and andesites do not show textures stongly indicative of shock metamorphism.

REFERENCES CITED

Berard, Jean, 1962, Summary geological investigations of the area bordering Manicouagan and Mushalagan lakes: Quebec Dept. Nat. Resources, Geol. Survey Prelim. Rept. 489.

Currie, K. L., 1965, Analogues of lunar craters in the Canadian Shield: New York Acad. Sci. Annals, v. 123, art. 2, p. 915-940.

Dence, M. R., 1965, The extraterrestrial origin of Canadian craters: New York Acad. Sci. Annals, v. 123, art. 2, p. 941-969.

Milton, D. J., and DeCarli, P. S., 1963, Maskelynite: formation by explosive shock: Science, v. 140, p. 670-671.

Short, N. M., 1965, A comparison of features characteristic of nuclear explosion craters and astroblemes: New York Acad. Sci. Annals, v. 123, art. 2, p. 573-616.

CRATERS PRODUCED BY MISSILE IMPACTS

By H. J. Moore

INTRODUCTION

A study of craters produced by the impact of missile warheads is being conducted jointly by the U.S. Geological Survey, the Commanding General of White Sands Missile Range, and the Ames Research Center of the National Aeronautics and Space Administration. The U.S. Geological Survey studies and maps the craters and prepares the reports. The Commanding General of White Sands Missile Range allows access to the impact craters, furnishes data on the kinetic energies of the missiles, and provides both ground and aerial photographs of the craters. Ames Research Center assists in mapping some craters and conducts some of the material property measurements.

The purposes of the crater study are to extend our knowledge of impact craters to those produced by projectiles with large kinetic energies and to compare the dimensions and characteristics of the craters with those produced by chemical explosives. In addition, comparison is being made of the morphologies and ejecta of these craters with those of lunar craters seen in the Ranger 7, 8, and 9 photographs as well as those photographed by Russia's Luna 9 and United States' Surveyor 1. The data will also be used for other space projects such as Unmanned Orbiter and Apollo.

This report provides data on impact craters produced by projectiles with energies between 2.10×10^{14} and 3.14×10^{15} ergs. The amount of material displaced during crater formation by projectile impact is nearly the same as the amount of material displaced during crater formation by chemical explosives when the kinetic energy of the projectile (which is corrected for the angle of impact) is equal to the equivalent energy of TNT of the

chemical explosive. The chemical explosives, however, must have small-scale depths of burial for this relationship to hold.

Materials in and around craters produced by missile impacts in cohesive materials may be divided into six mappable units: (1) target material, (2) thin to discontinuous ejecta, (3) thick ejecta, (4) tilted and broken target material, (5) shattered target material, and (6) slope material.

EXPERIMENTAL PROCEDURE

Missiles with kinetic energies between 2.10×10^{14} and 3.14×10^{15} ergs impacted dry to moist sand, alluvium, colluvium, and gypsum lake sediments. The missiles contained no explosives so that only the kinetic energy of the missile was available to form the crater. The projectile always impacted at angles between 58° and 45° from the ground surface. Accordingly, projectile energies must be corrected for the angle of impact. The correction employed was the same as that used for hypervelocity impacts at oblique angles in lead (Bryan, 1962, p. 527) and is equal to the sine of the angle of incidence measured from the ground surface.

Target densities ranged from 1.0 g per cm^3 for gypsiferous alluvium to 1.98 g per cm^3 for gypsum lake beds. Target densities and moisture contents were obtained using techniques outlined in the Earth Manual (U.S. Bur. Reclamation, 1963, p. 442-474). Target strengths measured with a shear vane were between 0 and 6 bars. The shear vanes used were 1.5 and 2.0 inches in diameter, and vane lengths were twice their diameters. Vanes were powered by hand, and the maximum reading on the torque wrench at the time of failure was recorded. Strength was determined using a standard formula (U.S. Bur. Reclamation, 1963, p. 572). Unconfined compressive strengths measured on small blocks and cores compared closely with shear vane strengths measured in the same material. Fenske (1956, p. 16-25) also found this to be true. Thus, the shear vane method is believed to yield a reasonable value for the unconfined target compressive strength. For noncohesive materials,

such as sand, the unconfined compressive strength is zero, but this does not mean the material has no bearing strength since bearing strength is related to the angle of internal friction of the sand, the normal stress exerted by the load, and other factors.

Topographic maps of the craters were prepared using a telescopic alidade, a planetable, a stadia rod, and a tape. Craters were mapped at scales of 1 : 24 and 1 : 48, depending on the size of the crater. Craters 9 and 14 were not mapped.

Crater volumes were obtained from the topographic maps with a compensating planimeter. They include only that portion of the crater below the original ground surface. Displaced mass was then computed by multiplying the density of the target material and the crater volume.

EXPERIMENTAL RESULTS

Crater Morphology and Structures

The relationships between the morphologies and structures of craters and ejecta have been reported previously (Moore and others, 1964), and the present results are essentially the same; therefore, only two craters will be discussed. Data on these and on all others mapped to date are reported in table 1.

Crater 17

Crater 17 was nearly circular in plan view with a rim to rim diameter near 20.6 feet and a depth of 4.6 feet (figs. 1, 2, and table 1). The crater walls sloped gently toward the crater floor except locally where slopes were near 60° and more. Slopes were steep just below the crater rim and on the crater wall underneath the missile trajectory. These steep slopes reflect the unconfined strength of the target material, which was measured as 1 to 3 bars.

Six mappable units of material were recognized in and around the crater. They include (1) target material, (2) thick ejecta, (3) thin to discontinuous ejecta, (4) tilted and broken target material, (5) shattered target material, and (6) slope material.

Table 1.--Data on missile impact craters

	Crater No. and target	Angle of impact	Kinetic energy[1] (10^{14} ergs)	Displaced mass (10^{6} g)	Crater diam[2]	Crater depth[3]
1.	Sand, very fine to medium, noncohesive, density 1.6 g/cm^3.	56.2°	3.62 3.00	0.94	2.86-2.62 9.4 -8.6	0.85 2.8
2.	Sandstone, medium-grained, large cohesion, density 2.5 g/cm^3.	56.8°	5.72 4.81	3.54	3.66-3.23 12.0-10.6	.76 2.5
3.	Gypsiferous sediments, mostly clay with some silt, weakly cohesive, density 1.1 g/cm^3.	50.4°	6.51 5.02	1.3	3.02-2.01 9.9 -6.6	.49 1.6
4.	Alluvium, silt- to clay-size grains, weakly cohesive, density 1.4 g/cm^3.	50.4°	5.92 4.56	2.2	3.66-2.93 12.0 -9.3	.58 1.9
5.	Interbedded gravelly sands and clays, weakly cohesive, density 1.4 g/cm^3.	51.0°	4.58 3.58	1.2	2.68-2.32 8.8 -7.6	.55 1.8
6.	Alluvium, silt with some fine sand, weakly cohesive, density 1.0 g/cm^3.	46.4°	13.8 9.93	7.8	5.36-5.17 17.6-13.7	.98 3.2
7.	Gypsum lake beds, clayey, 20 weight percent water, cohesive, density 1.2-1.6 g/cm^3.	45.9°	15.7 13.3	56.3	9.41-9.11 30.9-29.9	1.98 6.5
8.	Alluvium, silty with some very fine to fine sand, weakly cohesive, density 1.45 g/cm^3.	56.2°	4.23 3.52	2.6	2.5 -2.0 8.2 -6.7	.61 2.0
9.	Not mapped.	---	---	---	---	---
10.	Colluvium, soil with limestone fragments from silt size to several inches across, weakly cohesive, density 1.5 g/cm^3.	56.8°	2.95 2.48	1.2	2.4 -2.0 7.8 -6.5	.61 2.0
11.	Gypsum lake beds, 5-10 percent water, cohesive, density 1.98 g/cm^3.	51°	5.92 4.62	4.5	4.0 -3.1 13.0-10.2	.82 2.7
12.	Alluvium, silt- to sand-size grains, weakly cohesive, density 1.55 g/cm^3.	51°	5.21 4.06	2.0	3.0 -2.0 9.8 -6.6	.76 2.5
13.	Sand, fine to medium, moist, very weakly cohesive, density 1.55 g/cm^3.	51°	6.63 5.17	2.1	3.0 -2.5 9.9 -8.1	.85 2.8
14.	Not mapped.	---	---	---	---	---
15.	Alluvium, gypsiferous, silty, weakly cohesive, density 1.16-1.34 g/cm^3.	45.7°	24.1 17.4	17	5.56-5.69 18.3 -1.87	1.5 4.9
16.	Colluvium, soil with fragments from silt sizes to several inches across, weakly cohesive, density 1.33-1.4 g/cm^3.	45.0°	31.4 22.2	23	6.25-6.33 20.5-20.8	1.6 5.3
17.	Gypsum, silty to medium grained, cohesive, density 1.42-1.46 g/cm^3.	45.0°	19.7 14.0	24	6.21-6.46 20.4-21.2	1.4 4.6
18.	Gypsum sand, fine to medium, well-cemented, cohesive, density 1.40-1.44 g/cm^3.	45.7°	24.1 17.4	25	6.12-6.46 20.1-21.2	1.6 5.2
19.	Clayey silt, gypsiferous, moist, weakly cohesive, density 1.33 g/cm^3.	46°	20.7 14.5	20	5.80-6.34 19.04-20.8	1.59 5.2
20.	Clayey, silty and sandy, gypsiferous in part, very moist, weakly cohesive, density 1.92 g/cm^3.	45.8°	25.2 18.1	36	6.89-7.50 22.6-24.8	1.77 5.8
21.	Soil and colluvium overlying clay and siltstone, upper layers weakly cohesive. Avg. density 1.7 g/cm^3.	58.0°	2.10 1.78	2.5	2.93-3.7 9.6-10.6	.7 2.3

[1]Lower number corrected for angle of impact.
[2]Measurements are from rim crest to rim crest, in meters (upper) and in feet (lower).
[3]Measurements are from original ground surface, in meters (upper) and in feet (lower).

Figure 1.--Photograph of crater 17. Note few blocks in ejecta, gentle slopes of lower crater walls, and steep-slope crater wall beneath the missile trajectory. Open fracture is visible at edge of crater and outward of steep crater wall.

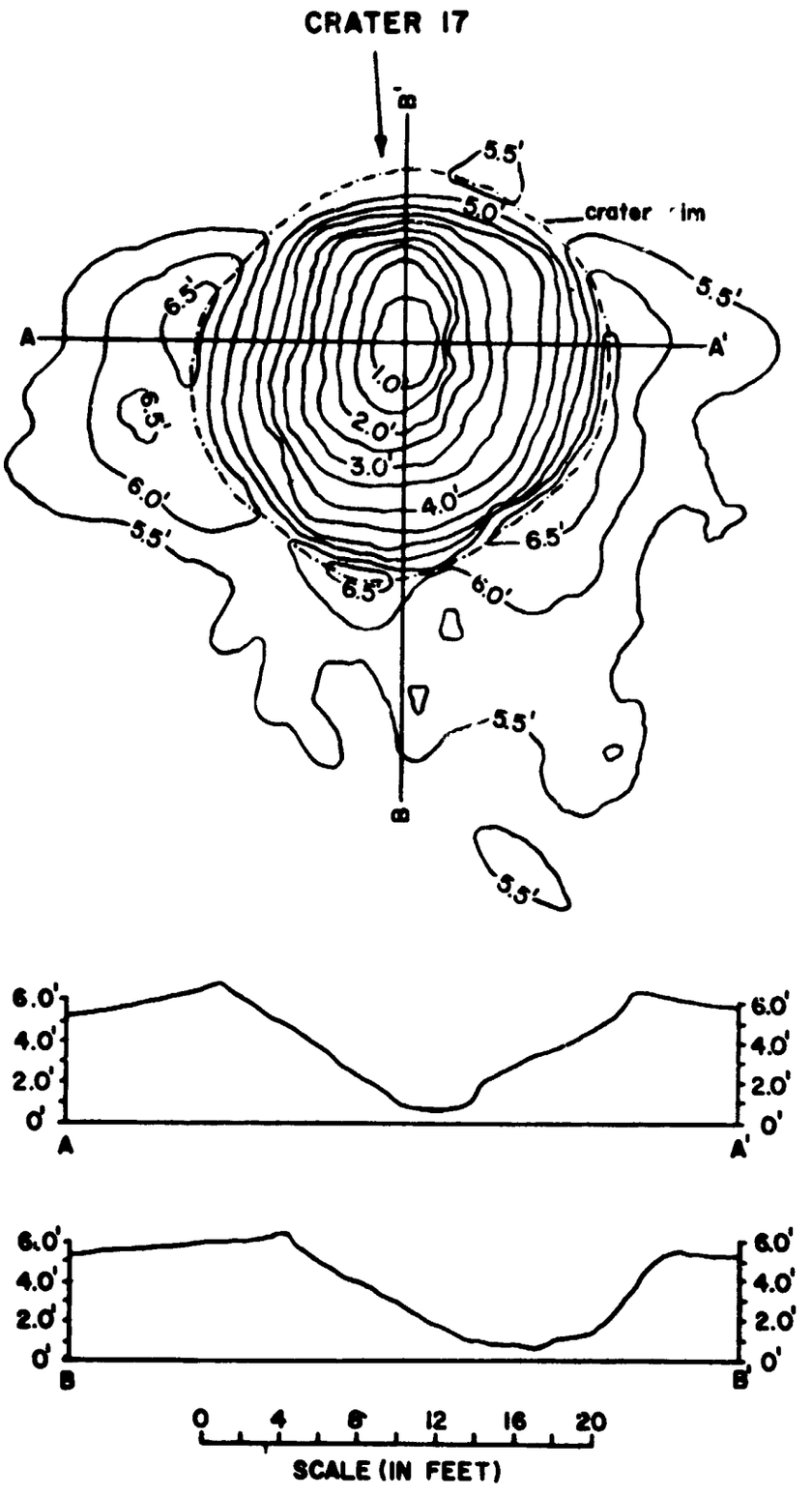

Figure 2.--Topographic map and profiles of crater produced in gypsum by missile impact. Arrow indicates approximate trace of missile path.

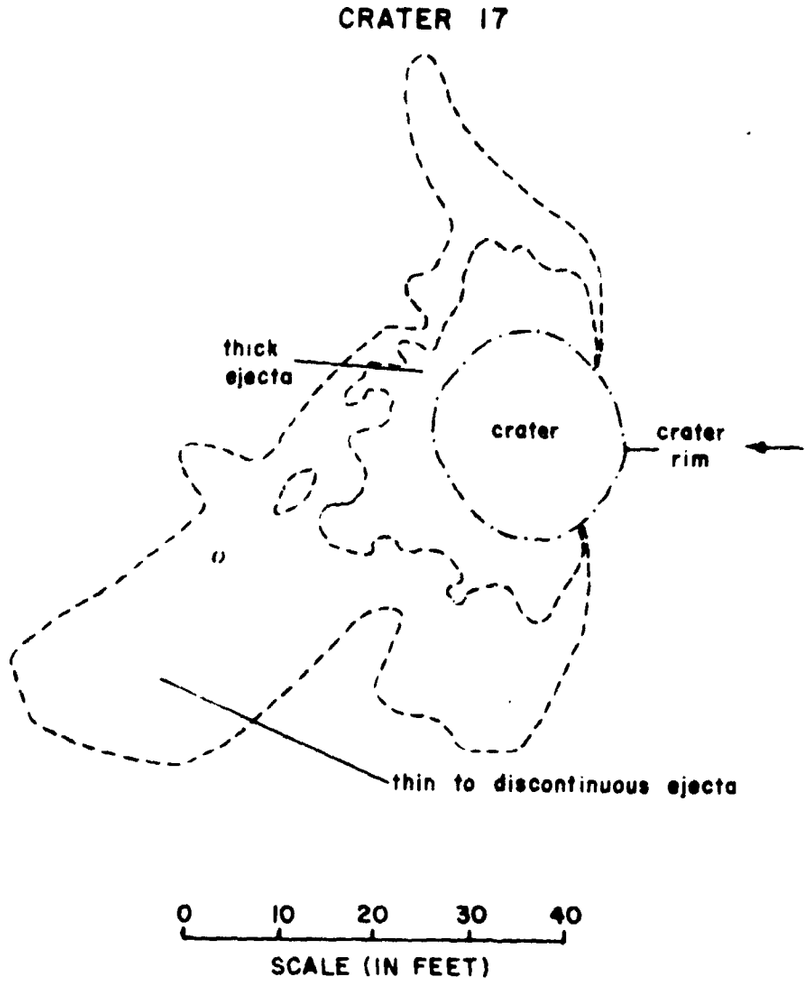

Figure 3.--Map showing ejecta distribution around crater in gypsum. Arrow indicates approximate trace of missile path.

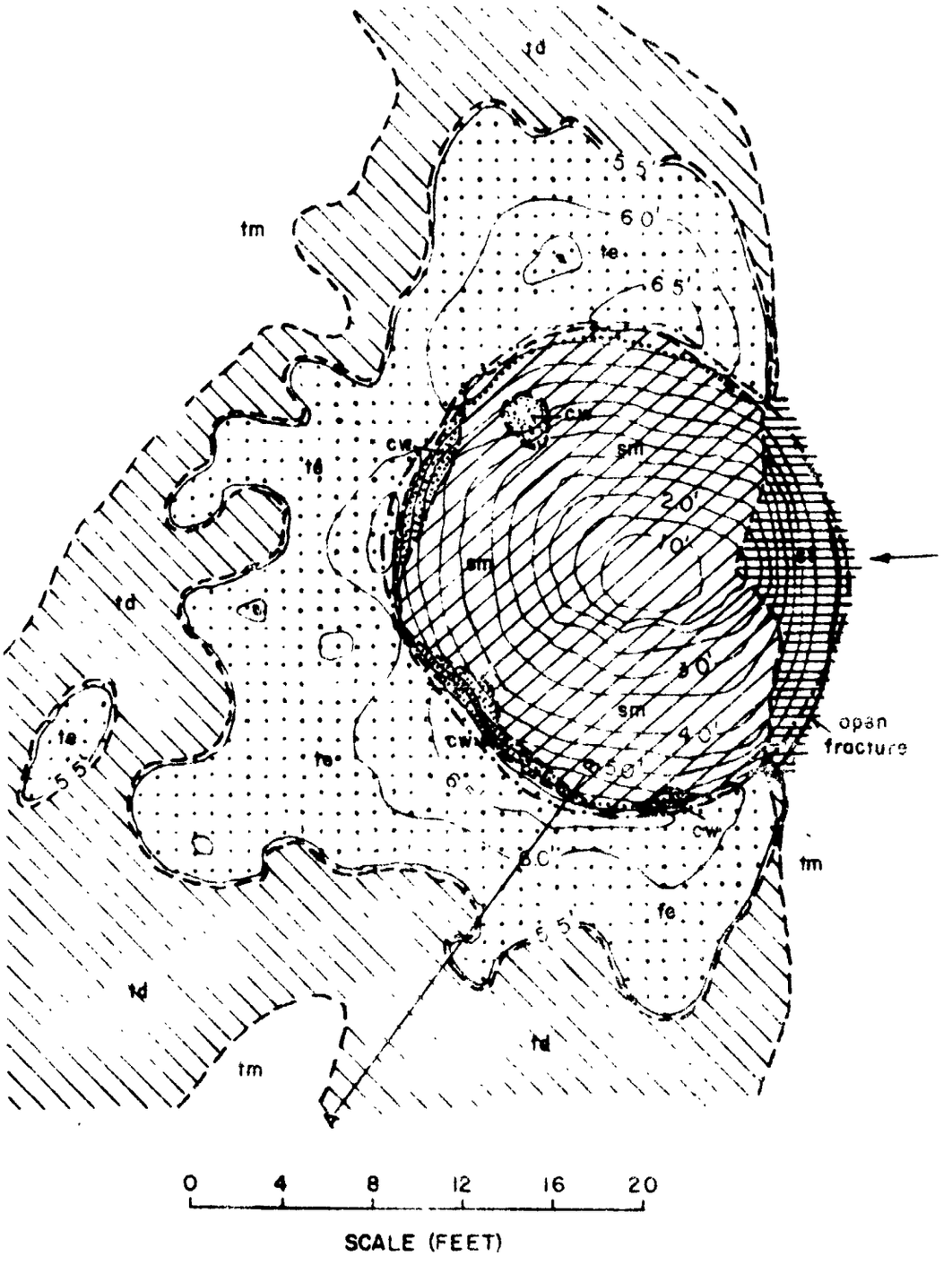

Figure 4.--Map of crater 17 showing lithologic and structural units.

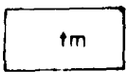

Target material.

Crater wall material, tilted and fractured target material.

Crater wall material, shattered, includes open fractures.

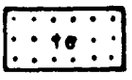

Thick ejecta composed of debris and large blocks ejected from crater, thickness greater than 0.3'.

Thin to discontinuous ejecta, composed of blocks and fragments.

Slope material composed of sand with some rubble.

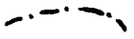

Crater rim.

Contact.

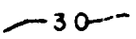

Contour, number indicates elevation above on arbitrary datum in feet.

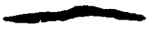

Open fracture.

The distribution of these materials is shown in figures 3 and 4.

Target material.--Target material consisted of undisturbed pale-yellow-gray cohesive gypsum overlain by pale-red-brown soil ranging in thickness from 0 to 18 inches. The pale-yellow-gray material is referred to as the lower soil horizon and the pale-red-brown material as the upper soil horizon in the cross section in figure 5 and later in this report.

The upper soil layer was principally silt (grains between 0.05 and 0.005 mm), and the lower soil layer was silty with some fine sand grains. X-ray diffraction patterns showed that the upper layer soil layer was composed of quartz, calcite, and feldspar and that the lower soil layer was gypsum. The grains of the upper layer were weakly cemented by calcite, whereas the grains of the lower layer were cemented by gypsum. Unconfined strengths were between 1.0 and 3.0 bars. The density of the target material was near 1.44 g per cm^3.

Thin to discontinuous ejecta.--Debris ranging from fine material to fragments a few inches across comprised thin to discontinuous ejecta. Fragments of sheared and compressed target material (see Moore and others, 1964) were found in this unit along with fragments of undeformed target material. Tongues of this ejecta extended at right angles to the missile trajectory up to 44 feet from the crater, and one tongue extended about 60 feet in the forward direction but at 45° to the plane of the missile trajectory (see fig. 3). Thin to discontinous ejecta do not represent the limit of throwout, which is about 400 feet from the crater where a few scattered fragments were found.

Secondary craters produced by the impact of ejecta from the crater were not found. Fragments that were ejected apparently broke upon impact or simply bounced without producing craters.

Thick ejecta.--Debris ranging in size from very fine to blocks up to 1 foot across comprised thick ejecta. The debris was composed principally of relatively undeformed target material from both soil horizons, but sheared and compressed target material

was found in local concentrations. Thick ejecta partly surrounded the crater and was nearly symmetrical about the plane of the missile trajectory. No thick ejecta was present beneath the missile trajectory. Small mounds of thick ejecta composed of fragmental debris were found isolated from the main body of thick ejecta (see figs. 3, 4). The thickness of this material ranged from a maximum of about 2.0 feet at the crater rim to about 0.2 ± 0.1 feet at points distant from the crater.

Small lenses of pale-red-brown ejecta from the upper soil layer were exposed locally on the crater walls (fig. 5). These lenses of ejecta were underlain by tilted target material composed of pale-red-brown soil and overlain by pale-gray ejecta from the lower layers. This inversion of the stratigraphic sequence occured only locally within the ejecta.

Tilted and broken target material.--Material that was not ejected formed the upper crater walls where slopes were greater than 60° in places. This material, which is composed of blocky units of target material, surrounded the crater except along a segment of the wall beneath the missile trajectory. The target material was locally tilted upward as much as 35°. The relationship between tilted target material and ejecta is shown in the cross section (fig. 5).

Shattered target material.--Shattered target material (see figs. 1, 4) was mapped on the crater wall beneath the missile trajectory. Slopes underlain by this material were locally vertical to overhanging, but the average slope was near 60° (see fig. 2). The unit includes several open fractures concentric with the crater edge. These fractures were nearly vertical at the surface (figs. 1, 4).

Slope material.--The most abundant material in the crater was slope material, a continuous spectrum of debris from fine particles to blocks nearly a foot across. Undeformed fragments of target material were dominant, but fragments of sheared and compressed target material were locally abundant. Except at the

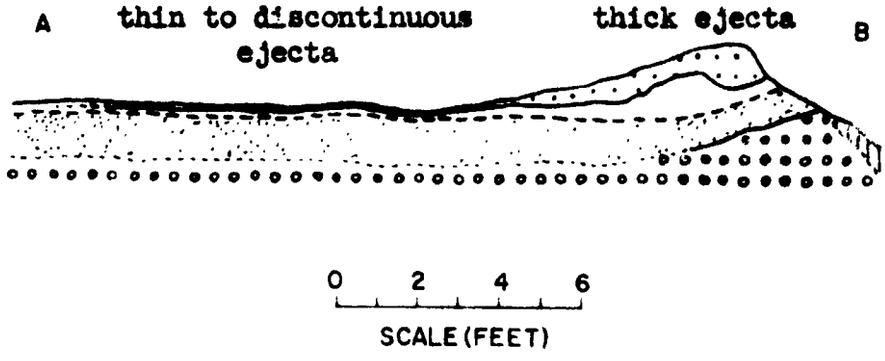

Figure 5.--Section A-B of crater 17 showing inverted layers in ejecta and tilting of ground surface at crater edge. Vertical and horizontal scales are equal.

bottom of the crater, the material formed slopes of nearly 30° because it lacked cohesiveness.

Crater 18

Crater 18 (figs. 6, 7) was similar in many respects to crater 17; however, it differed from crater 17 in that larger blocks were found in the ejecta, the slope material was composed principally of gypsum sand, and a reticulate jointing pattern was observed in the crater wall and in target material beneath the slope material.

The target material was pale-yellow to gray cohesive gypsum sand. The sand was strongly cemented near the surface and well cemented at depth. The target density was near 1.42 g per cm^3. Measurements of the target strengths with the sheer vane were erratic, especially at the surface where unconfined strengths were between 3.0 and 7.0 bars. At lower depths, strengths near 1.0 to 5.0 bars were measured.

Thin to discontinuous ejecta.--Extending as much as 60 feet from the crater in the direction of travel of the missile and as much as 50 feet at right angles to the plane of the trajectory were fingers of thin to discontinuous ejecta (figs. 8, 9). Fragments in this unit were generally larger than those in the same unit of crater 17. Again, secondary impact craters were absent.

Thick ejecta.--Thick ejecta was blocky in contrast with that of crater 17. Blocks up to 2½ feet long were found on the crater rim, and many blocks were more than 1 foot long (see figs. 6, 7). The blocks in the thick ejecta were composed of relatively undeformed target material, although some blocks exhibited open fractures. Smaller fragments in the thick ejecta consisted of relatively undeformed target material, fractured fragments, and sheared and compressed target material.

Crater wall material.--Tilted and broken target material that was not ejected was found in the upper crater walls (fig. 8). Steep walls formed in this unit because of its cohesion. Some

Figure 6.--Photograph of crater 18. Note abundant blocks and large blocks in ejecta, steep upper crater walls, and gentler slopes of lower crater walls.

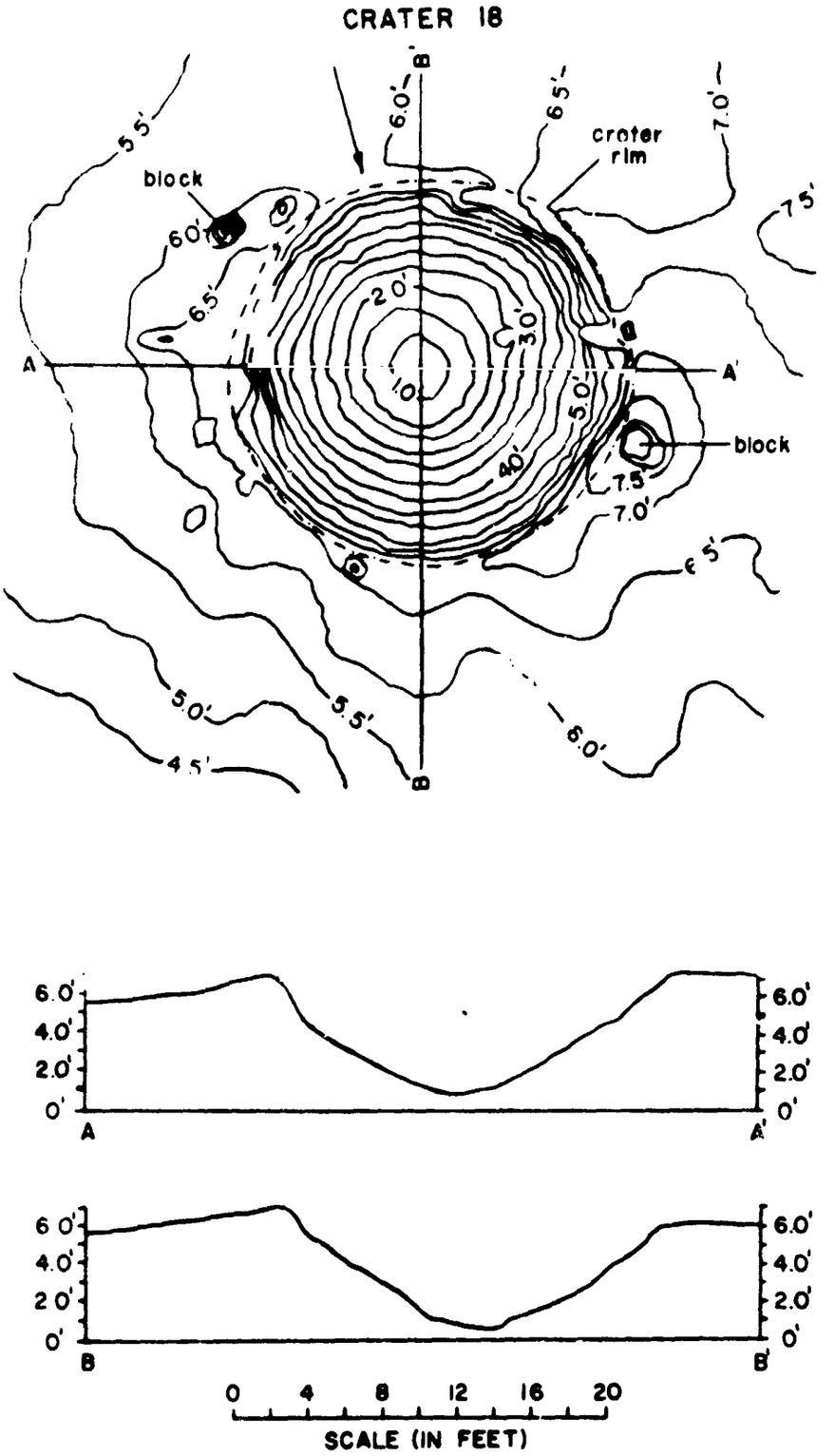

Figure 7.--Topographic map and profiles of crater produced in well-cemented gypsum sand by missile impact. Arrow indicates approximate trace of missile path.

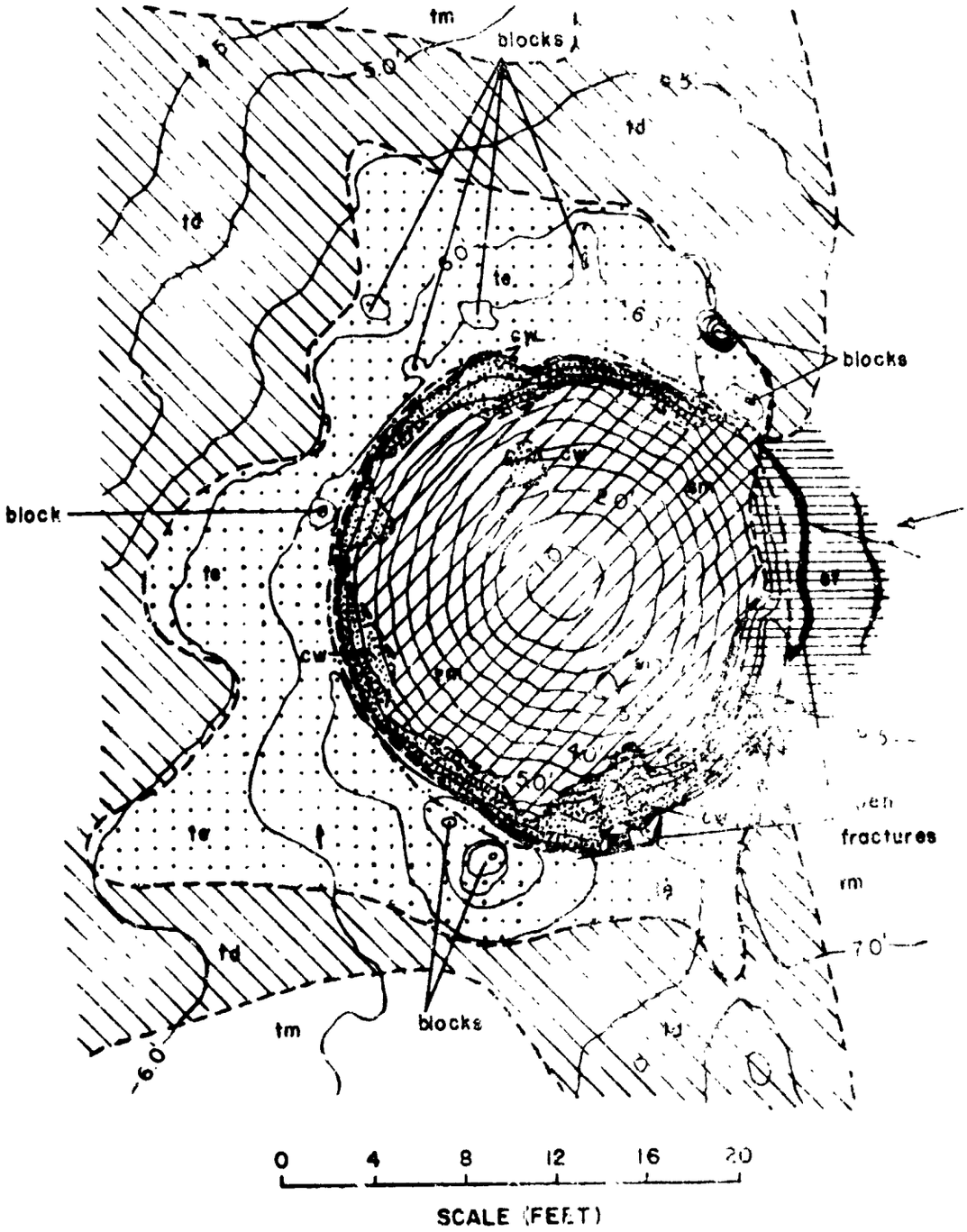

Figure 8.--Map of crater 18 showing lithologic and structural units.

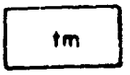

Target material.

Crater wall material, tilted and broken target material, composed of upper and lower soil horizons.

Crater wall material, shattered, includes open fractures.

Thick ejecta composed of debris and a few blocks ejected from crater, thickness greater than 0.3'.

Thin to discontinuous ejecta less than 0.3' thick, composed of debris ejected from crater.

Slope material composed of rubble.

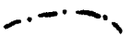

Crater rim.

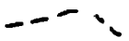

Contact.

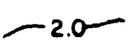

Contour, number indicates elevation above an arbitrary datum in feet.

Open fracture.

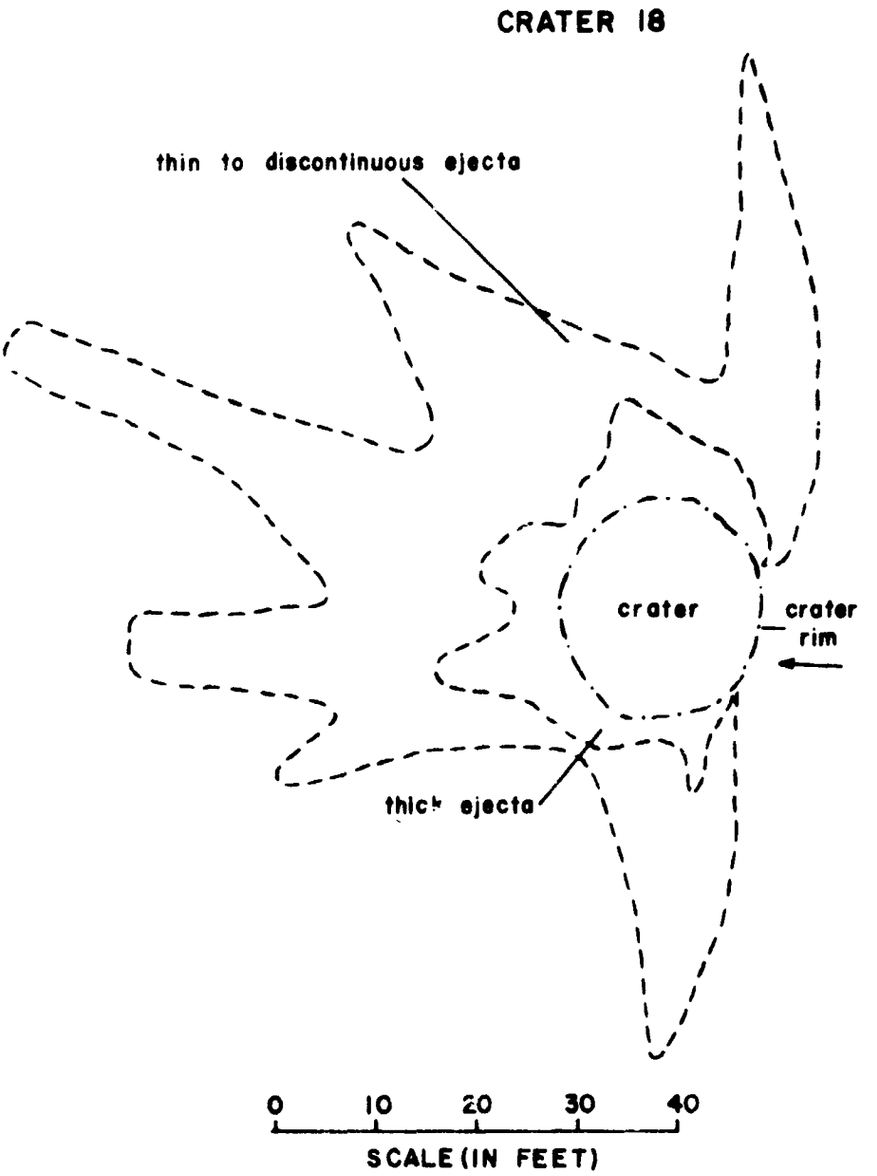

Figure 9.--Map showing ejecta distribution around crater in well-cemented gypsum sand. Arrow indicates approximate trace of missile path. Dashed line indicates ejecta pattern.

reticulate fractures, discussed below, were observed in the unit.

Shattered target material and open tensile fractures were found on the crater wall beneath the missile trajectory (see fig. 8). This unit was not as easily distinguishable as in crater 17.

Slope material.--Slope material was composed principally of desaggregated noncohesive sand of the target material, although a few blocks were present (fig. 6). Stress waves associated with the impact apparently caused breakage along boundaries of grains to produce the sand.

Fracturing.--A trench in the crater wall revealed a reticulate fracture pattern below the crater rim at about 4.8 feet. The fractures were inclined at angles of 57° away from and 3° toward the crater. The angle between the two sets was 60°. Higher (21 inches below the crater rim) in the crater wall in tilted and broken material, a similar but rotated fracture set was inclined 67° and 30° away from the crater. This set represents a fracture pattern produced by the impact and rotated shortly afterward. A P wave could produce such a fracture pattern, and the rotation could be due to the subsequent shear wave. Similar fractures and rotation of fractures have been observed in nuclear craters, and such fracture patterns have been observed around buried explosives (Allsman, 1960).

The limit of fracturing along the plane of the missile trajectory was detected by shear vane at depths near 1.0, 1.7, and 3.4 feet below the ground surface. At a depth of about 1.0 feet, the limit was between 10 and 13 feet from the crater rim where readings changed from about 2.9 to 5.7 bars. Two feet from the crater rim the readings were only 0.7 bars. At a depth of about 1.7 feet, the limit was between 6 to 10 feet where shear-vane strengths changed from 1.0 to 4.7 bars. Below the crater rim, reading was about 0.7 bars at 1.7 feet. At 3.4 feet below the surface the limit was very near 6 feet from the rim where a shear vane measurement of 4.3 bars was obtained; about 3 feet farther toward the crater a value of 1.2 bars was measured.

Comparison with Chemical Explosion Craters

Comparison of the data on missile impact craters indicates that the sizes of these craters are the same as those produced by chemical explosives (see fig. 10 and table 1). This apparently also holds for craters in water-saturated target materials (Moore and Lugn, 1965). However, in contrast with previous reports (Moore and others, 1964), the larger missile impact craters appear to be more comparable with craters produced by explosives at scale depths[1] near 0.5 ft per lb $^{1/3}$ rather than 0.2 ft per lb $^{1/3}$. This change is probably the result of differences in cratering phenomena. Missiles with lower specific energies may break up or only partly collapse. In addition, if they penetrate porous or weak target material they may entirely remain in it. Strong rocks, such as basalt or granite, could cause missiles with lower specific energies to bounce upon impact and produce little or no crater. Missiles with higher specific energies are completely fragmented, and pieces are found in the ejecta, in the crater, and dispersed below the crater. Missiles with higher specific energies would produce craters in all rock types. Such differences in material and projectile properties will result in varying crater dimensions, especially for projectiles with the lowest specific energies.

A sequence of experiments using diatomaceous earth with an unconfined compressive strength near 8 bars and a density near 1.0 g per cm^3 illustrates a wide variety of results under experimental conditions. A projectile (BB) fired from a BB gun into the diatomaceous earth at about 0.12 km per sec produced a tube in the diatomaceous earth about 3 BB diameters deep and 1 BB diameter across. A .22 caliber bullet fired into diatomaceous earth at about 1.5 km per sec produced a cavity filled with fragments of the target material and projectile. This cavity is similar to camouflets

---

[1]The scale depth employed here is equal to the depth of burial of the explosive (in feet) divided by the cube root of the weight (in pounds) of TNT equivalent of the explosive charge.

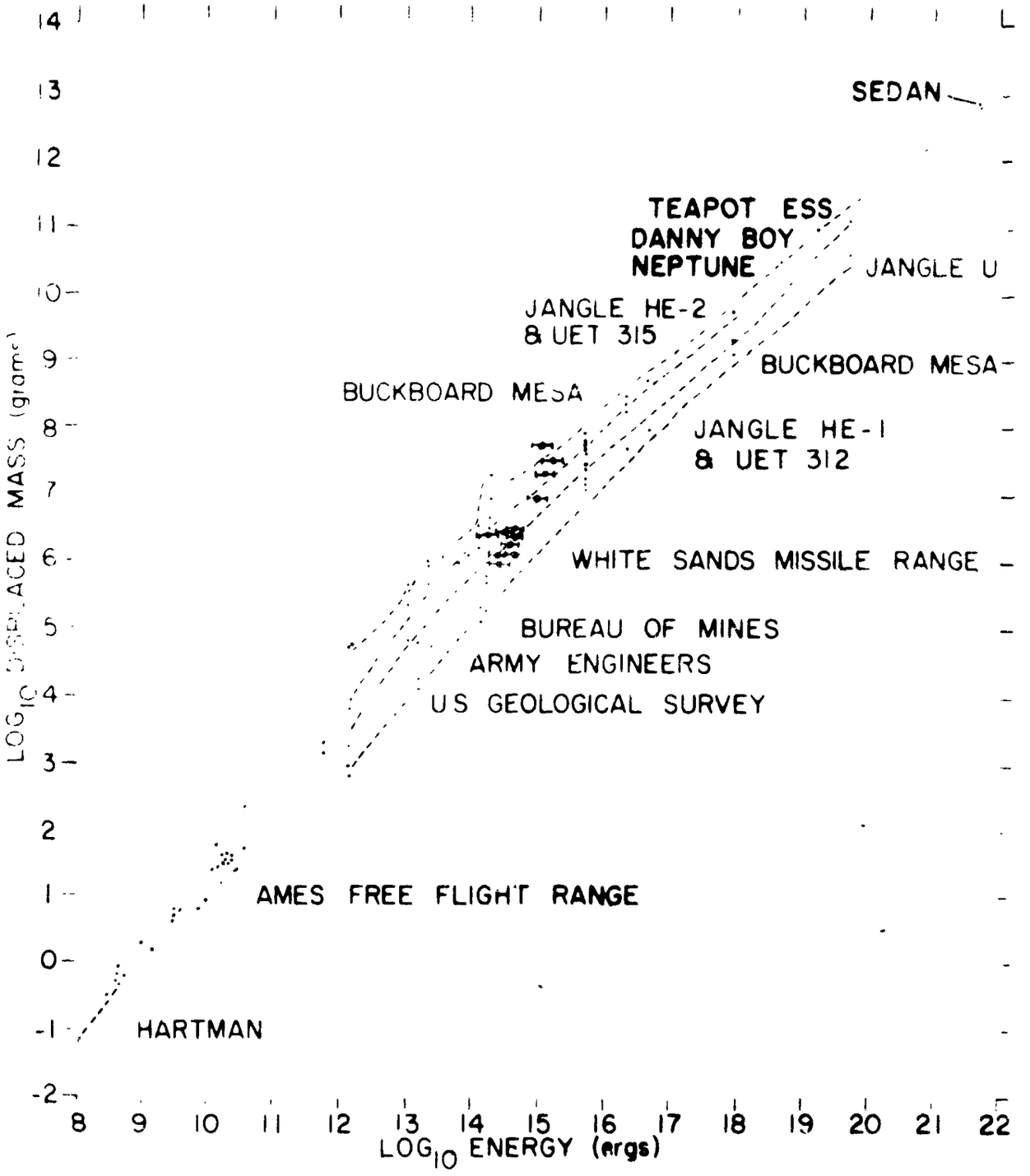

Figure 10.--Comparison between craters produced by impact and craters produced by chemical-nuclear explosives.

produced by deeply buried charges of chemical explosives which do not make craters (see, for example, U.S. Army Corps Eng., 1958). No crater is produced in the diatomaceous earth by the .22 projectile, and only a narrow hole connects the surface of the target block with the breccia-filled cavity. Presumably, a slightly higher projectile velocity would produce a crater with a large breccia cavity beneath it. At hypervelocities (4 km per sec) small projectiles of chrome steel produce craters in diatomaceous earth. In rocks such as the Vacaville basalt (Moore and others, 1964) missiles at velocities of 0.9 km per sec produce craters, but BB's at velocities near 0.12 km per sec simply bounce at impact and no crater is produced. Similar changes may be expected to occur with missile impact craters.

Biggest Block Relationship

Crater 18 provided new information on the maximum block size that may be expected around craters produced by explosives and impacts. The mass of the largest block in this crater (figs. 6, 7) has been plotted along with other data for indurated rocks (see fig. 11 and table 2). Although there is large scatter in the data, larger blocks are clearly associated with larger craters when the material within the crater is indurated. This block size is a function of the strength of the rock and the state of subdivision of the rock. Large blocks can only be expected around craters with large fracture spacings and in strong materials.

Table 2.--Explanation of points plotted in figures 10 and 11

Crater	Description	Reference
Sedan	Crater produced in alluvium at Nevada Test Site by 100 kiloton nuclear device.	Carlson and Roberts (1963).
Jangle U and Teapot ESS	Craters produced in alluvium at Nevada Test Site by 1.2 kiloton nuclear device.	Johnson (1959).
Danny Boy	Crater produced in basalt at Nevada Test Site by 0.42 kiloton nuclear device.	Unpub. data and Nordyke and Wray (1964).

Table 2.--Explanation of points plotted in figures 10 and 11--con.

Crater	Description	Reference
Neptune	Crater produced in tuff at Nevada Test Site by 0.09 kiloton nuclear device.	Shelton and others (1960).
Jangle HE-1, -2	Craters produced in sand and gravel mixture by 2,560 and 40,000 lb of TNT.	Sachs and Swift (1955).
UET 312, 315	Craters produced in dry clay by 2,560 and 40,000 lb of TNT.	Do.
Buckboard Mesa	Craters produced in basalt by 40,000 and 1,000 lb of TNT.	Unpub. data and Vortman and others (1960).
Yucca Flat--Mole	Craters produced in alluvium by 256 lb of TNT.	Murphey (1961), Sachs and Swift (1955).
Bur. Mines	Craters produced in granite and sandstone by 4.5 to 8 lb of TNT.	Duvall and Atchison (1957).
Army Eng.	Craters produced in clay and loess by 0.5 to 1 lb of TNT.	U.S. Army Corps Eng. (1958).
Ames Free Flight Range	Craters produced in basalt, dolomite, limestone, sandstone, and nephrite by hypervelocity projectile impacts at Ames Research Center (NASA), Moffett Field, Calif.	Unpub. data and Gault and others (1963).
Hartman	Craters produced in granite by wedge drill bits with low velocity.	Hartman (1962).
Meteor Crater, Ariz.	Natural crater produced in sandy limestone, dolomite, and sandstone by meteorite impact.	Gilbert (1896).
Dalgaranga, Western Australia	Natural crater produced in granite and laterite by meteorite impact.	Nininger and Huss (1960).
Project Chariot, Alaska	Crater produced in mudstone by 256 lb of TNT.	Kachadoorian (1961).
U.S. Geol. Survey	Craters produced in sandstone by 0.1, 1.0, and 10.0 lb of Hi Velocity Gel.	Unpub. data.
Ries Basin, Germany	Natural crater produced in sedimentary and metamorphic rocks by meteorite impact.	Branca and Fraas (1901).
White Sands N. Mex.	Crater produced in sandstone by missile impact.	Moore and others (1964).

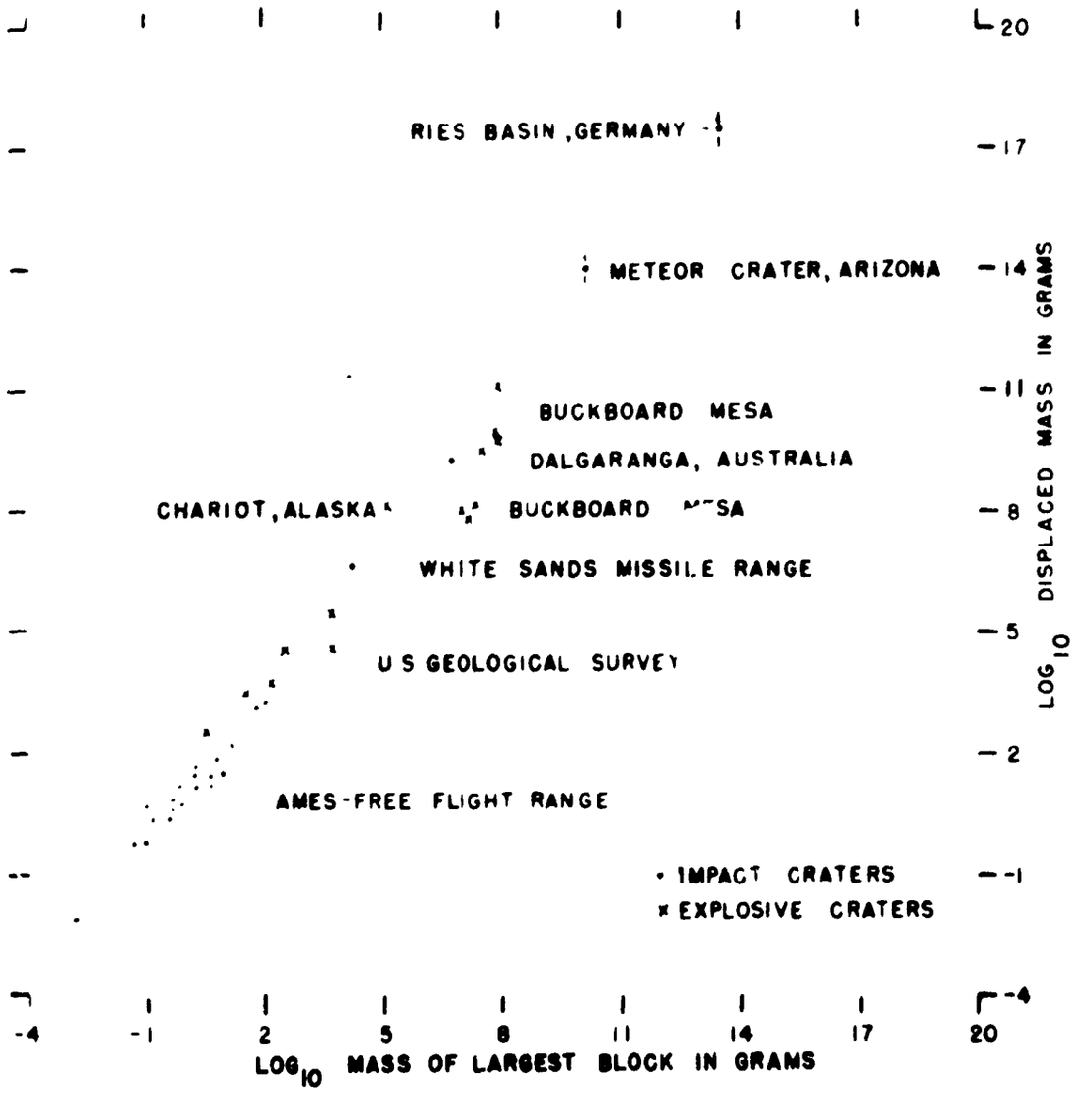

Figure 11.--Relationship between largest block and displaced mass of craters produced by impact and chemical-nuclear explosives in indurated rock.

SUMMARY

1. The materials in and around impact craters in cohesive materials may be mapped and classified in six units with differing properties. The units are: target material, thick ejecta, thin to discontinuous ejecta, tilted and broken target material, shattered target material, and slope material.

2. Missile impact craters are the same size as craters produced by chemical explosives detonated at shallow depths when the kinetic energy of the missile is the same as the TNT energy equivalent of the explosive. However, for missiles with low specific energies, the comparison is probably not valid.

3. Larger blocks may be ejected from larger craters if the rocks are well indurated and relatively unfractured.

REFERENCES CITED

Allsman, P. L., 1960, Analysis of explosive action in breaking rock: Am. Inst. Mining Metall. Petroleum Engineers Trans., v. 217, p. 469-478.

Branca, W., and Fraas, E., 1901, Das vulcanische Ries bei Nördlingen in seiner Bedeutung fur Fragen der allgemeinen Geologie: Akad. Wiss. Berlin Abh., Kl. Phys.-math., 169 p.

Bryan, G. M., 1962, Oblique impact of high velocity steel pellets on lead targets: Hypervelocity Impact Symposium, 5th, Denver 1961, Proc., v. 1, pt. 2, p. 511-534.

Carlson, R. H., and Roberts, W. A., 1963, Mass distribution and throwout studies, Project Sedan: U.S. Atomic Energy Comm., PNE-217F, 144 p.

Duvall, W, I., and Atchison, T. C., 1957, Rock breakage by explosives: U.S. Bur. Mines Rept. Inv. 5356, 52 p.

Fenske, C. W., 1956, Deep vane tests in Gulf of Mexico, in Symposium on Vane Shear Testing of Soils, Atlantic City, N. J., June 22, 1956: Am. Soc. Testing Materials Spec. Tech. Pub. 193, 70 p.

Gault, D. E., Shoemaker, E. M., and Moore, H. J., 1963, Spray ejected from the lunar surface by meteoroid impact: Natl. Aeronautics and Space Adm. Tech. Note D-1767, 39 p.

Gilbert, G. K., 1896, The origin of hypothesis, illustrated by the discussion of a topographic problem: Science, v. 3, no. 53, pl. 13.

Hartman, H. L., 1962, Crater geometry relations in percussive drilling: Mine and Quarry Eng., v. 28, p. 530-536.

Johnson, G. W., 1959, Mineral resource development by the use of nuclear explosives: U.S. Atomic Energy Comm., UCRL-5458, p. 10.

Kachadoorian, Reuben, 1961, Geologic results of November 1960 Project Chariot high explosive cratering experiment, Cape Thompson, Alaska: U.S. Geol. Survey Prof. Paper 424-D, p. D368-D371.

Moore, H. J., Kachadoorian, Reuben, and Wilshire, H. G., 1964, A preliminary study of craters produced by missile impacts, in Crater investigations, pt. B of Astrogeologic Studies Ann. Prog. Rept., July 1963-July 1964: U.S. Geol. Survey open-file report, p. 58-92.

Moore, H. J., and Lugn, R. V., 1965, A missile impact in water-saturated sediments, in Crater investigations, pt. B of Astrogeologic Studies Ann. Prog. Rept., July 1964-July 1965: U.S. Geol. Survey open-file report, p. 101-125.

Murphey, B. F., 1961, High explosive crater studies--desert alluvium: U.S. Atomic Energy Comm., SC-4614 (RR), p. 5-6.

Nininger, H. H., and Huss, G. I., 1960, The unique meteorite crater at Dalgaranga, Western Australia: Mineralog. Mag., v. 32, p. 619-639.

Nordyke, M. D., and Wray, W., 1964, Cratering and radioactivity results from a nuclear cratering detonation in basalt: Jour. Geophys. Research, v. 69, no. 4, p. 625-689.

Sachs, D. C., and Swift, L. M., 1955, Small explosion tests, Project Mole, final report on Project no. PU-876: Menlo Park, Calif., Stanford Research Inst., 2 v.

Shelton, A. V., Nordyke, M. D., and Goeckermann, R. H., 1960, The Neptune event, a nuclear explosive cratering experiment: U.S. Atomic Energy Comm., UCRI-5766, p. 3-5.

U.S. Bureau of Reclamation, 1963, Earth manual: 1st ed., Washington, U.S. Govt. Printing Office, 783 p.

U.S. Army Corps of Engineers, 1958, Cratering effects of surface and buried HE charges in loess and clay: Vicksburg, Miss., U.S. Waterways Expt. Sta. Tech. Rept. 2-482, 69 p.

Vortman, L. J., Chabai, A. J., Perret W. R., and Reed, J. W., 1960, Project Buckboard: U.S. Atomic Energy Comm., SC- 486 (RR), 76 p.

HYPERVELOCITY IMPACT CRATERS IN PUMICE

By H. J. Moore and F. G. Robertson

INTRODUCTION

The U.S. Geological Survey and Ames Research Center, Moffett Field, Calif., have been studying craters produced by impacts of hypervelocity projectiles with pumice as part of a cooperative program of research. This paper discusses the results of the studies using pumice blocks as targets.

Preliminary results indicate that the sum of ejected and fragmented material from craters produced by the impact of hypervelocity projectiles with pumice at velocities between 3.95 and 7.66 km per sec is proportional to the momentum of the projectile (corrected for the ratio of projectile and target densities). This momentum dependence is also suggested in the size distributions of the sum of the ejecta and fragmented pumice from the crater, as well as in the amount of crushed and partly fused pumice in the debris. This momentum dependence may only represent a transition between low-velocity impacts and hypervelocity impacts. The results contrast with those for craters in solid materials such as basalt and metals for which sizes are essentially dependent on the kinetic energy of the projectile.

The size distribution and petrography of the pumice debris imply that irreversible energy losses due to new surface and fusion may be the main factors in producing the momentum dependence of the sizes of craters in pumice.

EXPERIMENTAL PROCEDURE

Pyrex spheres 1/8 inch in diameter, iron cylinders 1/8 inch in diameter, and polyethylene cylinders 20 mm in diameter were fired at pumice blocks with light-gas guns (Charters and others, 1957; Curtis, 1962) in an atmosphere of air or nitrogen at pressures from

1 to 380 mm of mercury. The experiments were performed at the Free Flight Range of the Ames Research Center, Moffett Field, Calif., under the supervision of E. D. Heitowit and D. E. Gault. Metal and pyrex projectiles were mounted in nylon sabots which guided the projectiles down the launching tube and were separated from the projectiles after launch by aerodynamic drag. Projectile velocities, determined to within ± 0.01 km per sec by spark photography, ranged from 3.95 to 7.66 km per sec, and projectile kinetic energies ranged from 0.288×10^{10} to 127×10^{10} ergs. The projectiles impacted planed target surfaces at normal incidence.

Pumice targets were obtained from the U.S. Pumice mine near Lee Vining, Calif. The density of the pumice ranged from 0.48 to 0.76 g per cm^3. The pumice was banded and vesicular, with vesicles ranging in size from $1.5 \times 1.5 \times 4$ mm to $0.02 \times 0.02 \times 0.27$ mm. The vesicles were alined parallel to the banding. The pumice was composed chiefly of glass; a fraction of a percent consisted of microlites. The pumice was composed of the following (in percent):

SiO_2	75.7
Al_2O_3	13.0
Na_2O	4.0
K_2O	4.5
$H_2O(+)$	.71
Fe_2O_3	.626
FeO	.44

Minor amounts of MgO, $H_2O(-)$, TiO_2, P_2O_5, and MnO were also present.

Size distributions of ejected pumice, as well as fragmented pumice remaining in the crater, were obtained individually for six experiments. The fragmented pumice remaining in the crater was removed by dumping the loose material into water and gently washing out the crater. Standard sieving screens and techniques were used in conjunction with settling and centrifuging to obtain the size distributions of the debris. Indicated recoveries obtained by comparing the target mass loss with

mass recovered were between 85.3 and 98.1 percent for the experiments. Losses were not confined to the finest portions since large pieces adhered to the tape binding one side of the collection box and were not recoverable.

Masses of pumice fragmented and ejected were computed from: (1) the weight lost by the target block after impact and (2) the weight of recovered ejecta and fragmented pumice removed from the crater. Volumes were determined by computation from the masses and target densities.

DESCRIPTION

Small craters in pumice resemble bottles; initial crater walls are overhangs. The upper walls of larger craters are spall surfaces; their initial slopes are less than 30°. Steep crater walls and overhangs are found below the spalled surfaces. Photographs of craters in pumice have appeared previously (Moore and others, 1964, p. 128-129). Depth to diameter ratios for small craters are near 1 to 0.6, whereas ratios for larger craters are near 1 to 1.2.

Comparison of the size distributions of ejecta and fragmented pumice from the craters reveals the presence of many spalled fragments from the large craters and their absence in the ejecta and fragmented pumice from small craters (compare figs. 1 and 2). The histograms of the size distributions, however, suggest that the fragmentation of the pumice was similar for sizes less than 2.8 to 5.6 mm. Inspection of the coarse ejecta from the large craters shows that many fragments have the flat surfaces of the planed face of the target block and were formed by spalling. Indeed, many of these large pieces may be replaced in the crater in "jigsaw puzzle" fashion. The mode in the histograms near 0.125 mm is probably related to the modal distance between vesicles in the pumice.

Much of the ejecta is composed of aggregates of pumice that have been intensely crushed and partly fused, but most fragments are unaltered. Photographs of the aggregates of crushed and fused pumice have appeared previously (Moore and others, 1964, p. 140-143).

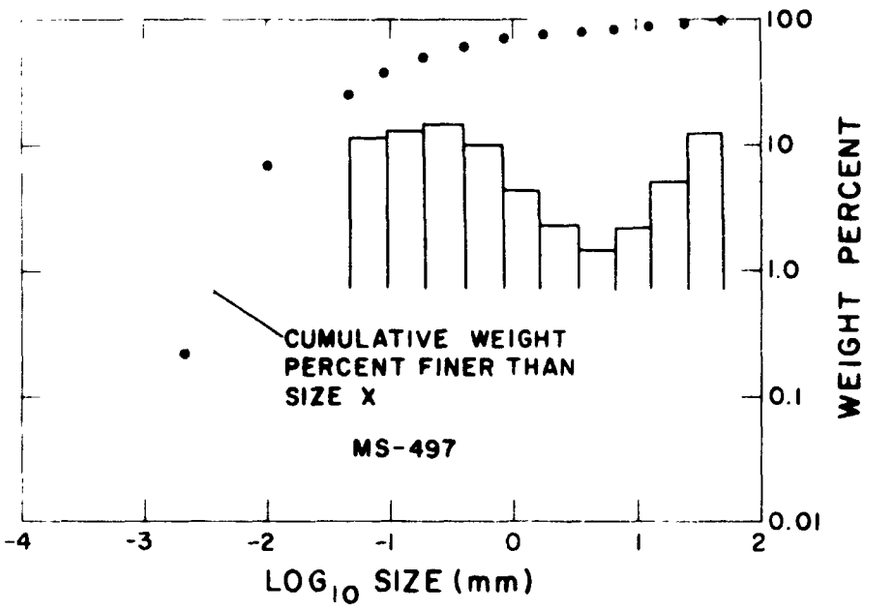

Figure 1.--Ejecta and fractured pumice from large crater in pumice. Note presence of abundant spalled fragments in coarsest sizes.

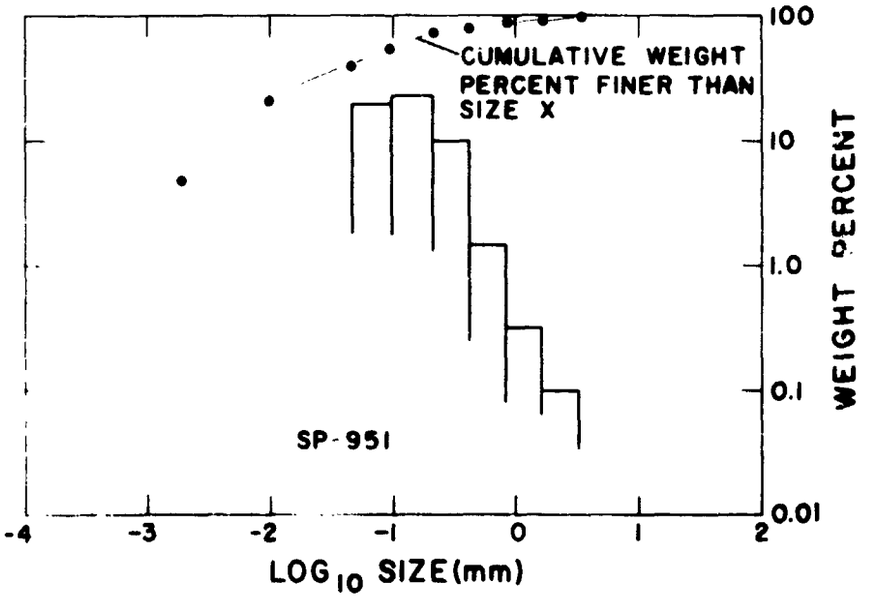

Figure 2.--Ejecta and fractured pumice from small crater in pumice. Note absence of spalled fragments in coarsest sizes.

Petrographic studies of the aggregates of crushed and partly fused pumice show that about 25 percent of the ejecta and fragmented pumice from craters produced at the highest velocities is composed of this material. In addition, the amount of crushed and fused aggregate is nearly proportional to the projectile velocity.

CORRELATION OF DATA

The data were correlated by comparing projectile properties with: (1) the sum of the masses of ejected pumice and fragmented pumice removed from the craters, (2) the sum of the volumes of ejected pumice and fragmented pumice, (3) the results of size-distribution analyses, and (4) the results of petrographic analyses. No attempts were made to correlate the ejecta, alone, with projectile properties because of the erratic behavior of the ejecta.

Initial attempts at correlation were based on previous works, such as those for craters in metals (Summers, 1959), for shaped charges (Birkhoff and others, 1948), and for craters in rocks (Moore and others, 1965). Subsequent refinements were made by trial and error. For the two largest craters (table 1), it was necessary to account for spalling, which is virtually absent in the smaller craters. Even this procedure did not remove scatter, because one experiment produced a very large crater (table 1, MS-498).

Mass of ejected and fragmented pumice.--Comparison of the data (see table 1) on the sum of the masses of ejecta and fragmented pumice removed from the crater with the kinetic energy of the projectile (corrected for the density ratio) revealed no simple correlation (see fig. 3). Inspection of the data for pyrex projectiles (fig. 3) suggested that some function proportional to the projectile momentum might be appropriate.

A relationship between the ejected and fragmented pumice and projectile momentum, which has been corrected for the projectile and target density ratio, proved to be a reasonable correlation of the data, provided that the effect of spalling for the largest

Table 1.--Data on hypervelocity impact craters in pumice

[All targets were pumice from Mono Craters, Calif.]

Target		Projectile				Crater	
No.	Density (g per cm^3)	Material[1] and mass (g)	Shape[2] and diam	Velocity (km per sec)	Kinetic energy (10^{10} ergs)	Depth (cm)	Ejected and total[3] mass (g)
			in.				
SP732	0.67	Py, 0.0368	S, 1/8	6.49	0.775	2.9	1.4, nd
SP943	.52	Py, .0370	S, 1/8	4.33	.346	3.6	.60 2.43
SP944	.55	Py, .0368	S, 1/8	5.31	.519	3.8	.46 3.25
SP945	.46	Py, .0367	S, 1/8	6.66	.815	3.2	2.08 3.22
SP946	.50	Py, .0369	S, 1/8	6.58	.80	3.4	1.98 3.82
SP947	.51	Py, .0368	S, 1/8	nd	nd	3.5	.58 2.24
SP948	.48	Py, .0370	S, 1/8	6.74	.839	3.2	1.63 3.56
SP949	.48	Py, .0369	S, 1/8	5.22	.501	4.1	.95 3.21
SP950	.55	Py, .0369	S, 1/8	4.5	.376	3.2	.69 2.62
SP951	.50	Py, .0369	S, 1/8	3.95	.288	4.0	.51 2.11
SP952	.47	I, .1248	C, 1/8	5.28	1.74	4.9	4.60 9.00
SP953	.52	I, .1264	C, 1/8	5.36	1.81	4.0	7.43 8.32
SP954	.55	Py, .0369	S, 1/8	6.84	.86	3.3	1.68 3.70
SP955	.55	I, .1235	C, 1/8	5.35	1.77	5.2	2.48 8.93
			mm				
MS497	.76	Po, 4.25	C, 20	5.24	58.2	13.7	491
MS498	.76	Po, 4.33	C, 20	7.66	127	15.8	1,444.5

[1]Py, pyrex; I, iron; Po, polyethylene.
[2]S, sphere; C, cylinder.
[3]Total mass includes ejected mass and fragmented mass removed from crater.

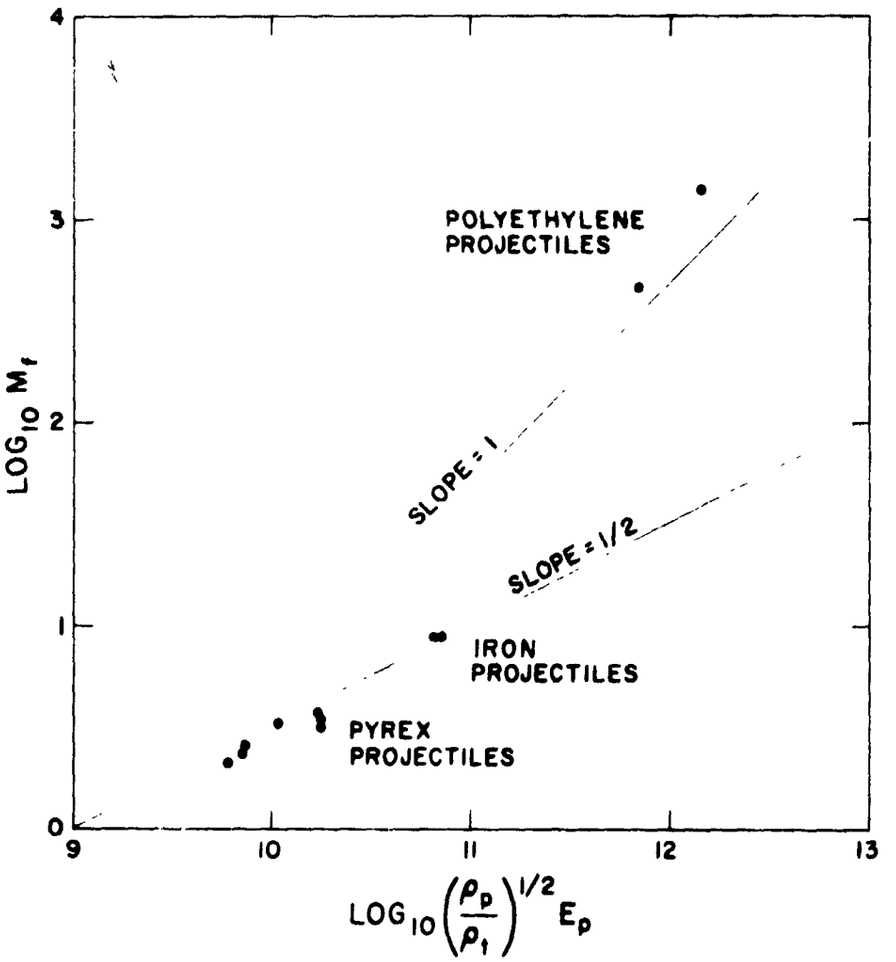

Figure 3.--Comparison of sum of ejected and fragmented pumice from craters with the kinetic energy of the projectiles (corrected for the density ratio).

craters was taken into account (see fig. 4). The equation for the line in figure 3 is:

$$M_f = 10^{6.26} \left[\frac{\rho_p}{\rho_t}\right]^{-1/8} m_p V_p \qquad (1)$$

where:

M_f = mass of ejecta and fragmented pumice from craters (grams)
ρ_p = projectile density (g per cm^3)
ρ_t = target density (g per cm^3)
m_p = projectile mass (grams)
V_p = projectile velocity (cm per sec).

The exponent of the density ratio term was obtained by trial and error using equations derived from those like equation 1:

$$\frac{M_f}{E_p} = -0.9 \left[\frac{\rho_p}{\rho_t}\right]^{+1/8} V_p + 11.71 \qquad (2)$$

where:

E_p = kinetic energy of the projectile (10^{10} ergs)
M_f = mass of ejected and fragmented pumice from crater (grams)
V_p = velocity of projectile (km per sec).

It was found that, for the density ratio term of equation 2, exponents of 1/4 and 0 introduced more scatter of the data points for the various projectile types than an exponent of 1/8 (see fig. 5). However, the largest crater produced in pumice by a polyethylene projectile could not be correlated with the terms used above. This will be discussed later.

Volume.--Equation 1 can be recast to yield equations similar to those used for cratering experiments in metals (Charters and Summers, 1959). An equation which approximately fits the data is:

$$\frac{Vol_f}{Vol_p} = 18.5 \left[\left(\frac{\rho_p}{\rho_t}\right)^{7/4} V_p^{\,2}\right]^{1/2} \qquad (3)$$

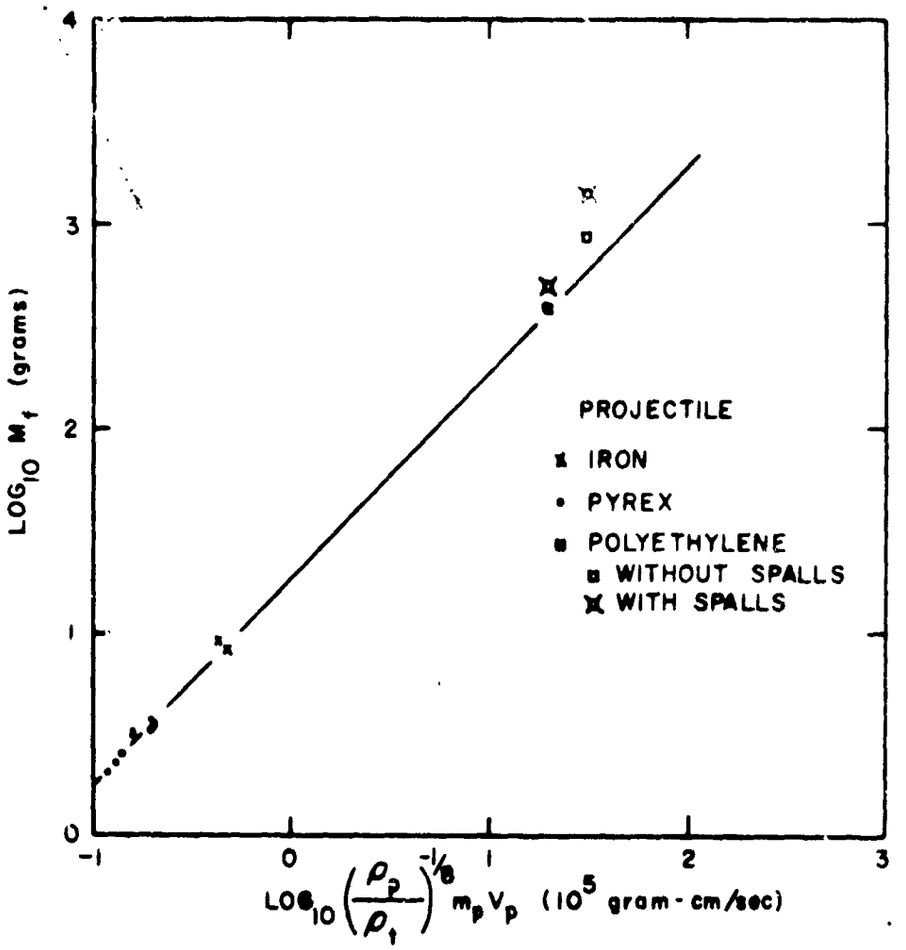

Figure 4.--Comparison of the sum of ejected and fragmented pumice from craters with the momentum of the projectiles (corrected for the density ratio).

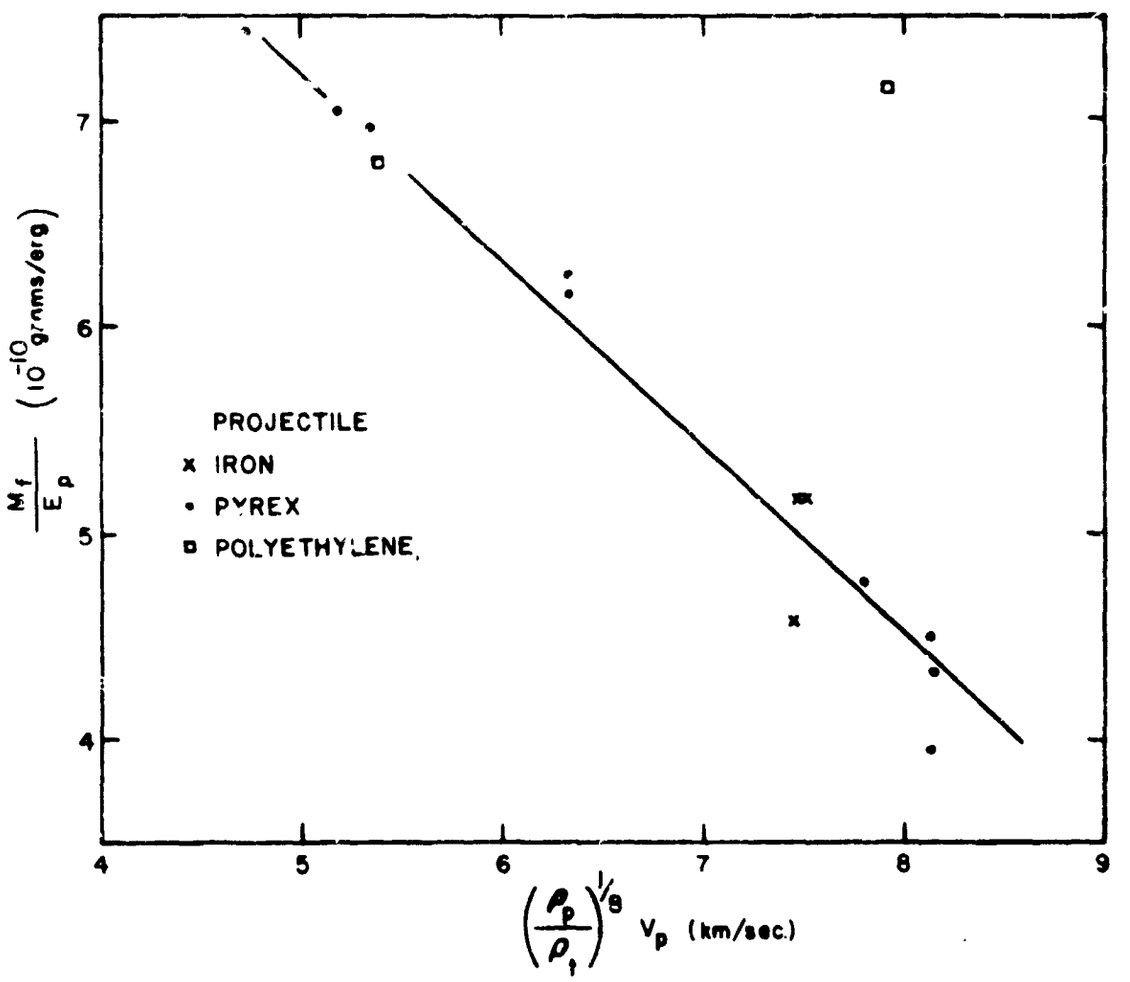

Figure 5.--Comparison of ejected and fragmented pumice and kinetic energy of projectile with velocity of projectile and density ratio.

where:

V_p = velocity of projectile (km per sec)

Vol_f = volume of ejecta and fragmented pumice

Vol_p = volume of projectile.

The correlation of the data (fig. 6) is reasonable, except for the largest craters produced by polyethylene projectiles. The second largest crater can be correlated if the material due to spalling is taken into account.

Size distributions.--Comparison of the volume of fragmented pumice passing a screen with 1.0 mm openings and projectile properties (fig. 7), yields an equation similar to equation 3:

$$\text{Vol passing 1.0 mm screen} = 16.2 \left[\left(\frac{\rho_p}{\rho_t}\right)^{7/4} V_p^{\,2}\right]^{1/2}. \quad (4)$$

Again, the largest crater which was produced by polyethylene does not correlate.

The form of equation 4 also adequately describes the volume of fragmented pumice passing screens with 0.10 and 0.043 mm openings. For these screen sizes the constants become 11.5 and 6.3 respectively.

The size of openings in screens which will pass one gram of fragmented pumice is nearly inversely proportional to the momentum of the projectile (see fig. 8). No endeavor has been made in figure 8 to alter the density ratio exponent, since the relationship is adequately illustrated. However, a smaller exponent would be appropriate as in equation 2.

Spalling.--Inspection of the size distributions of ejecta from large and small craters in pumice (figs. 1, 2) reveals that they differ markedly in the coarse sizes. This is the result of spalling in the larger pumice craters and the absence of it in the smaller ones. Spalling partly accounts for the difficulty in correlating the data. In figures 4, 5, and 6, the largest pumice craters, which were produced by polyethylene projectiles, are each represented by two points: one counting the spalls and one omitting the spalls.

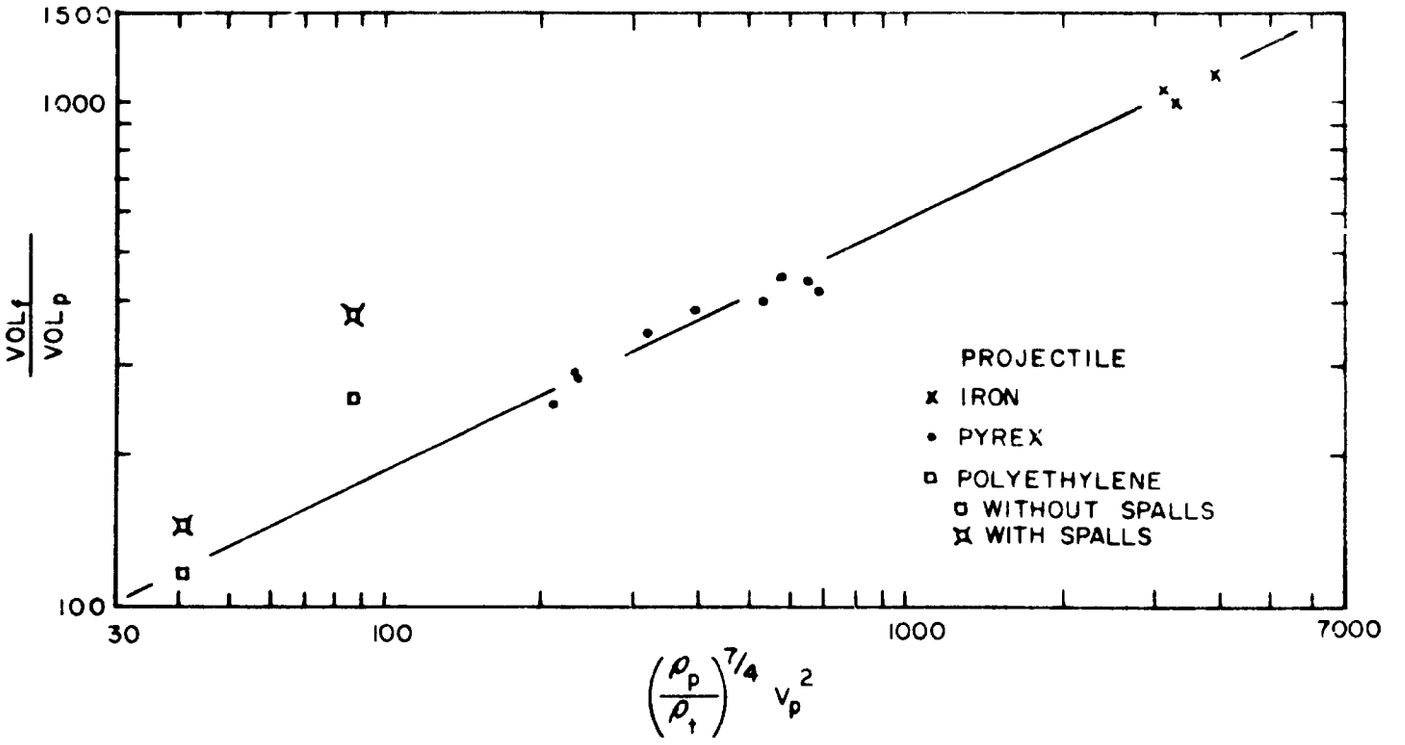

Figure 6.--Comparison of ratio of volume of ejecta and fragmented pumice with projectile velocity and ratio of projectile and target densities.

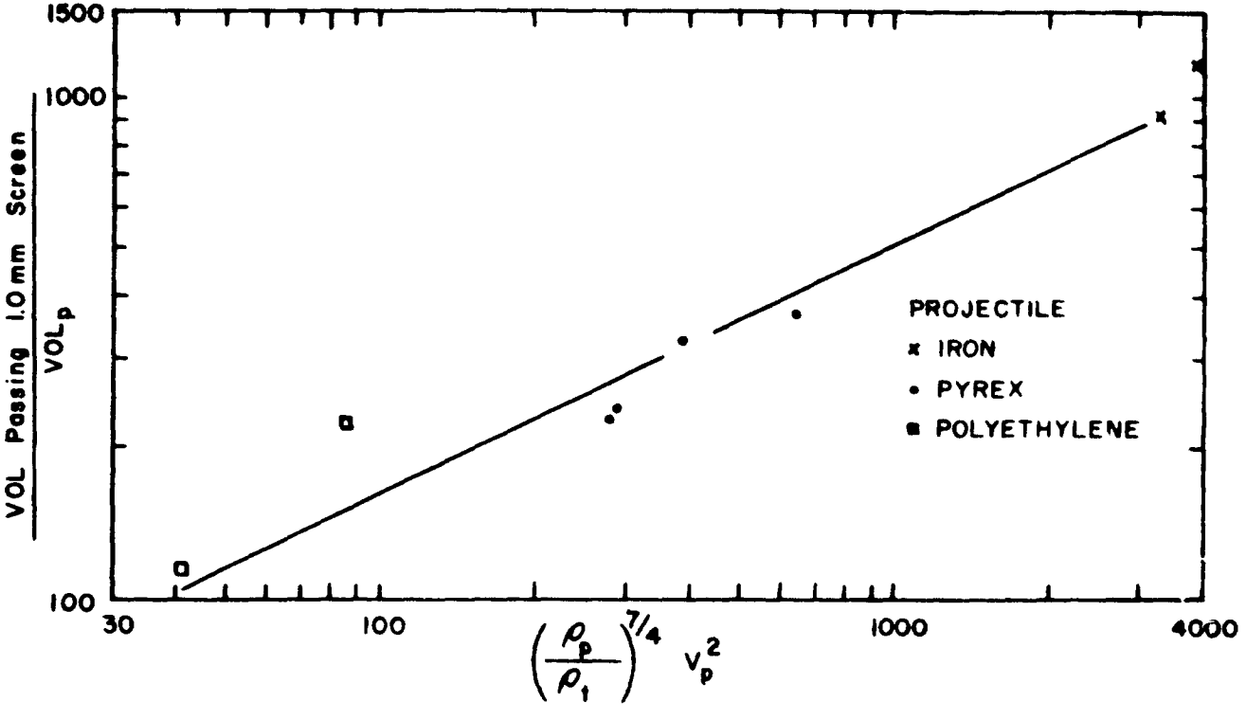

Figure 7.--Comparison of ratio of volume of ejecta and fragmented pumice passing a 1.0 mm screen with projectile velocity and ratio of projectile and target densities.

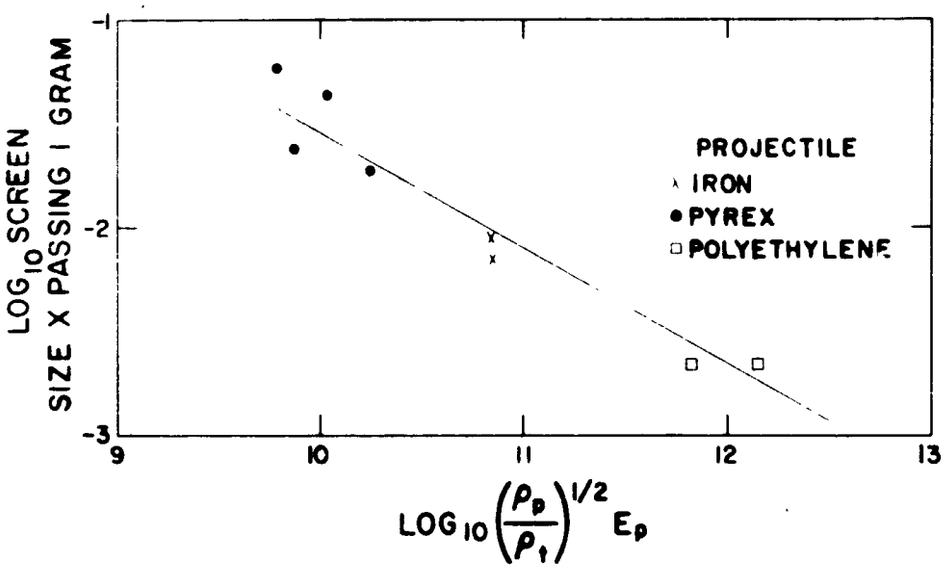

Figure 8.--Comparison between screen opening passing 1.0 g of fragmented pumice with projectile kinetic energy (approximately corrected for density ratio).

In all cases, the omission of the spalls improved the correlation. However, nothing seems to remove the scatter due to the largest crater produced by polyethylene. Perhaps, some additional term, which is dependent on size, is required (Moore and others, 1965).

Aggregates of crushed and fused pumice.--Studies of the ejecta indicate that a significant amount of material in the ejecta and material removed from the craters is composed of aggregates of crushed and fused pumice. The amount of aggregate is also proportional to the velocity of the projectile. This result is consistent with the results in equations 3 and 4.

DISCUSSION OF DATA

The results of the data on pumice are significantly different from those for other materials such as basalt and metals. For a given projectile, the amount of pumice fragmented is proportional to the square root of the kinetic energy of the projectile. This is in marked contrast with craters produced by projectile impacts in basalt, for which the ejected mass is proportional to the 1.19 power of the kinetic energy of the projectile (Moore and others, 1965). For craters in metals, the volumes of craters are nearly proportional to the kinetic energies of projectiles, although some authors have reported a weak velocity dependence (Halperson, 1965). Ejected mass-projectile energy relationships for craters in aluminum are somewhat like those in basalt (Denardo, B. P., personal commun.).

Energy losses due to irreversible heat losses and fragmentation of the pumice account for the data on craters in pumice. The data show that for a given projectile the amount of pumice ejected and fragmented is proportional to the velocity of the projectile or the square root of the kinetic energy of the projectile (eq 1, fig. 4). Such a relationship was also found for the amount of debris passing 1.0, 0.10, and 0.043 mm seiving screens (eq 4, fig. 7), as well as the amount of aggregate of partially fused and crushed pumice.

In their theory on impact crater formation, Charters and Summers (1959) suggest that the effective deformation strength can be computed. Although the Charters-Summers theory needs to be and can be modified to take into account the fact that momentum is a vector quantity, it does have utility. The general implications of their theory have been discussed by Gault and Moore (1965). In addition, it has been successfully used to calculate effective strengths of temporary craters in water produced by falling drops of water (Moore and others, 1963). The theory also is consistent with the results of craters produced by missile impacts in wet and dry natural materials (Moore and Lugn, 1965).

The Charters-Summers theory requires that the effective strength of the target (S_{eff}) be proportional to the ratio of the kinetic energy of the projectile (E_p) and the crater volume (Vol_c):

$$S_{eff} \propto \frac{E_p}{Vol_c}; \qquad (5)$$

and, dividing both sides of the proportionality by the target density (ρ_t):

$$\frac{S_{eff}}{\rho_t} \propto \frac{E_p}{M_f}. \qquad (6)$$

In equations 5 and 6, the term $\frac{S_{eff}}{\rho_t}$ has the dimensions of ergs per gram and may be thought of as a specific energy of deformation, and M_f is the sum of the amounts of ejecta and fractured pumice removed from the crater. For this interpretation of the data, equation 1 requires that:

$$\frac{S_{eff}}{\rho_t} \propto E_p^{\frac{1}{2}}, \qquad (7)$$

for a given projectile and when spalling is neglected for very large craters. Thus, the theory requires that the effective target strenth and deformation energy be proportional to the square root

of the kinetic energy of the projectile, for a given projectile.

The result in equation 7 is in agreement with both the size distribution and the amount of aggregate of crushed and fused pumice. The amount of surface energy lost irreversibly should be proportional to the amount of material finer than a given size (excluding spalling). The variation of the amount of material finer than 1.0, 0.10, and 0.043 mm sizes (eq 4, fig. 7) was found proportional to the projectile momentum for pyrex projectiles impacting pumice. Thus, the surface energy lost irreversibly is also proportional to the projectile momentum--a result consistent with equation 7. The amount of crushed and partly fused pumice, which is taken to represent irreversible energy losses, is also proportional to the projectile momentum. This is consistent with equation 7. Thus, the results using the Charters-Summers theory to calculate deformation energy losses and effective target strengths are in agreement with the expectations for these strengths and energy losses using the data on size distributions and petrographic studies.

The density ratio term, $\left[\frac{\rho_p}{\rho_t}\right]^{-1/8}$, also relates to irreversible energy losses due to fragmentation and fusion. Larger pressures and larger volume changes would be attained for more dense projectiles than for less dense projectiles with the same velocities. In this case, irreversible heat losses would be larger for the dense projectiles, and the exponent for the density ratio, -1/8, is in the correct sense for equation 1 (see fig. 4). Unfortunately, Hugoniots are not available for pumice, and refined analyses are not possible at this time.

The largest craters, which spalled, present a special problem. Spalling is virtually absent in the small pumice craters. The results here are similar to those reported by Hartman (1959) for drill-bit craters in synthetic aggregates. Hartman found that a certain critical energy was required before spalling occurred. Such a relationship is present in these data, but much more data are needed to define it.

SUMMARY

The sum of ejected material and fragmented material removed from craters formed in pumice targets by hypervelocity impact is proportional to the momentum of the projectile and 1/8 power of the ratio of the target density and projectile density. This result, which may represent a transition from low velocity to hypervelocity phenomena, is in marked contrast with such data on craters in most metals and basalt, which are essentially energy dependent.

Size distribution and petrographic studies are consistent with the results and indicate that irreversible energy losses due to fragmentation and heating have produced the momentum dependency of the amount of ejected material and fragmented material.

Spalling produces larger craters than would be expected when the kinetic energy of the projectile exceeds a certain value.

REFERENCES CITED

Birkhoff, Garnett, Macdougall, D. P., Pugh, E. M., Taylor, Sir Geoffrey, 1948, Explosives with lined cavities: Jour. Appl. Physics, v. 19, p. 563-582.

Charters, A. C., Denardo, B. P., and Rossow, V. V., 1957, Development of a piston-compressor type light-gas gun for the launching of pre-flight models of high velocity: U.S. Natl. Advisory Comm. Aeronautics, Tech. Note 4143, 95 p.

Charters, A. C., and Summers, J. L., 1959, Some comments on the phenomena of high-speed impact, in Decennial symposium, May 26, 1959, White Oak, U.S. Naval Ordnance Lab., Silver Spring, Md., p. 1-21.

Curtis, J. S., 1962, An accelerated reservoir light-gas gun: Natl. Aeronautics and Space Adm. Tech. Note D-1144, 22 p.

Gault, D. E., and Moore, H. J., 1965, Scaling relationships for microscale to megascale impact craters: Hypervelocity Impact Symposium, 7th, Orlando, Fla., Proc., v. 6, p. 341-351.

Halperson, S. M., 1965, Comparisons between hydrodynamic theory and impact experiments: Hypervelocity Impact Symposium, 7th, Orlando, Fla., Proc., v. 5, p. 235-257.

Hartman, Howard L., 1959, Basic studies of percussion drilling: Mining Eng., v. 11, p. 69-75.

Moore, H. J., Gault, D. E., and Heitowit, E. D., 1965, Change of effective target strength with increasing size of hypervelocity impact craters: Hypervelocity Impact Symposium, 7th, Orlando, Fla., Proc., v. 4, p. 35-45.

Moore, H. J., Gault, D. E., Heitowit, E. D., and Lugn, R. V., 1964, Hypervelocity impact craters in porous cohesive targets, in Crater investigations, pt. B of Astrogeologic Studies Ann. Prog. Rept., July 1963-1964: U.S. Geol. Survey open-file report, p. 93-143.

Moore, H. J., and Lugn, R. V., 1965, A missile impact in water-saturated sediments, in Crater investigations, pt. B of Astrogeologic Studies Ann. Prog. Rept. July 1964-July 1965: U.S. Geol. Survey open-file report, p. 101-126.

Moore, H. J., MacCormack, R. W., and Gault, D. E., 1963, Fluid impact craters and hypervelocity--high-velocity impact experiments in metals and rock: Hypervelocity Impact Symposium, 6th, Cleveland, Ohio, Proc., v. 2, pt. 2, p. 367-399.

Summers, J. L., 1959, Investigation of high-speed impact--regions of impact and impact at oblique angles: Natl. Aeronautics and Space Adm. Tech. Note D-94, 18 p.

N 67-19395

COMPILATION OF DATA ON CRATERS PRODUCED BY EXPLOSIVES

By Francis G. Robertson

INTRODUCTION

High-resolution photographs of the small-scale features of the lunar surface taken by Rangers 7, 8, and 9 and Surveyor 1 show that the topography of the moon is dominated by shallow depressions or craters. Most of the craters may be the result of impacts of objects from space and ejecta from other craters. Thus, an understanding of craters is necessary for a clearer understanding of the lunar surface, since it has been shown that craters produced by projectile impact and by explosives are comparable (Moore and others, 1964; Shoemaker, 1960).

The literature contains a wealth of information about craters produced by chemical and nuclear explosives with energies between about 10^{10} and 10^{24} ergs. Previous data compilations do not include the results of newer experiments, nor do they report all the quantities of interest to the space scientist studying the moon. In addition, most compilations do not carefully examine variables such as rock and material properties.

For the reasons above, a new compilation has begun, using a format modified from the most complete previous work, a compilation by the U.S. Army (Sager and others, 1960). Where possible, their work has been verified against original sources, as well as for internal consistency. From their work and from other sources, data on a total of 1,246 craters have now been collected for which there is sufficient information concerning the explosive and the resulting crater. The information has been further standardized for recording on punched cards, so that machine processing can be used for sorting, plotting, and computational purposes.

COLLECTION AND RECORDING OF DATA

Data were collected from available literature. The compilation of the Army Corps of Engineers was used as a guide (Sager and others, 1960), and their data represent the only available source for 745 craters.

The following information was recorded on worksheets and then transferred to punched cards:

1. Agent producing crater, chemical or nuclear explosive and type.
2. Target material, rock and material type; moisture content, frozen or unfrozen, complex layering, etc.
3. Energy of explosive, measured in ergs using TNT equivalent of explosive as a standard measure.
4. Apparent volume of crater, volume of crater below original ground surface, measured from topography of crater, includes some estimates using apparent depth below original ground surface and apparent radius for calculation.
5. Displaced mass, the product of the density of the medium in which the crater was produced and the apparent crater volume.
6. Apparent depth, the depth of the crater below the original ground surface.
7. Apparent radius, the average radius of the crater; one-half the average crater diameter measured between crater walls at original ground surface.
8. Rim height, the average height of the rim of the crater above the original ground surface.
9. Rim radius, the average radius; one-half the average diameter measured between rim crests (note difference from apparent radius).
10. Scaled depth, the ratio of the depth of burial of the explosive, in feet, to the cube root of the weight of TNT equivalent of the explosive, in pounds.
11. Item number, crater number in this compilation, in order of acquisition.

12. Source number, identification of reference.
13. Shot number, test number as reported in reference.
14. Charge weight, actual weight of explosive charge in pounds.
15. TNT equivalent, weight of TNT which has same energy release as the explosive charge used.
16. Charge depth, depth of burial of explosive below original ground surface.
17. True volume, volume of crater measured from the original ground surface to the limit of fracturing.
18. True depth, depth of crater measured from the original ground surface to the limit of fracturing.
19. True radius, average radius of crater measured from the center of the crater to the limit of fractured material at the original ground surface.
20. Cone angle, slope of crater wall at the original ground surface.

Crater dimensions and explosive energies are recorded in cgs units (centimeter-gram-second) on the punched cards, whereas scaled depths and charge weights are recorded in units of feet and pounds as described. These quantities are expressed on the punched cards in terms of logarithms to the base 10 to facilitate plotting of the data, which cover a range of some 14 orders of magnitude. Scaled depths are simply recorded as decimal numbers.

With the data so arranged, machine sorting of the punched cards easily provides the results of cratering experiments with any desired characteristics. The data are then readily available for machine plotting and computational purposes.

RESULTS

Examination of the data in this compilation reveals that: (1) craters in very wet materials may obey different scaling laws than those in dry materials over the whole energy range from 10^{14} to 10^{22} ergs; (2) the difference in crater sizes as a result of moisture content of the material is particularly distinct at energies near

10^{15} ergs; and (3) sizes of craters produced by explosives with energies near 10^{13} ergs are strongly dependent upon cohesion and rock type of the material. Part of the data of the compilation is graphically summarized in figure 1.

Scaling laws.--Comparison of displaced masses of craters produced by explosives with zero scaled depth of burial in dry alluvium and soils with those produced in very wet material shows that the scaling laws cannot be the same for these two classes of material (fig. 1). The curve for craters in dry alluvium is much straighter than that for craters in the wet materials. The curve for craters in wet materials seems to be composed of two distinct branches. One of these, for explosive energies above 10^{15} ergs, has a gentler slope than the curve for dry alluvium; and the other, for energies below 10^{14} ergs, has a steeper slope than the curve for dry alluvium.

For the craters in wet materials plotted in figure 1, the moisture content exceeded about 15 percent for craters produced by explosives with energies larger than 10^{14} ergs. For the craters produced by explosives with energies at $10^{13.27}$ ergs (1.0 lb TNT), moisture content ranged from 5 to 22 percent.

The two largest craters reported in this compilation are Castle I and Castle III. Because of difficulties in measuring these two craters, the validity of the estimated displaced mass may be in doubt. Castle I was not included in the plot, but the data for Castle III seem more reasonable from consideration of the cratering experiment (Vaile, 1961), and Castle III was included as the largest crater on the plot. In any case, the data for other large craters, including the Suffield Crater at $10^{19.3}$ ergs (Rooke and Chew, 1965), are known to be valid.

Wet and dry materials.--A more detailed plot of data from the compilation is shown in figure 2. For these energy ranges, it is clear that craters produced in very wet materials are significantly larger than those in dry materials. Comparisons of this kind must

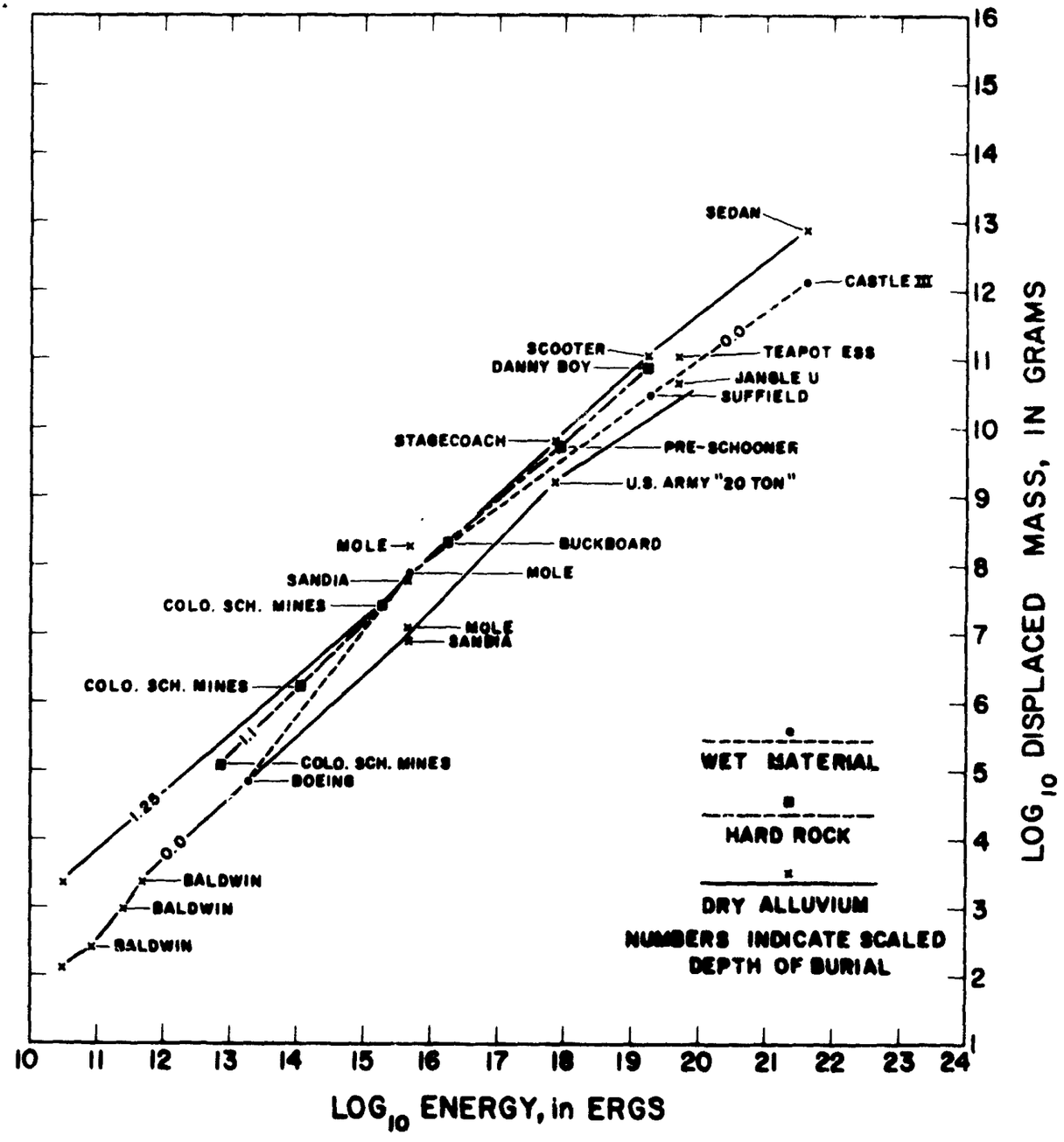

Figure 1.--Summary plot for craters produced by chemical and nuclear explosives in three classes of material. Note the size difference of craters in wet materials and in dry alluvium for scaled depth of 0.00.

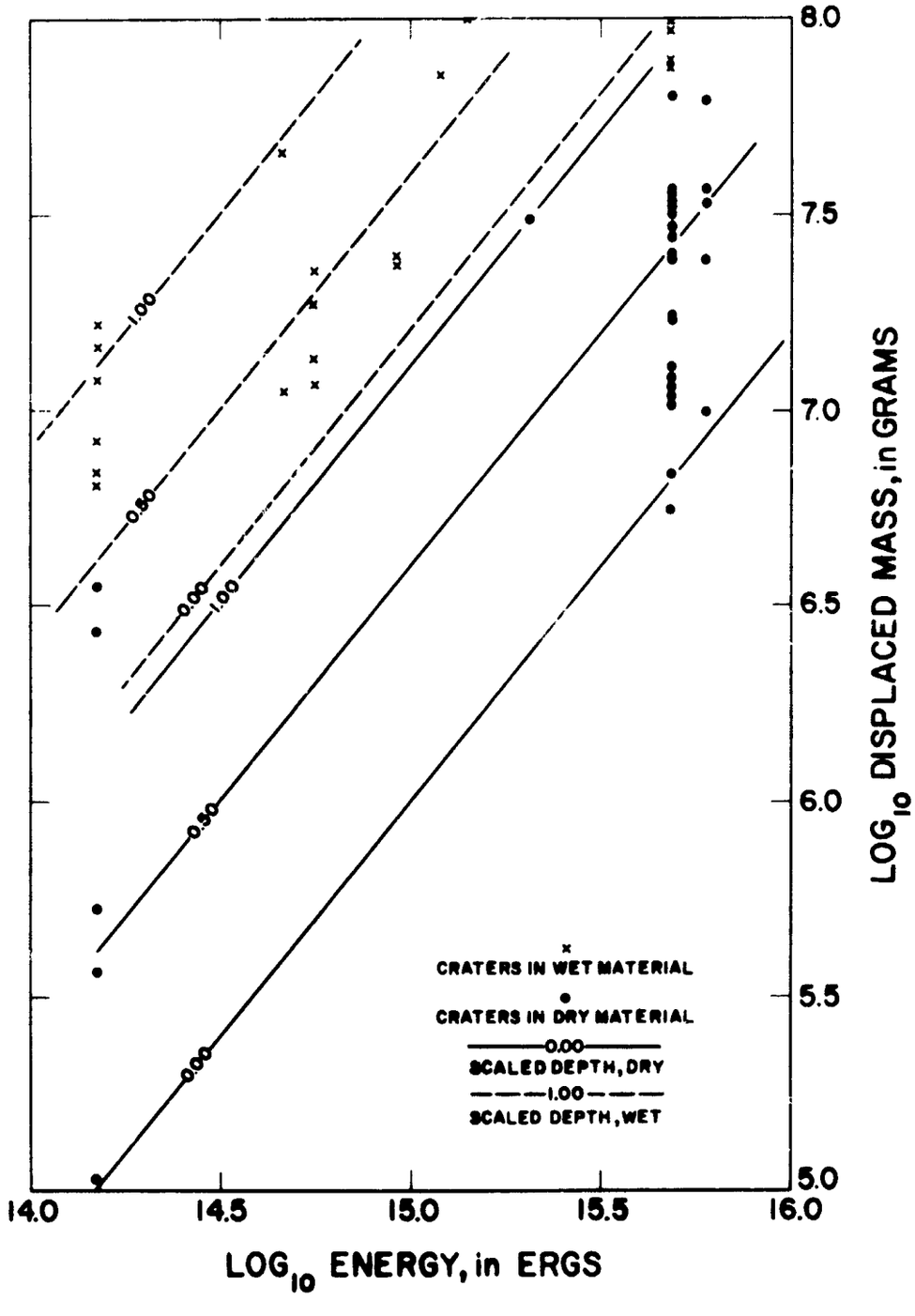

Figure 2.--Comparison of size of craters produced by chemical explosives in dry and very wet materials for scaled depths of burial of 0.00, 0.50, and 1.00.

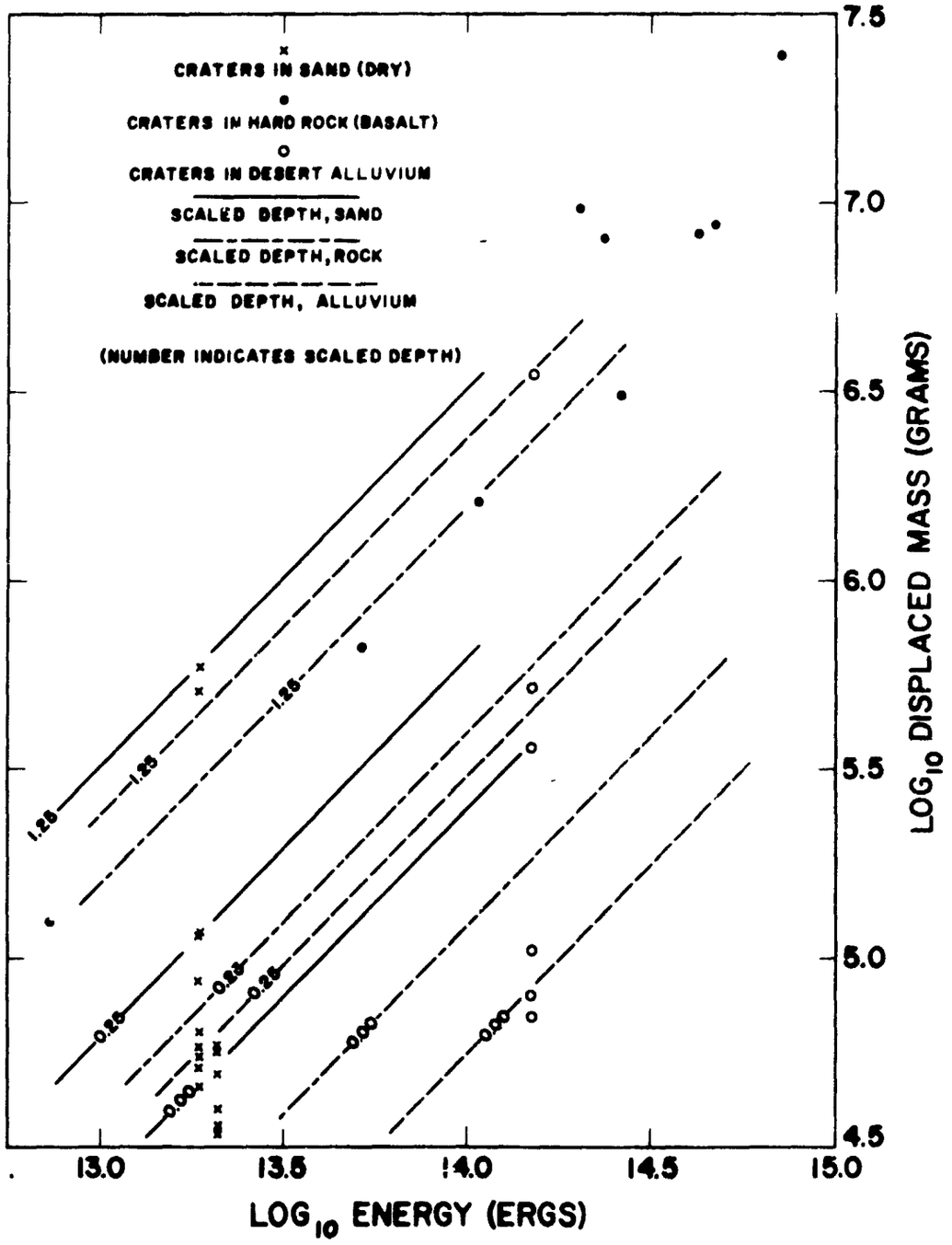

Figure 3.--Plot of craters produced by chemical explosives in dry sand, hard rock, and alluvium at scaled depths of burial of 0.00, 0.25, and 1.25.

be made carefully for materials within definite ranges of moisture content to avoid confusing results. For this reason, this plot was drawn for only the very wet and very dry materials.

Cohesion.--Cohesion and rock properties affect the sizes of craters produced by explosives with energies near 10^{13} ergs (see fig. 3). In all cases, craters in noncohesive materials such as sand are larger than their counterparts in rocks and cohesive soils. In addition, craters in cohesive soils tend to be larger than those in hard rocks, except at scaled depths below about 0.4. This result is consistent with data on hypervelocity—high-velocity impacts using projectiles with kinetic energies near 10^{10} ergs (Moore and others, 1964). Rock type apparently becomes less important at higher energies, but the difference still exists (see fig. 1).

REFERENCES CITED

Moore, H. J., Gault, D. E., Heitowit, E. D., and Lugn, R. V., 1964, Hypervelocity impact craters in porous cohesive targets, in Crater investigations, pt. B of Astrogeologic Studies Ann. Prog. Rept., July 1963-July 1964: U.S. Geol. Survey open-file report, p. 93-143.

Moore, H. J., Kachadoorian, Reuben, and Wilshire, H. G., 1964, A preliminary study of craters produced by missile impacts, in Crater investigations, pt. B of Astrogeologic Studies Ann. Prog. Rep., July 1963-July 1964: U.S. Geol. Survey open-file report, p. 58-92.

Rooke, A. D., Jr., and Chew, T. D., 1965, Operation Snowball--Crater measurements and earth media determinations, interim report: Vicksburg, Miss., U.S. Waterways Expt. Sta. Misc. Paper 1-764, p. 20-21, 27, 29.

Sager, R. A., Denzel, C. W., and Tiffany, W. B., 1960, Cratering from high explosive charges--Compendium of crater data: Vicksburg, Miss., U.S. Waterways Expt. Sta. Tech. Rept. 2-547, 32 p., 10 tables.

Vaile, R. B., Jr., 1961, Pacific craters and scaling laws: Jour. Geophys. Research, v. 66, no. 10, p. 3413-3433.

IMPACT METAMORPHISM

By E. C. T. Chao

INTRODUCTION

The origin of many circular structures and craters such as the cryptoexplosive structures, located in nonvolcanic terrains, is often obscure and difficult to ascertain. If the crater morphology is well preserved, the crater geometry, the raised rim, and the type and distribution of fragmental material can provide useful information regarding its origin. If the crater is well exposed, then detailed geologic mapping, geologic sections, and the structural features and stratigraphic sequence of the crater walls and rim can provide critical information regarding the mechanism of formation of the structure. If the structure is buried, gravity anomalies and drilling can provide useful and definitive information regarding its origin. If the state of preservation of the structure is not perfect, results of many of these studies are not always conclusive.

One of the most effective methods of investigating the origin of circular structures or craters is the detailed study of the mineralogical and petrographic changes of the rock material in which the structure is located or excavated. Generally, this method is effective for the study of large craters, in excess of 1,000 feet in diameter. Nevertheless it has been shown to be effective in the study of the Wabar crater of Saudi Arabia, which has a diameter of about 300 feet.

Meteorite impact metamorphiam is the change in rocks and minerals caused by hypervelocity meteorite impact. The major objective of study of this metamorphism is to establish criteria so that craters of meteorite impact origin can be distinguished from circular structures of other origins.

It is generally accepted that the occurrence of meteoritic material associated with a circular crater structure in a non-volcanic terrain is conclusive evidence of meteorite impact. Among the craters which satisfy this criterion are the Meteor Crater of Arizona, the Wabar crater near Al Hadida in east-central Saudi Arabia, the Odessa crater of Texas, and the Henbury craters of central Australia. Petrographic evidence derived from rocks of these known meteorite impact structures may then be extended to such structures as the Ries crater of Bavaria, south Germany (Shoemaker and Chao, 1961), and the Lake Bosumtwi crater of Ghana (Littler and others, 1962) where remains of the impacting body have not been conclusively identified.

This paper reviews and presents data on diagnostic criteria in order to establish progressive stages or degrees of impact metamorphism. The evidence presented is based on studies of materials collected principally by the author from Meteor Crater, Ariz.; Ries crater, southern Bavaria, Germany; Lake Bosumtwi crater, Ghana; Wabar crater, Saudi Arabia; and the Henbury craters, Northern Territory, Australia.

DIAGNOSTIC PETROGRAPHIC CRITERIA OF HYPERVELOCITY METEORITE IMPACT

Unique microstructures, selective phase transitions, formation of vitreous phases without evidence of viscous flow or vesiculation, the occurrences of high-pressure polymorphs, and evidence of extremely high temperatures are criteria considered by this author to be characteristic of hypervelocity meteorite impact metamorphism. Shatter cones as evidence of shock have been adequately discussed elsewhere (Dietz, 1963).

Microstructures

The occurrence of a single set of megascopic, discontinuous, tension fractures in the rock, the occurrence of multiple sets of closely spaced planar fractures in quartz, and kink-bands in micas are characteristic microstructures and worthy of careful study and consideration.

Fractures

Fracture patterns are developed both in brittle minerals, such as quartz, and in rock. Those developed in rock are megascopic evidence of shock that can be readily observed in hand specimens.

Megascopic fractures.--The impact metamorphosed sandstones from the Meteor Crater of Arizona, the Wabar crater of Arabia, and the Henbury craters of central Australia show megascopically a single set of parallel, discontinuous, sinuous tension fractures (fig. 1). These fractures are generally oriented at a steep angle to the bedding whether the bedding was originally horizontal or moderately dipping. The fractures are lenticular, a few tenths of a millimeter to several millimeters in width and depth and up to a few centimeters in length. The long axes of the openings are generally parallel to the bedding. In some rocks such openings appear to be concentrated in certain beds, perhaps because of the grain size or the porosity of those beds (fig. 1). These tension openings and their relation to bedding are clearly observed microscopically (figs. 2, 6). Some openings cut across single grains of quartz (fig. 2). None of these cavities are coated by quenched products or fused vitreous matter. The fractures are believed by the author to be oriented radially and perpendicular to the shock wave because the original bedding was nearly horizontal, therefore only a single set was formed.

In a more advanced stage, a pronounced set of fractures not distinguishable from shear fractures occurs at steep angles to the bedding. They have been observed only in strongly sheared Coconino Sandstone and dolomitic Kaibab Limestone of the Meteor Crater.

Tension fractures of tectonic origin are normally more continuous and better defined and occur in more than one set caused by folding of beds. The minute scale, the single set, and the sinuous discontinuous nature of these openings are perhaps characteristic of impact or shock compression.

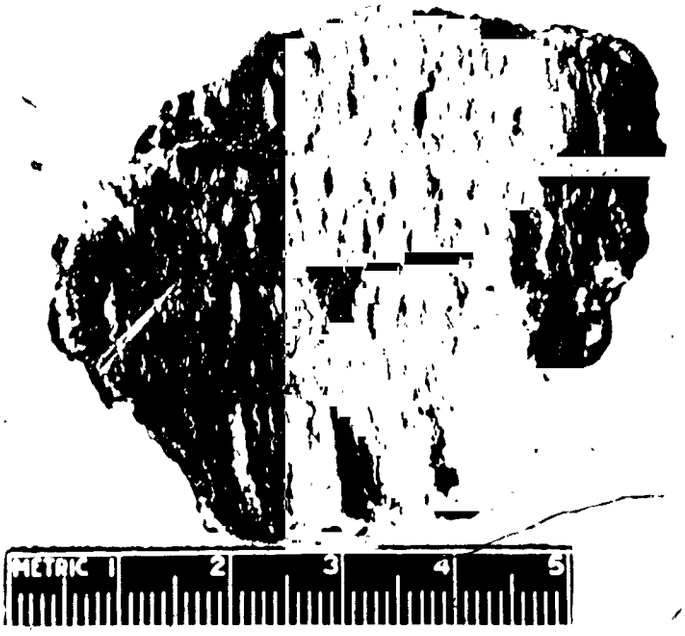

Figure 1.--Shocked Coconino Sandstone from Meteor Crater, Ariz., showing a set of discontinuous tension fractures nearly normal to the bedding.

Figure 2.--Photomicrograph of shocked Coconino Sandstone showing fractured quartz and the tension openings (white). The dark areas consist of weathered glass with some coesite. Reflected light.

Microscopic planar structures.--Quartz, which is normally free of cleavage and parting, shows multiple sets of closely spaced planar fractures and basal deformation lamellae in impact metamorphosed sandstones and granitic rocks. Bunch and Cohen (1964) reported that fractures in quartz in Coconino Sandstone from Meteor Crater were oriented as follows (in decreasing frequency of occurrences): $\{10\bar{1}1\}$ or $\{01\bar{1}1\}$, $\{0001\}$, $\{11\bar{2}2\}$, $\{10\bar{1}0\}$ and $\{11\bar{2}0\}$, and $\{11\bar{2}1\}$. Engelhardt and Stöffler (1965) described such planar structure in quartz in some of the shocked granitic rocks from the Ries (fig. 3). In decreasing frequency of occurrence, they are: $\{0001\}$, $\{10\bar{1}3\}$ and $\{01\bar{1}3\}$, $\{10\bar{1}1\}$ and $\{01\bar{1}1\}$, $\{10\bar{1}2\}$ nd $\{01\bar{1}2\}$, $\{10\bar{1}0\}$ and $\{1\bar{1}20\}$, $\{21\bar{3}1\}$ and $\{12\bar{3}1\}$, and $\{51\bar{6}1\}$. Some of them do not have rational crystallographic indices. Multiple sets of closely spaced planar fractures have not been observed in quartz from tectonically metamorphosed rocks. The significant differences between the planar microstructures in shocked quartz and quartz deformed at ordinary geologic strain rates have been described by Carter (1965). Shocked quartz studied by Carter includes specimens from Vredefort Ring, South Africa; the Meteor Crater of Arizona; Clearwater Lakes, Quebec; Ries, Germany; and from the Lac Couture and Brent structures of Canada.

Kink-bands

Development of kink-bands in micaceous minerals from tectonites is well known. Artificially produced kink-bands in mica from the Innsbruck mica schist have been analyzed (Turner, 1964). Kink-bands are well developed in biotite from metamorphosed granitic fragments in suevite of the Ries. Both the kink-bands and the herringbone texture in these biotites clearly indicate strong influence of crystallographic orientation. The development of kink-bands is most effective where the basal cleavage of the biotite is parallel to the direction of hydrostatic or shock-wave compression, as demonstrated by Turner(1964) and Cummings (1965). The herringbone

Figure 3.--Photomicrograph of quartz with multiple sets of closely spaced planar fractures in a weakly shocked biotite granite gneiss fragment in suevite; crossed nicols; Ries.

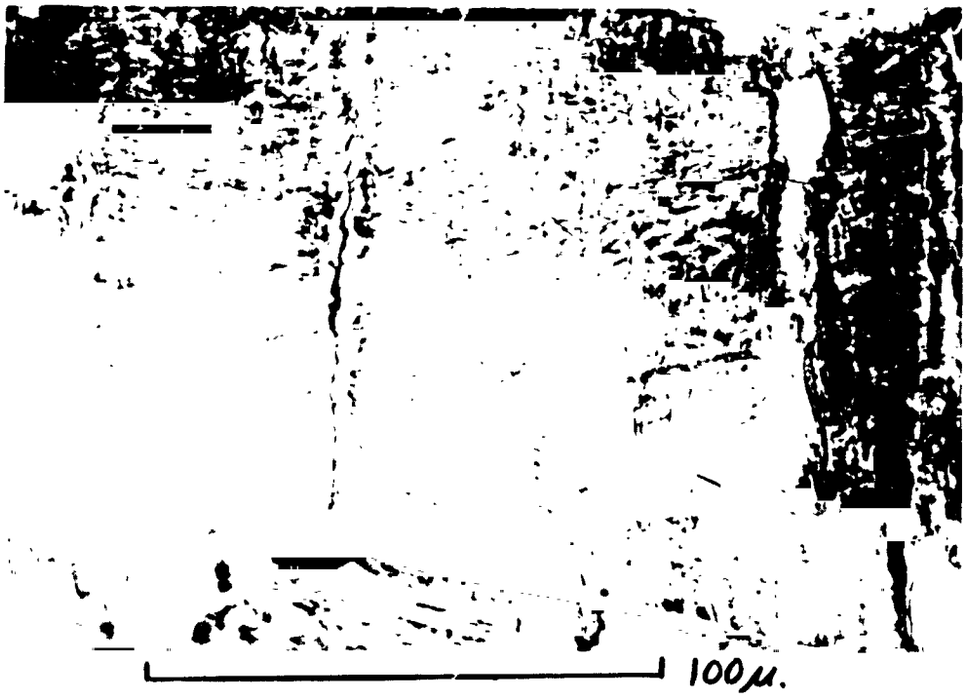

Figure 4.--Photomicrograph of a biotite showing herringbone texture due to kinking from a biotite-quartz schist fragment; reflected light; Otting quarry, Ries.

texture (fig. 4) was also preferentially developed in biotite crystals with their basal cleavage nearly normal to the direction of compression. Biotite crystals with basal cleavage normal to the compression show little or no sign of kinking (fig. 5). Kink-banded biotites occur in granitic rock and quartz-mica schist which exhibit selective shock transformation of minerals. They are nevertheless not exclusively of shock origin.

Selective Phase Transitions

If a given mineral or minerals of a rock have undergone phase transition and the remaining minerals are unchanged, the process is defined as a selective phase transition. It is a unique criterion of shock and is prevalent in specimens which have undergone impact metamorphism.

The best examples of selective phase transitions are the micaceous sandstones from the Henbury craters of Australia and the granitic rocks and biotite-quartz schist in suevite[1] of the Ries crater of southern Germany.

A fine-grained micaceous snadstone from the northeastern ejecta blanket of the largest crater at Henbury shows visible discontinuous tension fractures. The bedding is shown by the oriented elongated grains of transformed quartz which lie nearly perpendicular to the tension fractures (figs. 6, 7). Under crossed nicols, all the detrital quartz grains are isotropic. The index of refraction is 1.462, and X-ray studies of such grains show them to be glass. The sericite or fine-grained muscovite, as well as a few scattered grains of detrital feldspar, remain birefringent and crystalline. The quartz grains have therefore been selectively transformed into silica glass, but the original detrital grain boundaries and texture are retained. I propose the term "thetomorphic" to describe such silica glass. The word is derived from the Greek word "thetos,"

[1]A rock which resembles a tuff-breccia but is of nonvolcanic origin (Chao and Littler, 1963).

Figure 5.--Photomicrograph of strongly kinked biotite in a moderately shocked biotite granite. Shock compression parallel to the basal cleavage results in the development of strong kink bands. If the compression is nearly normal to the basal cleavage, shock effect is not evident. Reflected light. Au Mühle quarry near Hainfarth, Ries.

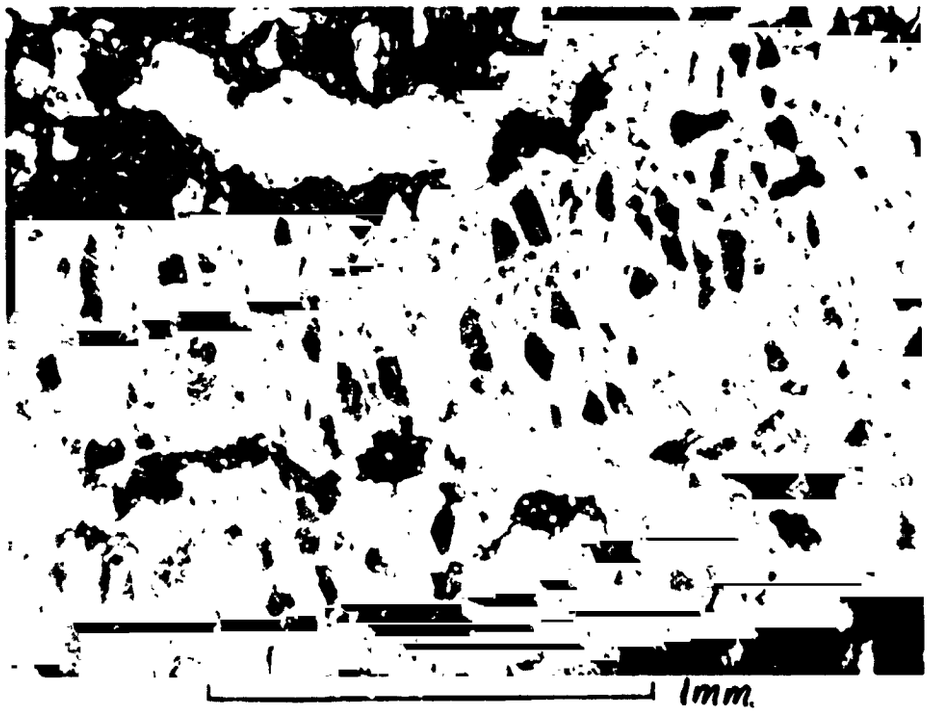

Figure 6.--Photomicrograph of a fine-grained micaceous sandstone showing alinement of the quartz grains or bedding and the tension openings normal to the bedding. Henbury, Australia.

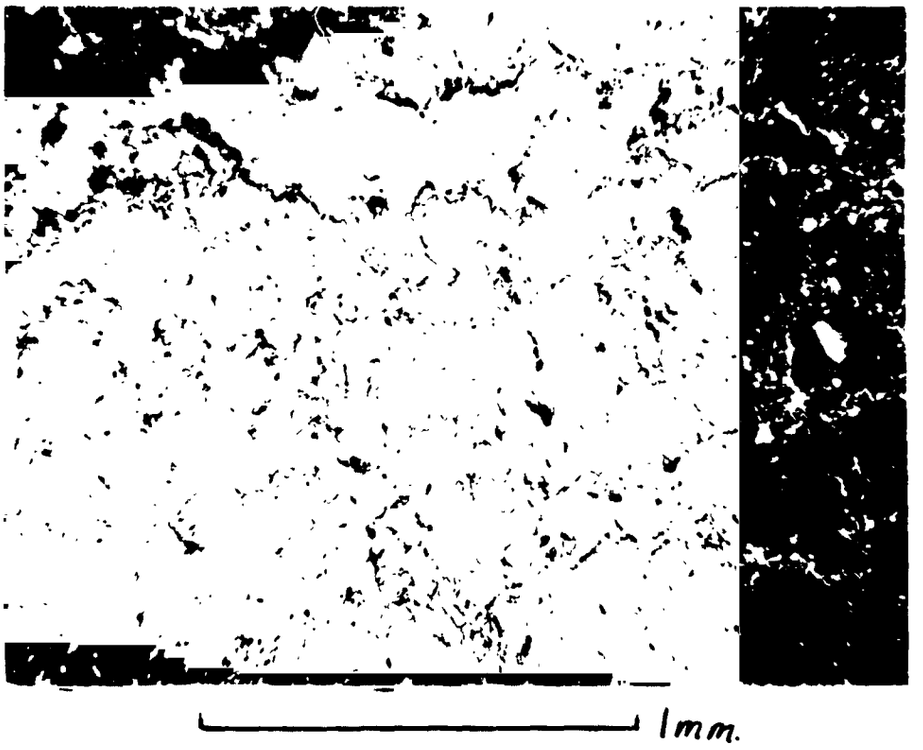

Figure 7.--Same as in figure 6; crossed nicols showing that the detrital quartz has been transformed to isotropic silica glass. Muscovite in the matrix remained crystalline.

Figure 8.--Photomicrograph of a moderately shocked biotite granite with selectively shock-transformed thetomorphic silica glass (Si) and thetomorphic plagioclase glass (pl). Reflected light. Au Mühle quarry near Hainfarth, Ries.

meaning adopted, and "morphe," form. The term can be used to describe any glassy phase transformed by shock from the host mineral in the solid state. The transformation of quartz accompanied by the lack of reaction of the fine-grained micaceous matrix material suggests a high pressure and low temperature history.

De Carli and Jamieson (1959) have shown experimentally that quartz can be transformed to silica glass by shock at an estimated peak pressure of 360 to 600 kb. In the case of the Henbury micaceous sandstone, the peak pressure may not have been as high as suggested by the above experiment. The denser mica in the matrix however may have reacted with the passage of the shock wave in such a manner as to raise the local pressure and focus the shock effect into the more compressible quartz which it surrounds.

Fine-grained biotite granite fragments in suevite collected and studied by the author from the Au Mühle quarry near Hainfarth of the Ries, Germany, show the same selective phase transitions as the Henbury sandstone. Megascopically the shocked fine-grained biotite granite fragment is indistinguishable from a normal fine-grained biotite granite. In thin sections (figs. 8, 9) the granoblastic texture is well preserved. The quartz and plagioclase feldspars have been transformed to glass, whereas the biotite and the fine-grained muscovite in the plagioclase remain birefringent and crystalline (fig. 9). The index of refraction of the thetomorphic silica glass is 1.46, that of the water-clear thetomorphic feldspar glass is 1.506. Neither of the transformed isotropic phases cause diffraction of X-rays. Some biotite developed kink-bands and has reduced birefringence, but all remains crystalline.

Milton and De Carli (1963) have demonstrated experimentally the transformation of plagioclase by shock into maskelynite, a glass of identical composition. The plagioclase of the dynamically loaded gabbro in their experiment was transformed at an estimated pressure of 250 kb.

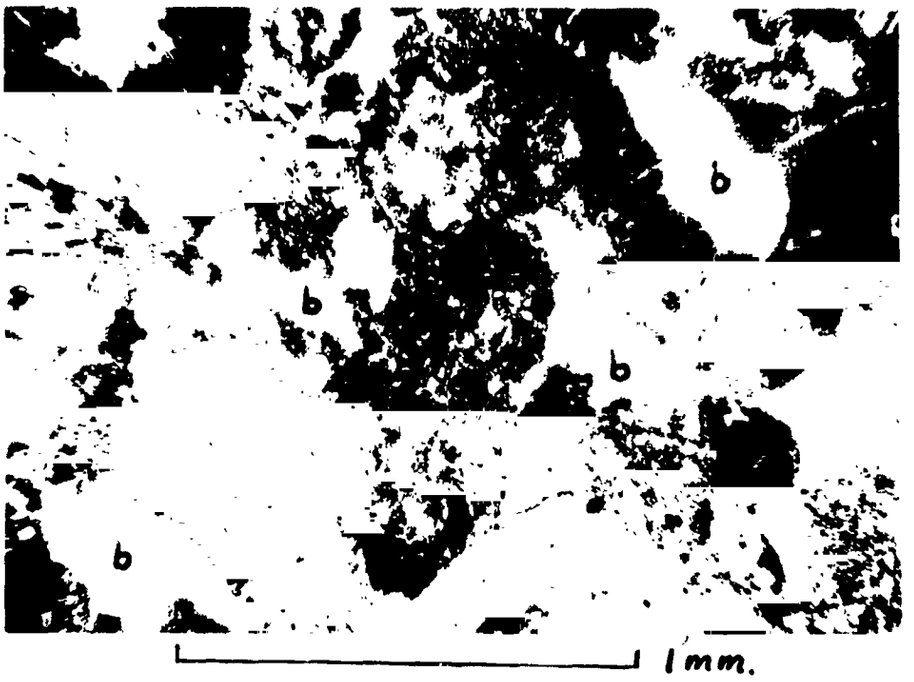

Figure 9.--Same as in figure 8; crossed nicols. Note the isotropic thetomorphic silica glass and plagioclase glass. Biotite (b) remained crystalline.

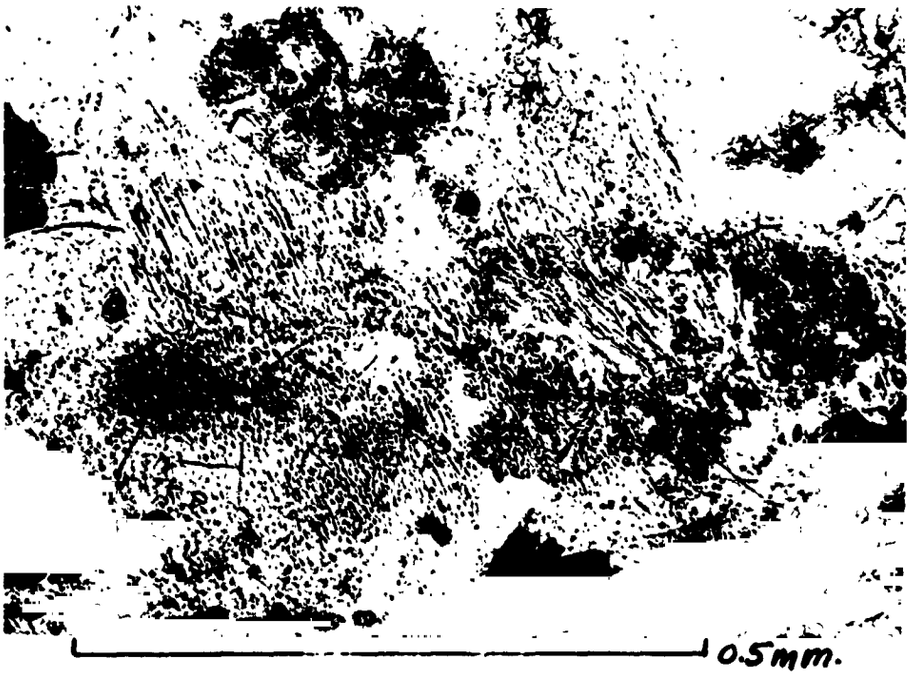

Figure 10.--Photomicrograph of perthite and myrmekite glass in a moderately shocked biotite granite. Note preservation of perthitic texture (on the left) and myrmekitic texture (on the right). Plain reflected light. Au Mühle quarry near Hainfarth, Ries.

The impact-metamorphosed fine-grained biotite granite fragment from Hainfarth has had a high pressure and moderately low temperature history. The pressure may have been higher than that experienced by the Henbury micaceous sandstone since in this case the plagioclase has also been transformed. Similar selective phase transitions have been observed in granitic gneisses, biotite-quartz schist, diorite, plagioclase amphibolite, and other crystalline fragments in suevite from several quarries of the Ries where the quartz has been transformed to glass and the biotite and amphiboles remain crystalline.

This author believes that the criterion of selective phase transition is an indisputable evidence of hypervelocity meteorite impact or strong shock. It is characteristic of disequilibrium conditions at high pressure and low to moderate temperature, and is perhaps a safer and more reliable criterion than the occurrence of coesite in a specimen.

Formation of Vitreous Phases Without Viscous Flow and Vesiculation

Isochemical transformation of a crystalline to an amorphous phase in the solid state without melting can be distinguished from vitrification by melting and cooling. The vitreous phase transformed in the solid state retains the fine internal texture and external crystal forms and outline without being destroyed by viscous flow or vesiculation. Such transformation is achieved uniquely by shock.

Grains of perthite and myrmekite are present in the previously described fine-grained biotite granite fragment from Hainfarth (figs. 10, 11). The relative values of indices of refraction are consistent since the lenses of plagioclase glass in the perthite are higher in index than the matrix potassium feldspar glass, and the ribs of silica glass in the myrmekite are distinctly lower than the matrix plagioclase glass. Although there are surely volume changes in such transitions, these were not discernable microscopically. Such vitreous phases may be denser than those of identical

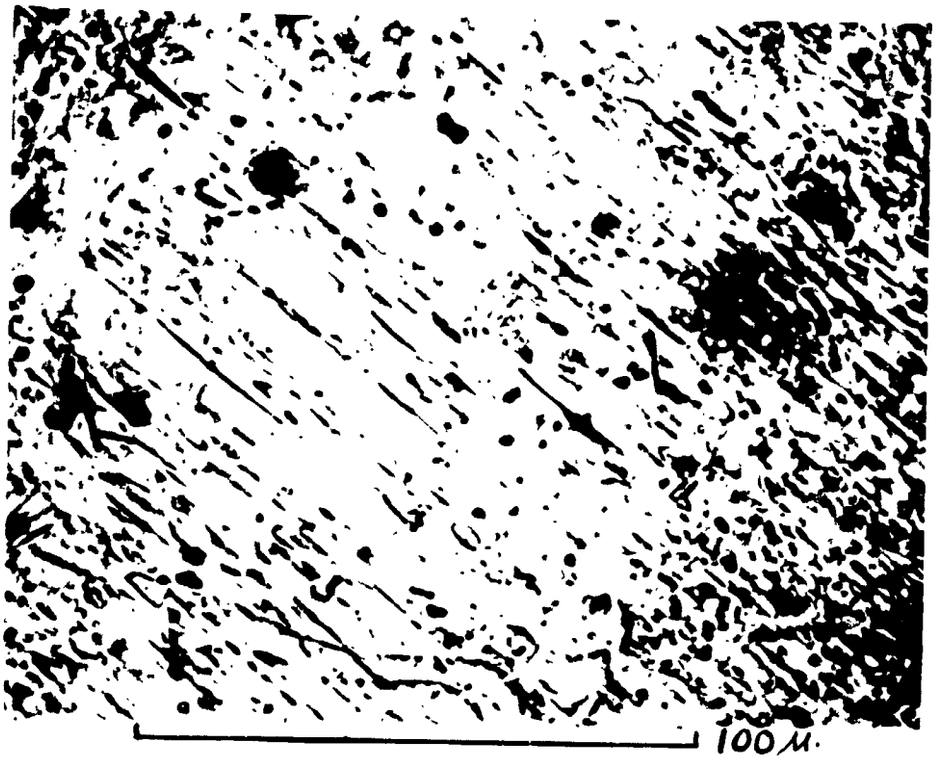

Figure 11.--Same as figure 10; enlarged view of the perthite glass.

Figure 12.--Photomicrograph of a partially transformed plagioclase. The dark bands along the composition plane are isotropic. Crossed nicols, Otting quarry, Ries.

composition formed at 1 atmosphere. Work in progress will settle this question.

Partial vitrification of plagioclase along composition-twin planes is shown in figures 12 and 13. The thin bands of glass are distinctly isotropic and lower in index of refraction than the adjacent untransformed plagioclase. The twin planes appear to have served as nucleation sites.

The formation of vitreous phases without viscous flow and vesiculation is typical of moderately high shock pressure and moderately low shock-induced temperatures. Flowage and vesiculation are to be expected if the shock pressures and temperatures are very high. The crystalline to vitreous phase transition must be extremely rapid, so that little diffusion is permitted. The author believes that reactions such as albite to jadeite plus quartz which require diffusion and time for reaction do not occur under conditions of meteorite impact which probably lasted only a few microseconds to a few seconds. Failure to find jadeite in shocked feldspathic rocks from the suevite of the Ries substantiates this opinion.

Occurrence of High-Pressure Polymorphs

The most widely known high-pressure mineral is diamond from the kimberlite breccia pipes of Africa. Lipschutz and Anders (1961) first suggested that diamonds in the Canyon Diablo iron meteorite were formed by shock upon impact with the earth during the formation of the Meteor Crater of Arizona. A few weeks later coesite was found in the shocked Coconino Sandstone (Chao and others, 1960). Still later, stishovite, a higher pressure polymorph of SiO_2 than coesite, was discovered in coesite-bearing Coconino Sandstone (Chao and others, 1962). Very high pressures are needed in order to form these polymorphs in the laboratory (Coes, 1953; Boyd and England, 1960; Stishov and Popova, 1961; Ringwood and Seabrook, 1962; Wentorf, 1962; Sclar and others, 1962). It therefore seems evident that the occurrences of such high-pressure polymorphs are diagnostic criteria for meteorite

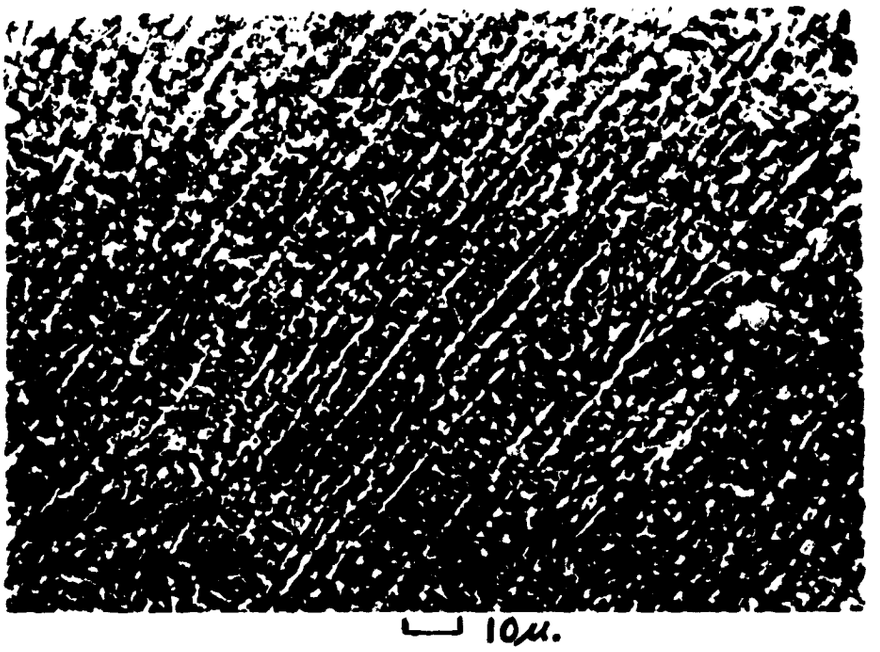

Figure 13.--Same as in figure 12; enlarged view of the partially transformed plagioclase. The narrow bands of glass have distinctly lower index of refraction than the adjacent plagioclase. Reflected light.

impact, since they are found in siliceous sediments occurring at shallow depths and are associated with craters in nonvolcanic terrains.

Since natural coesite was first discovered, in Meteor Crater, it has been found in the Ries crater (Shoemaker and Chao, 1961), the Wabar crater (Chao and others, 1961), the Holleford Crater in Canada (Bunch and Cohen, 1963), the Lake Bosumtwi crater of Ghana (Littler and others, 1962), and in the circular structure of Lake Mien (Swenson and Wickman, 1965). Coesite has also been reported from the Kentland structure (Cohen and others, 1961) and the Richat structure of French West Africa (Cailleux and others, 1964). The last two occurrences are unconfirmed.

Although all these occurrences of coesite are in rocks associated with a circular structure in a nonvolcanic terrain, and may therefore be of meteorite impact origin, it is not a foregone conclusion that coesite may not occur in a tectonic environment formed by concentrated shearing stress. Coesite has not been searched for as extensively in tectonic breccia and shear zones and volcanic explosive craters as it has been in suspected meteorite crater structures. This author therefore regards the occurrence of coesite as evidence of high pressure but not infallible evidence of meteorite impact.

The formation of stishovite requires hydrostatic pressures in excess of 75 kb. Because of such high pressures and the thermal and mechanical instability of stishovite, Skinner and Fahey (1963) concluded that its occurrence on the surface of the earth must be considered very compelling evidence for meteoritic impact. It has so far been found only at Meteor Crater, Ariz., and Ries crater (Chao and Littler, 1963; Hörz, 1965).

Both diamonds (De Carli and Jamieson, 1961) and stishovite (De Carli and Milton, 1965) have been successfully synthesized by explosive shock. The estimated pressures of formation for diamonds are about 300 kb and for stishovite 150-280 kb.

Evidence of Extremely High Temperatures

Evidence of extremely high transient temperatures produced by meteorite impact can be derived either from the fusion of the impact body or the fusion of the minerals of the target rock or both. It is well known that globules, spherules, or spheroids of nickel-iron, a few microns to millimeters in diameter, were formed and embedded in the fused glass or impactite as a result of impact-fusion of the impacting body, such as the Canyon Diablo iron meteorite or the Wabar iron meteorite. The fusion of refractory minerals in impact-heated rocks has been studied less extensively.

Nickel-iron spherules and spheroids from the soil from Meteor Crater, Ariz., are enriched in nickel as well as in phosphorus and sulfur (Mead and others, 1965). Nickel-iron spherules from the impactites of Wabar crater are enriched in nickel (Larson and others, 1964). Metallic spherules have also been discovered in the Ries glass (Chao, 1963; Schüller and Ottemann, 1963, El Goresy, 1964), and from Lake Bosumtwi (El Goresy, 1966). Nickel-iron spherules were also discovered in tektites (Chao and others, 1964). The occurrence and formation of all these nickel-iron spherules are attributed to fusion of the body by impact. The melting temperature of iron with 7-8 weight percent Ni is about 1,500°C (Hansen and Anderko, 1958). The form and quenched textures indicate that the Meteor Crater and Wabar spherules have been melted. The stretched silica glass inclusions in the Ries and tektite glass indicate even higher temperatures. Such high temperatures are generally not attained by natural events within the earth's crust.

As a result of the renewed interest in the origin of the Ries, the impactites from there are being studied by several laboratories. The occurrence of droplets of once-molten rutile, globules of pseudobrookite, the occurrence of baddeleyite as a melting product of zircon (El Goresy, 1965), spherules and stringers of troilite (El Goresy, 1964), and abundant stretched lechatelierite inclusions are all suggestive of high temperatures. Similar features have

also been observed by the author (unpub. data) and by El Goresy (1966) on the impactites from Lake Bosumtwi. Precise estimates of temperatures are not possible; however, as the temperature range of stability of silica glass is greater than 1,728°C (Schick, 1960), the estimated temperature rise should be around 2,000°C.

The petrographic evidence presented and reviewed has led us a long way towards solving the mystery of the origin of many circular structures on the surface of the earth. The evidence of shock-produced, closely spaced planar fractures in quartz and kink-bands in biotite, the evidence of selective solid state phase transitions in shocked biotite granites, the presence of coesite and stishovite, the presence of metallic spherules and the presence of fused and decomposed refractory minerals indicating an extremely high temperature environment, all point to a meteorite impact origin for the Ries. Much similar evidence points to the same origin for Lake Bosumtwi.

PROGRESSIVE STAGES OF METEORITE IMPACT METAMORPHISM

The ejecta from meteorite impact craters presents a rare opportunity for studying the sequence of phase changes of a single mineral species, and an opportunity to observe textural and chemical changes of a specific rock type resulting from different pressures and temperatures. Preliminary results of such studies are presented here.

Sandstone Series

The sandstones from Meteor Crater, Wabar crater, and the Henbury craters illustrate the progressive stages or increasing degree of impact metamorphism. Evidence of high pressure and low to moderate temperatures is listed in columns 1-3 of table 1. Evidence of very high temperatures is listed in column 4. The impactites of Meteor Crater, Ariz., represent a glass probably derived from mixtures of sandstone and dolomitic limestone. They do not belong in the sequence of shock-metamorphosed Coconino Sandstone.

Table 1.--Impact metamorphism of some sandstones

[Columns 1-4 are in order of increasing degree of metamorphism]

	1	2	3	4
Coconino Sandstone Meteor Crater, Ariz.	Quartz with multiple sets of closely spaced fractures.	Intensely fractured quartz with traces of silica glass and coesite along grain boundaries.	Intensely fractured quartz with traces of silica glass, a few percent of coesite, and trace of stishovite.	Vesiculated sandstone or glass bombs with more than 80 percert glass. Little or no coesite or stishovite.
Wabar sandstone Saudi Arabia	--do--	--do--	n.r.	White to black impactite glass with nickel-iron spherules.
Pertatataka shaly sandstone, Henbury craters, Australia	n.r.	Thetomorphic silica glass transformed from detrital quartz; crystalline muscovite.	n.r.	Bloated shale and impactites with more than 80 percent glass; containing minute nickel-iron spheroids.

n.r. = not represented.

The criteria applicable to the advanced stages of shock or impact metamorphism of sandstones follow closely the degree of shock transformation of quartz. Evidence of shock first appears where the quartz grains show multiple sets of closely spaced planar fractures visible microscopically in parallel reflected light. This is followed by complete shock transformation of quartz into thetomorphic silica glass of index of refraction of 1.46. The transformation occurred in the solid state since the details of the quartz grain boundaries and textures are preserved. This type of transition is similar to that which occurred in the experiment on single quartz crystals by De Carli and Jamieson (1959). A higher degree of shock is indicated by the occurrence of coesite along the grain boundaries and the appearance of stishovite in localized areas of high pressure. In the intensely metamorphosed sandstones, the residual shock-induced temperature was so high that the high pressure phases were destroyed, resulting in a rock with a high percentage of silica glass with little or no coesite or stishovite.

Granite and Granitic Gneiss Series

Granite and granitic gneiss fragments in the Ries suevite show various degrees of impact metamorphism. Five hand specimens illustrate increasing degree of shock (fig. 14). Specimen A is a weakly shocked granite gneiss from suevite from the Otting quarry. It contains chiefly chloritized biotite, plagioclase feldspar, potassium feldspar, and quartz. Quartz shows multiple sets of closely spaced planar fractures (fig. 15). The gneissic structure is well displayed. Specimen B is a moderately shocked biotite granite gneiss with thetomorphic silica and feldspar glass and crystalline biotite (fig. 16); the same phases occur in moderately shocked biotite granite (figs. 8, 9). Specimen C is a moderately strongly shocked granite gneiss which is visibly vesicular in hand specimen. Coesite is easily observed optically in the silica glass (figs. 17, 18). The gneissic structure is just

Figure 14.--Hand specimens of granitic gneiss fragments in suevite from the Ries crater showing the various degrees of impact metamorphism: A, Weakly shocked; B, moderately shocked; C, moderately strongly shocked; d, strongly shocked; and E, intensely shocked.

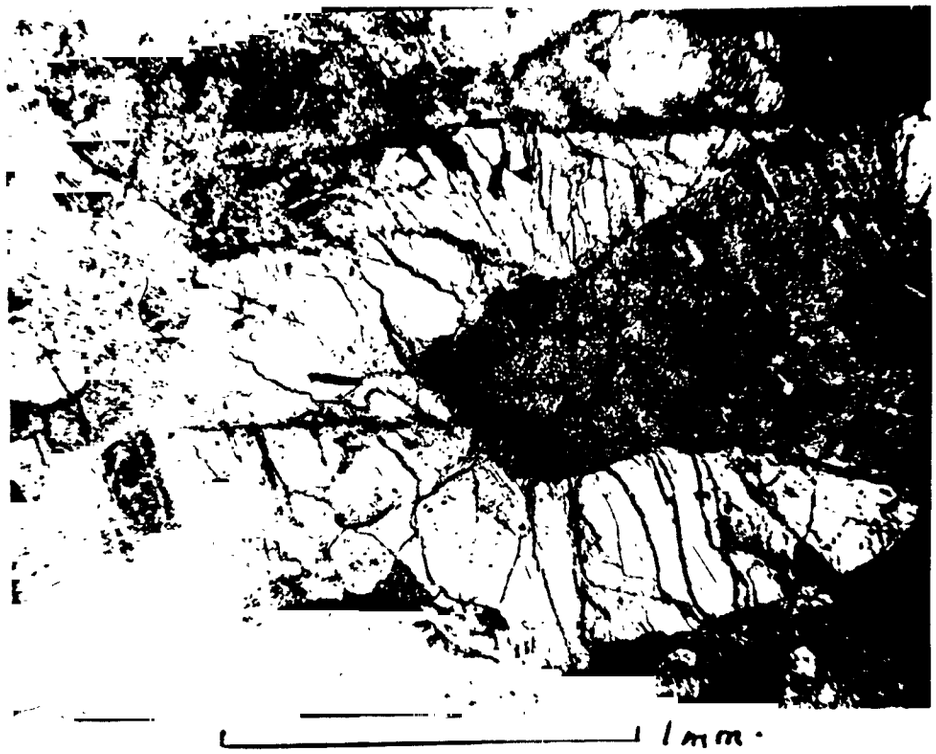

Figure 15.--Photomicrograph of a weakly shocked granite gneiss showing quartz with closely spaced planar fractures. Otting quarry, Ries.

Figure 16.--Photomicrograph of a moderately shocked granite gneiss showing silica glass (Si) with stringers of recrystallized quartz, and slightly vesiculated turbid plagioclase glass (Pl). Reflected light, Otting quarry, Ries.

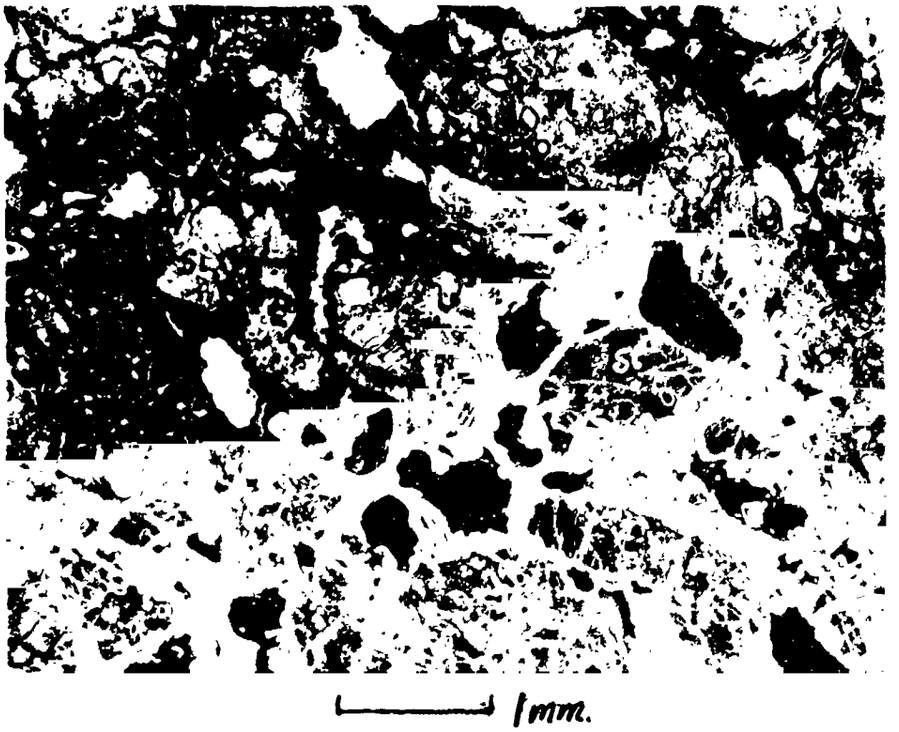

Figure 17.--Photomicrograph of a vesicular moderately strongly shocked granitic rock with silica glass (Si) containing stringers of coesite and vesicular feldspar glass (Pl). Iron-oxide-rich glassy material lines the large vesicles. Reflected light. Otting quarry, Ries.

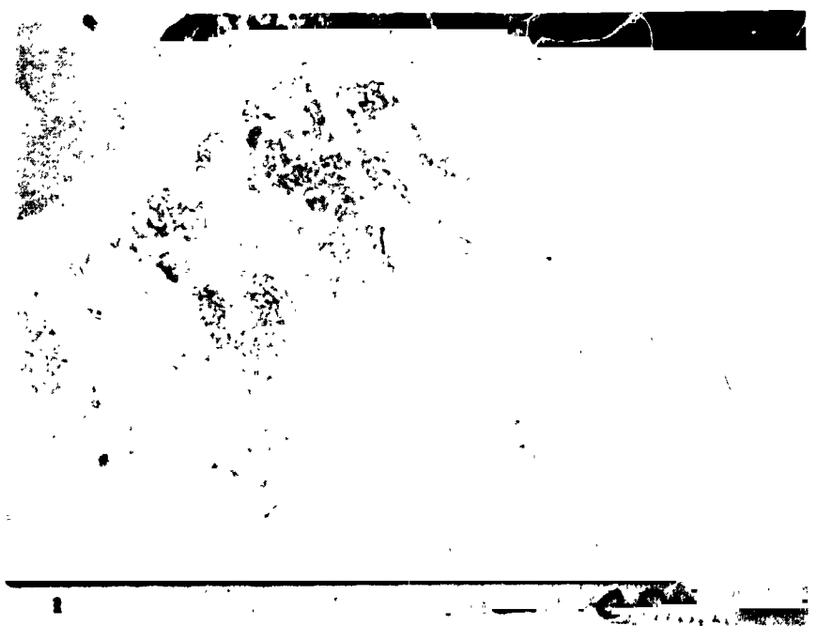

Figure 18.--Photomicrograph of a grain of silica glass (Si) with aggregates of coesite (C) with high refringence, low birefringence. Plain reflected light. Otting quarry, Ries.

perceptible. Specimen D is a strongly shocked granite gneiss which locally contains a brown glass with well-developed flow structures (fig. 19). Specimen E represents an intensely shocked material. It is a sparsely vesicular dark glass with scattered angular mineral fragments which were captured by the glass and inclusions of stretched lechatelierite (fig. 20). The mineralogic and petrographic characteristics of these five specimens are summarized in table 2.

Sequences of other crystalline rocks such as biotite-quartz gneiss, diorite, and plagioclase amphibolite can also be classified into degrees of impact or shock metamorphism on the basis of the shock damage and phase transitions of the associated minerals.

In summary, the various shock effects in quartz in the Ries material are represented as follow with increasing degree of shock:

1. Weakly shocked quartz with multiple sets of closely spaced planar fractures, normal optical properties.
2. Weakly to moderately shocked quartz with anomalous biaxial optical properties, lower mean index of refraction and lower birefringence than normal quartz and partial phase transition to silica glass.
3. Moderately shocked quartz, complete transformation from quartz to thetomorphic silica glass in the solid state.
4. Moderately strongly shocked quartz, represented by silica glass with numerous stringers of recrystallized alpha quartz and traces of coesite.
5. Strongly shocked quartz, represented by nonvesicular silica glass containing abundant aggregates of coesite and some traces of stishovite (not observed optically).
6. Intensely shocked quartz, represented by irregular, embayed, to severely stretched lechatelierite.

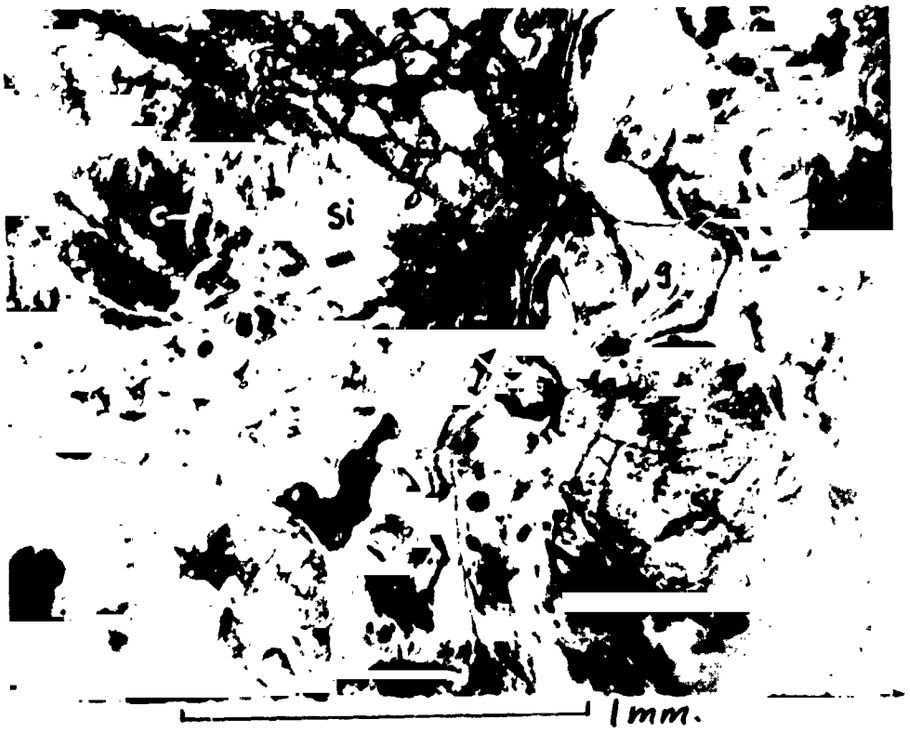

Figure 19.--Photomicrograph of strongly shocked granitic rock showing patches of mixed glass with well-developed schlieren (g) and relict inclusions of silica glass (Si), with stringers of coesite (C). Reflected light, Otting quarry.

Figure 20.--Photomicrograph of intensely shocked granitic material showing glass with sparse mineral fragments, well-developed schlieren, and severely stretched and coiled lechatelierite inclusions. Reflected light. Otting quarry, Ries.

Table 2.--Petrographic characteristics of progressively impact-metamorphosed granite gneisses of the Ries crater, Germany

Specimen----	A (weakly shocked)	B (moderately shocked)	C (moderately strongly shocked)	D (strongly shocked)	E (intensely shocked)
Quartz	Well-developed multiple sets of closely spaced planar fractures (figs. 3, 15).	Partially or completely transformed to thetomorphic silica glass (figs. 8, 9).	Silica glass with stringers of recrystallized quartz and traces of coesite (fig. 16).	Nonvesicular silica glass with abundant stringers of coesite; trace of stishovite (figs. 17-19).	Stretched and coiled lechatelierite (fig. 20).
Plagioclase (K-feldspar)	Sign or effect of shock not detectable optically or by X-ray.	Partially or completely transformed to thetomorphic plagioclase glass (figs, 8, 9, 12, 13); some show well-developed closely spaced planar fractures.	Vesiculated plagioclase glass (fig. 16).	Vesicular to flowed feldspar glasses forming a mixed glass by incorporating iron oxide.	Mixed glass, no longer identifiable as feldspar glass.
Biotite	Normal to slightly kinked.	Some are strongly kinked with reduced birefringence.	Oxidized or decomposed to iron oxide and glass.	Small iron oxide particles, drawn out in the mixed glass and partially dissolved in the glass.	Iron oxide completely dissolved in the glass.
Accessory and opaque minerals	Normal.	Normal.	Slightly oxidized.	Ilmenite with reaction rims of pseudobrookite or magnetite.	Relicts of ilmenite; perhaps a trace of wüstite; droplets of rutile, baddeleyite and spherules of troilite and metal.
Texture	Gneissic texture intact.	Gneissic texture largely intact.	Gneissic texture vaguely visible.	Strongly vesiculated.	Slightly vesiculated glass with well-developed schlieren.

Plagioclase feldspar shows similar changes with increasing shock:

1. Weakly to moderately shocked plagioclase with closely spaced planar fractures and partial transformation from a crystalline to glassy state along and across twinning lamellae.
2. Moderately shocked plagioclase, represented by complete transformation in the solid state from crystalline to thetomorphic glass with inherited details of cleavage and grain boundaries.
3. Moderate to strongly shocked plagioclase, represented possibly by a dense plagioclase glass.
4. Strongly shocked plagioclase, represented by vesiculated plagioclase glass.
5. Intensely shocked plagioclase, represented by vesicular glass with pronounced flow structures.

IMPLICATIONS OF THE SEQUENCE OF PHASE TRANSITIONS AND ESTIMATED PRESSURES AND TEMPERATURES DURING PASSAGE OF A SHOCK WAVE

The shock equation of state of natural material may depend upon its modal mineral composition, bulk specific gravity or porosity, grain size, matrix, and crystallographic orientation and textural layering. Under a given peak shock pressure, the completeness of transformation of a given phase probably depends on its density, compressibility, grain size, crystallographic orientation, and the geometry or the interlocking nature of the adjacent associated minerals and their compressibility. It is particularly important to know the shock equation of state, for example, of plagioclase of a certain composition in a matrix of amphibole crystals in a plagioclase amphibolite rock, so that the peak pressure and the residual temperature in the plagioclase with the passage of strong shock can be calculated. Identical information is needed for the prediction of shock effects in terms of phase transitions for the amphibole in a matrix of plagioclase feldspar. In a similar manner, for a biotite granite, the shock equation of state of quartz in a matrix of feldspars and biotite of that

particular granite should be known. To the author's knowledge, there are no experimental data on the shock equation of state of crystalline rocks for which the peak pressures and the corresponding residual temperature have been calculated.

Detailed mineralogic and petrographic studies of the shocked crystalline rocks in suevite from the Ries show that the pressure and temperature histories reflected by any single mineral species are independent of the chemical composition of the associated minerals. Chemical reaction by diffusion is at a minimum under such transient nonequilibrium conditions. Hence, the mineral facies concept of Eskola will not be applicable to rocks with shock histories. This is true particularly if the shock pressures were high but the induced residual temperatures were low. Coesite has been found only within silica glass and never outside it. It has never been found in a shock-transformed albitic plagioclase as a product of the reaction coesite plus jadeite, for example. Where temperature was high, as in some of the glasses in the suevite of the Ries, the high-pressure phases were largely destroyed, except for relicts or inclusions of silica glass with aggregates of coesite. Under these circumstances, diffusion of iron oxide into the mixed glass, and the decomposition and melting of refractory accessory minerals such as ilmenite, rutile, and zircon are observed (El Goresy, 1964, 1965).

Detailed data of the shock effects in individual rock-forming minerals and associated minerals up to 1,600 kb and 2,500°C, were presented by the author at the symposium on shock metamorphism on natural materials held at Goddard Space Flight Center, Greenbelt, Md., April 14-16, 1966. The data should appear in the symposium volume of that conference.

IMPACT METAMORPHIC FEATURES IN METEORITES AND TEKTITES AND THE STUDY OF RETURNED LUNAR SAMPLES

The study of impact metamorphism not only helps in resolving the origin of crater structures, but also is of value in determining the effect of nuclear devices on natural materials.

Features in meteorites have also been attributed to shock by collisions (Fredriksson and others, 1963). It is also recognized that impact shock affected the concentration and distribution of rare gases in meteorites (Fredriksson and De Carli, 1964; Peter Signer, oral commun., 1964). Equally significant, though controversial, is the origin of diamonds in meteorites (Carter and Kennedy, 1964; Anders and Lipschutz, 1966). The evidence of shock in meteorites is of particular interest because it modifies our understanding of the size and history of breakup and accretion of primary and secondary bodies and of the cooling or heating cycle of meteorites. Lunar material recovered on earth as the result of ejection of such fragments by large meteorite impacts should also bear evidence of shock.

The study of impactites has greatly improved the understanding of the mechanism of formation of tektites (Chao and others, 1964). Although there is no proof that tektites are of lunar origin, aerodynamic evidence indicates that it is a serious possibility (Chapman, 1964). It is easy to recognize the possible importance of the widespread occurrence of vesicular and glassy material on the lunar surface. Photographs taken by Lunik IX and Surveyor I encourage this belief. Whether the glassy lunar surface material formed by consolidation of extruded lunar magma, or is due to cosmic radiation or solar proton bombardment or to meteorite impact shock, the study of shock or impact metamorphism should provide basic data for comparison as well as the identification of constituent phases of shock origin in the study of lunar samples.

REFERENCES CITED

Anders, Edward, and Lipschutz, M. E., 1966, Critique of paper by N. L. Carter and G. C. Kennedy, "Origin of diamonds in the Canyon Diablo and Novo Urei meteorites": Jour. Geophys. Research, v. 71, no. 2, p. 643-661.

Boyd, F. R., and England, J. L., 1960, The quartz-coesite transition: Jour. Geophys. Research, v. 65, no. 2, p. 749-756.

Bunch, T. E., and Cohen, A. J., 1963, Coesite and shocked quartz from Holleford Crater, Ontario, Canada: Science, v. 142, no. 3590, p. 379-381.

_____1964, Shock deformation of quartz from two meteorite craters: Geol. Soc. America Bull., v. 75, no. 12, p. 1263-1266.

Cailleux, André, Guillemaut, Armel, and Pomerol, Charles, 1964, Présence de coesite, indice de hautes pressions, dans l'accident circulaire des Richât (Adrar Mauritanien): Acad. sci. [Paris] Comptes rendus, v. 258, p. 5488-5490.

Carter, N. L., 1965, Basal quartz deformation lamellae - a criterion for recognition of impactites: Am. Jour. Sci., v. 263, no. 9, p. 786-806.

Carter, N. L., and Kennedy, G. C., 1964, Origin of diamonds in the Canyon Diablo and Novo Urei Meteorites: Jour. Geophys. Research, v. 69, no. 12, p. 2403-2422.

Chao, E. C. T., 1963, The petrographic and chemical characteristics of tektites, chap. 3 of O'Keefe, J. A., ed., Tektites: Chicago, Univ. Chicago Press, p. 51-94.

Chao, E. C. T., Dwornik, E. J., and Littler, Janet, 1964, New data on the nickel-iron spherules from Southeast Asian tektites and their implications: Geochim. et Cosmochim. Acta, v. 28, no. 6, p. 971-980.

Chao, E. C. T., Fahey, J. J., and Littler, Janet, 1961, Coesite from Wabar Crater, near Al Hadidah, Arabia: Science, v. 133, no. 3456, p. 882-883,

Chao, E. C. T., Fahey, J. J., Littler, Janet, and Milton, D. J., 1962, Stishovite, SiO_2, a very high pressure new mineral from Meteor Crater, Arizona: Jour. Geophys Research, v. 67, no. 1, p. 419-421.

Chao, E. C. T., and Littler, Janet, 1963, Additional evidence for the impact origin of the Ries basin, Bavaria, Germany: Geol. Soc. America Spec Paper 73, p. 127.

Chao, E. C. T., Shoemaker, E. M., and Madsen, B. M., 1960, First natural occurrence of coesite: Science, v. 132, no. 3421, p. 220-222.

Chapman, D. R., 1964, On the unity and origin of the Australasian tektites: Geochim. et Cosmochim. Acta, v. 28, no. 6, p. 841-880.

Coes, L., Jr., 1953, A new dense crystalline silica: Science, v. 118, no. 3057, p. 131-133.

Cohen, A. J., Bunch, T. E., and Reid, A. M., 1961, Coesite discoveries establish cryptovolcanics as fossil meteorite craters: Science, v. 134, no. 3490, p. 1624-1625.

Cummings, David, 1965, Kink-bands: shock deformation of biotite resulting from a nuclear explosion: Science, v. 148, no. 3672, p. 950-952.

De Carli, P. S., and Jamieson, J. C., 1959, Formation of an amorphous form of quartz under shock conditions: Jour. Chem. Physics, v. 31, no. 6, p. 1675-1676.

_____1961, Formation of diamond by explosive shock: Science, v. 133, no. 3467, p. 1821-1822.

De Carli, P. S., and Milton, D. J., 1965, Stishovite: synthesis by shock wave: Science, v. 147, no. 3654, p. 144-145.

Dietz, R. S., 1963, Cryptoexplosion structures: a discussion: Am. Jour. Sci., v. 261, p. 650-664.

El Goresy, Ahmed, 1964, Die Erzmineralien in den Ries-Bosumtwi-Krater-Gläsern und ihre genetische Deutung: Geochim. et Cosmochim. Acta, v. 28, no. 12, p. 1881-1891.

El Goresy, Ahmed, 1965, Baddeleyite and its significance in impact glasses: Jour. Geophys Research, v. 70, no. 14, p. 3453-3456.

_____1966, Metallic spherules in Bosumtwi crater glasses: Earth and Planetary Sci. Letters, v. 1, no. 1, p. 23-24.

Engelhardt, W. V., and Stöffler, D., 1965, Spaltflächen im Quartz als Anzeichen für Einschläge grosser Meteoriten: Die Naturw., v. 52, no. 17, p. 489-490.

Fredriksson, Kurt, and De Carli, P. S., 1964, Shock emplaced argon in a stony meteorite: Jour. Geophys. Research, v. 69, no. 7, p. 1403-1411.

Fredriksson, Kurt, De Carli, P. S., and Aaramäe, A., 1963, Shock-induced veins in chondrites: Space Research III, 3rd Int. Space Sci. Symposium, Washington 1962, Proc., p. 974-983.

Hansen, Max, and Anderko, Kurt, 1958, Constitution of binary alloys: New York, McGraw Hill.

Hörz, Friedrich, 1965, Untersuchungen an Riesgläsern: Beitr. z.: Min. u. Pet., v. 11, p. 621-661.

Larson, R. R., Dwornik, E. J., and Adler, Isidore, 1964, Electron-probe analysis of "cosmic" particles: New York Acad. Sci. Annals, v. 119, p. 282-286.

Lipschutz, M. E., and Anders, Edward, 1961, The record in meteorites - 4, Origin of diamonds in iron meteorites: Geochim. et Cosmochim. Acta, v. 24, nos. 1, 2, p. 83-105.

Littler, Janet, Fahey, J. J., Dietz, R. S., and Chao, E. C. T., 1962, Coesite from the Lake Bosumtwi crater, Ashanti, Ghana: Geol. Soc. America Abstracts for 1961, Spec. Paper 68, p. 218.

Mead, C. W., Littler, Janet, and Chao, E. C. T., 1965, Metallic spheroids from Meteor Crater, Arizona: Am. Minerologist, v. 50, nos. 5, 6, p. 667-681.

Milton, D. J., and De Carli, P. S., 1963, Maskelynite: formation by explosive shock: Science, v. 140, no. 3567, p. 670-671.

Ringwood, A. E., and Seabrook, Merren, 1962, Some high-pressure transformations in pyroxenes: Nature, v. 196, no. 4857, p. 883-884.

Schick, H. L., 1960, A thermodynamic analysis of the high-temperature vaporization properties of silica: Chem. Rev., v. 60, p. 331-362.

Schüller, A., and Ottemann, J., 1963, Vergleichende Geochemie und Petrographie meteoritischer und volkanischer Gläser: Neues Jahrb. Miner. Abh., v. 100, p. 1-26.

Sclar, C. B., Young, A. P., Carrison, L. C., and Schwartz, C. M., 1962, Synthesis and optical crystallography of stishovite, a very high pressure polymorph of SiO_2: Jour. Geophys. Research, v. 67, no. 10, p. 4049-4054.

Shoemaker, E. M., and Chao, E. C. T., 1961, New evidence for the impact origin of the Ries Basin, Bavaria, German: Jour. Geophys. Research, v. 66, no. 10, p. 3371-3378.

Skinner, B. J., and Fahey, J. J., 1963, Observations on the inversion of stishovite to silica glass: Jour. Geophys. Research, v. 68, no. 19, p. 5595-5604.

Stishov, S. M., and Popova, S. W., 1961, New dense polymorphic modification of silica [in Russian]: Geokhimya, no. 10, p. 837-839.

Swenson, N. D., and Wickman, F. E., 1965, Coesite from Lake Mien, southern Sweden: Nature, v. 205, no. 4977, p. 1202-1203.

Turner, F. J., 1964, Analysis of kinks in micas of an Innsbruck mica schist: Neues Jahrb. Miner. Abh. Br. Sander v., p. 347-356.

Wentorf, R. H., Jr., 1962, Stishovite synthesis: Jour. Geophys. Research, v. 67, no. 9, p. 3648.

N67-19397

NICKEL-IRON SPHERULES FROM THE AOUELLOUL GLASS OF MAURITANIA, AFRICA

By E. C. T. Chao, E. J. Dwornik, and
Celine W. Merrill

The origin of the Aouelloul glass is a subject of current interest to investigators studying terrestrial meteorite impact glasses (impactites) and tektites of possible lunar origin. The Aouelloul crater, 350 m in diameter in Ordovician sandstone, is at lat 20°15' N. and long 12°41' W. in Mauritania, Africa. It was first described by Monod and Pourquié (1951). The associated Aouelloul glass occurs around the crater and has been described by Smith and Hey (1952). Later studies of the Aouelloul glass have been mostly on specific aspects (Barnes, 1963; Cohen, 1958; Senftle and Thorpe, 1959; Cohen and Anania, 1960; Zähringer, 1963; Wagner, 1966; and El Goresy, 1965), none of which reveal much about the origin of the glass.

Although the Aouelloul glass is associated with a well-developed and well-preserved crater, its origin is uncertain. The problem is threefold: (1) Is the Aouelloul crater a genuine meteorite crater? (2) How did the Aouelloul glass form? and (3) Was it derived from the underlying bedrock of the Aouelloul crater?

Several useful and diagnostic mineralogic and petrographic criteria for the identification of meteorite craters have been developed in recent years (Chao, in preparation). Among the criteria pertinent to the study of the origin of the Aouelloul glass are (1) the characteristic microstructures of minerals formed by shock at extremely high strain rates, (2) the occurrence of high-pressure polymorphs, (3) the occurrence of nickel-iron spherules, and (4) evidence of the breakdown of molten products of refractory accessory minerals. So far only baddeleyite, derived

from decomposed zircon, has been reported from the Aouelloul glass (El Goresy, 1965). This paper reports the occurrence of nickel-iron spherules in the Aouelloul glass.

In February 1964, one of us (Chao) accompanied by Prof. Th. Monod, visited the Aouelloul crater in Mauritania, Africa. In addition to a reconnaissance geologic study, more than 2,000 pieces of the Aouelloul glass were collected for detailed mineralogical, petrographic, and chemical studies. Nearly 100 of the medium to large (2-5 cm long) Aouelloul glass samples were sliced into wafers 0.5-1 mm thick. Each wafer was then examined under the binocular and petrographic microscopes in search for nickel-iron spherules and inclusions and structures of special interest. Since none of the sandstone and quartzite samples collected at the crater show any macroscopic evidence of shock or impact metamorphism, it was hoped that some of the inclusions deeply embedded in the Aouelloul glass might contain high-pressure phases or bear evidence of shock.

Approximately 600 wafers of Aouelloul glass were examined microscopically. Thin sections were made of 20 selected wafers, and polished sections of an additional 30 wafers. Nickel-iron spherules were found in several wafers of a single Aouelloul glass specimen, which also contains a partly fused sandstone inclusion 4-5 mm long.

Figures 1 and 2 show the occurrences and the shape of the nickel-iron spherules in the Aouelloul glass. They range from about 0.2 μ, the limit of resolution of the optical microscope, to 50 μ in diameter. Those spherules larger than 20 μ are only partly spherical, with many protuberances. Those smaller than 20 μ are almost perfectly spherical. Figure 1 shows two of the largest spherules recovered so far. Each has a jagged side thus giving the impression that they were torn apart from a larger molten globule and then quenched.

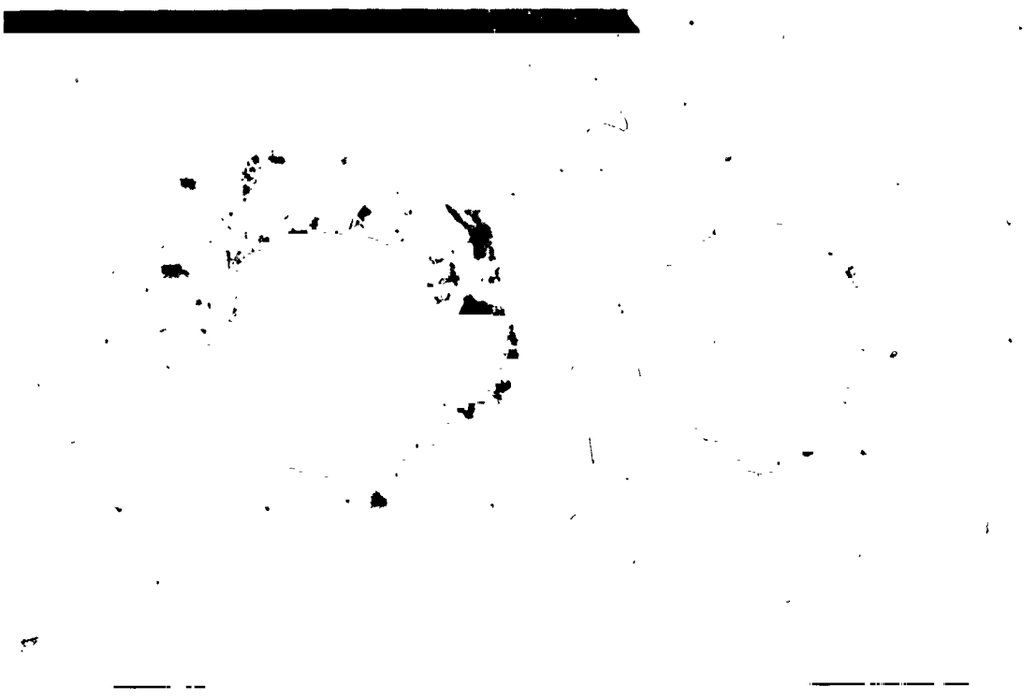

Figure 1.--Photomicrograph of polished wafer showing two partly spherical nickel-iron spherules. Incident light.

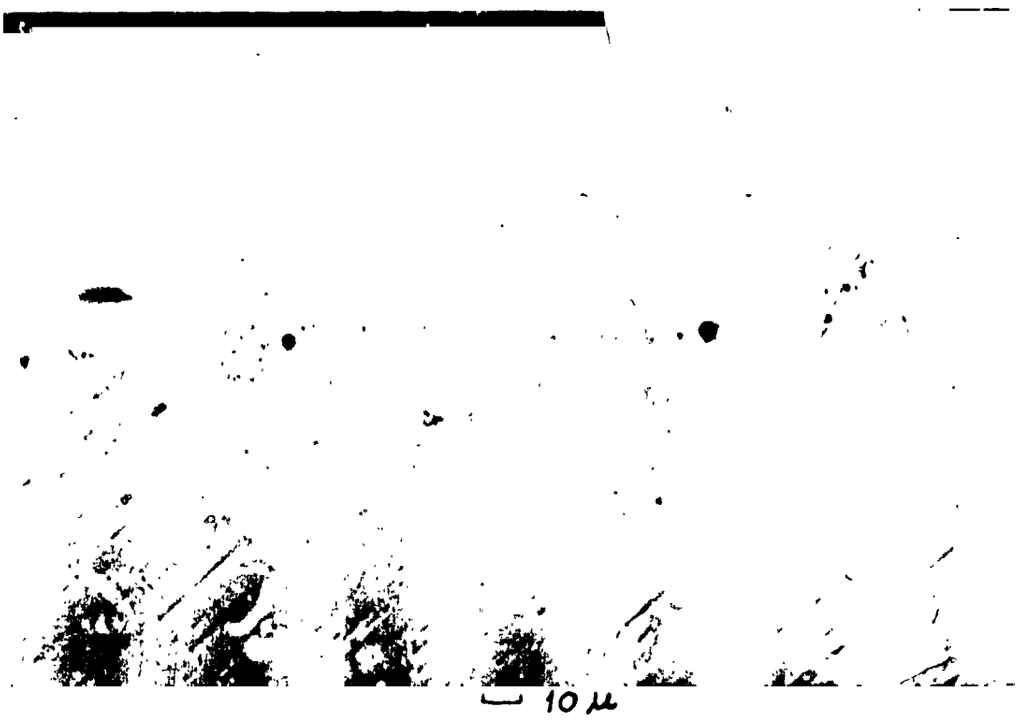

Figure 2.--Photomicrograph of small nickel-iron spherule concentrated in a narrow band of glass. Incident light, polished wafer.

The nickel-iron spherules are clearly concentrated in narrow lenses or layers of bluish-gray to gray glass. The gray glass ranges from wisps or stretched lenses a few microns in width to bands as much as 1 mm wide that extend through the length of the entire specimen. This discrete distribution of the spherules is the principal reason why they are so difficult to find. Each gray lens or band is in turn embedded in a thin sheath of colorless glass within the normally brown Aouelloul glass (fig. 3). Under χ 1,000 magnification, literally thousands of nickel-iron spherules are visible in a band of gray glass. Most of these are less than 0.5 μ in diameter. Viewed in incident light, the spherules sparkle like the stars in the Milky Way.

More than 50 spherules have been studied optically. Of these, 10 are larger than 20 μ, and more than half are larger than 5 μ. Unetched polished sections of these spherules are pale yellowish white in reflected light and are isotropic. These properties are consistent with nickel-iron. Nital etching of two large spherules revealed circular and slightly polygonal grain boundaries of kamacite within the spherule. No other phases were detected.

Several spherules were extracted from the glass for X-ray study. They are strongly magnetic, nearly perfectly spherical, silvery white, and bright and shiny. One of these measuring about 35 μ in diameter was mounted on the tip of a blank X-ray spindle and X-rayed in a Debye-Scherrer camera. The pattern shows a small number of rather sharp spots in both the front and back reflecting regions, indicating that the spherule contains a small number of crystals. The pattern, however, can easily be identified as kamacite or α-iron with a unit cell of $\underline{a} = 2.865$ A $\pm$ 0.005.

Eleven spherules, all larger than 5 μ, were analyzed by an electron microprobe using analyzed kamacite from the Canyon Diablo iron meteorite with 7.0 percent Ni as a standard. The results were not corrected for absorption and fluorescence, because the matrix effect is similar to that of the standard used. The analyse

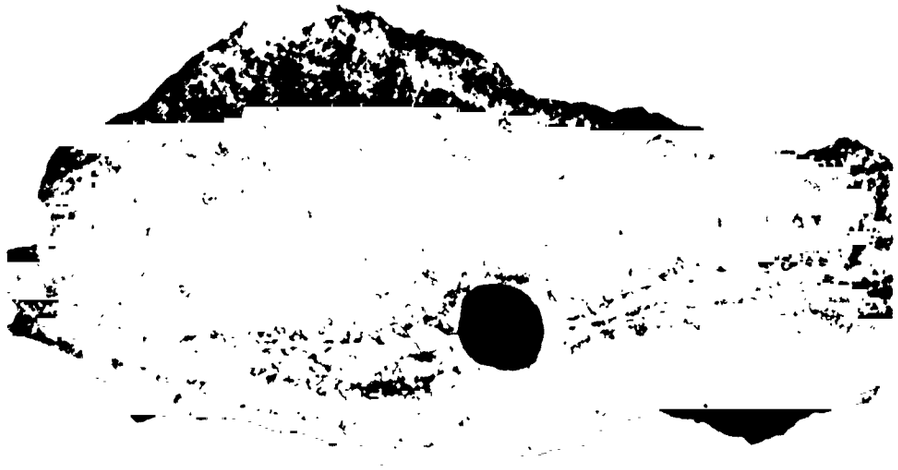

Figure 3.--Photomicrograph of an Aouelloul glass wafer with a hole in it showing the discrete occurrence of the nickel-iron spherules in three lenses (black areas) within a sheath of clear glass (white areas bordering the black) in the matrix brown glass (gray). Each dark lenticular area contains thousands of nickel-iron spherules. Transmitted light.

show that the spherules consist mostly of iron, with a nickel content ranging from 1.7 to 9.0 percent (table 1). These analyses are similar to those of nickel-iron spheroids recovered from the Meteor Crater of Arizona which range from 2 to 24 percent Ni (Mead, Littler and Chao, 1965). The analyses are consistent with a meteoritic origin for the spherules. We therefore conclude that the occurrence of nickel-iron in the Aouelloul glass is proof that the Aouelloul crater is a genuine meteorite crater.

Table 1.--Ni content of Ni-Fe spherules from the Aouelloul glass

Spherule No.	Diameter (μ)	Wt percent Ni
1	39	1.9
2	50	2.2
3	26	2.6
4	10	7.0
5	6	2.6
6	18	3.1
7	13	4.8
8	21	2.9
9	25	2.2
10	9	1.7
11	10	9.0

Note.--Excitation voltage 25 kv, specimen current 0.01 μa. Not corrected for absorption and fluorescence. Precision of the analyses is within 5 percent of the amount present.

Can we be sure that Aouelloul glass is not a tektite of possible lunar origin, since tektites also contain nickel-iron spherules of comparable nickel content (Chao, Dwornik and Littler, 1964)? As pointed out by Chao in his study of nickel-iron spherules and the variation of iron content in tektites (Chao, 1963), iron must be oxidized before it can be dissolved in a silicate melt. Furthermore,

Brett (1966) has reported that the matrix glass immediately surrounding nickel-enriched nickel-iron spherules in terrestrial impact glasses commonly shows pronounced enrichment of iron, probably caused by oxidation in the atmosphere and diffusion before the glass was completely cooled. Although the lack of iron enrichment in the glass does not prove vacuum conditions during its formation, which would be required for a lunar origin, the presence of such enrichment is strong evidence for formation in an oxygen-rich environment (Brett, 1966).

Electron microprobe analyses of the iron content along a traverse across the gray glass, clear glass, and the brown matrix glass were made. The standards used consisted of an analyzed moldavite with 1.35 percent Fe, an analyzed australite with 2.73 percent Fe, and an Ivory Coast tektite with 5.06 percent Fe. Because of the comparable amount of iron and similarity in matrix, no correction for absorption and fluorescence, etc., was made. Table 2 shows clearly that the various parts of the gray glass in which the nickel-iron spherules were embedded contain more iron than the brown matrix Aouelloul glass. In one spot analyzed, the gray glass contained twice as much iron as the brown glass. The iron content of the brown matrix glass, 1.8-2.0 percent, agrees well with data on four Aouelloul glass samples, analyzed by X-ray flourescence (Chao, Merrill, Cuttitta, and Annell, 1966). The iron content of the sheath of clear glass around the gray glass is below the limit of detection.

In order to determine whether the enrichment of iron in the spherule-bearing gray glass is due to discrete disseminated nickel-iron spherules or to dissolved iron, optical and X-ray studies were made. Several bands of the spherule-bearing gray glass with a sheath of colorless glass and attached brown matrix glass were carefully cut out and crushed into small fragments. Chips of gray glass that under χ 150 magnification showed no nickel-iron spherules and gray

Table 2.--Fe content of gray glass (containing Ni-Fe spherules), clear glass, and matrix Aouelloul glass

		Spot position analyzed[1]	Percent Fe
In gray glass	1.	20μ to right of spherule 8	2.8
	2.	Between spherules 8 and 9	4.0
	3.	20μ to left of spherule 9	3.2
	4.	5 μ	2.6
	5.	30 μ	2.0
In clear glass	6.	70 μ	< .2
	7.	95 μ	< .2
In brown Aouelloul glass	8.	125 μ	1.9
	9.	155 μ	2.0
	10.	195 μ	1.8
	11.	260 μ	1.8
	12.	325 μ	1.8

Note.--Excitation voltage 25 kv, specimen current 0.01 μa. Not corrected for absorption and fluorescence. Precision of the analyses is within 5 percent of the amount present.

[1]The distances listed for 4 through 12 are traverse distance from spherule 9 toward viewer and across the boundaries of the gray glass, clear glass, and the brown matrix Aouelloul glass.

glass with visible spherules were mounted on top of separate blank spindles and X-rayed for 24 hours with a microfocus X-ray diffraction unit. The specimen with spherules yielded a film that showed a weak but clear reflection at d = 2.02 A for kamacite; the other showed no reflections.

Under the microscope, the boundaries between the gray glass, the colorless glass, and the brown matrix glass are very sharp. Two types of colorless glass are present: One has an index of refraction of 1.465 ± 0.002 and is nearly pure silica; the other has an index of 1.473 ± 0.001. The matrix brown glass has an

index of 1.479 ± 0.001. Some of the gray glass tends to splinter into elongated lenses and rods. They show notable birefringence, which indicates compression, a feature consistent with impact origin. Other gray glass fragments are completely isotropic and show no strain. Discrete nickel-iron particles are disseminated irregularly in the gray glass; certain parts are almost free of them. The gray glass has a much higher index of refraction (1.504 ± 0.001, fig. 4). This rise in index could not be due to the presence of discrete nickel-iron particles. It must be the result of incorporation of dissolved oxidized iron from the meteorite source. This fact and the enriched nickel content in one of the spherules (9 percent Ni) with respect to normal kamacite of iron meteorites, indicate that the fusion event took place in an oxidizing environment such as the earth's atmosphere (Brett, 1966).

The brown Aouelloul glass contains many partially digested and undigested sandstone inclusions. It must have been molten during the cratering event. Since its gross chemical composition is nearly identical with that of the underlying Zli sandstone (Chao, Merrill, Cuttitta, and Annell, 1966), we believe that this glass is derived from the Zli sandstone. We also believe that it was fused by a meteoritic impact and, thus, that much of the iron content in the Aouelloul glass is of meteoritic origin. The gray glass is derived from addition of nickel-iron to a silica glass fused perhaps from either the Zli sandstone or the Oujeft quartzite (Chao, Merrill, Cuttitta, and Annell, 1966). These discrete lenses of high-silica glass were engulfed by the more abundant brown glass during the violent event of the formation of the Aouelloul crater.

The Aouelloul glass is similar in texture to some tektites. Like these it contains numerous lechatelierite inclusions. In composition, however, it is nearly identical with the Zli sandstone which underlies the crater. Its geographic distribution is restricted to the immediate vicinity of the Aouelloul crater. We conclude from the evidence presented that the Aouelloul glass is an impactite of terrestrial origin and is not a tektite.

Figure 4.--Photomicrograph of a fragment of spherule-bearing gray glass (a) with an index of refraction N of 1.504, surrounded by clear glass (b) with N = 1.473, and clear glass (c) with N = 1.463. Black spots in the gray glass (a) are nickel-iron spherules. Transmitted polarized light, grain immersed in oil with N = 1.491.

REFERENCES CITED

Barnes, V. E., 1963, Tektite strewn-fields, in O'Keefe, J. A., ed., Tektites: Chicago, Univ. of Chicago Press, p. 25-50.

Brett, Robin, 1966, Metallic spherules in tektites and impactites [abs.]: Am. Geophys. Union Trans., v. 47, no. 1, p. 145.

Chao, E. C. T., 1963, The petrographic and chemical characteristics of tektites, in O'Keefe, J. A., ed., Tektites: Chicago, Univ. of Chicago Press, p. 51-94.

_____Impact metamorphism, in Researches in geochemistry: v. 2, New York, John Wiley & Sons, Inc. (in preparation).

Chao, E. C. T., Dwornik, E. J., and Littler, Janet, 1964, New data on the nickel-iron spherules from southeast Asian tektites and their implications: Geochim. et Cosmochim. Acta, v. 28, p. 971-980.

Chao, E. C. T., Merrill, C. W., Cuttitta, F. C., and Annell, Charles, 1966, The Aouelloul crater and the Aouelloul glass of Mauritania, Africa [abs.]: Am. Geophys. Union Trans., v. 47, no. 1, p. 144.

Cohen, A. J., 1958, The absorption spectra of tektites and other natural glasses: Geochim. et Cosmochim. Acta, v. 14, p. 279-286.

Cohen, A. J., and Anania, John, 1960, Nickel in moldavites [abs.]: Jour. Geophys. Research, v. 65, p. 2482.

El Goresy, Ahmed, 1965, Baddeleyite and its significance in impact glasses: Jour. Geophys. Research, v. 70, no. 14, p. 3453-3456.

Mead, C. W., Littler, Janet, and Chao, E. C. T., 1965, Metallic spheroids from Meteor Crater, Arizona: Am. Mineralogist, v. 50, no. 5/6, p. 667-681.

Monod, Théodore, and Pourquié, A., 1951, La cratère d'Aouelloul (Adrar, Sahara Occidental): L'Inst. francais d'Afrique Noire Bull., v. 13, p. 293-304.

Senftle, F. E., and Thorep, A., 1959, Magnetic susceptibility of tektites and some other glasses: Geochim. et Cosmochim. Acta, v. 17, no. 3/4, p. 234-247.

Smith, W. C., and Hey, M. H., 1952, The silica-glass from the crater of Aouelloul (Adrar, western Sahara): L'Inst. francaise d'Afrique Noire Bull., v. 14, no. 3, p. 763-776.

Wagner, Güther, 1966: Zeitschr. Naturf., v. 21a, no. 6, p. 733-745.

Zähringer, J., 1963, Isotopes in tektites, in O'Keefe, J. A., ed., Tektites: Chicago, Univ. of Chicago Press, p. 137-149.

LARGE-SCALE PLANE WAVE SHOCK EXPERIMENTS DESIGNED FOR SAMPLE RECOVERY

By T. J. Ahrens,[1] D. D. Keough,[1]
and D. J. Milton

Several petrographic features ascribed to shock during impact events have been reproduced by subjecting rock specimens to explosive shock loading in the laboratory. In a typical experiment (Milton and De Carli, 1963), specimens of gabbro the size and shape of a small coin were enclosed in a steel container and shock loaded by impacting the assembly with a steel flying plate accelerated by a plane-wave generator. The pyroxenes of the gabbro remained crystalline, whereas the plagioclase underwent a solid-state transformation to glass (maskelynite). The product closely resembles the rare meteorites of the shergottite class and plutonic rocks from the Clearwater Lakes and Ries craters that are presumably shock metamorphosed. The principal difference between the experimentally shocked gabbro and shergottite is the intense brecciation of the gabbro, the result of interaction of shock waves originating at interfaces and boundaries of the specimen and its container. A problem more serious than poor correspondence to the natural environment is that considerable uncertainty is introduced into calculation of the pressure and temperature history of the multiply shocked laboratory specimen.

It would be advantageous to perform experiments on a semi-infinite rock target (such as a smooth-surfaced outcrop) in which the shock can dissipate without reflections. Another advantage of a large-scale in situ experiment is that the rock may be subjected to shock pressures of longer duration than the several microseconds now possible in the laboratory. The longer time scale of such

[1]Poulter Laboratories, Stanford Research Inst., Menlo Park, Calif.

experiments would more realistically simulate the shock loading associated with the impact of meteorites with planetary surfaces. Planarity of the shock front is critical in the design of the experiment. We expect that if a sufficiently planar shock wave is induced into a homogeneous rock, radial material flow should not take place, so that a crater would not form and shock-metamorphosed rock would remain in place for post-shot sampling.

An experimental assembly designed at Poulter Laboratories of the Stanford Research Institute produces a planar shock wave and an associated relatively planar particle velocity flow field over an area of nearly half a square meter. Such an assembly is expected to deliver a peak shock pressure on the order of 250 kilobars for perhaps 10 microseconds with a reasonable weight of explosive. The explosive configuration should allow the pressure profile induced in a given rock type to be later measured in the laboratory (using, for example, a tombstone-sized sample of rock) and to be calculated using a one-dimensional time-dependent computer code. Techniques have been developed and are currently being employed at Poulter Laboratories for measuring shock-wave profiles in rocks and other solids (Berstein and Keough, 1964; Keough and others, 1964; Keough, 1964). The artificial viscosity type of computer code used to describe the shock propagation in space and time resulting from the interaction of a detonating high explosive with a solid such as a rock was described by Erkman (1965).

The assembly (figs. 1, 2) is an adaptation of the "mousetrap" plane wave generator. A sheet-metal geodesic surface covered by sheet explosive serves as a line initiator (Erkman, 1959). The detonation wave originates at the apex and reaches all points on the opposite edge of the geodesic surface simultaneously as a line wave, which detonates a plane sheet of explosive. The detonation of this sheet throws an aluminum plate against a pad of explosive in contact with the target. The mousetrap angle between the flyer plate and the explosive pad (fig. 1) is chosen so that the sum of

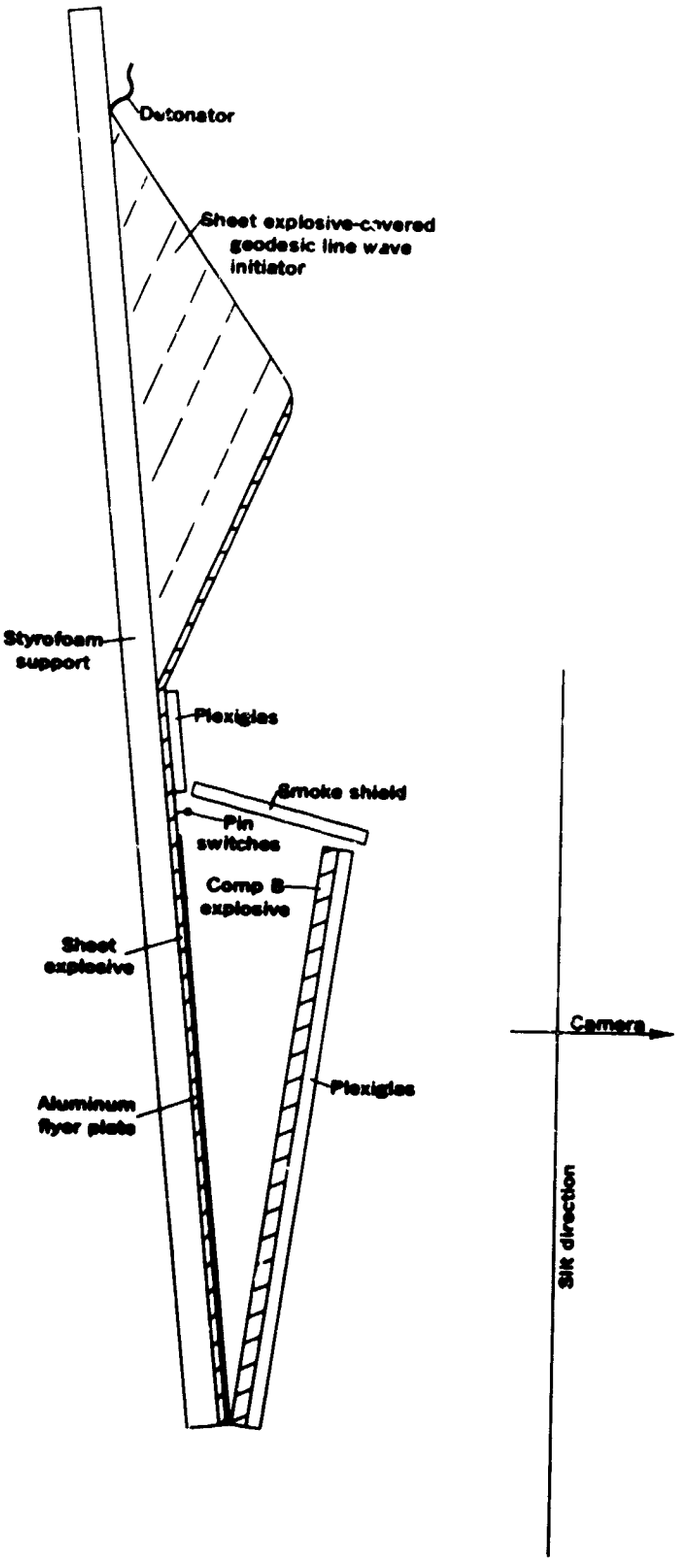

Figure 1.--Prototype explosive assembly, as set up for smear photography.

Figure 2.--Prototype explosive assembly on firing mound, Calaveras Test Site.

time required for the shock front to reach a point on the flyer plate and the time of flight of that point of the plate is constant for all points. Thus the explosive pad is detonated simultaneously over its entire face by simultaneous impact of the flyer plate, and a planar shock wave is transmitted into the target.

Two assemblies have been tested at the Calaveras Test Site of SRI. In the first (figs. 1, 2), sheet explosive 0.2 inch thick was used to cover the geodesic surface and to drive a 1/16-inch aluminum flyer plate against a 24χ24χ1/2-inch pad of Composition B explosive resting against a Plexiglas plate. The flash produced as the shock wave reached the air trapped between the explosive pad and the Plexiglas was recorded by a smear camera as viewed through 15 slits (fig. 3b), in positions corresponding to the dark lines of figure 3a. The smear camera also recorded the flash from a segment of the sheet explosive between the geodesic surface and the flyer plate (this portion of the smear photograph is omitted in fig. 3c). In addition, eight pin contacts were placed on the sheet explosive just above the flyer plate to record the time of detonation electronically. The slope of the streaks in the smear-camera record (fig. 3c) indicates the closure time, which depends on the mousetrap angle. In this case, the angle was 0.9° ± 0.15° smaller than it should have been for simultaneous detonation of the Composition B explosive pad. The spacing and the irregularities of the streaks indicate other deviations from simultaneity of detonation in the explosive pad. Serious departure occurred in the upper few inches of the pad. The cause may have been either air resistance to the flyer plate where its path is longest or interference by the shock wave propagated in the air from the explosive of the geodesic surface. Over the larger part of the explosive pad, however, the detonation was (allowing for the effect of the mousetrap angle error) instantaneous within ± 1 microsecond. The same limits were indicated for detonation of the sheet explosive above the flyer plate by the smear photograph and the pin switch record.

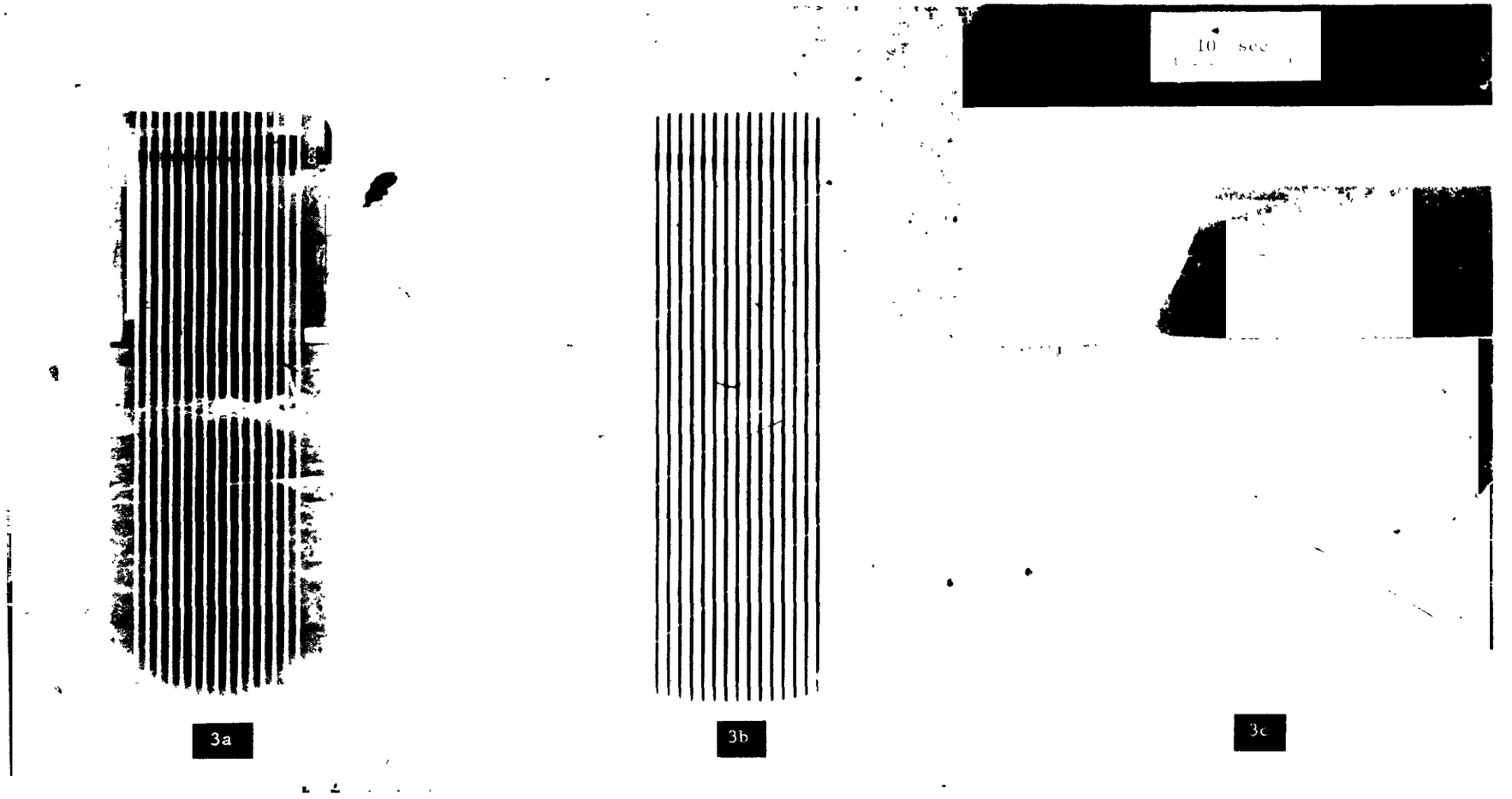

Figure 3.--Smear-camera photography. 3a, Still view, with position of slits indicated by black grid lines. From top to bottom: end of geodesic Plexiglas recorder on sheet explosive, smoke shield, Plexiglas recorder on explosive pad, chair stand, ground; 3b, still view through slits; 3c, portion of smear photograph showing detonation of explosive pad, smear from right to left.

In the second experiment, a heavier (1/8 inch) flyer plate accelerated by a thicker (0.4 inch) sheet of explosive was used to overcome the air resistance, the geodesic was turned over so that the flat explosive-covered surface lay against the styrofoam support, and the mousetrap angle was corrected. In this experiment, detonation instantaneous within ± 1 microsecond occurred over the entire explosive pad. This gives a satisfactorily planar wave, and the design of the explosive assembly is regarded as complete.

A site on Bear Ridge, Fresno County, in the Sierra Nevada has been selected for the field experiments. Glaciated outcrops of granodiorite provide smoothly curved convex surfaces on which experiments can be placed about 30 feet from any visible vertical joints. Horizontal sheeting is unusually wide spaced in the area--the first major sheet fracture is probably at least 15 feet down. Since the outcrops are rough on a scale of 1 or 2 inches, it will be necessary to grind the target area to a plane.

REFERENCES CITED

Bernstein, D., and Keough, D. D., 1964, Piezoresistivity of Manganin: Jour. Appl. Physics, v. 35, p. 1471-1474.

Erkman, J. D., 1959, Simultaneous detonation along a line: Rev. Sci. Instruments, v. 30, p. 818-820.

_____1965, Elastoplastic effects in the attenuation of shock waves: Naval Ordnance Lab. Symposium on Detonation, 4th, Oct. 13-15, 1965.

Keough, D. D., 1964, Pressure transducers for measuring shock wave profiles; phase IX, additional gage development: Natl. Aeronautics and Space Adm. Rept. 1414-1.

Keough, D. D., Williams, R. G., and Bernstein, D., 1964, Piezoresistive pressure transducer: Am. Soc. Mech. Eng. Pub. 64-WA/PT-5.

Milton, D. J., and De Carli, P. S., 1963, Maskelynite: formation by explosive shock: Science, v. 140, p. 670-671.

INFLUENCE OF STRESS HISTORY ON LOW-TEMPERATURE THERMOLUMINESCENCE OF HALITE

By Carl H. Roach

INTRODUCTION AND ACKNOWLEDGMENTS

A study of thermoluminescence characteristics of rocks from several geological environments was started by the U.S. Geological Survey in May 1961 to investigate the extent to which thermoluminescence could be used to determine the temperature, radiation, pressure, and chemical history of rock-forming minerals. It was soon discovered that some rocks exposed at rock quarries, terrestrial meteorite craters, and along large fault systems where they had been exposed to unusual shock or stress histories had different thermoluminescence characteristics than the same rock bodies in nearby localities that had been subjected to less stress. This relationship made it desirable to study the influence of stress history on thermoluminescence properties of common rock-forming minerals. Although several different rock types have been studied, this report will discuss only the results of a study of the influence of stress history on low-temperature thermoluminescence of halite (rock salt).

Laboratory triaxial testing procedures were used to stress samples of halite at low strain rates, and laboratory shock-loading techniques were used for obtaining high rates of strain. Through cooperative arrangements with the Advanced Research Projects Agency, U.S. Department of Defense, and the U.S. Atomic Energy Commission, thermoluminescence studies were made of the effects on surrounding halite (rock salt) of two underground nuclear explosions conducted by the U.S. Atomic Energy Commission.

This research program was conducted on behalf of the Advanced Research Projects Agency, U.S. Department of Defense, whose support the author greatly appreciates.

The author is especially indebted to Mr. Lorin R. Stieff (Headquarters, U.S. Air Force) and to Mr. Theodore George (Advanced Research Projects Agency) for handling all field support and logistics requirements for the study of the Gnome and Salmon underground nuclear explosions. The Laue back-reflection X-ray photographs were graciously provided by Dr. Richard Barton, Colorado School of Mines, and most of the low-temperature thermoluminescence glow curves were prepared by Mr. Gordon R. Johnson, U.S. Geological Survey. Mr. T. S. Sterrett supervised the drilling operations for obtaining the subsurface cores.

THEORY OF THERMOLUMINESCENCE

Thermoluminescence is the light, or radiation, emitted by some minerals as they are heated from a convenient low temperature (usually room temperature or lower) to a higher temperature that is below the temperature of incandescence (Curie, 1963; Leverenz, 1950). The thermal energy supplied during heating causes electrons to move from electron traps, where they are in a metastable excited state, to luminescence centers where the electrons undergo deexcitation and assume a lower energy state. The light emitted is a result of the drop in energy level that occurs as the electrons move from electron traps to luminescence centers.

Thermoluminescent minerals may undergo excitation by receiving thermal, optical, high-energy ionizing radiation, mechanical, or chemical forms of energy. Excitation by these methods may provide enough energy to raise some electrons into the conduction band and allow them to migrate through the crystal and eventually become trapped in electron traps. Electron traps are formed by several types of crystal imperfections that have the ability to localize an electron at an excited energy level. At least six types of primary imperfections may serve as electron traps: (1) phonons, (2) free electrons and positive holes, (3) excitons, (4) vacant lattice sites and interstitial atoms, (5) foreign atoms in either interstitial or substitutional positions, and (6) structural dislocations (Gray,

1957). Each of these crystal imperfections, or combinations thereof, may be important in electron trapping. Electron trapping is a fundamental process for storing energy in electronically active solids, but the physical details of the process are not completely known.

Most thermoluminescent minerals have some of their electron traps loaded as they exist in their natural environment. The percentage of electron traps that are loaded, or occupied, is controlled by the geological or physical history of each mineral. In applying thermoluminescence techniques to the study of shock- or stress-induced changes in solid-state characteristics of rocks, the investigator is concerned with the degree to which the mechanical and thermal energy associated with a high-energy shock or stress wave will change either the total number of electron traps or the number of filled, or occupied, electron traps. Thermoluminescence measurements of equivalent shocked and unshocked samples is the method used to determine how a shock event will alter the number of occupied electron traps in a rock or mineral. The degree to which a shock event will alter the total number, or population, of electron traps in a rock or mineral can be estimated by first filling all traps by means of irradiation methods and then comparing thermoluminescence measurements of the shocked and unshocked samples.

THERMOLUMINESCENCE MEASUREMENTS

Thermoluminescence is studied most conveniently by the "glow curve" technique. A glow curve is a graph showing intensity of thermoluminescence, in relative units, as a function of temperature while the sample is being heated. The U.S. Geological Survey is currently obtaining glow curves by heating samples through two ranges of temperature: "high-temperature" glow curves are obtained by heating samples from room temperature to 400°C, and "low-temperature" glow curves are obtained by heating the samples from the boiling point of liquid nitrogen (-195.8°C) up to the temperature of melting ice (0°C). Only low-temperature glow curves are discussed in this report, because the high-temperature thermoluminescence

of halite has not been found to vary diagnostically with shock.

Low-Temperature Glow Curves

Low-temperature glow curves are made by lowering the temperature of the specimen to the temperature of liquid nitrogen (-195.8°C), loading or filling the electron traps by X-ray excitation, and heating the specimen to 0°C.

The sample holder used to obtain low-temperature glow curves is a cylindrical brass chamber consisting of two parts that can be joined in such a way as to allow the chamber to be evacuated (fig. 1). The sample holder is used in the following manner: The specimen is inserted into the sample holder, the two pieces are joined, and the chamber is evacuated to a pressure of about 100 microns of mercury. Next, the evacuated chamber containing the specimen is immersed in a dewar flask that is nearly filled with liquid nitrogen. The temperature of the specimen is monitored by an iron-constantan thermocouple that is inserted into the bottom of the sample holder and is encased in ceramic tubing outside the holder for protection during handling. After the thermocouple reading indicates that the sample has been at liquid-nitrogen temperature for about 2 minutes, the sample is subjected to X-radiation through the mica window at the top of the chamber. The time of exposure of X-radiation varies considerably with the mineral being studied. Halite was X-rayed at 80 kilovolts and 15 milliamps for 15 seconds. After X-ray excitation, a photomultiplier tube (RCA No. 6655A), with a peak response in the visible near-ultraviolet region, is mounted vertically above the mica window; then the dewar is removed, exposing the base of the sample holder to a jet of heated air. The air jet is supplied by a blower-type resistive heater that is mounted at a fixed position beneath the chamber. The light, or radiation, emitted during heating is detected by the photomultiplier tube, amplified, and fed into the Y-axis input of an X-Y recorder. The electrical potential of the iron-constantan thermocouple in the sample holder drives the X-input of the same recorder. Thereby,

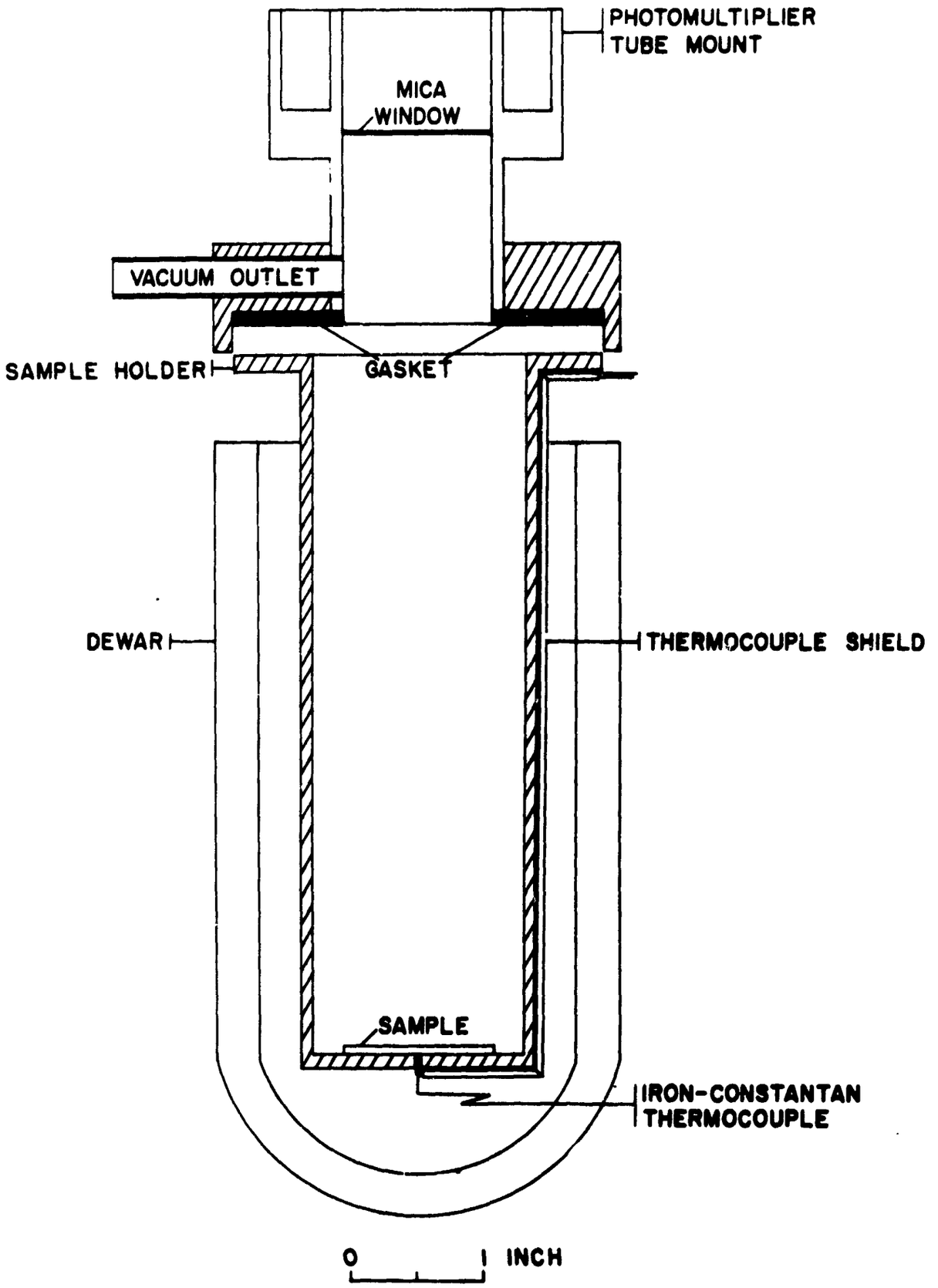

Figure 1.--Sample holder for obtaining low-temperature glow curves.

the intensity of thermoluminescence is automatically plotted against the rise in temperature of the sample, producing a low-temperature glow curve (fig. 2). Although the apparatus is simple in design, the reproducibility of glow curves is very good.

Glow curves of halite samples studied to date have one prominent peak that occurs at about -95°C (fig. 2). A secondary peak on most glow curves occurs near 0°C, and minor peaks of much lower intensity occur between the main peak and liquid nitrogen temperature. Since all these peaks behave in the same way relative to stress history, only the main peak is used as an indicator of intensity of stress on the halite. Thin wafers of halite with parallel sides were used for thermoluminescence measurements. The parameter used for comparing thermoluminescence of solid wafers was determined by dividing the peak intensity of thermoluminescence of the main peak by the area of the wafer.

Autoluminographs

Previous research by the author has revealed that high-energy shock will induce enough thermoluminescent traps in halite so that its low-temperature thermoluminescence will expose a nearby film. Photographs obtained by utilizing the light emitted from minerals during the thermoluminescence process are known as autoluminographs and have been previously described by Baskerville and Kunz (1904), by Iimori and Iwase (1931), and by Brown (1933). Autoluminographs are especially valuable because they allow one to determine the distribution of thermoluminescence with respect to microscopic crystallographic features. Since it is of great importance to learn as much as possible about the physical characteristics of shock-induced thermoluminescence, an apparatus was developed for obtaining high-resolution low-temperature autoluminographs of thin wafers of halite.

The photographic technique for obtaining the autoluminographs is as follows: Thin wafers of halite are cooled to the boiling point of liquid nitrogen (-195.8°C), X-rayed for 60 seconds at a

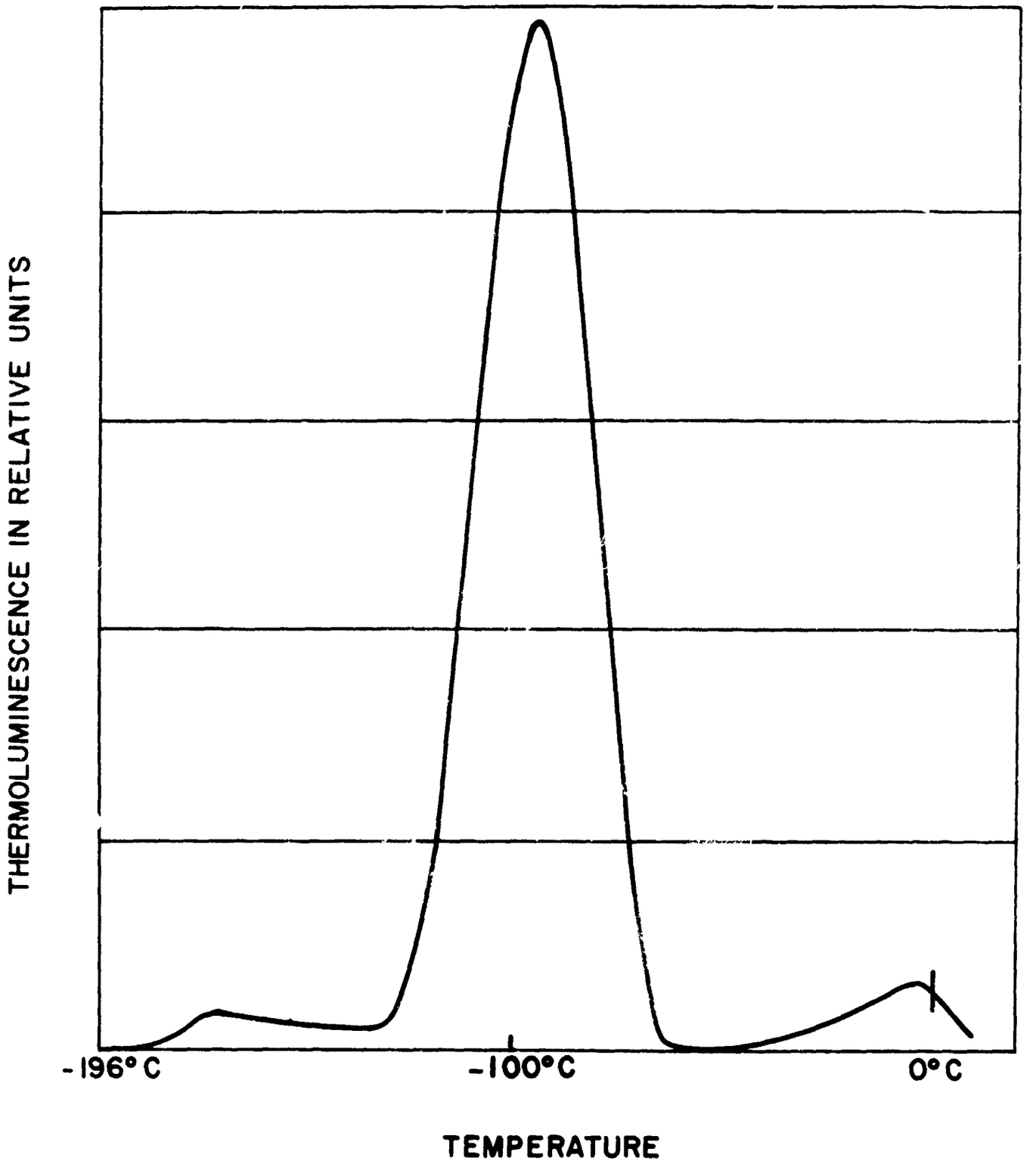

Figure 2.--Low-temperature glow curve of halite from Project Gnome, Carlsbad, N. Mex.

distance of 10 inches from the source of X-rays, placed in a light-tight chamber, and heated to room temperature in much the same manner as for obtaining low-temperature glow curves. The thermoluminescence emitted from the samples during heating exposes a Polaroid film, and therefore produces a photograph of the thermoluminescent area. The photographic equipment consists of a Polaroid model MP-3 copy camera with a 75-mm Biotar f-1.5 lens mounted backward on the lens board, and standard-length extension tubes between the lens and the light-tight sample holder to obtain varying magnifications. The f- opening is varied to suit the intensity of thermoluminescence. Polaroid type 47--3000-speed print film is used. Selected polaroid prints can be photographed to obtain clear negatives from which duplicate prints are obtained.

EXPERIMENTAL STUDIES OF SHOCK- AND STRESS-INDUCED LOW-TEMPERATURE THERMOLUMINESCENCE IN HALITE

Experimental studies were conducted to determine, under known conditions, if the low-temperature thermoluminescence characteristics of halite could be significantly altered by a shock or stress event. In a typical laboratory experiment, a cylindrical core of previously unshocked halite from the site of the Salmon underground nuclear explosion near Hattiesburg, Miss., was used for a shock-loading experiment. The core sample had a diameter of 5.0 inches and a length of 10.0 inches. A No. 6 electric blasting cap was tied securely to one end so that the length of the blasting cap was parallel to the axis of the core sample (fig. 3). The core sample was shock loaded by detonating the elctric blasting cap after the core had been immersed in a container of sand to confine the explosion.

After detonation of the electric blasting cap, the core was sawed in a direction normal to the core axis to obtain disks at varying distances from the shocked end of the core sample. These disks, as sawed, were approximately 1/4 inch thick. The disks were trimmed to obtain a square plate, 1 square inch in area,

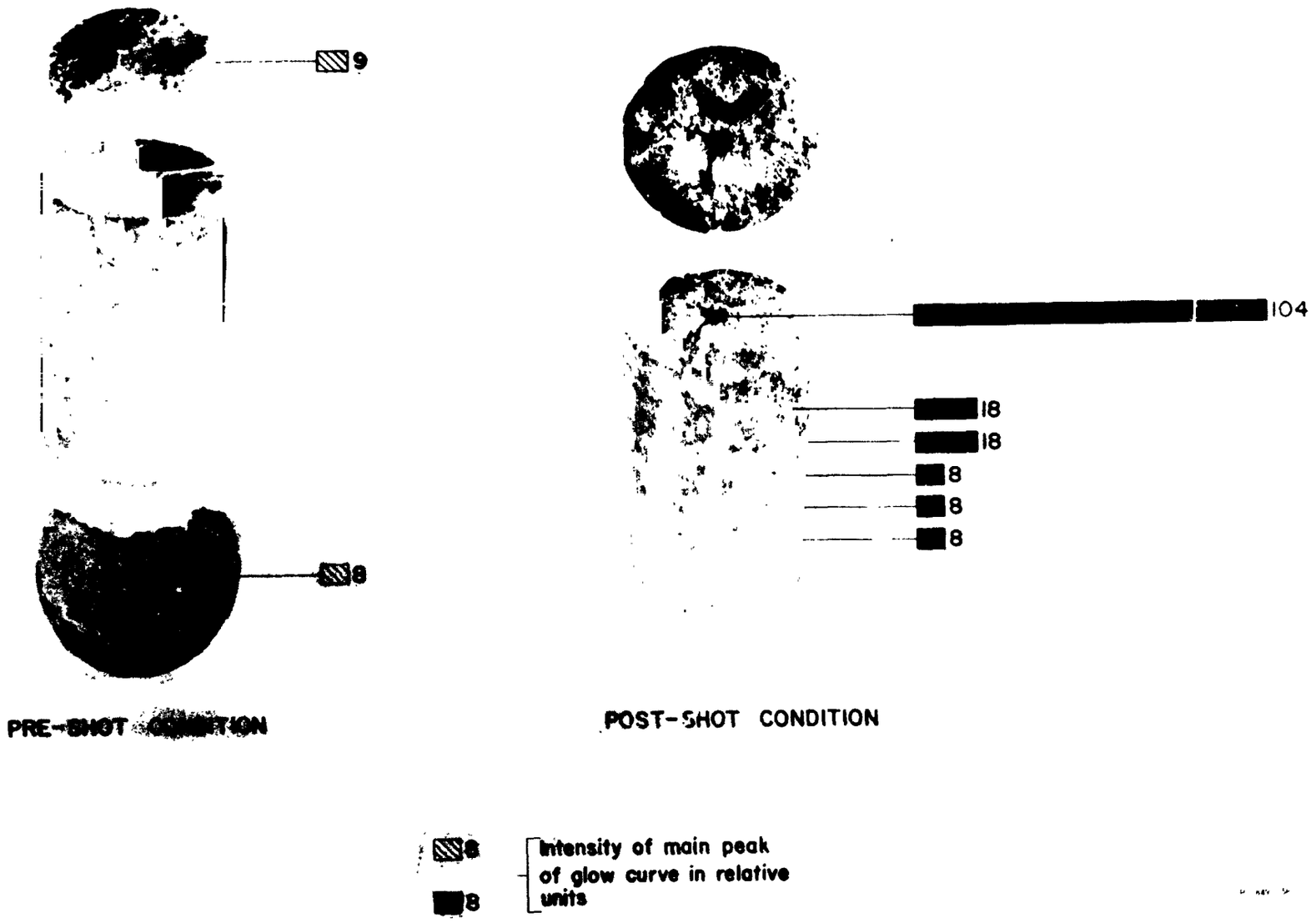

Figure 3.--Shock-induced low-temperature thermoluminescence of halite from the Dribble (Salmon) site, Hattiesburg, Miss.

from the central part of the original core. The central part of the disk was selected for study to eliminate the outer edges of the core cylinder, which may have been shocked or stressed during drilling operations when the core was obtained. The thin plates were then hand lapped on fine emery paper to avoid harsh treatment during preparation of the wafers. The wafers were hand lapped slowly on the emery paper to an average thickness of about 0.1 inch. Low-temperature glow curves were obtained from each thin wafer of the shocked halite in the manner previously described. Comparison of glow curves of the shocked samples with glow curves of unshocked samples revealed that shock derived from the detonation of the electric blasting cap induced significant amounts of low-temperature thermoluminescence in the halite near the point of origin of shock (fig. 3). The shock-induced thermoluminescence did not extend beyond about 3 1/2 inches from the point of origin of shock. Results of numerous experiments not discussed here show that if homogeneous specimens are used for shock-loading experiments of this kind, the shock-induced thermoluminescence decreases exponentially and continuously with distance from point of origin of the shock. However, if the shock-loaded specimen contains prominent physical irregularities such as open fractures, stylolitic seams, or thin layers of contrasting mineralogy, the shock wave may interact with these physical features in such a way as to modify slightly the shock-induced thermoluminescence gradient. These relations suggest that the shock loading experiment was scaled properly inasmuch as the shock-induced thermoluminescence did not extend to the end of the core. Had the shock wave been reflected from the free surface at the end of the core specimen, perturbation effects would have been introduced. This shock-loading experiment provided direct evidence that a high-energy shock wave alters the low-temperature thermoluminescence of halite from the Salmon site, and suggested that an underground nuclear explosion in the rock salt at the Salmon site would alter the low-temperature thermoluminescence of the adjacent halite. Similar shock-loading experiments on natural

halite specimens from other localities and on artificially grown halite crystals produced similar results.

The U.S. Bureau of Reclamation Laboratory in Denver, Colo., conducted triaxial compression tests on eighteen 5-inch-diameter pre-shot cores of rock salt from the Dribble (Salmon) site (U.S. Bur. Reclamation, 1962). These tests were conducted for the U.S. Atomic Energy Commission to determine the shear-strength characteristics of the salt in terms of the equation of Mohr's envelope. A low-temperature thermoluminescence measurement was made on a specimen obtained from each of the 18 cores to determine if the stress history associated with the triaxial compression tests affected the thermoluminescence properties of the halite, and if affected, whether the changes in low-temperature thermoluminescence were proportional to the magnitude of the principal stresses generated during the compression tests. The triaxial compression and low-temperature thermoluminescence data for the salt cores are summarized in table 1. Inasmuch as the average background low-temperature thermoluminescence of unshocked and unstressed Dribble halite is about 6.5 units, all triaxial compression tests induced some low-temperature thermoluminescence in the Dribble halite. However, no simple and consistent relationship was found between the amount of low-temperature thermoluminescence of the halite and the magnitude of either the lateral or axial pressure to which the halite was subjected. Autoluminographs revealed that the induced low-temperature thermoluminescence had an extremely variable distribution within the stressed cores and seemed to be most concentrated along fractures where failure occurred or at places where certain crystals were favorably oriented to receive the maximum stress under a given set of pressure conditions (fig. 4). The size of the thermoluminescence specimen was very small relative to the volume of the cores tested triaxially, and therefore a simple and consistent relationship was not found between the amount of stress-induced low-temperature thermoluminescence and the pressures generated during the triaxial tests. The

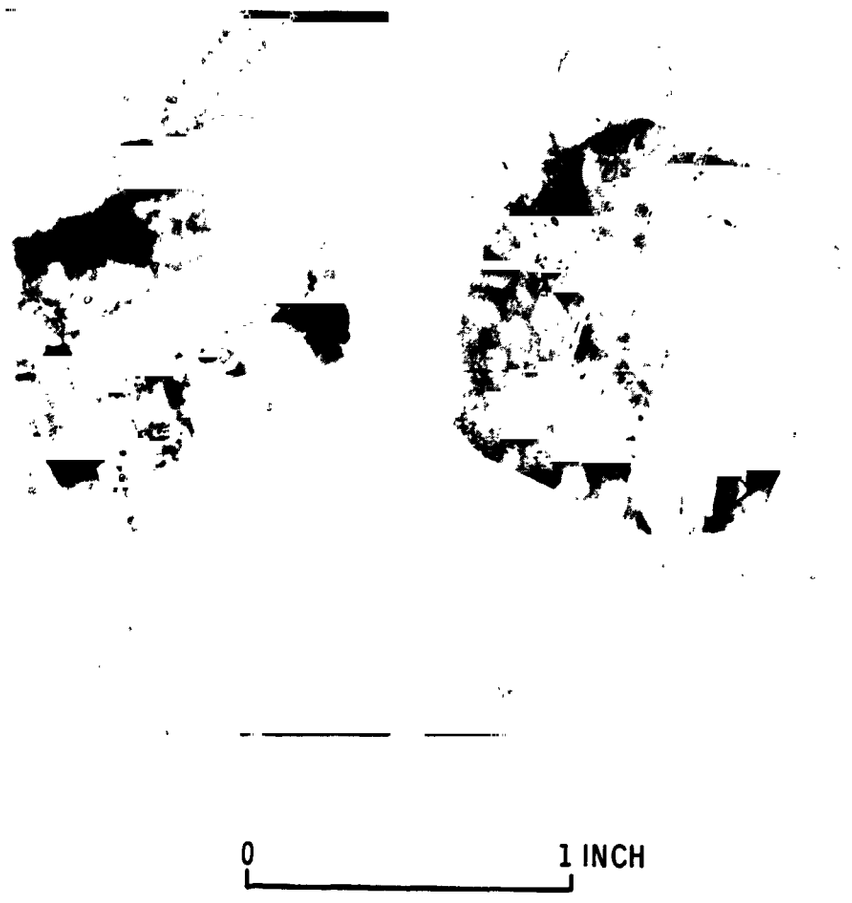

Figure 4.--Autoluminographs of Dribble halite subjected to triaxial compression by the U.S. Bureau of Reclamation.

Table 1.--Triaxial compression and low-temperature thermoluminescence data for USBR test cores of Dribble halite

Specimen No. (depth in feet)	Lateral S_3 (psi)	Axial S_1 (psi)	Thermoluminescence (relative units)	Remarks
2392	0	3,487	11	
2359	0	3,586	17	
2438	0	3,630	19	
2663	500	8,272	65	
2366	500	8,627	106	
2253	500	8,627	78	
1683	1,500	13,501	68	
2669	1,500	13,359	16	
2269	1,500	13,572	49	
1697	2,500	17,877	23	Sheath ruptured.
2680	2,500	17,877	12	Do.
2294	2,500	17,877	12	Do.
2689	3,500	20,474	100	Do.
2337	3,500	20,616	10	Do.
1701	3,500	20,901	34	
2346	5,000	22,661	21	Do.
1726	5,000	23,373	13	Do.
2695	5,000	23,088	38	Do.

S_3 = unit lateral pressure on specimen.
S_1 = actual unit axial pressure on specimen.

random orientation of halite crystals within the cores and highly anisotropic distribution of surfaces of failure mean that many of the thermoluminescence specimens were taken from positions poorly located for studying the relationship between low-temperature thermoluminescence and the magnitude of the principal stresses to which the cores were exposed. Stress-induced low-temperature thermoluminescence studies of single crystals of halite are planned

to see whether a simple relationship does in fact exist between maximum pressures of triaxial compression tests and the stress-induced low-temperature thermoluminescence of halite.

Unconfined compressive tests were conducted on specimens of Dribble (Salmon) halite to determine the minimum stress difference necessary to initiate stress-induced low-temperature thermoluminescence. These tests indicated that, under unconfined compressive conditions, a stress difference of about 750 psi was sufficient to initiate stress-induced low-temperature thermoluminescence and also to exceed the yield strength of the halite. The yield strength of halite can be defined as the maximum stress difference at the beginning of large deformation by plastic flow.

These experimental studies indicate that both shock waves and relatively slow rates of applied stress accompanying triaxial compression tests significantly alter the low-temperature thermoluminescence of halite. From these results, it would be expected that stress waves generated by underground nuclear explosions in halite would induce low-temperature thermoluminescence in the halite near the explosion, and that its magnitude would tend to decrease exponentially with distance from the point of origin of shock.

PROJECT GNOME

On December 10, 1961, a nuclear device was detonated in rock salt in an underground tunnel at the Gnome site, about 25 miles southeast of Carlsbad, N. Mex. (fig. 5). The total yield of this nuclear device has been estimated at 3.0 ± 0.75 kilotons (Weart, 1962). The nuclear detonation, known as the Gnome event, was the first experiment of the Plowshare Program for the peaceful uses of atomic energy. The technical objectives were to test the feasibility of recovering heat and certain isotopes from an underground nuclear explosion in rock salt, and to measure resonance neutron activation.

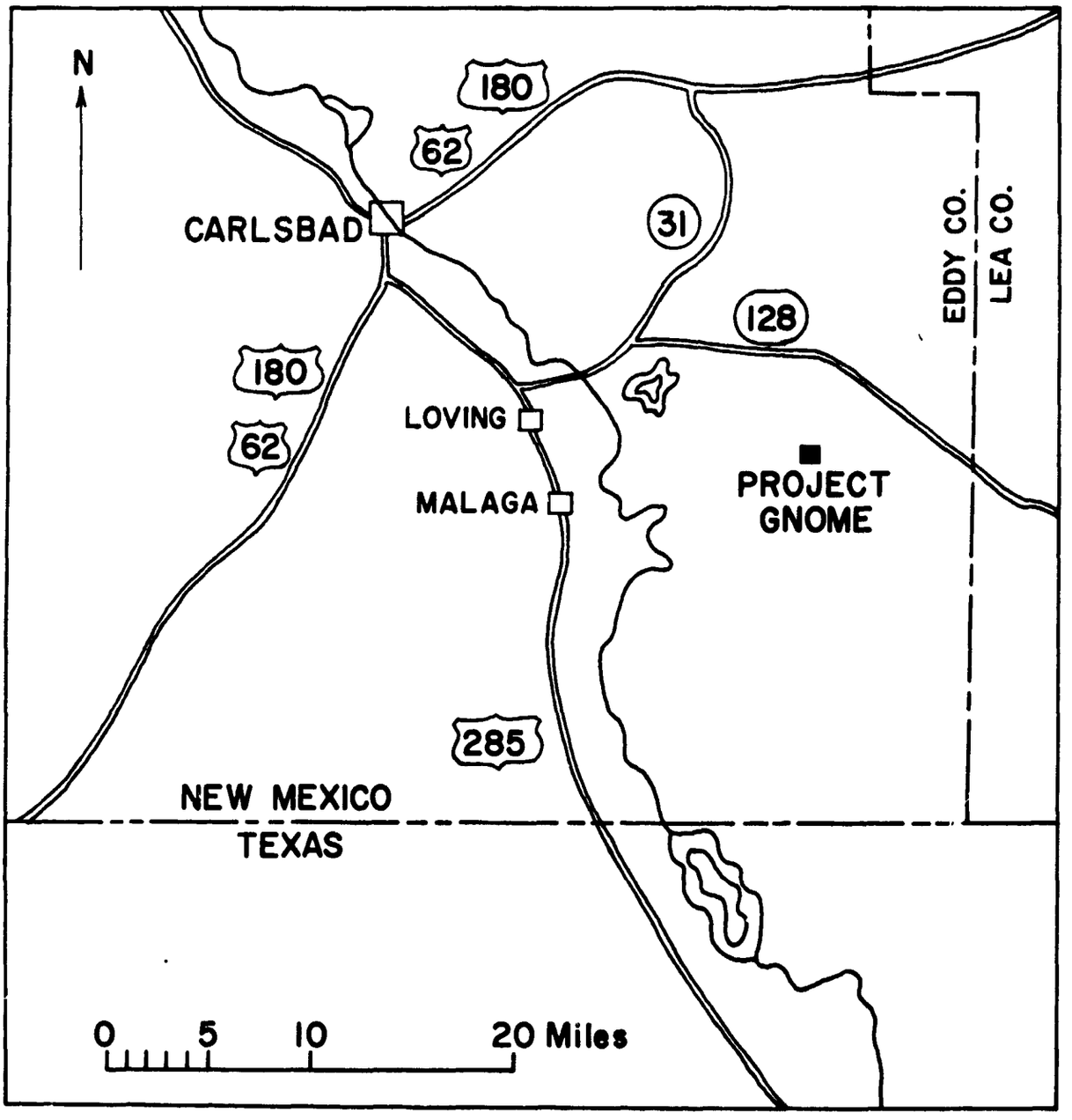

Figure 5.--Index map showing location of Gnome site.

The author participated in Project Gnome to determine if strong shock waves associated with the detonation of an underground nuclear explosion would significantly alter the low-temperature thermoluminescence of enclosing halite, as was suggested by previously conducted shock-loading and triaxial testing experiments on halite.

Geologic Setting

The nuclear device was detonated at the end of an 1,100-foot-long tunnel, 1,184 feet below the ground surface (fig. 6). The detonation took place in the Salado Formation, of Permian age, which consists principally of rock salt (halite) with minor amounts of interbedded anhydrite and polyhalite. The rocks penetrated by the Gnome shaft are briefly described in table 2.

The upper part of the Salado Formation is known as the leached member, and is approximately 60 feet thick in the vicinity of the Gnome site. The leached member consists mainly of reddish-brown to gray-green clay and silt with minor amounts of interbedded gypsum and anhydrite. The Salado Formation is separated from the overlying Rustler Formation by a disconformable contact.

The remainder of the Salado Formation consists of well-bedded halite with minor amounts of interstratified thin beds of argillaceous halite, polyhalite, anhydrite, and clay. The halite ranges in color from clear through pink to reddish orange. The orange color is mainly dependent on the amount of polyhalite that is disseminated in the halite. Some of the beds of halite contain appreciable amounts of disseminated and banded clay that ranges in color from reddish brown to greenish gray. Several thin beds of dark-reddish-brown polyhalite, which contrast markedly with the adjacent lighter colored beds of halite and are continuous over a large area, are very useful as marker beds in the Gnome area. One such polyhalite bed (marker bed 121) is 9.0 feet below the point of detonation of the nuclear device and is especially useful in placing the stratigraphic position of post-shot samples of halite with respect to the point of origin of shock of the nuclear detonation. The Vaca Triste Sandstone

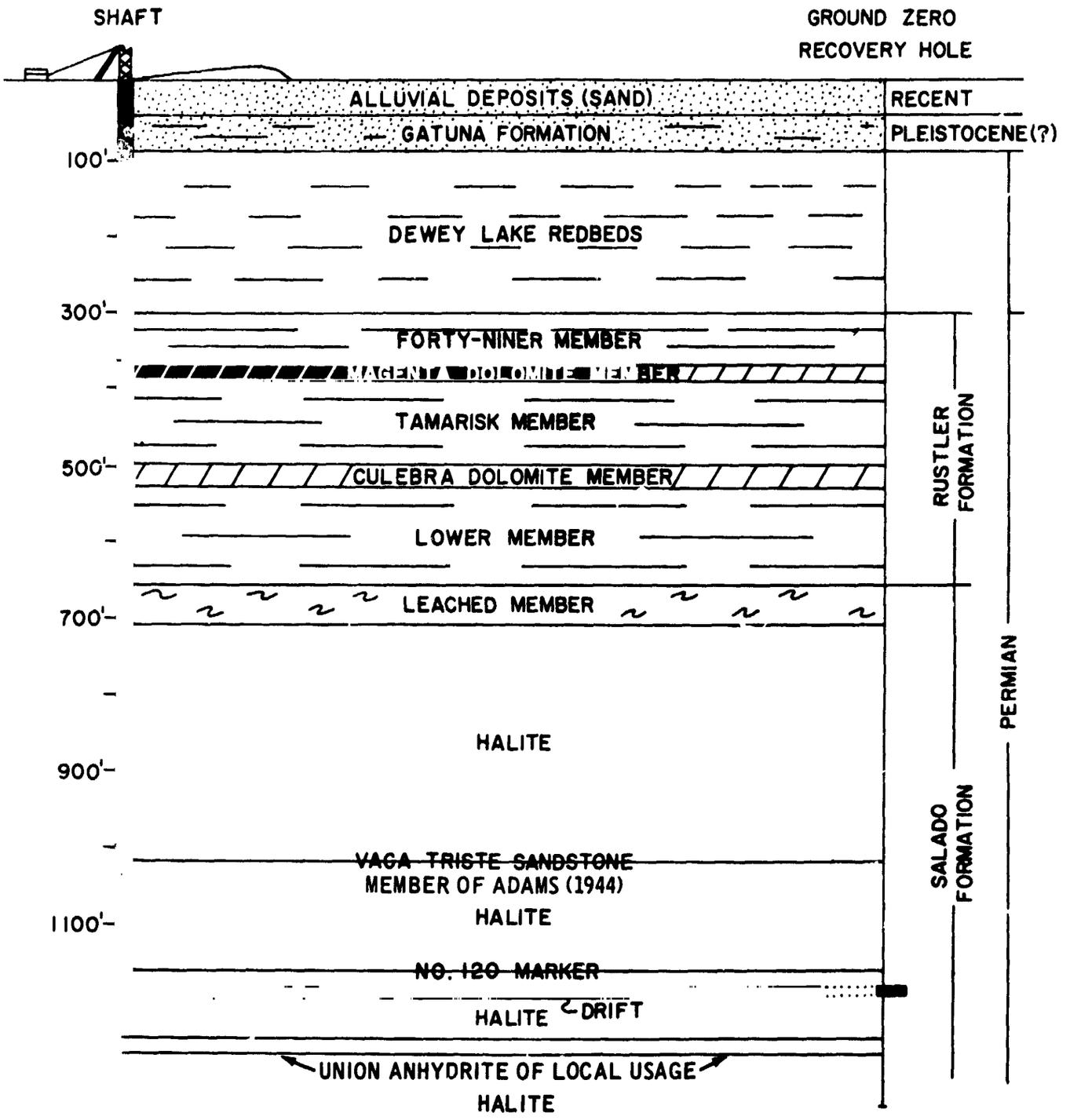

Figure 6.--Geologic section showing rocks penetrated by the Gnome shaft and tunnel. Modified from Gard, Cooper, and others (1962).

Table 2.--Generalized stratigraphic section of rocks exposed in the Gnome shaft

[Modified from Gard, Cooper, and others, 1962]

Age	Unit	Lithology	Depth below surface (feet)	Thickness (feet)
Recent	Alluvial bolson deposits.	Unconsolidated sand.	0- 43	43.0
Pleistocene(?)	Gatuna Formation	Friable sandstone and conglomerate.	43- 92	49
Late Permian	Dewey Lake Redbeds.	Thin-bedded siltstone.	92- 294	202.1
Do.	Rustler Formation:			
	Forty-niner Member.	Chiefly gypsum and anhydrite.	294- 361	67
	Magenta Dolomite member.	Silty dolomite	361- 382	21
	Tamarisk Member	Chiefly anhydrite and gypsum.	382- 496	114
	Culebra Dolomite Member.	Dolomite	496- 524	28
	Lower member	Chiefly clay and silt, with some gypsum and anhydrite.	524- 651	127
Do.	Salado Formation:			
	Leached member	Chiefly claystone and siltstone.	651- 709	58
	Unleached part	Chiefly impure halite rock, with some anhydrite, polyhalite, and siltstone.	709-1,202	493
	(Bottom of shaft.)			

Member of Adams (1944) is a good marker bed about 160 feet above the shot point and serves as a convenient reference point for locating samples vertically above the nuclear detonation. The Union anhydrite of local usage, about 45 feet below the shot point, serves as a good marker bed for locating post-shot samples vertically below the shot point.

In the vicinity of the Gnome site, individual beds in the Salado Formation strike N. 89° E. and dip less than 1/2° N. The constant attitude of the Salado beds facilitates greatly the lateral correlation between pre- and post-shot drill-hole samples. Inasmuch as lateral facies and attitude variations within the overlying Rustler Formation would complicate the accurate correlation of pre- and post-shot samples, all samples selected were from the Salado Formation. Low-temperature thermoluminescence measurements have been made for several of the rock units above the Salado Formation, but the data obtained are inconclusive because pre- and post-shot samples cannot be accurately correlated.

Shock-Induced Low-Temperature Thermoluminescence of Rock Salt at Gnome Site

Methods of study

Low-temperature glow curves of stratigraphically equivalent pre- and post-shot samples of halite were compared to determine if high-energy shock derived from the Gnome event caused significant changes in the thermoluminescent characteristics of the halite in the Salado Formation. All samples used were obtained from drill core of pre- and post-shot drill holes. Pre-shot samples were obtained from the S.R. 1 pre-shot drill hole (figs. 7-9). The S.R. 1 recovery hole was drilled about 2 1/2 to 3 years prior to the Gnome event for the purpose of evaluating geologic conditions at Ground Zero. Post-shot samples of halite were obtained from four post-shot drill holes (fig. 7).

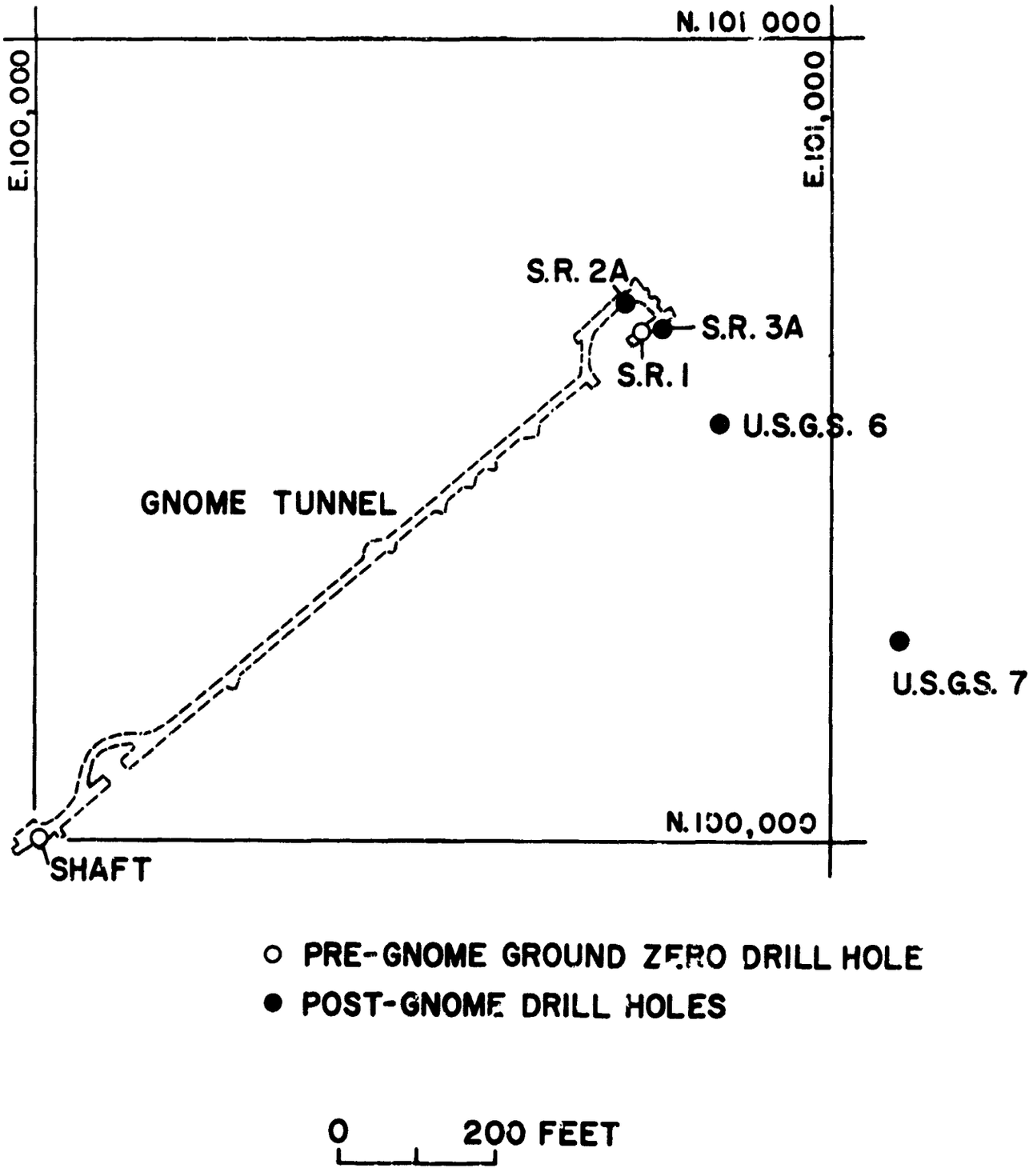

Figure 7.--Map showing location of pre- and post-shot drill holes at the Gnome site.

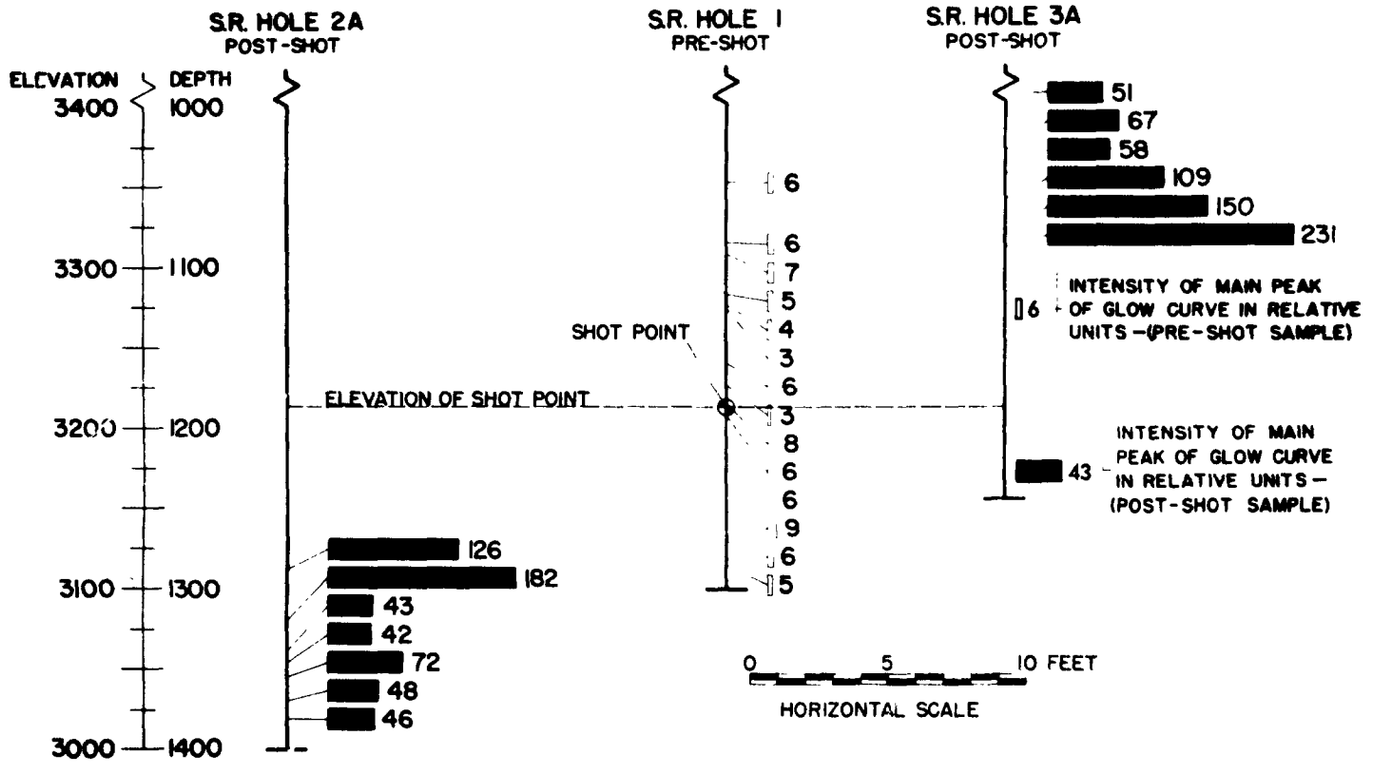

Figure 8.--Low-temperature thermoluminescence of pre- and post-shot halite, Project Gnome (near-in effects).

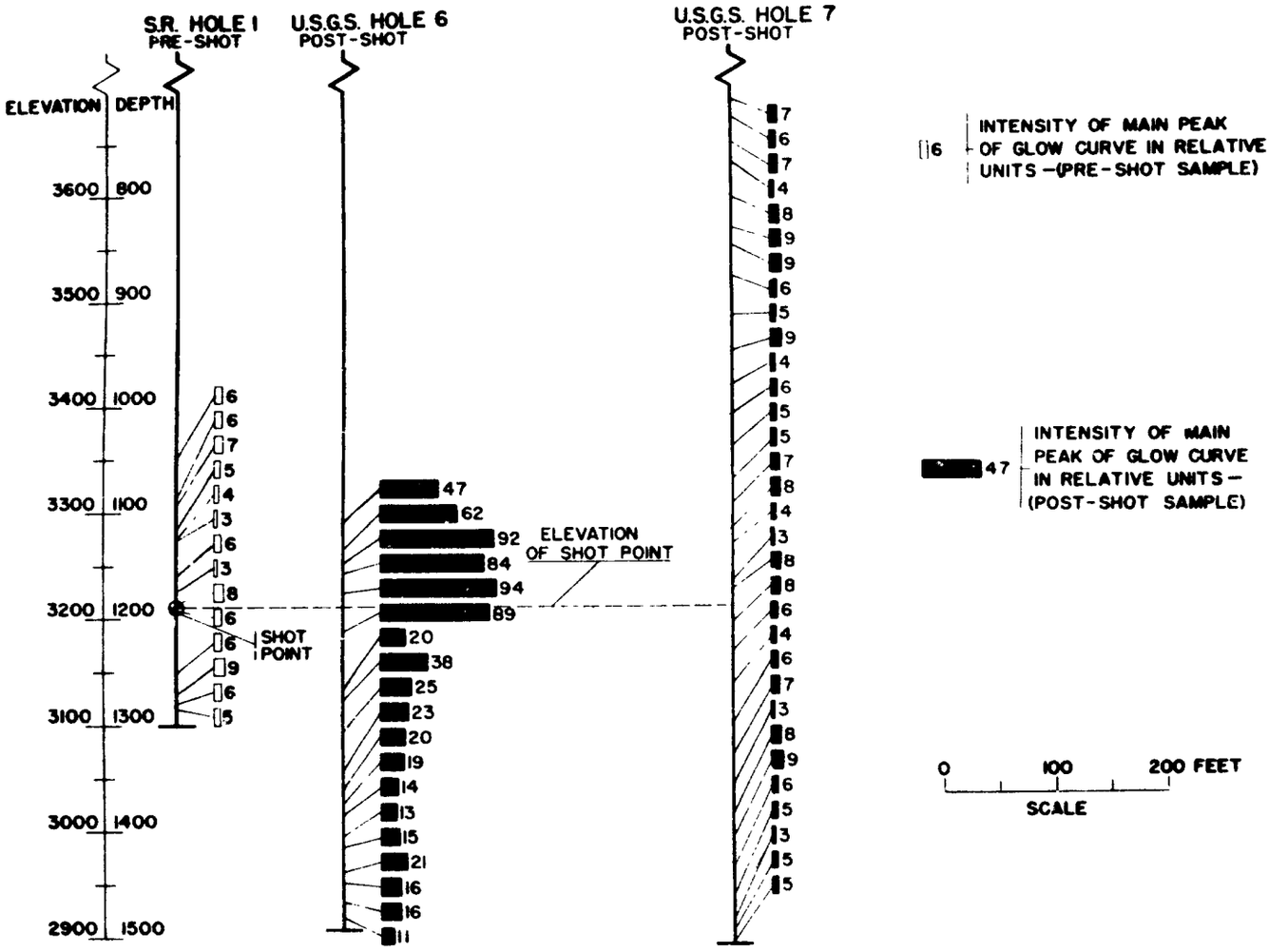

Figure 9.--Low-temperature thermoluminescence of pre- and post-shot halite, Project Gnome (faraway effects).

Samples for thermoluminescence studies were obtained by sawing disks from the drill cores in the manner previously described. Only relatively pure halite specimens were selected, and these samples were taken from each relatively pure halite layer in the core.

Results of study

Background low-temperature thermoluminescence of the halite in the Salado Formation was determined by obtaining a glow curve of each sample taken from drill core of the S.R. 1 pre-shot drill hole. Some difficulty, however, was encountered in trying to obtain completely unstressed samples, because all core available for these studies had previously been split, by other investigators, from its original diameter of 3 1/2 inches by the use of core splitters. It had previously been established that significant amounts of low-temperature thermoluminescence could be induced in the halite by moderate to severe crushing action. Samples from the core segments that had not been stressed during the drilling activities or the core-splitting operation were selected for pre-shot studies.

Autoluminographs were prepared for each sample from the pre-shot hole to determine if any low-temperature thermoluminescence had been artificially induced in the samples by the core-drilling or core-handling operations. The autoluminographs indicated that some pre-shot samples had anomalously high thermoluminescence that could be attributed to preparation of the samples. Autoluminographs showed low-temperature thermoluminescence (1) adjacent to the original core surface (probably induced by the stress created during drilling operations) (fig. 10), (2) immediately adjacent to some of the core-splitting surfaces; and (3) in the holes, or negative crystals, filled with the fine halite powder created during grinding or polishing (the fine powder created during polishing operations is highly stressed). Pre-shot samples whose autoluminographs indicated anomalously high thermoluminescence of these types were excluded from consideration when natural pre-shot background thermoluminescence of

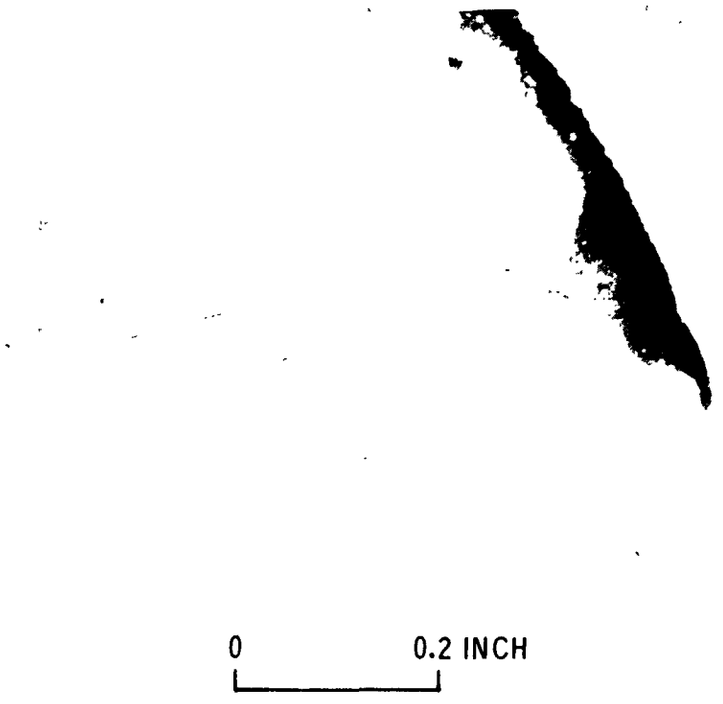

Figure 10.--Autoluminograph of pre-shot halite showing low-temperature thermoluminescence along edge of core that was induced by stress created by diamond core bit, Project Gnome.

halite at Project Gnome was determined. Autoluminographs of normal pre-shot samples indicate that the true background thermoluminescence is not intense enough to expose the film. Studies of unshocked or unstressed halite from other localities indicate that the above procedure was completely justified.

The amount of low-temperature thermoluminescence induced by shock of the Gnome event was determined by comparing the intensity of the main peak of glow curves of pre- and post-shot drill-hole samples near Ground Zero (figs. 8, 9). Within about 200 feet radial distance of the Gnome shot point, all samples have significant amounts of shock-induced low-temperature thermoluminescence (fig. 8). Samples of radioactive halite were not studied, since the purpose of this investigation was to study only shock-induced low-temperature thermoluminescence characteristics. Also, all samples within 100 feet of the shot point were eliminated to avoid any shock-induced thermoluminescence resulting from the mining operation. Shock-induced low-temperature thermoluminescence of halite from these two post-shot drill holes tends generally to decrease exponentially with distance from point of origin of shock. Minor reversals in this thermoluminescence gradient may be related to interference effects associated with boundaries between beds with contrasting bulk density or impedance. Some relatively low thermoluminescence was due to the presence of weakly thermoluminescent minerals in the halite. The most distant samples of halite in the S.R. 2A and S.R. 3A post-shot drill holes are about 200 feet radially from Ground Zero, and are about eight times as thermoluminescent as the average comparable pre-shot samples.

The maximum distance to which thermoluminescence was induced was determined by studying glow curves of core samples obtained from the U.S.G.S. 6 and U.S.G.S. 7 post-shot drill holes that were located 150 and 500 feet horizontally from the Gnome explosion point (fig. 9). Since the depth interval from 700 to 1,100 feet was not cored in the U.S.G.S. 6 drill hole, post-shot samples were not available from that part of the Salado Formation in this drill hole. However, the

greatest amount of shock-induced thermoluminescence in the U.S.G.S. 6 drill hole was concentrated at about the same elevation as the shot point (depth 1,184 feet), and should have decreased exponentially above the shot point as it did below the shot point. Toward the bottom of the U.S.G.S. 6 drill hole (fig. 9), the intensity of thermoluminescence of the halite approached but was still above the average intensity of pre-shot halite. Therefore, some shock-induced thermoluminescence was registered at a radial distance of approximately 325 feet from the explosion point. Glow curves of 32 post-shot samples of halite collected from the top 800 feet of the Salado Formation in core from the U.S.G.S. 7 drill hole indicate that the shock-induced thermoluminescence in the halite did not extend as far as 500 feet horizontally from the Gnome explosion point. Extrapolation of the data indicated that the shock-induced thermoluminescence probably extended outward at least 350 feet from the Gnome shot point.

Autoluminographs of highly shocked samples of halite show that sufficient amounts of thermoluminescence were induced in the halite to make minute details of crystalline structure easily visible (fig. 11). Autoluminographs of pre-shot halite from Gnome are either completely dark and featureless or show evidence of stress-induced thermoluminescence created by drilling or sample-preparation operations.

Single-Crystal X-ray Studies

Single-crystal X-ray studies showed that those post-shot samples of halite that had low-temperature thermoluminescence induced by the Gnome nuclear explosion also had their crystalline structure altered. Comparison of back-reflection Laue patterns of pre- and post-shot samples of a halite bed 100 feet above the Gnome shot point showed that the Laue spots of the post-shot halite were greatly smeared, an indication that the nuclear explosion caused severe crystal strain or distortion (fig. 12). The back-reflection Laue pattern of the stratigraphically equivalent pre-shot halite sample contained round, relatively sharp spots, indicating that this sample had a more nearly ideal structure and had not been exposed to much stress. Laue

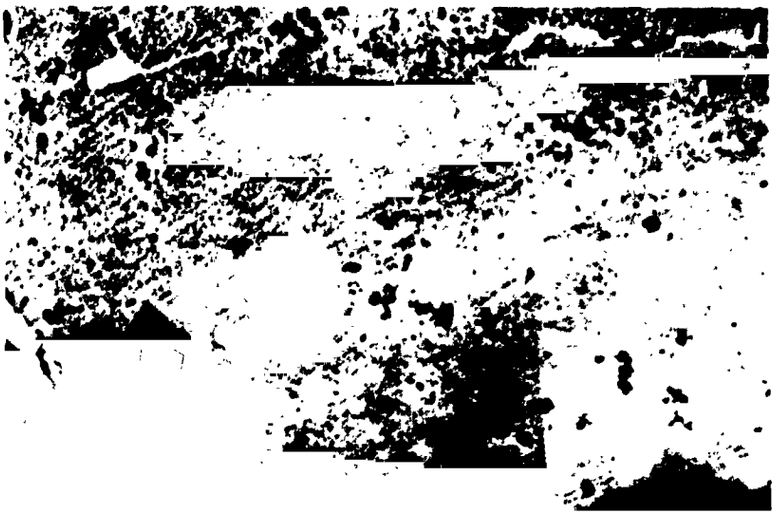

Figure 11.--Autoluminograph of post-shot halite sample 100 feet vertically above Gnome shot point.

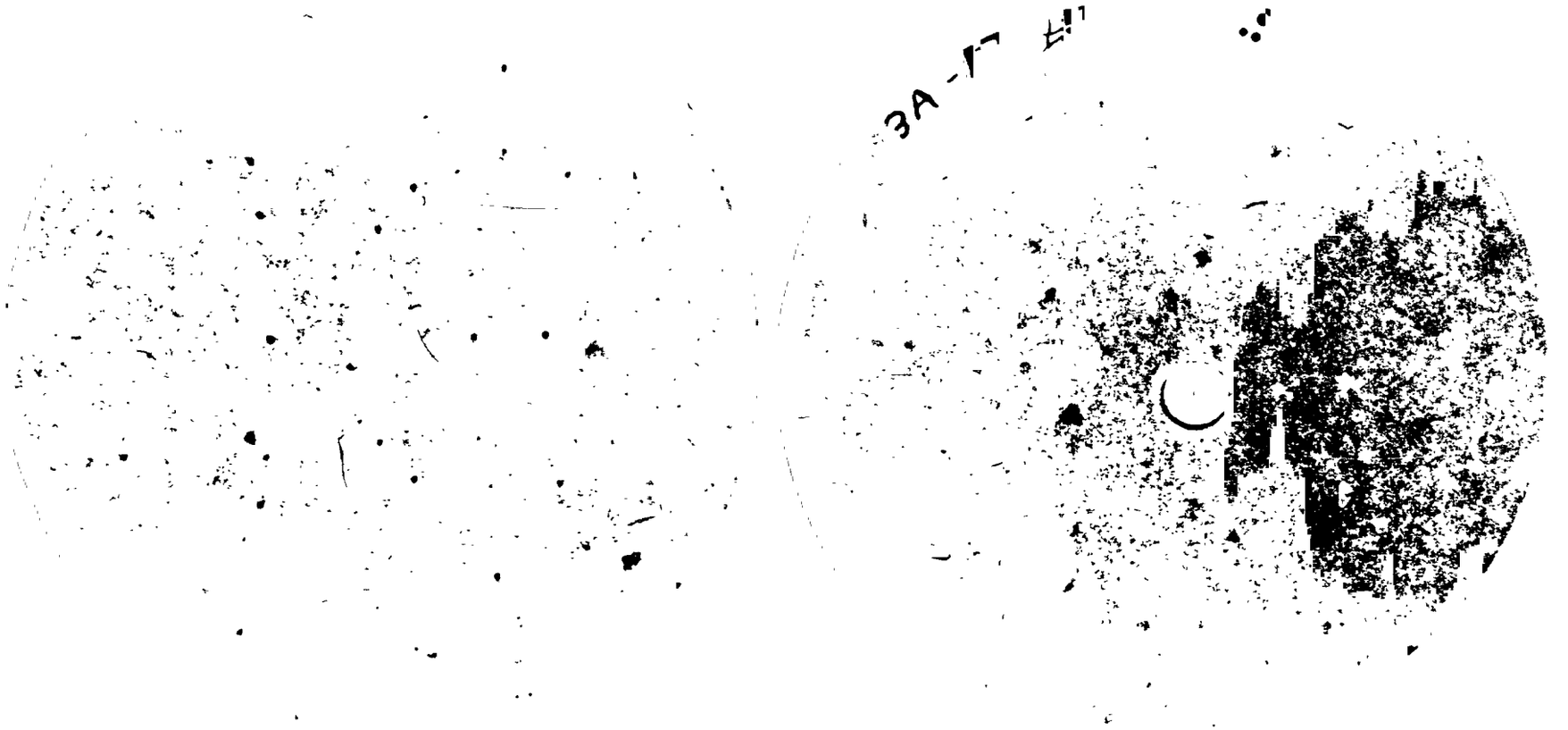

Pre-shot sample
(AEC No. 1 drill hole)

Post-shot sample
(100 feet above shot point)

Figure 12.--Laue back reflection patterns of pre- and post-shot samples of halite at Gnome site (near-in effects).

patterns showed that post-shot samples of halite 150 feet laterally from the Gnome shot point were also strained in comparison to their pre-shot condition (fig. 13). The maximum distance at which shock-induced crystal distortion can be observed by single-crystal X-ray methods is not known at present.

Conclusions

This preliminary study indicates that shock derived from the Gnome nuclear explosion induced significant amounts of low-temperature thermoluminescence in the halite adjacent to the point of origin of shock. The maximum distance to which the low-temperature thermoluminescence was induced in the halite could not be precisely determined owing to the lack of some properly spaced post-shot samples. The available data seem to justify the conclusion that shock of the Gnome explosion did induce thermoluminescence in the adjacent beds of halite for a distance of about 350 feet radially from the point of origin of shock.

Single-crystal back-reflection Laue X-ray techniques also offer potential for studying shock or stress history of halite.

PROJECT DRIBBLE, SALMON EVENT

On October 22, 1964, a nuclear device was detonated at a depth of 2,700 feet in the Tatum salt dome in Lamar County, about 25 miles southwest of Hattiesburg, Miss. (figs. 14, 15). This nuclear detonation had an energy yield of about 5 kilotons and was known as the Salmon event of Project Dribble, conducted by the U.S. Atomic Energy Commission.

The author participated in the Salmon event to determine if stress waves associated with an underground nuclear explosion in a salt dome would significantly alter the low-temperature thermoluminescence characteristics of the enclosing halite, as was previously found in the horizontally stratified rocks at the Project Gnome site.

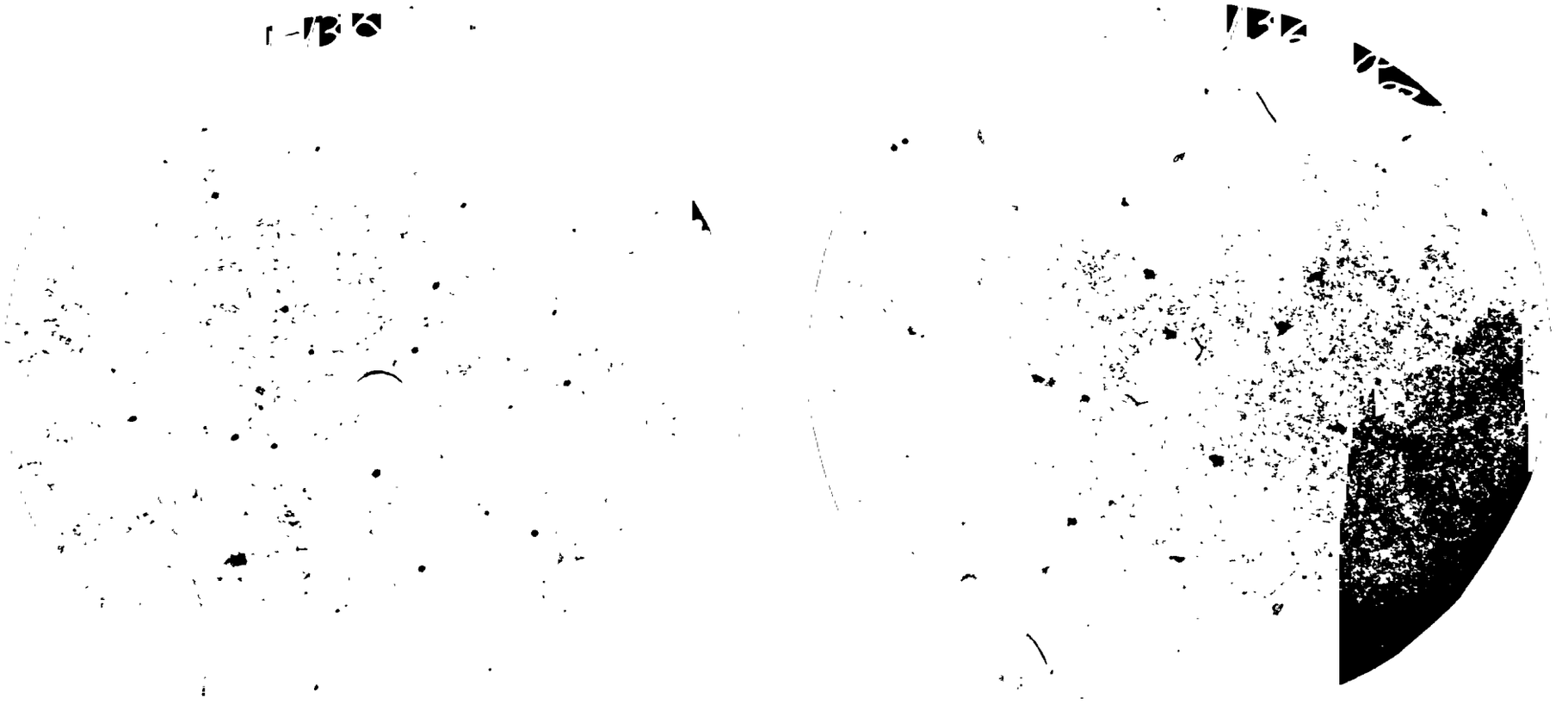

Pre-shot sample
(AEC No. 1 drill hole)

Post-shot sample
(150 feet laterally from shot point)

Figure 13.--Laue back reflection patterns of pre- and post-shot samples of halite at Gnome site (faraway effects).

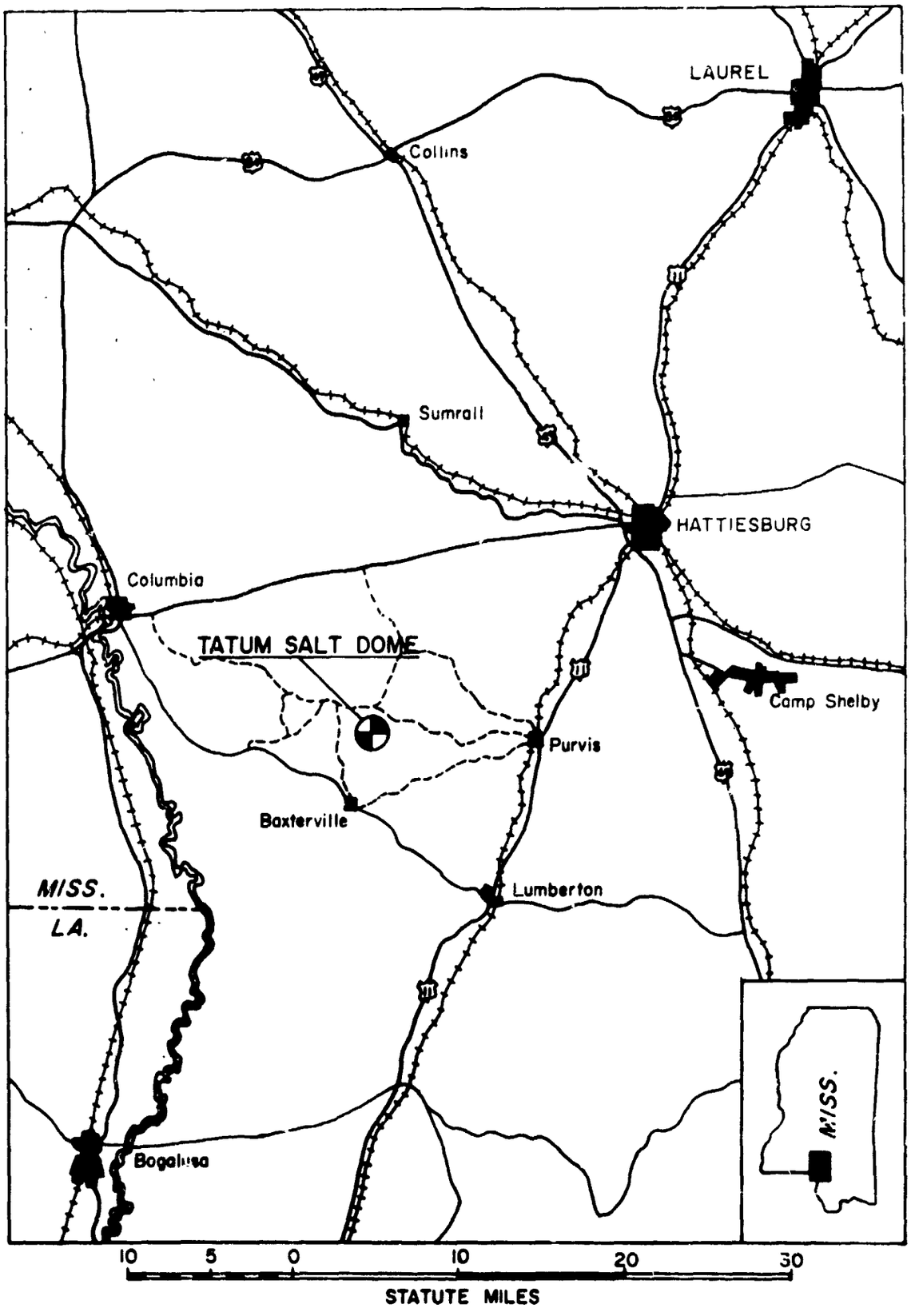

Figure 14.--Index map showing location of Tatum salt dome.

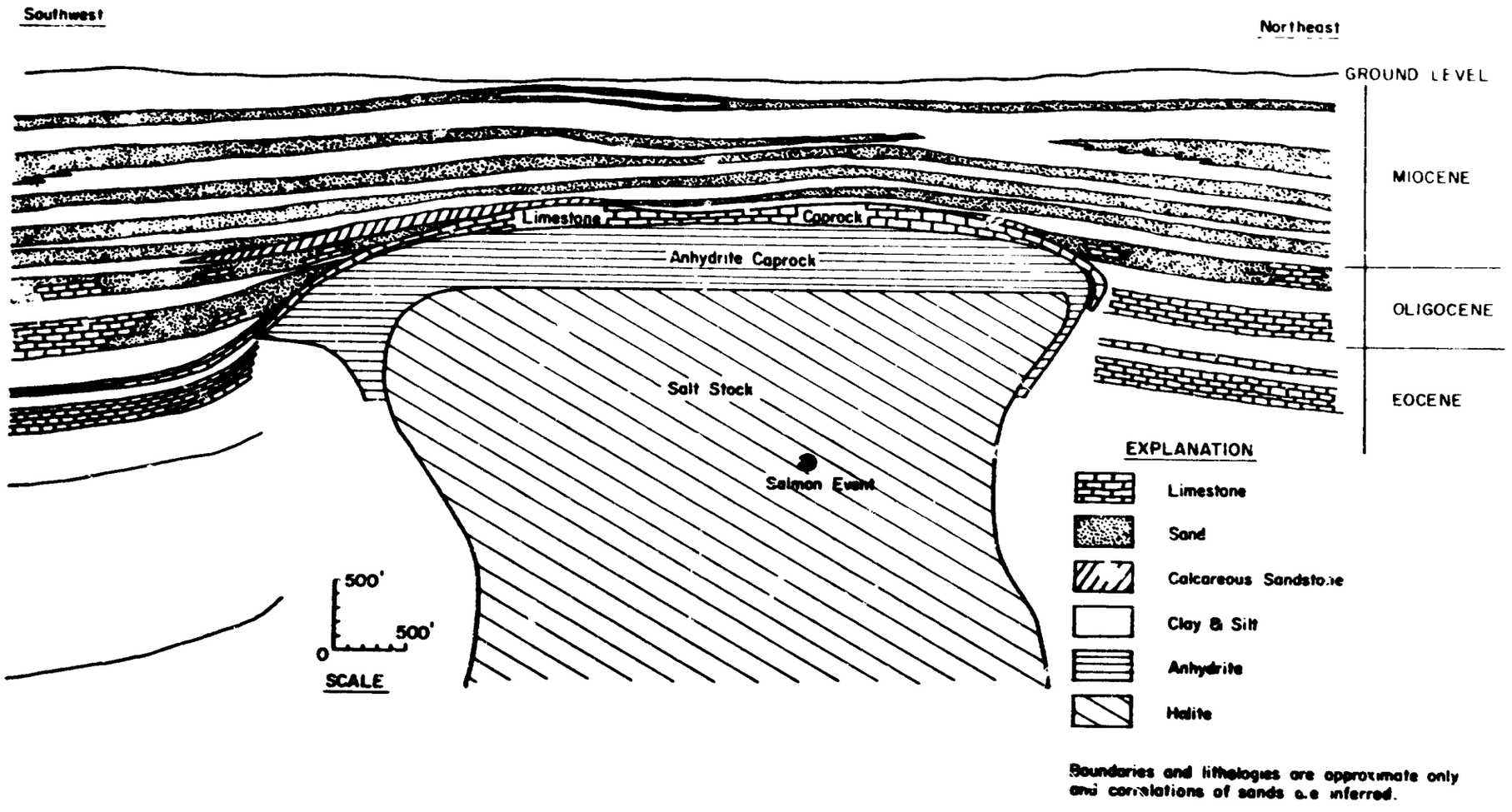

Figure 15.--Geologic section of Tatum salt dome, Lamar County, Miss.

Geologic Setting

The Tatum dome is one of 9 shallow salt domes in southeastern Mississippi, and one of more than 50 shallow salt domes in the Mississippi salt basin (Braunstein, 1958). It consists of a salt stock with a proved thickness of more than 3,000 feet, an average diameter of about 5,000 feet, and a caprock composed of an upper limestone unit and a lower anhydrite unit with an average aggregate thickness of 650 feet (fig. 15). The dome is overlain by Miocene to Recent unconsolidated sediments to an average depth of about 600 feet, and has not apparent surface expression. According to D. H. Eargle, J. F. Stanford, and B. O. Davis (unpub. data), the Tatum dome probably was one of the most recently active of the nine domes in southeastern Mississippi and has penetrated rocks as young as Oligocene (formations of the Vicksburg Group).

Tatum Salt Dome

Studies by R. A. Black, W. S. Twenhofel, and D. H. Eargle of the Geological Survey show that the salt dome is irregular in shape and flares at the top. Such salt overhangs are fairly common among salt domes (Murray, 1961, chap. 5), but the extension of caprock so far (850 feet) beyond the limits of salt is unusual. The top of the salt is remarkably flat, having a relief of less than 50 feet; the top of the caprock has a maximum relief of about 900 feet, and the thicknesses of the upper limestone and lower anhydrite parts of the cap range from 7 to 205 feet and from 60 to 465 feet, respectively.

The most prominent internal structure in the salt is a near-vertical interlayering between comparatively fine-grained salt with anhydrite inclusions and inclusion-free, coarser grained, lighter colored salt. The layers range in thickness from about 1/4 inch to 6 inches. Steeply inclined layers of inclusions generally have a low-angle cross foliation defined by overlapping sheets of anhydrite inclusions two or three crystals thick. Elongate salt grains in adjacent inclusion-free layers have their long axes in or near this cross foliation. Offsets of the steep plane of layering

parallel to the cross foliation are rare.

Steep layering in the salt is abruptly truncated at the caprock contact, and both anhydrite and limestone zones of the cap are characterized by a flat layering. Layering in anhydrite is dominantly a banding of light and dark anhydrite resulting from granulation and recrystallization in the light bands. Elongate anhydrite grains in both the partly recrystallized bands and the dark bands are oriented parallel to the plane of layering. Recrystallized bands sometimes bifurcate and commonly have irregular wavy contacts and lenticular shapes. Subhorizontal banding of this type is called katatectic banding by Julius Schlocker (written commun., 1963), and commonly grades into zones of extremely irregular, intensely deformed, and largely recrystallized anhydrite, or is truncated by irregular bands with a complex internal structure. Layering in the limestone cap results from variations in proportions of different minerals; this banding is also intensely deformed in places and brecciated carbonate layers are recemented by celestite and strontianite.

Shock-Induced Low-Temperature Thermoluminescence of Rock Salt at the Salmon Site

Methods of study

Low-temperature glow curves of equivalent pre- and post-shot samples of halite were compared to determine whether high-energy shock derived from the Salmon event caused significant changes in the thermoluminescent characteristics of halite in the Tatum dome. All samples used were of core from pre- and post-shot drill holes. Pre-shot samples were obtained from the STA-1 and STA-1A pre-shot drill holes. All post-shot halite samples were obtained from the Salmon post-shot 2 drill hole (PS-2), about 100 feet north of station -1A, the ground zero emplacement drill hole (fig. 16). Pre- and post-shot halite specimens selected for low-temperature thermoluminescence measurements were obtained by sawing disks from the drill cores in the manner described previously. Specimens selected

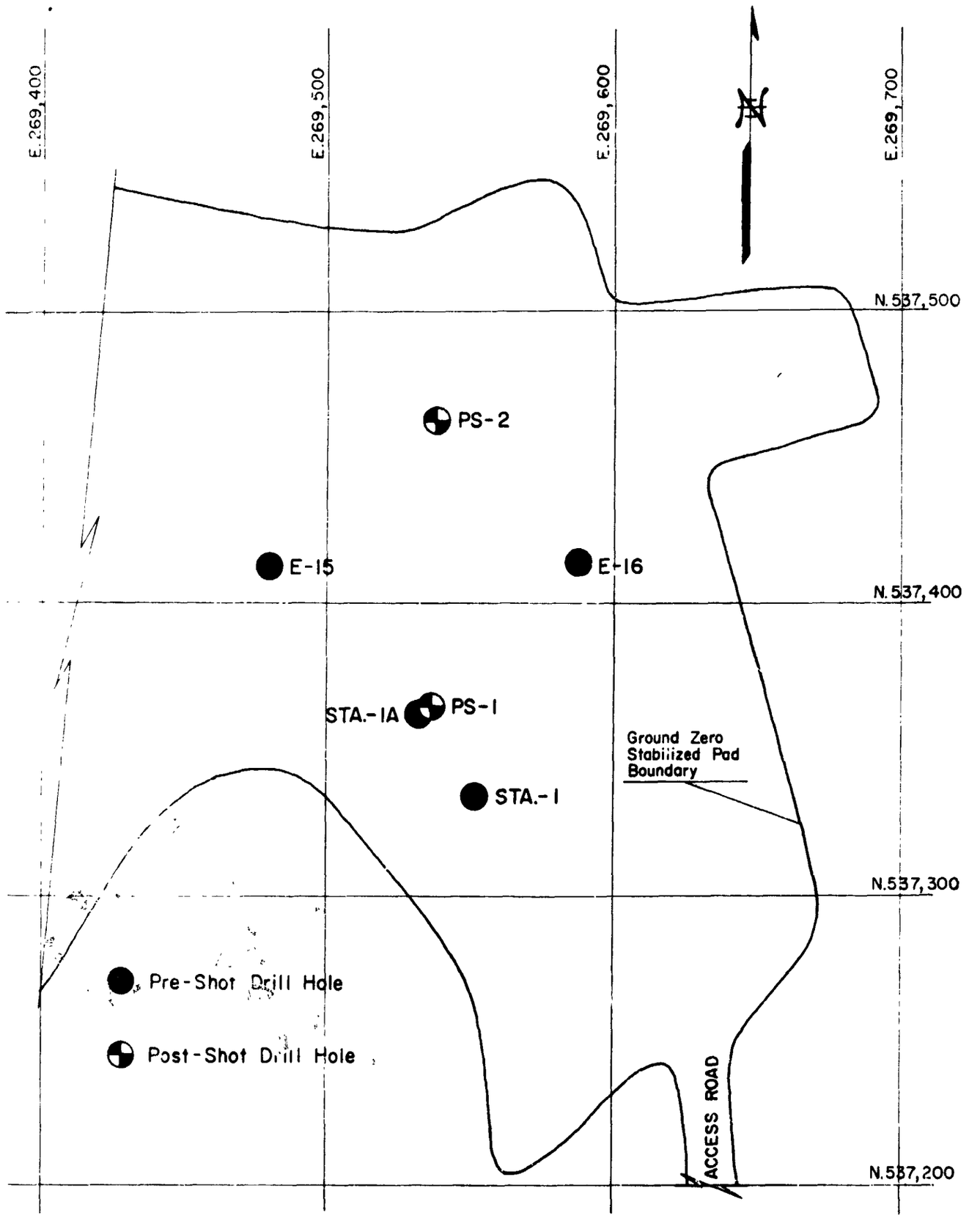

Figure 16.--Surface locations of drill holes at Salmon site.

for study were of relatively pure halite, from parts of the core that were as far as possible from manmade breaks in the core.

Results of study

Autoluminographs of pre-shot samples of halite from the Tatum dome were black, or only faintly visible, indicating that the background low-temperature thermoluminescence of completely unstressed halite was not intense enough to expose the film. Autoluminographs of halite samples that had been stressed mechanically (fig. 4) or by high-energy shock that accompanied the Salmon event had sufficient amounts of low-temperature thermoluminescence to make minute details of crystalline structure easily visible.

The amount of low-temperature thermoluminescence induced in halite by shock accompanying the Salmon event was determined by comparing the intensity of the main peak of glow curves of pre- and post-shot drill-hole samples at various distances from the Salmon explosion point (fig. 17). The low-temperature thermoluminescence of halite in the WP-1 pre-shot drill hole ranges from 5 to 9 relative units and averages 7 units. Post-shot halite samples having at least 10 relative units of low-temperature thermoluminescence are thought to have been affected by stress waves associated with the Salmon event.

All halite samples from the depth of the Salmon shot point (2,700 feet) upward to a depth of 2,369 feet (345 feet radial distance from the shot point) have shock-induced low-temperature thermoluminescence (fig. 17). Throughout this interval the low-temperature thermoluminescence increases fairly continuously to a high of 190 relative units at a depth of 2,654 feet (46 feet above the depth of the Salmon shot point). Autoluminographs of the halite samples throughout this interval reveal that the shock-induced low-temperature thermoluminescence is fairly evenly distributed throughout the specimens.

From a depth of 2,654 feet to the total depth (3,024 feet) in the post-shot 2 drill hole, the amount of shock-induced low-

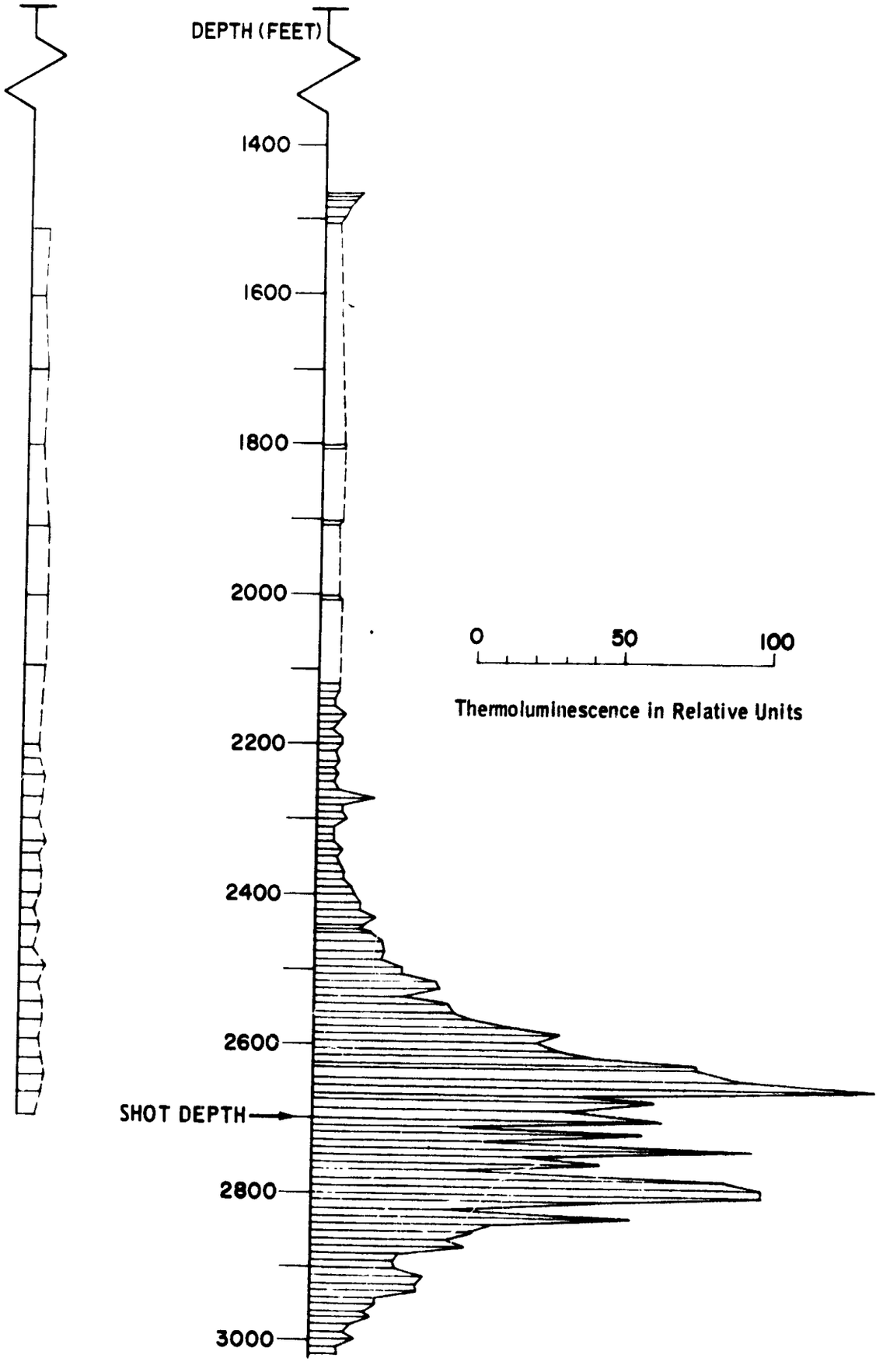

Figure 17.--Low-temperature thermoluminescence of pre- and post-shot halite, Salmon event, Project Dribble.

temperature thermoluminescence in the halite decreases very erratically to a value near, but still greater than, the normal value for unstressed halite. Autoluminographs of samples in this depth interval show that the shock-induced thermoluminescence is very erratically distributed among the component halite crystals in each specimen.

A thin isolated zone of shock-induced low-temperature thermoluminescence was found at a depth of 2,273 feet, which corresponds to a radial distance from the shot point of 437 feet (fig. 17).

A thin completely isolated zone of halite having higher than normal amounts of low-temperature thermoluminescence was found immediately below the anhydrite caprock at a depth interval of 1,466 to 1,476 feet (fig. 17). Although this interval of halite is far above the strongly affected halite, it may have had its thermoluminescence characteristics modified slightly by the complex interaction of stress waves encountering the anhydrite-halite contact that separates the two rock types having different shock impedances. Shock experiments performed on pre-shot Dribble halite cores indicate that contacts between anhydrite and halite can cause small amounts of low-temperature thermoluminescence to be induced in the halite adjacent to anhydrite, even though it is not connected with the stress-induced thermoluminescence next to the explosion point. It is possible that the level of thermoluminescence was related to stress generated by slight movements along the anhydrite-halite contact in relatively recent geologic time. More detailed study of the thermoluminescence characteristics of halite adjacent to the caprock is necessary before the anomalous thermoluminescence in that zone can be fully explained.

Conclusions

The results of this study show that stress waves associated with detonation of the 5-kiloton Salmon nuclear device induced significant amounts of low-temperature thermoluminescence in the halite adjacent to the point of origin of shock. Maximum shock-induced thermoluminescence in the Salmon post-shot 2 drill hole was

at a radial distance of about 110 feet and at an upward angle of about 24° from the Salmon shot point. From the point of maximum intensity, the amount of shock-induced thermoluminescence decreased rapidly and nearly continuously upward to a radial distance of 345 feet, whereas it decreased rapidly and very erratically downward to the total depth of the drill hole, which was about 340 feet radially from the shot point. Shock-induced low-temperature thermoluminescence was definitely found at a radial distance of 437 feet and was tentatively identified at the anhydrite-halite contact at the base of the caprock, a radial distance of about 1,225 feet from the shot point.

INTERPRETATION AND GEOLOGICAL APPLICATION OF RESULTS

Triaxial and unconfined compression tests on core specimens have shown that stress-induced low-temperature thermoluminescence is initiated in halite where the maximum stress difference exceeds the yield strength of the halite. For deformation with slow rates of strain, stress-induced low-temperature thermoluminescence of halite appears to be closely associated with the stress domain of plastic deformation.

Field studies have shown that halite stressed under conditions of high rates of strain achieved by use of chemical or underground nuclear explosions develops stress-induced low-temperature thermoluminescence whose distribution and intensity are closely related to the distribution and intensity of plastic deformation in the halite adjacent to the explosive sources of energy. The maximum radial distance of 437 feet at which shock-induced low-temperature thermoluminescence was found in halite adjacent to the Salmon underground nuclear explosion is essentially equal to the 135-meter (443-foot) distance that Lawrence Radiation Laboratory scientists directly measured and computed for the location of the plastic-elastic boundary near the Salmon cavity (Dr. Leo Rodgers, oral commun., 1965). Also, the approximate 350-foot radius of shock-induced low-temperature thermoluminescence found in Gnome halite agrees

very well with the location of the plastic-elastic boundary near the Gnome cav ty as directly measured and computed by Lawrence Radiation Laboratory personnel. Although the radius of shock-induced low-temperature thermoluminescence near the Gnome nuclear explosion is known to have extended slightly beyond 350 feet, this distance compares very closely with the radial distance of 122 meters (400 feet) where the mathematical relation between measurements of peak radial acceleration and radial distance from the detonation was found to change slope (Weart, 1962). This change in slope between these two parameters may occur at the plastic-elastic boundary.

The above relations strongly suggest that low-temperature thermoluminescence techniques can be very useful in delineating or mapping the three-dimensional extent of halite that is plastically deformed adjacent to underground nuclear explosions. The physics of plastic deformation adjacent to large underground chemical and nuclear explosions is poorly understood as compared to that of the hydrodynamic and elastic zones, and therefore the thermoluminescence techniques discussed in this report should contribute toward developing a better understanding of the fundamental mechanisms of plastic deformation in halite. Preliminary studies also indicate that thermoluminescence techniques can probably be successfully used to study plastic deformation in other common rock types.

Studies at the Gnome and Dribble sites and numerous laboratory shock and stress experiments show that the amount of stress-induced low-temperature thermoluminescence at any particular point in a body of plastically deformed halite is very sensitively affected by the presence of physical irregularities such as open fractures, stylolitic seams, and boundaries or contacts between layers of contrasting mineralogy. Such irregularities in the halite represent boundaries separating two media having contrasting shock impedances and therefore interfere with the transmission of shock or stress waves through the rock body. These data indicate that

thermoluminescence techniques have great potential application in that field of rock mechanics dealing with the transmission of strong shock or stress waves through a rock body. The experimental data available indicate also that thermoluminescence techniques have great potential application in other fields of rock mechanics where slow rates of strain are involved, such as slow creep and plastic deformation associated with the occurrence of large earthquakes, plastic deformation in rocks associated with the occurrence of large earthquakes, plastic deformation in rocks associated with large lateral fault systems like the San Andreas fault system in California, and plastic deformation in contact metamorphic rocks adjacent to some igneous intrusions and in regionally metamorphosed areas.

The results of solid-state investigations from which data for this report were obtained indicate that thermoluminescence techniques have great potential application to the broad field of rock mechanics as well as to many related geological problems.

REFERENCES CITED

Adams, J. E., 1944, Upper Permian Ochoa series of Delaware Basin, west Texas and southeastern New Mexico: Am. Assoc. Petroleum Geologists Bull., v. 28, no. 11, p. 1596-1625.

Baskerville, C., and Kunz, G. F., 1904, Kunzite and its unique properties: Am. Jour. Sci., v. 18, p. 25.

Braunstein, Jules, 1958, Habitat of oil in eastern Gulf Coast, in L. G. Weeks, ed., Habitat of oil: Tulsa, Okla., Am. Assoc. Petroleum Geologists, p. 511-522.

Brown, W. L., 1933, Photo-phosphorescence in minerals: Univ. Toronto Studies, Geol. Ser., no. 35, p. 19-35.

Curie, D., 1963, Luminescence in crystals: New York, John Wiley & Sons, Inc., 332 p.

Gard, L. M., Cooper, J. B., and others, 1962, Hydrologic and geologic studies for Project Gnome: U.S. Geol. Survey Proj. Gnome Rept. PNE-130F, 1961. (Available from Clearinghouse for Sci., Federal, and Tech. Inf., U.S. Dept. Commerce, Springfield, Md.)

Gray, T. J., The defect solid state: New York, Interscience Publishers, Inc., 511 p.

Iimori, S., and Iwase, E., 1931, The solarization of fluorite and the law of lumino transformation: Sci. Papers Inst. Phys. Chem. Research, Tokyo 16, p. 41-67.

Leverenz, H. W., 1950, An introduction to luminescence of solids: New York, John Wiley & Sons, Inc., 569 p.

Murray, G. E., 1961, Geology of the Atlantic and Gulf coastal province of North America: New York, Harper & Bros., 692 p.

U.S. Bureau of Reclamation, 1962, Triaxial compression tests of salt rock cores for the United States Atomic Energy Commission--Project Dribble: U.S. Bur. Reclamation Concrete and Structural Br. Lab. Rept. C-1043, 16 p.

Weart, W. D., 1962, Particle motion near a nuclear detonation in halite: Seismol. Soc. America Bull., v. 52, no. 5, p. 981-1005.

GEOLOGY OF THE MOSES ROCK INTRUSION SAN JUAN COUNTY, UTAH

By Thomas R. McGetchin

INTRODUCTION AND REGIONAL SETTING

The Moses Rock intrusion is being studied as a possible terrestrial analog to the subsurface geology of some of the lunar rilles. It is one of five known intrusive pipes or dikes of kimberlite (micaceous serpentine breccia) on the Colorado Plateau; all are within the Navajo Indian Reservation, in southeast Utah and northeast Arizona. Three (Moses Rock, Mule Ear, Garnet Ridge) are just south of the San Juan River along Comb Ridge, a pronounced topographic feature formed by differential weathering of rocks in the Comb monocline. This fold forms the eastern border of the Monument upwarp, which is a major structural feature of this part of the Colorado Plateau. The intrusions are localized within 2 or 3 miles of the axis of this fold.

The intrusion at Moses Rock has not been described in detail previously but was mentioned by Shoemaker (1962). The pipe at Mule Ear has been mapped in detail by Shoemaker and Moore (unpub. map); the pipes at Garnet Ridge, approximately 13 miles south of Moses Rock, were described by Malde (1954), and Malde and Thaden (1963). The only published map of the dike at Red Mesa is a small-scale sketch map by Shoemaker (1962, p. 297). A serpentine intrusion at Buell Park, near Fort Defiance in northeast Arizona, occurs on the west flank of the Defiance monocline (Allen and Balk, 1954).

Previous geological reports of the immediate vicinity are by Gregory (1938), Baker (1935, 1936), and O'Sullivan (1965). References to very early surveys in the region may be found in Bartlett (1962).

MOSES ROCK

The intrusion at Moses Rock is about 7 miles east-southeast of Mexican Hat, Utah, in red beds of the Permian Cutler Formation. Detailed stratigraphic sections were measured at the contacts of the Moses Rock dike and nearby to establish correspondence between specific stratigraphic horizons and blocks contained in the breccia within the dike.

The Moses Rock intrusion lies at the east end of Monument Valley. The Cutler rocks there dip gently eastward between the open Raplee anticline and the Comb monocline. In the monocline they locally attain dips of 40°. Two types of intrusive rocks are present: serpentine breccia (kimberlite) and minette, a potassium-rich lamprophyre (see Williams, 1936). Both types occur in dikes trending generally north.

STRUCTURE OF THE DIKE

The Moses Rock breccia dike strikes generally north and dips steeply westward. Its total length is unknown because the south end is buried beneath Recent sand dunes, but it is well exposed for more than 4 miles of its length, particularly at the north end. Its width is approximately 1,000 feet. The relative topographic relief depends on the relative resistance of dike rock and the rocks now exposed at the contacts. The north end of the dike cuts the relatively resistant Halgaito Member, and its surface expression is a trench; the south end cuts the relatively incompetent gypsiferous Cedar Mesa Member and forms a ridge.

Figure 1 is a generalized geologic map at a scale of 1 inch = 1,000 feet; it is generalized from detailed maps at a scale of 1 inch = 200 feet. The locations of 29 detailed geologic sections (1 inch = 200 feet) are shown in figure 2; some of these appear in figure 3.

Figure 1.-- GENERALIZED GEOLOGIC MAP OF THE MOSES ROCK INTRUSION

San Juan County, Utah

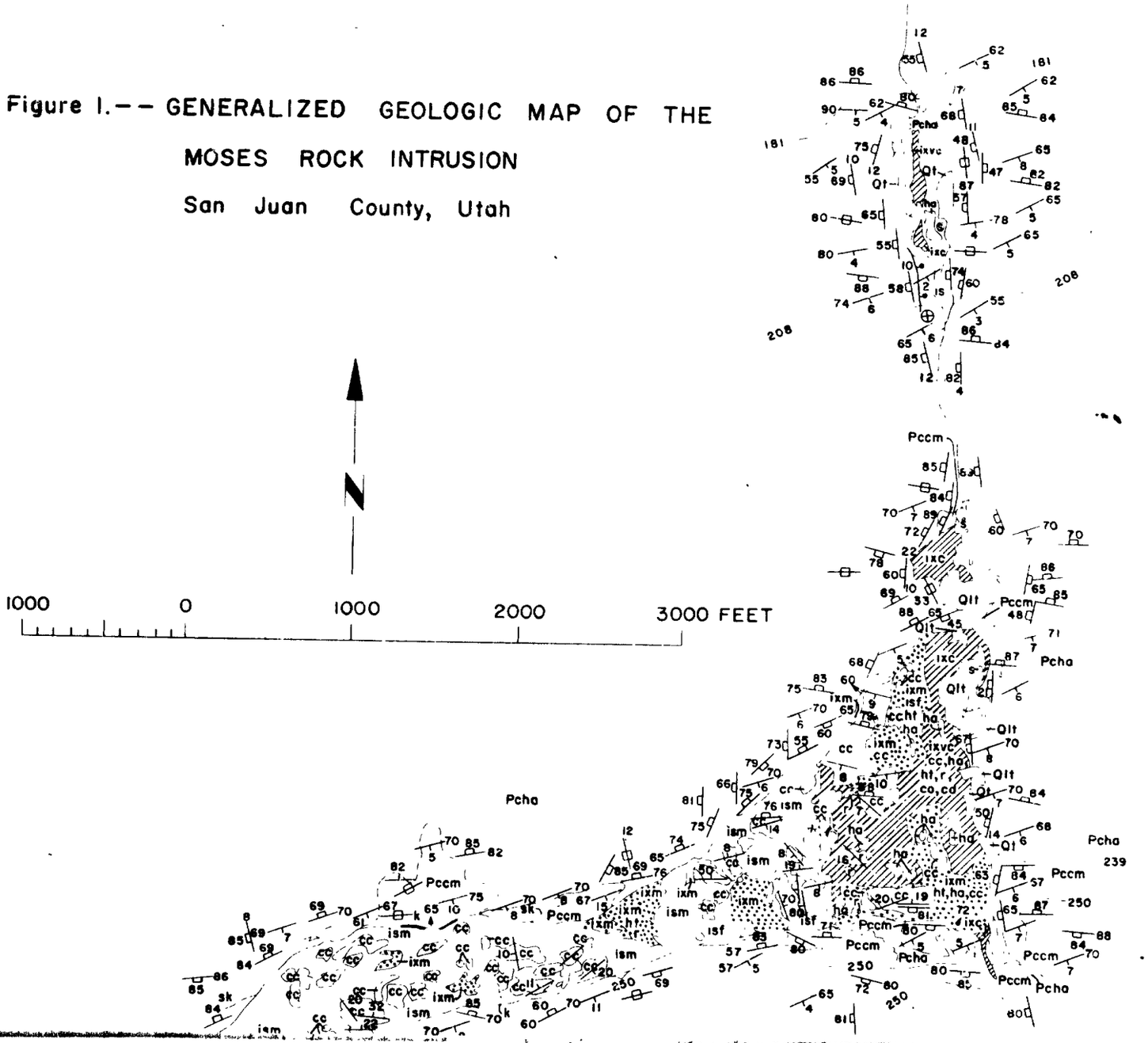

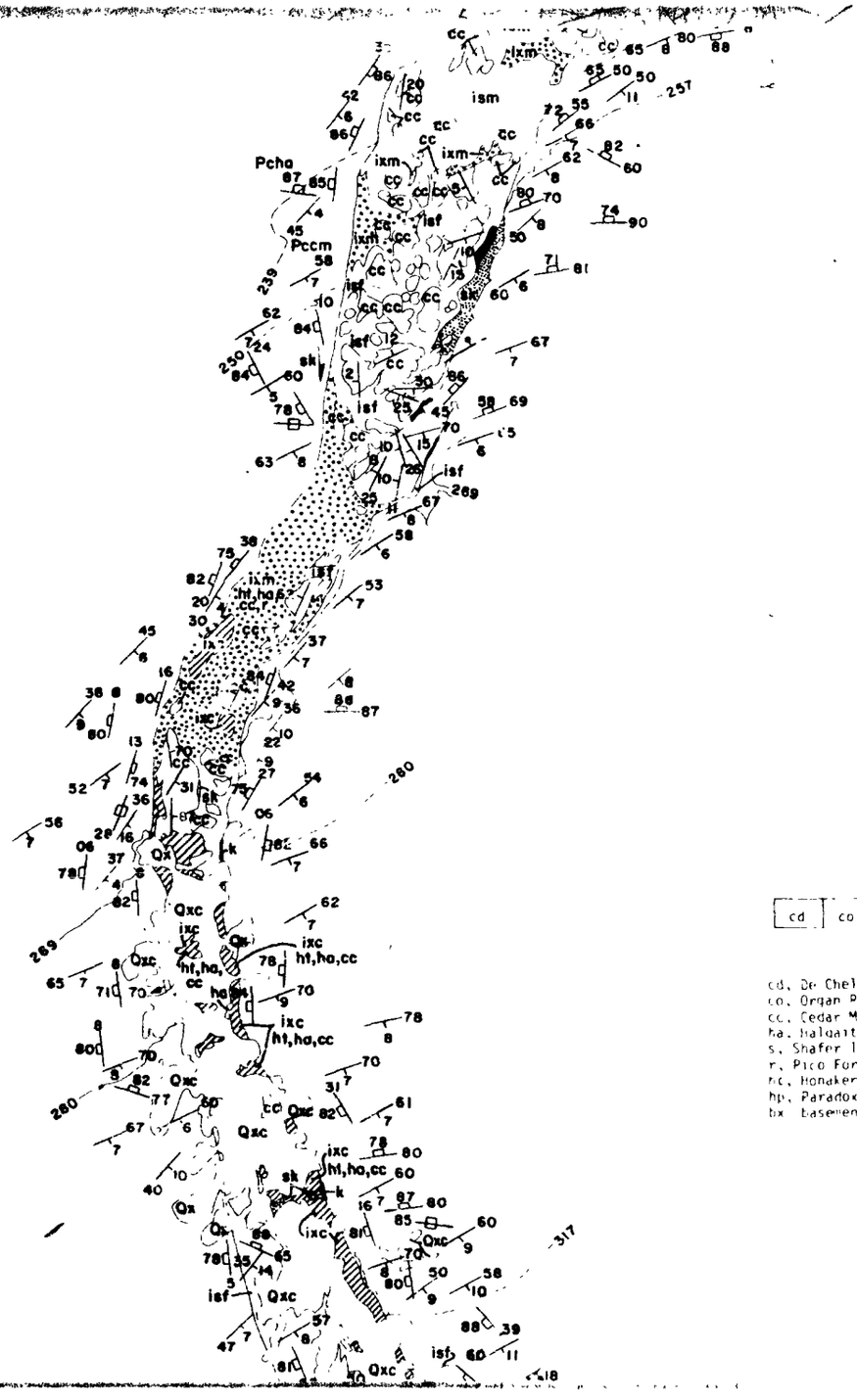

I-2

EXPLANATION

Qal

Alluvium

Qt

Talus

Qtl

Talus composed of limestone blocks

Qx | Qxvc | Qxc | Qxm

Surface rubble composed of basement rocks

Qx, cobble size
Qxvc, larger than 12 in
Qxc, larger than 6 in
Qxm, larger than 1 in

Qsd

Dune sand

Qs

Sedimentary deposit commonly capped with caliche

cd | co | cc | ha | r | ht | hp | bx

Breccia blocks within dike

cd, De Chelly Sandstone Member of Cutler Formation
co, Organ Rock Member of Cutler Formation
cc, Cedar Mesa Sandstone Member of Cutler Formation
ha, Halgaito Member of Cutler Formation
s, Shafer Limestone (local usage) of Rico Formation
r, Rico Formation
ht, Honaker Trail Member of Hermosa Limestone
hp, Paradox Member of Hermosa Limestone
bx, Basement rock

ixvc | ixc | ixm
is | ism | isf
sk
k

Intrusive rocks filling dike

ixvc, breccia with serpentine-bearing matrix, basement-rock inclusions exceed 12 in. in diameter
ixc, similar to ixvc, except basement rock inclusions only exceed 6 in. in diameter
ixm, similar to ixvc, except basement rock inclusions only exceed 1 in. in diameter
is, breccia composed predominately of blocks of Cutler Formation together with minor amounts of serpentine and basement-rock rock types
ism, basement-rock inclusions larger than 1 in. in diameter
isf, basement-rock inclusions smaller than 1 in. in diameter
sk, comminuted clastic material of the Cutler Formation mixed with kimberlite
k, kimberlite, dark-green serpentine-bearing rock; breccia containing pyroxene, ilmenite, garnet, and phlogopite inclusions and numerous kinds of rock and mineral fragments

QUATERNARY

TERTIARY

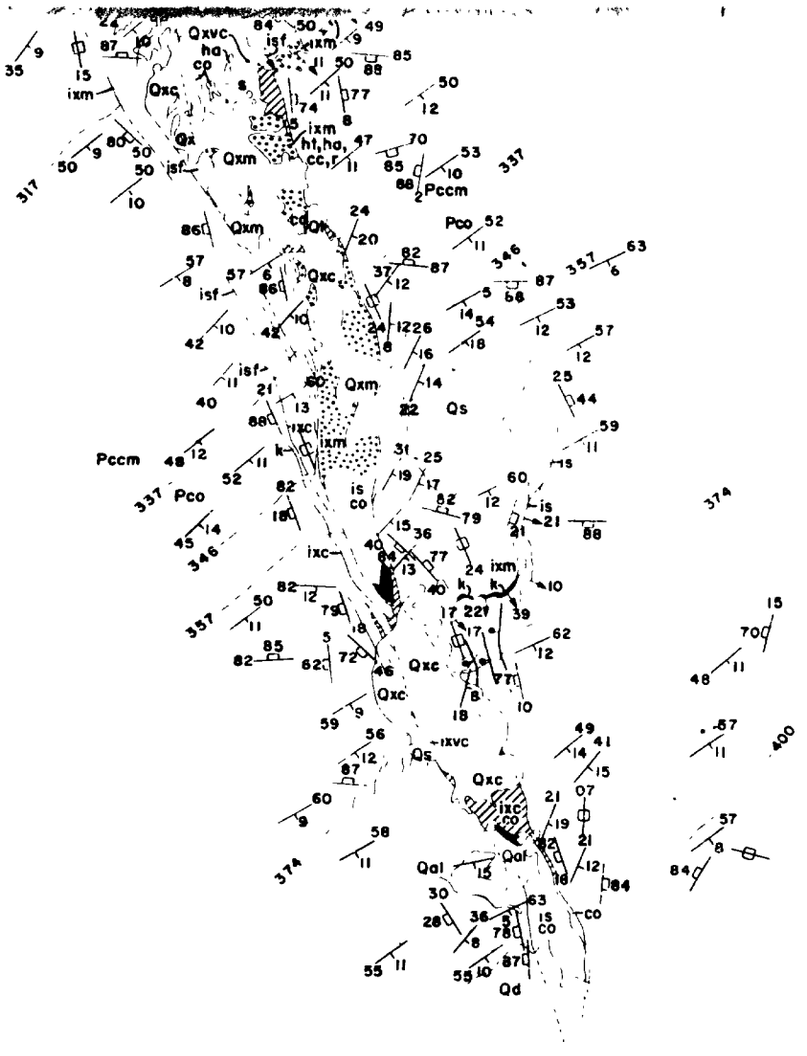

Pcd
Pco
Pccm
Pcha

Cutler Formation

Pcd, De Chelly Sandstone Member (230 feet)
Pco, Organ Rock Member (220 feet)
Pccm, Cedar Mesa Sandstone Member (201 feet)
Pcha, Halgaito Member (41 feet)

Pr

Rico Formation

Contact

Dashed where approximately located, dotted where concealed. Number refers to specific stratigraphic horizon indexed to detailed measured stratigraphic column

Strike and dip of bedding

Inclined Vertical
Attitude of fracture or joint

Fault

Dashed where approximately located, dotted where concealed. Bar and ball on downthrown side

Figure 2.-- INDEX MAP OF MOSES ROCK INTRUSION
San Juan County, Utah
Showing Roads, Geologic Sections, and Sample Localities

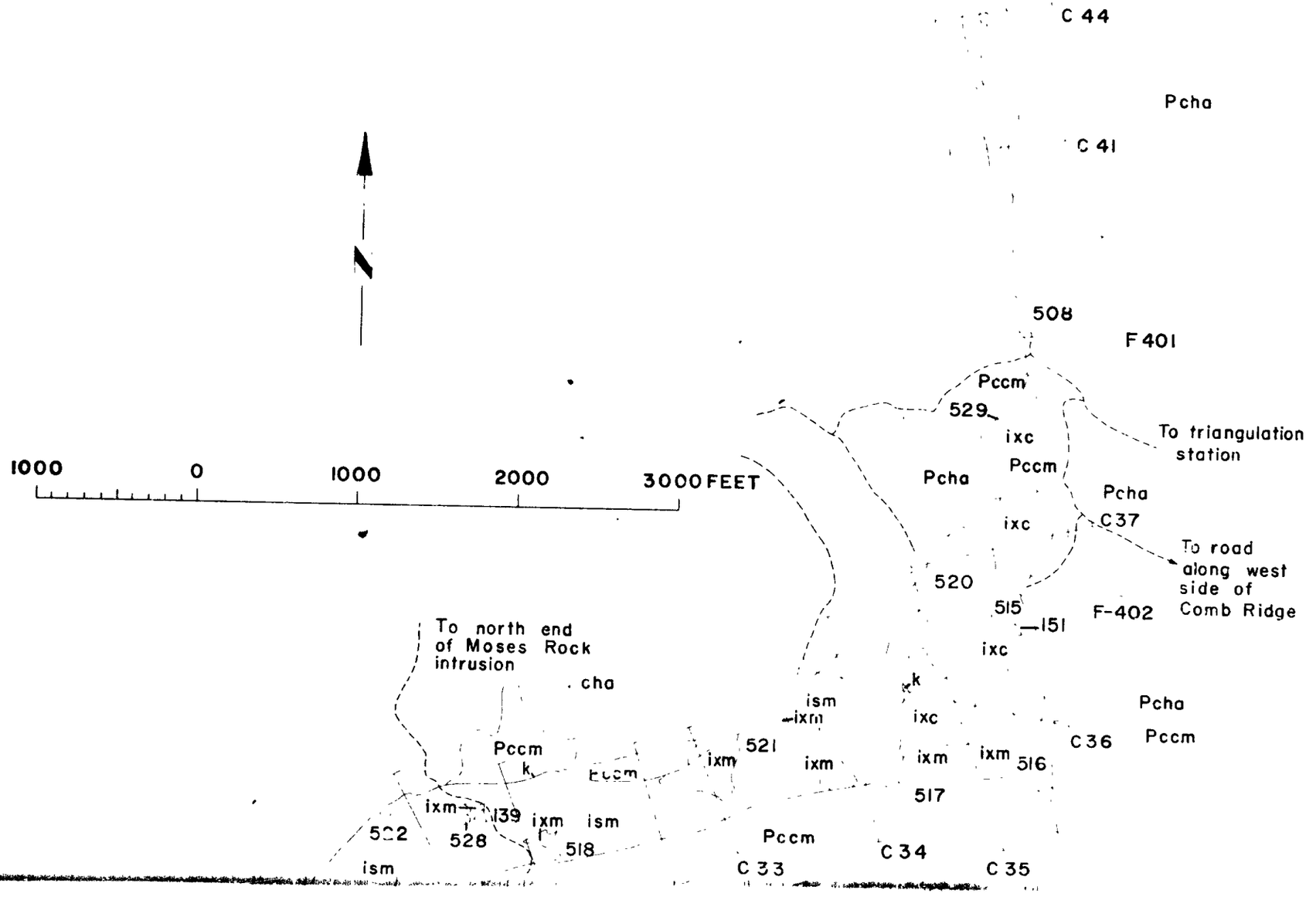

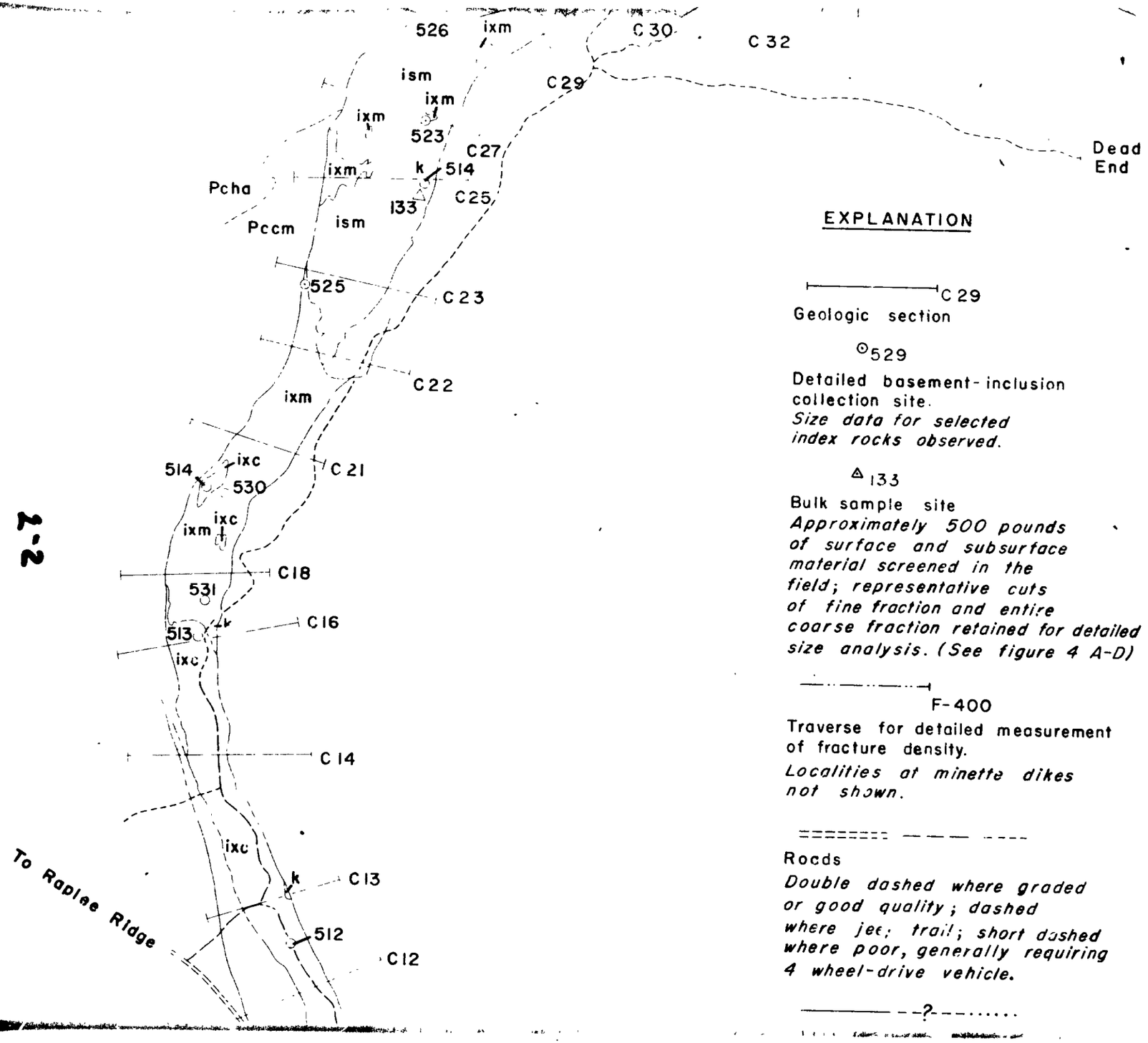

2-2

EXPLANATION

C 29
Geologic section

529
Detailed basement-inclusion collection site.
Size data for selected index rocks observed.

133
Bulk sample site
Approximately 500 pounds of surface and subsurface material screened in the field; representative cuts of fine fraction and entire coarse fraction retained for detailed size analysis. (See figure 4 A-D)

F-400
Traverse for detailed measurement of fracture density.
Localities of minette dikes not shown.

Roads
Double dashed where graded or good quality; dashed where jeep trail; short dashed where poor, generally requiring 4 wheel-drive vehicle.

?

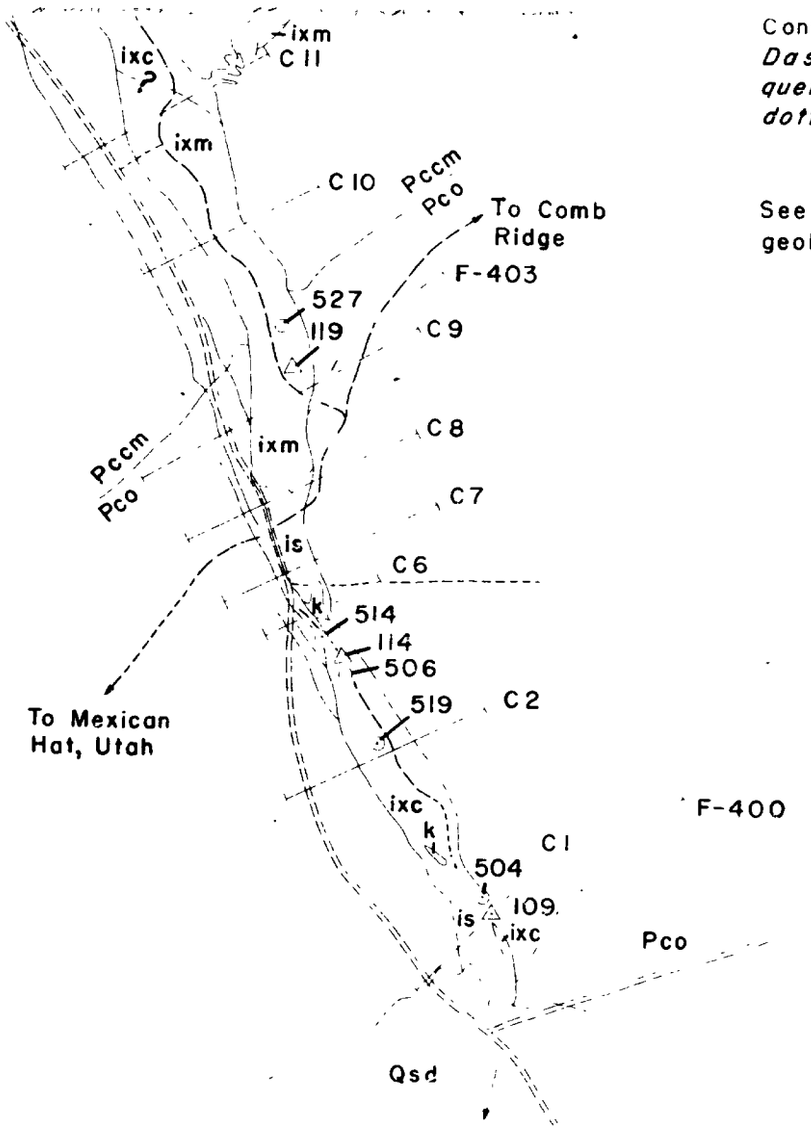

Contact
Dashed where approximate; queried where indefinite; dotted where concealed.

See figure 1 for explanation of geologic symbols.

To Comb Ridge-Mexican Water, Arizona or Vanadium Corporation of America #2 mine and Mexican Hat, Utah.

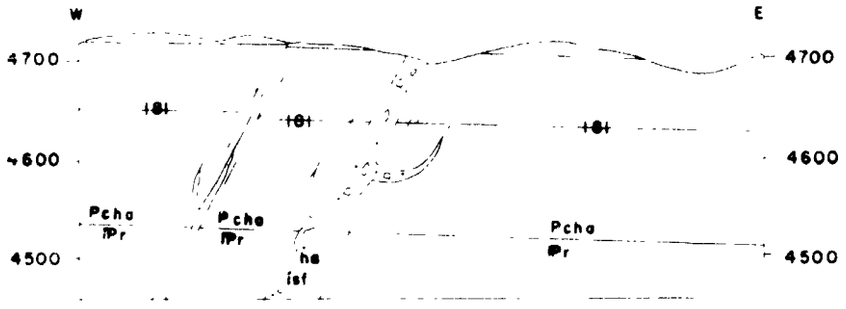

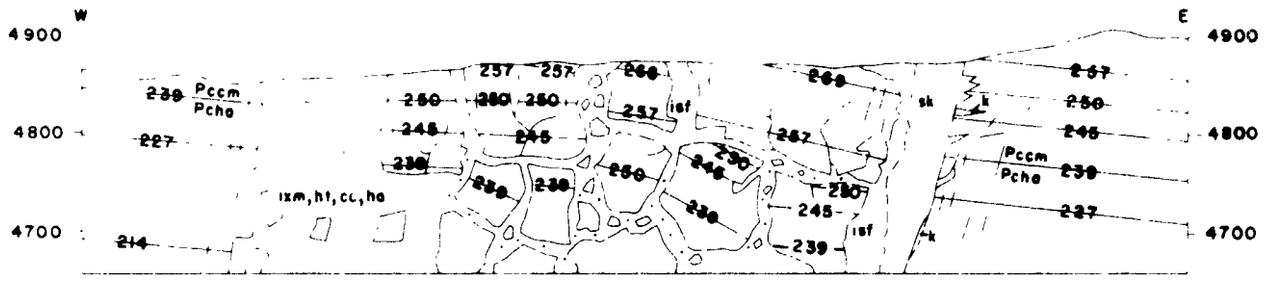

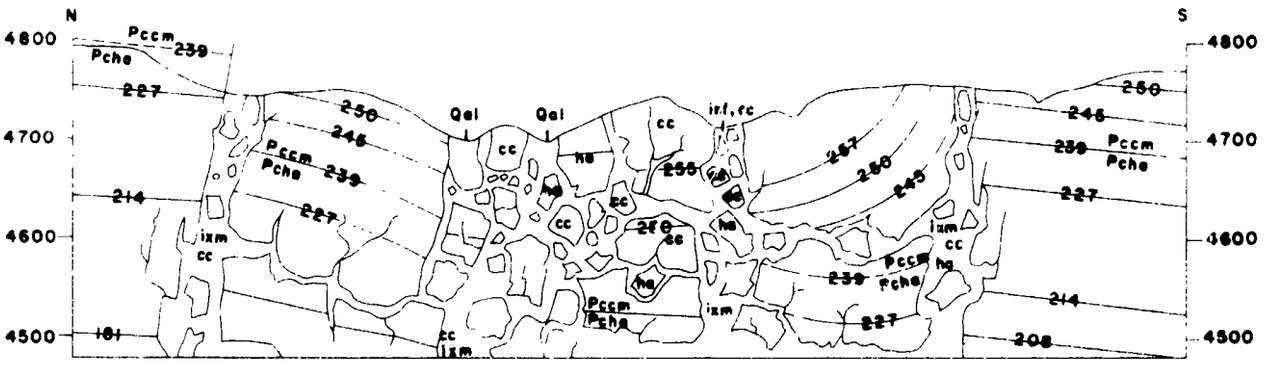

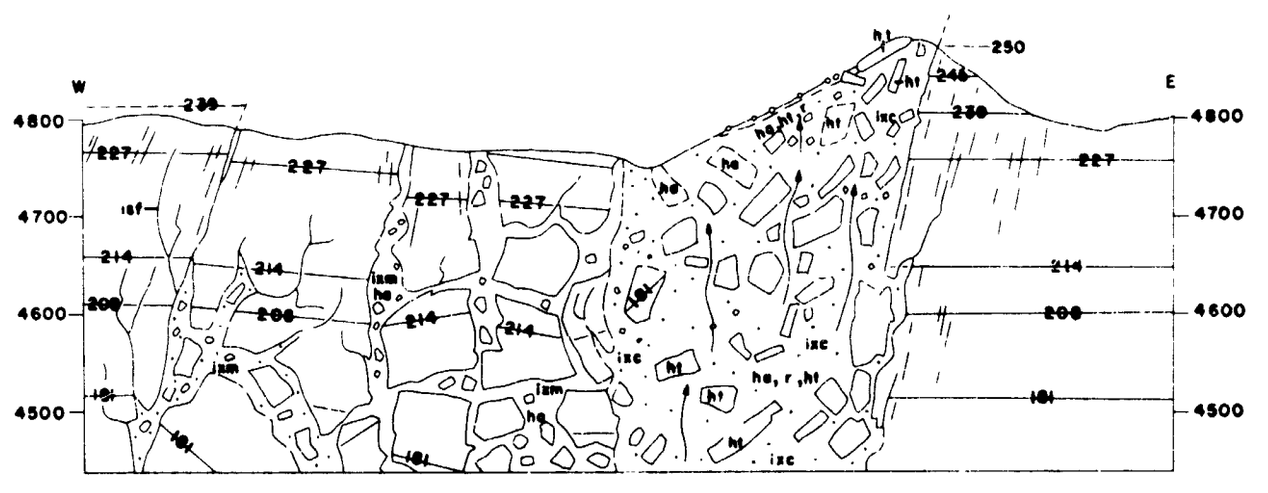

Figure 3.--Geologic sections through Moses Rock diatreme. Horizontal and vertical scale: 1 inch = 200 feet. See figure 2 for location of sections; see figure 1 for explanation of geologic symbols. Marker horizons within Cutler Formation are numbered.

The dip of the dike contacts ranges from vertical to about 70° W. A well-developed fracture system in the country rock parallels the contact. The density of fractures (fractures per linear foot) decreases approximately as an inverse power of the distance from the dike contact. Fracture density parallel to the regional joint trend (which near the dike strikes about N. 80° W., dips nearly vertical) also decreases away from the contact but not as abruptly. Fractures in the red sandstone and siltstone wallrocks at the contact are commonly bleached along zones typically 2-3 mm wide. Fractures paralleling the contacts generally disappear 200-300 feet from the contact; where present, bleaching effects on fractures disappear generally within about 10 feet of the contact, and everywhere within 50 feet.

A similar fracture pattern is present near the minette dikes. The fracture density decreases with distance in the same way; bleaching effects are more marked. The data are insufficient to make any definitive statement about the effect of lithology on the fracture density, although the measurements on Alhambra Rock suggest that the limey-siltstone red beds were more easily fractured than the limestone.

Deformation of the wallrocks is generally very slight. Beds are locally uparched, but most are largely undeformed and are simply truncated at the contact. Metamorphism and alteration at the contact are restricted to the bleached zones described above.

INTRUSIVE MATERIAL

The dike comprises lithologically distinct, but gradational, breccia units, which are mixtures of three components: (1) kimberlite--serpentine breccia containing olivine, pyroxene, garnet, calcite, and small, generally angular, rock and mineral fragments; (2) inclusions of Precambrian metamorphic and igneous rock fragments, not exposed locally; and (3) inclusions of sedimentary rocks, which can be usefully subdivided into limestone and clastic sedimentary rock debris derived from Paleozoic and Mesozoic strata now exposed at the surface in nearby river canyons or known from drilling records.

Units have been mapped within the intrusion on the basis of the relative abundance of these materials and the size of inclusions, which varies considerably from place to place (see fig. 1).

To determine the nature of these breccias, approximately 500 pounds of samples was obtained from the surface and from six subsurface localities at which the overburden was removed (fig. 2). The composition of the material and size frequency distributions of the various components were determined for all the material. Data on the subsurface samples are presented in figure 4 and table 1. Not all map units were sampled, but the range of compositions is representative, except that the unit called "is" (or "ism") is almost entirely clastic sedimentary debris with very little kimberlite or basement debris.

Dense kimberlite occurs as small dikelike bodies within the intrusion at at least four known localities. The degree of dilution of kimberlite with various types of debris ranges from almost none to at least six parts debris to one part kimberlite (table 1). The dilution probably exceeds 10 to 1 in much of the dike. The bulk samples suggest that the degree of dilution of kimberlite with debris increases as the size of the basement (and limestone) fragments increases.

The size frequency distributions of the clastic sedimentary material in the bulk samples (fig. 4 C, D) are characteristic of curves for material comminuted in ball mills (or other mechanical processes such as impact; see Meloy, 1963; Moore and others, 1963). Curves for limestone and basement inclusions are not as clearly characteristic of comminution and may reflect greater resistance to grinding and perhaps some differences in their history within the vent. Size frequency curves for basement inclusions collected in surface samples may reflect and represent the populations--at least with respect to size distribution.

The size of the basement inclusions varies greatly from place to place. The largest observed basement inclusions are ellipsoidal

Figure 4.--Size distribution and composition of six bulk samples of intrusive material. See figure 2 for location of samples. For each sample four diagrams are given. Diagrams for entire subsurface sample are A, size distribution of all components; B, debris components in various size fractions. Diagrams for each debris component in subsurface sample and for basement-rock fragments observed in sample totaled to 100 percent and treated independently of each other are C, composition of various size fractions; D, cumulative composition.

Explanation

B diagrams:

k, serpentine fragments and olivine, pyroxene, and garnet crystals not obviously derived from crystalline rock fragments

ss, sandstone and siltstone mostly derived from Cutler Formation

ls, limestone debris derived from Paleozoic rocks underlying the Cutler Formation

bx, rock fragments derived from the Precambrian crystalline basement

C and D diagrams:

△—·—△ Basement crystalline rocks observed in surface sample

▲——▲ Basement crystalline rocks in subsurface sample

⊡- -⊡ Limestone fragments derived from Paleozoic rocks underlying the Cutler Formation in subsurface sample

⊙-···⊙ Clastic sedimentary rock fragments and debris; mostly red sandstone and siltstone derived from Cutler Formation in subsurface sample

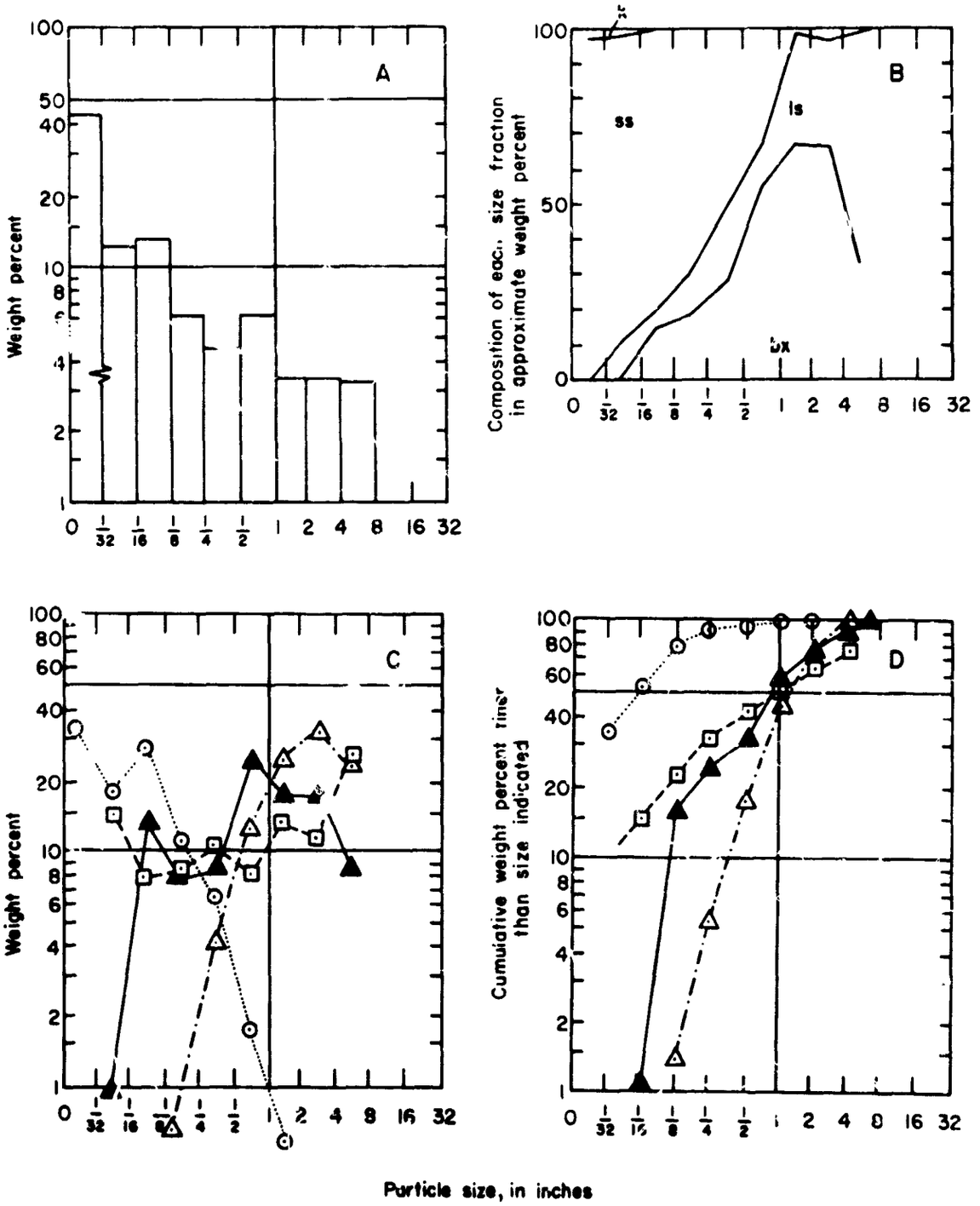

Figure 4.--Sample 151.

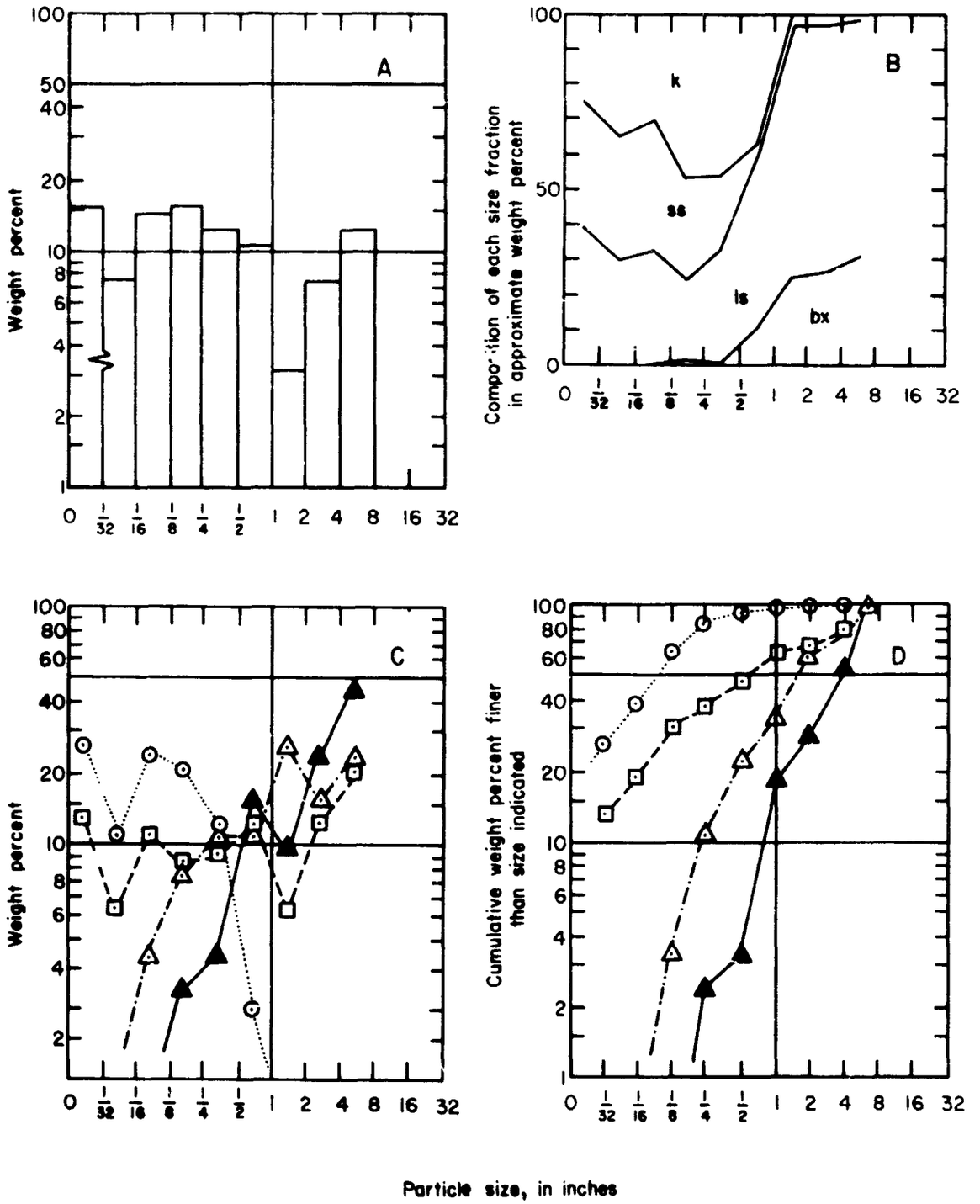

Figure 4.--Sample 109.

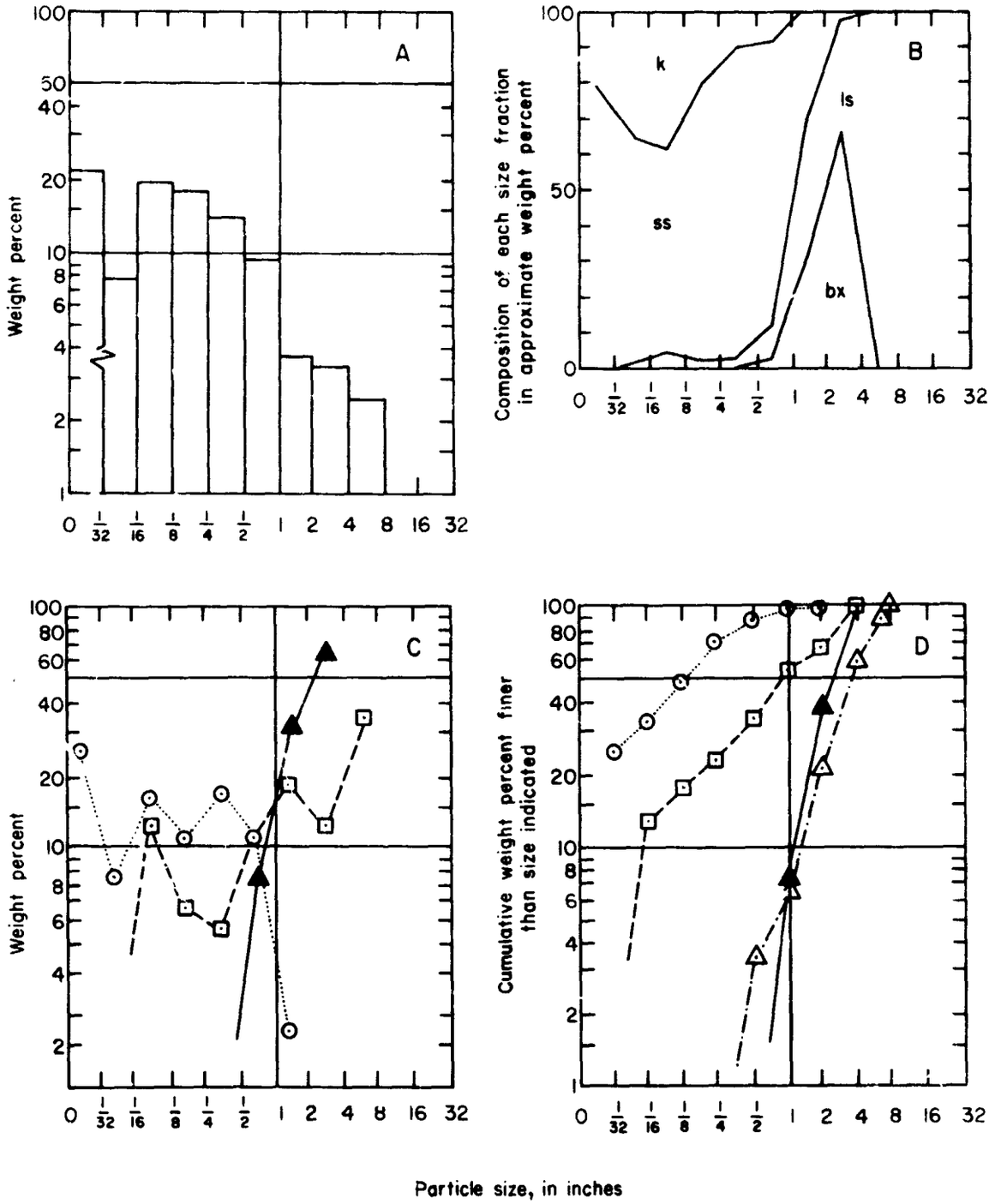

Figure 4.--Sample 114.

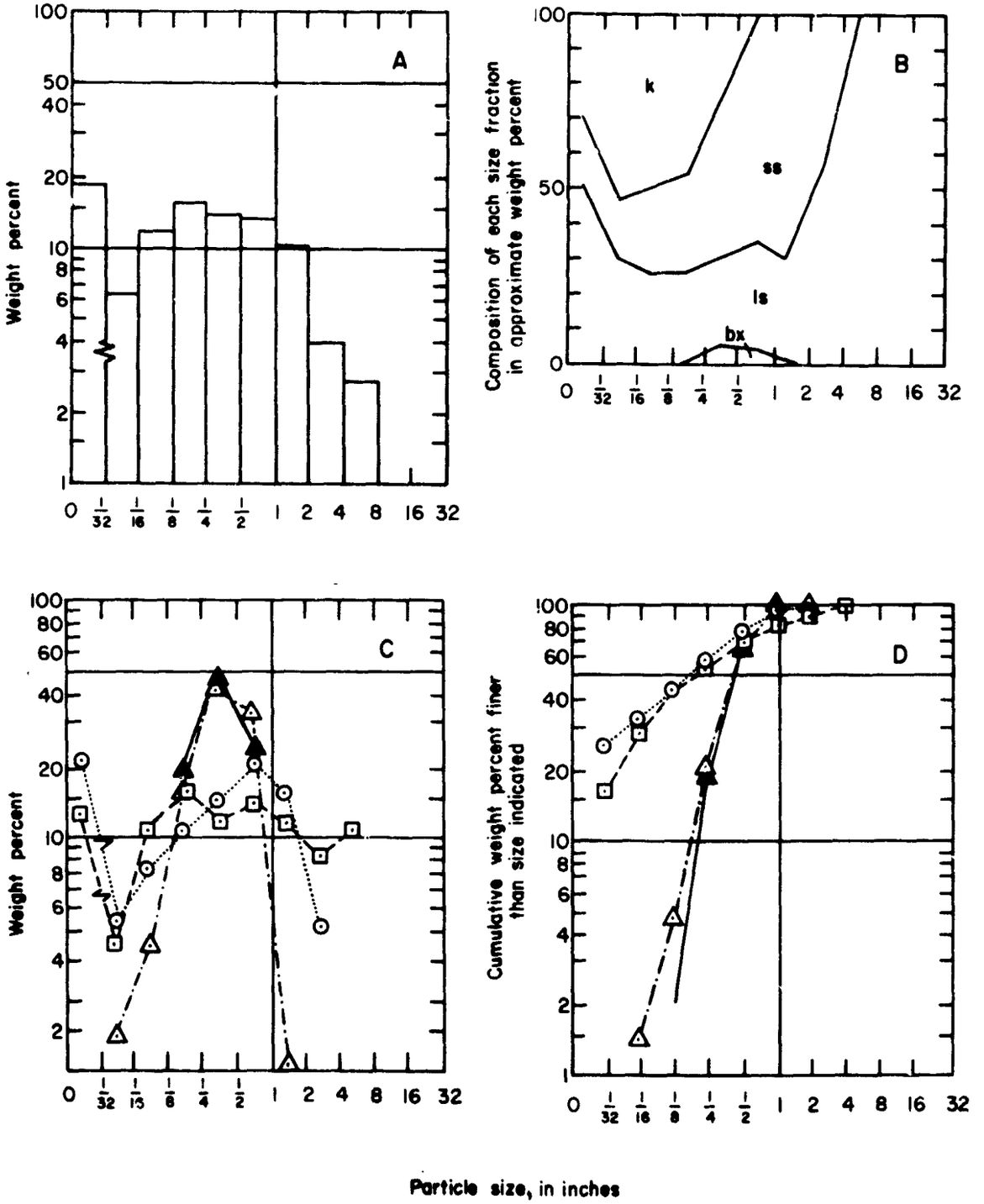

Figure 4.--Sample 139.

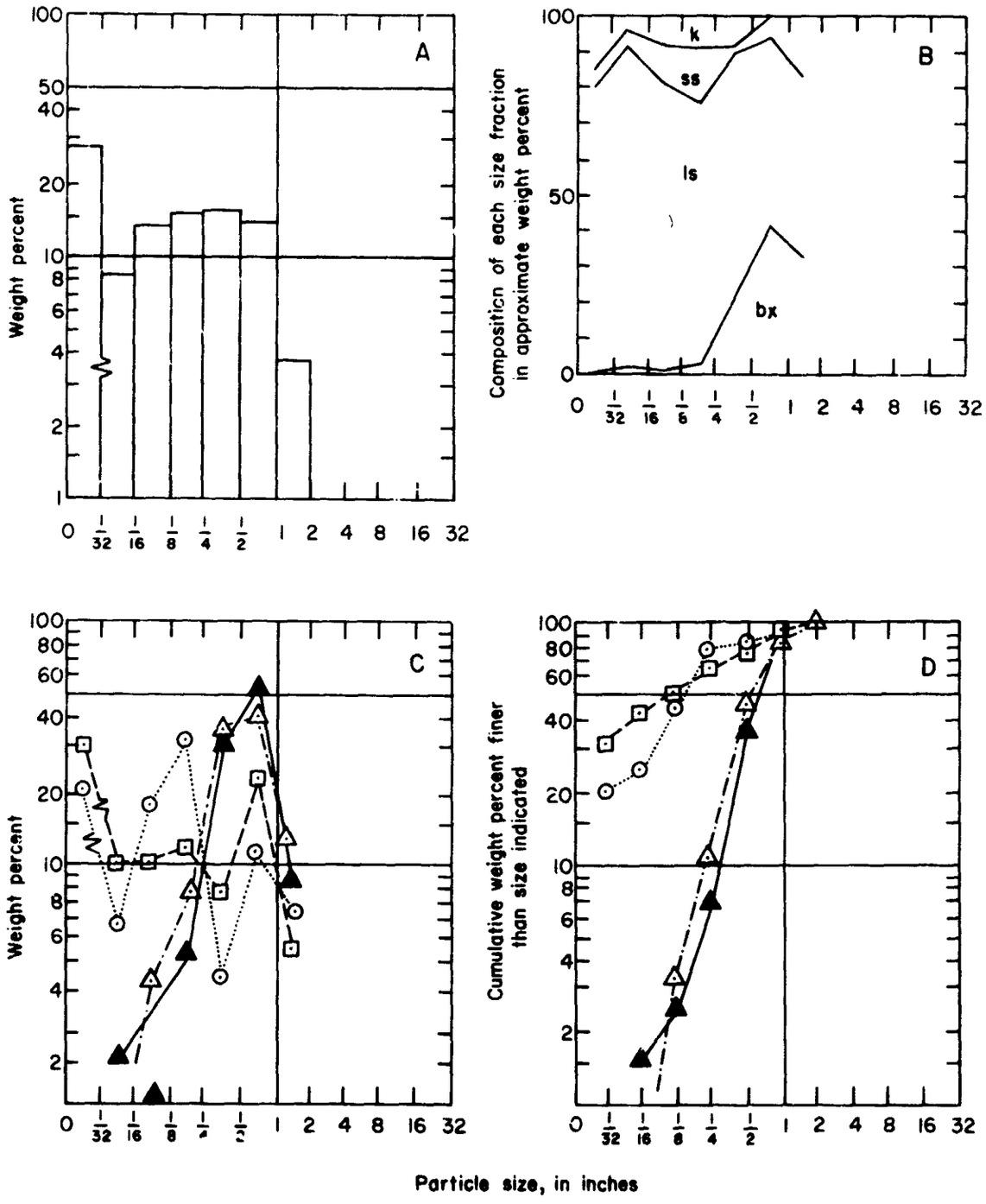

Figure 4.--Sample 119.

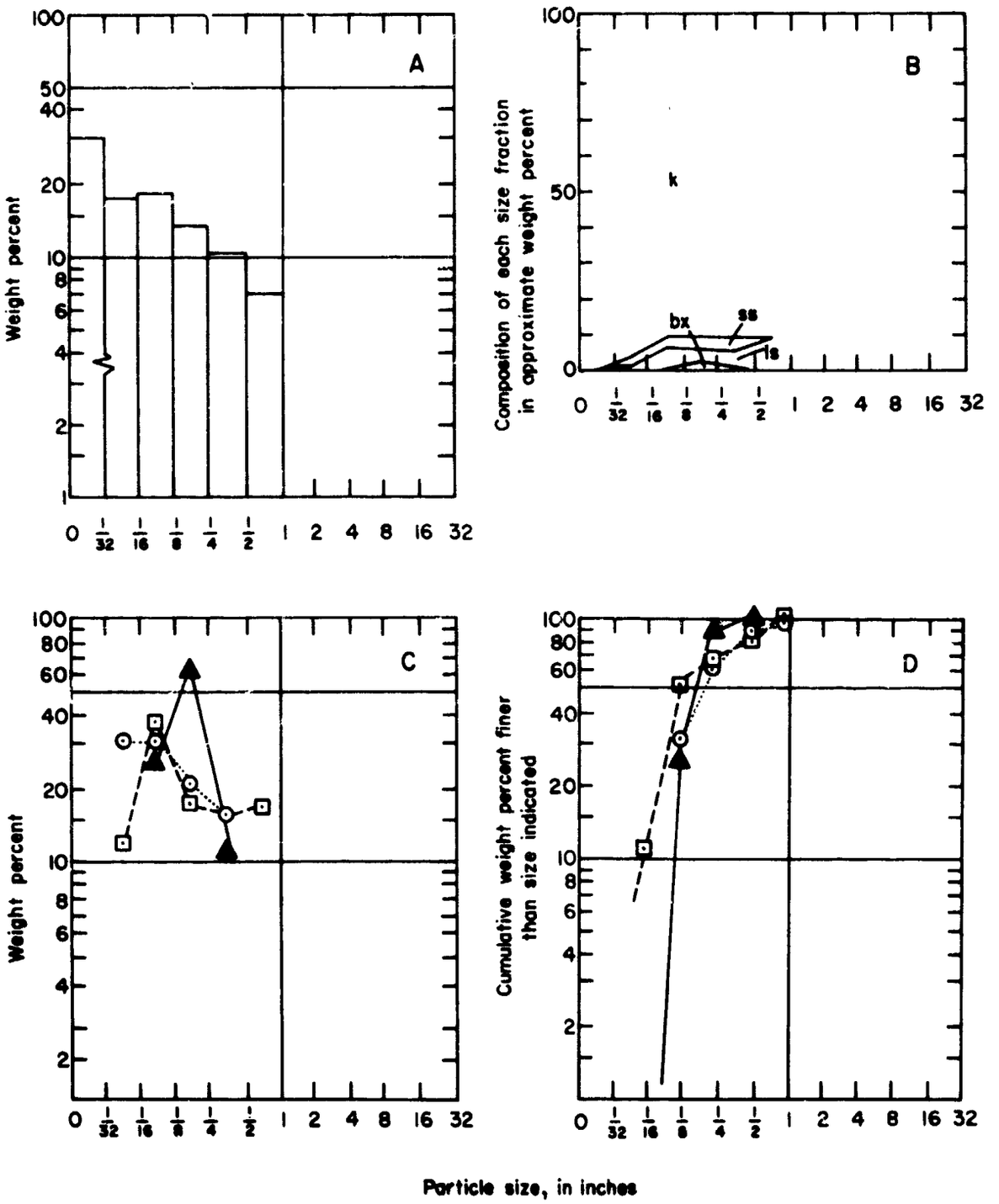

Figure 4.--Sample 133.

Table 1.--Composition of bulk samples of the intrusive material

Sample No.	151	109	114	139	119	133
A, Weight percent of all material in subsurface bulk sample						
Kimberlite	13.4	28	20.7	27	50	95.0
Precambrian basement rock	13.8	8	3.8	2	11	.7
Limestone	8.7	42	7.5	28	32	3.1
Clastic material	64.1	22	68.0	43	7	1.2
Total	100.0	100	100.0	100	100	100.0
B, Intrusive material normalized to kimberlite (dilution of kimberlite)						
Kimberlite	1.00	1.00	1.00	1.00	1.00	1.00
Precambrian basement rock	1.03	0.29	0.18	0.07	0.22	0.01
Limestone	.65	1.46	.36	1.04	.64	.03
Clastic material	4.72	.79	3.29	1.59	.14	.01
Total	6.40	2.54	3.83	2.70	1.00	.05
C, Largest fragments observed						
Part of bulk subsurface sample (g):						
Precambrian basement rock	2,079	2,788	1,341	34	66	1
Limestone	2,095	4,795	2,832	2,455	11	9.8
Local occurrence, maximum dimension (cm):						
Precambrian basement rock	37	40	27	13	14	3.5
Limestone	60	35	22	30	12	4.5

blocks of biotite granite gneiss, about 4 feet in diameter. Basement inclusions are largely unaltered, although commonly weathered. Detailed collections of basement inclusions were made at 28 localities.

Large blocks in the intrusion were derived from the Paleozoic and Mesozoic sedimentary rocks lining the vent and are as much as several hundred feet long (see fig. 3). Block and fragment size varies continuously from these large blocks to silt-sized grains represented in the bulk samples. It was possible to identify the specific stratigraphic horizons from which breccia blocks within the dike were derived and to determine the displacement of the blocks accurately. In general, very large blocks are displaced downward relative to their original stratigraphic position; however, within certain zones very large blocks have been transported upward hundreds of feet.

Large blocks are generally angular; smaller blocks, more spherical. Metamorphism and alteration of included blocks, including those derived from red beds and limestones, are minor or absent; deformation is minor.

The history of individual blocks is of interest since it is largely determined by the fluid density and velocity of the fluidized flow system within the intrusion. Whether a block introduced into the flow will sink or rise depends on its size, density, shape and orientation (if it is nonspherical). Once introduced into the flow it is subjected to transport, abrasion and comminution. Large blocks may initially subside relative to the walls, but as comminution and abrasion proceed the debris will eventually be carried upward. One would like to know the size of the largest block which the medium was capable of transporting upward. Thus, it is of interest to examine the size of blocks as a function of stratigraphic displacement. Ideally "size" is defined as the diameter of an equivalent sphere to account for nonspherical shapes as is common practice in fluid mechanics. However, in outcrops only two dimensions are usually seen, and the true size and shape of blocks

must be estimated or inferred. To avoid introduction of additional bias, the maximum exposed dimension of a block was used as an index of its size, and this was plotted against stratigraphic displacement for the Moses Rock intrusion. The data plotted in figures 5A-5C provide the basis for the conclusions drawn in the four sections that follow.

Estimated Equilibrium Block Size

Since blocks are observed stratigraphically displaced both upward and downward, it seems clear that sufficiently large blocks sank in the flow. Knowledge of the equilibrium size (with some independent means of estimating the fluid density and drag coefficient) would permit evaluation of the fluid velocity locally. The important field observation, therefore, is the size of the largest block displaced upward.

At Garnet Ridge, Cane Valley, and Mule Ear diatremes, the blocks displaced upward are smaller than the blocks resolved on the maps. However, at Mule Ear, crystalline basement blocks (nearly spherical) 20 feet in diameter were observed (E. M. Shoemaker, oral commun.); at Garnet Ridge crystalline basement boulders 5 to 6 feet in diameter are present.

The best data available are at Moses Rock: there, blocks from the Rico Formation 200 feet across are displaced upward about 500 feet; numerous Pennsylvanian (Hermosa Group) limestone blocks up to 100 feet across are displaced upward 800 to 2,500 feet. The largest basement crystalline blocks (spherical blocks of biotite granite gneiss) are 4 to 5 feet in diameter. The large limestone blocks are commonly tabular in form, thus the size of the equivalent sphere varies almost from their maximum to their minimum dimension depending on their orientation (flat side or edge to the flow). However, the diameter of the "equilibrium sphere" at the Moses Rock diatreme appears to be of the order of 100 feet.

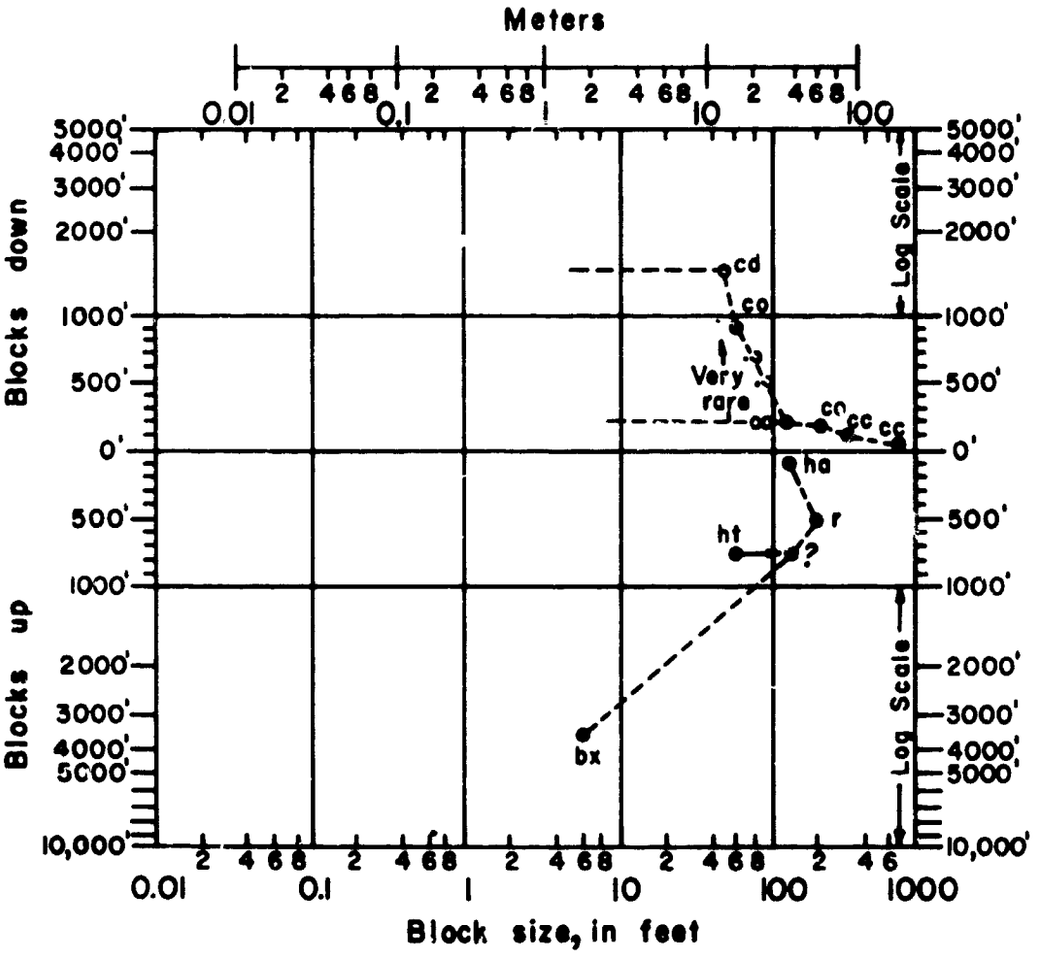

Figure 5A.--Maximum exposed dimension of blocks plotted against stratigraphic displacement of each block--entire body. See figures 1 and 4 for explanation of geologic symbols.

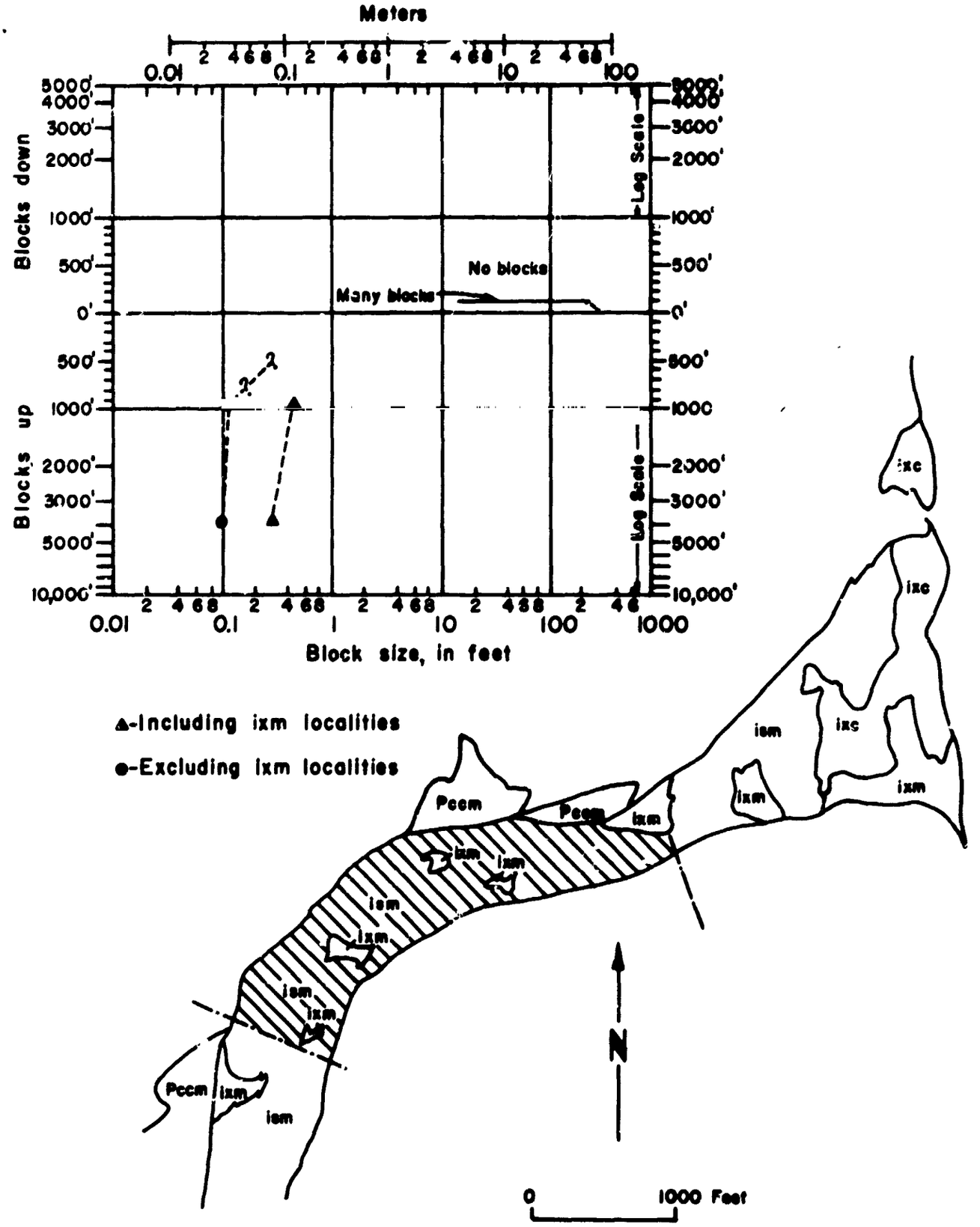

Figure 5B.--Maximum exposed dimension of blocks plotted against stratigraphic displacement of each block--central part. See figures 1 and 4 for explanation of geologic symbols.

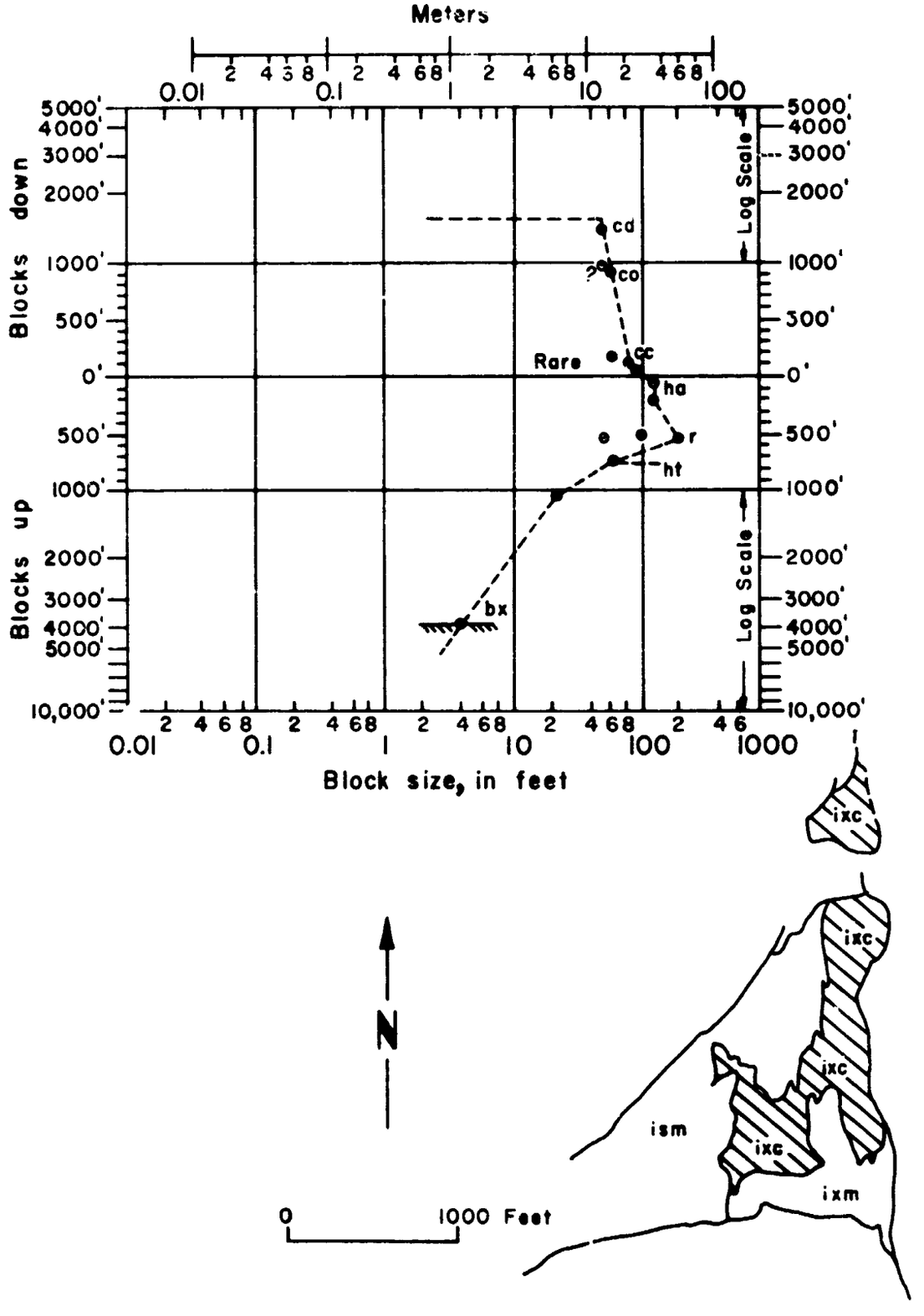

Figure 5C.--Maximum exposed dimension of blocks plotted against stratigraphic displacement of each block--north end. See figures 1 and 4 for explanation of geologic symbols.

Maturity of Flow or Duration of Eruption

Differences between diatremes probably reflect differences in duration of the eruption as well as differences in flow history. At Mule Ear, the eruption lasted long enough to ream out the vent. Differences also exist within individual intrusions. Compare, for example, two areas within the Moses Rock intrusion: the central portion sketched in figure 5B contains large blocks displaced short distances downward and only rare and small basement inclusions; by contrast, at the north end (see fig. 5C), blocks are displaced greater stratigraphic distances, both up and down. The interpretation here is that the eruption was of relatively short duration in the central portion, whereas at the north end channels formed and flow through the vent continued for some time.

Size-Depth Relationship for Upward Displaced Blocks

At Moses Rock, for fragments derived from stratigraphic units below the present surface, the deeper the source, the smaller the maximum block size (see fig. 5C). This observation is the empirical basis for interpreting the relative depth of origin of the basement inclusions where the stratigraphy is not known. If a similar size-depth relationship holds, the vertical section represented by the basement inclusions can be reconstructed.

Thickness of the Overburden

No locks stratigraphically above the Cutler Formation were observed in the Moses Rock intrusion. Large blocks of Burro Canyon conglomerate and Mancos Shale are present in the Mule Ear diatreme (E. M. Shoemaker and H. J. Moore, unpub. map, 1957). Assuming the Mule Ear and Moses Rock diatremes to be roughly contemporaneous, and, since they are only 2 miles apart, the ground surface at the time of their emplacement was at least 3,000 feet above the present surface.

EMPLACEMENT OF THE MOSES ROCK INTRUSION

The inferred history of emplacement of the Moses Rock intrusion is illustrated in figure 6.

The surface expression of the Moses Rock dike was probably a long rift with several well-developed maar-type craters along it, each surrounded by an ejecta blanket. The material in this ejecta is probably represented by the various intrusive units, now exposed at depth. The stratification of this material therefore reflected the changing composition of the intrusive material with time. Thus, these beds should reflect the sequence described above but in inverted stratigraphic sequence. The basal layer should be nearly pure kimberlite tuff, becoming diluted with other debris including progressively larger blocks as one moves upward through the section.

The distribution of material around the vent (or exterior ballistics) is determined by the ejection velocity and angle, size of the block, and atmospheric conditions.

The original surface expression of this intrusion was probably very similar to certain rilles on the surface of the Moon, for example, the Hyginus rille, the Stadius crater chain, and in particular, the prominant rille in the eastern part of the floor of the crater Alphonsus, as shown in the Ranger IX photographs. Nothing can be said regarding possible similarity of the intrusive or extrusive material; however, the forms are suggestive of a possible similar type of violent eruptive volcanism.

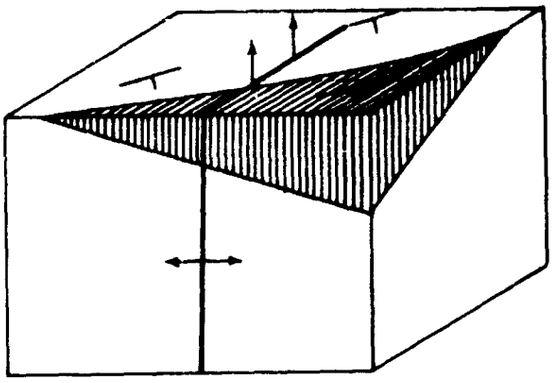

Fracture propagates upward. Intrusive material is initially largely gaseous, with small amount of serpentine and little or no wallrock debris. At this stage, fluid pressure exceeds the local lithostatic load, plus the effective strength of the rocks.

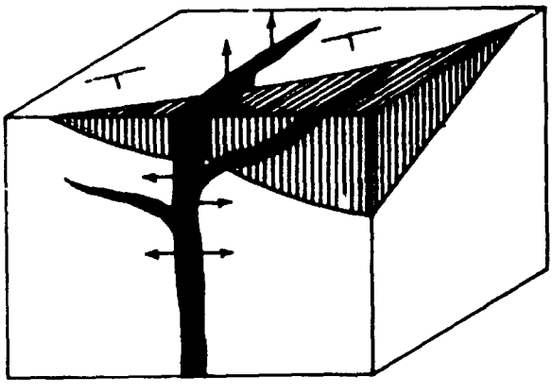

Fracture opens forcibly by fluid over-pressure within the fissure; sills and dikes emplaced locally along weaknesses, and local deformation at the walls may occur. Intrusive material is gas with serpentine entrained with small amounts of basement rock fragments; very little sedimentary wallrock debris present.

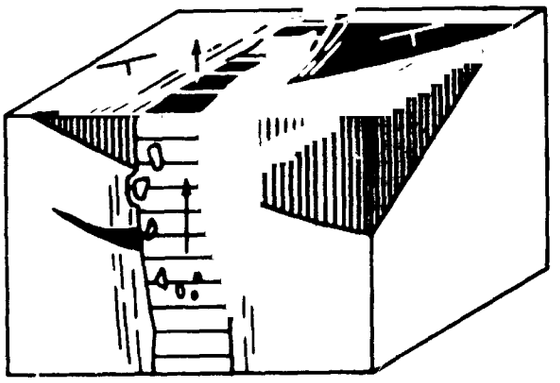

As flow continues, the dike widens slightly and probably vents locally at the surface, the fluid velocity increases. The fluid pressure drops as a result. When this pressure drop becomes extreme the walls fail and blocks are introduced into the flow which rise or sink depending on the local fluid velocity and density and the size, shape, and orientation of the block. As these blocks become comminuted, the debris is mixed with the intrusive serpentine and gas. The fragments of crystalline basement rocks entrained are small initially, but larger blocks are entrained as the eruption progresses.

(See p. 252 for key to patterns.)

Figure 6.--Inferred sequence of events during emplacement.

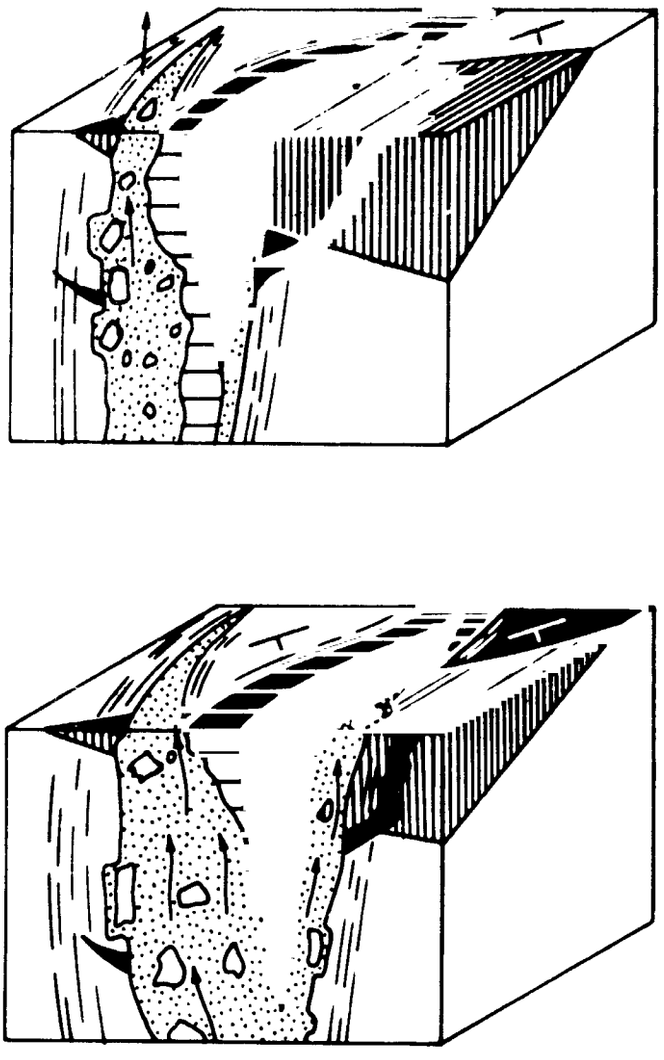

As the eruption matures, the mixture of serpentine, breccia blocks from various sources, and debris produced by comminution of the breccia blocks, entrained in upward flow may be considered as a gas-solid fluidized system--or perhaps at greater depths as a fluid-solid fluidized slurrie where the fluid density is great. The upward movement of such a heterogeneous medium is not uniform, rather the flow becomes restricted preferentially into channels. (In industrial fluidized systems such channels are a common problem; they are referred to as "ratholes".) Within these channels the upward flow velocities become large. Basement inclusions are large and spherical; wallrock blocks are large and locally displaced upward from their original position; serpentine content of the breccia is low owing to the dilution by material derived from the vent walls.

The sequence of events appears unambiguous; however, it may represent a single eruption or a series of eruptions separated slightly in time.

Figure 6.--Inferred sequence of events during emplacement--Continued.

REFERENCES CITED

Allen, J. E., and Balk, Robert, 1954, Mineral resources of Fort Defiance and Tohatchi quadrangles, Arizona and New Mexico: New Mexico Bur. Mines and Mineral Resources Bull. 36, 192 p.

Baker, A. A., 1935, Geologic structure of southeast Utah: Am. Assoc. of Petroleum Geologists Bull., v. 19, pt. 2, p. 1472-1507.

_____1936, Geology of the Monument Valley-Navajo Mountain region, San Juan County, Utah: U.S. Geol. Survey Bull. 865, 106 p.

Bartlett, R. A., 1962, Great surveys of the American West: Univ. of Oklahoma Press, 408 p.

Gregory, H. E., 1938, The San Juan country: U.S. Geol. Survey Prof. Paper 188, 123 p.

Malde, H. E., 1954, Serpentine pipes at Garnet Ridge: Science, v. 119, p. 618.

Malde, H. E., and Thaden, R. E., 1963, Serpentine at Garnet Ridge: U.S. Geol. Survey Bull. 1103, p. 54-61.

Meloy, T. P., 1963, Cumulative and weight retained tables for the Gaudin-Meloy size distribution: Am. Inst. Mining Metall. Engineers Trans., v. 226, p. 357-361.

Moore, H. J., Gault, D. E., and Lugn, R. V., 1963, Experimental impact craters in basalt: Am. Inst. Mining Metall. Engineers Trans., v. 226, p. 258-262.

O'Sullivan, R. B., 1965, Geology of the Cedar Mesa-Boundary Butte area, San Juan County, Utah: U.S. Geol. Survey Bull. 1186, 128 p.

Shoemaker, E. M., 1962, Interpretation of lunar craters, in Kopal, Z., ed., Physics and astronomy of the Moon; London, Academic Press, p. 283-359.

Williams, Howel, 1936, Pliocene volcanoes of the Navajo-Hopi country: Geol. Soc. America Bull., v. 47, p. 111-172.